VISUAL PERCEPTION OF SPATIAL ORDER

visuele waarneming van spatiele orde

VISUAL PERCEPTION OF SPATIAL ORDER

visuele waarneming van spatiele orde

(MET EEN SAMENVATTING IN HET NEDERLANDS)

PROEFSCHRIFT

TER VERKRIJGING VAN DE GRAAD VAN DOCTOR IN DE WISKUNDE EN NATUURWETENSCHAPPEN AAN DE RIJKSUNIVERSITEIT TE UTRECHT, OP GEZAG VAN DE RECTOR MAGNIFICUS PROF. DR. J.A. VAN GINKEL, VOLGENS BESLUIT VAN HET COLLEGE VAN DECANEN IN HET OPENBAAR TE VERDEDIGEN OP MAANDAG 9 MAART 1987 DES NAMIDDAGS TE 2.30 UUR

DOOR

ALEXANDER TOET

GEBOREN OP 12 OKTOBER 1955 TE APELDOORN

PROMOTOR: Prof. Dr. J.J. Koenderink
CO-PROMOTOR: Dr. B. Nienhuis

cum homo calculat fit spatium

E. Cassirer.
The concept of group and
the theory of perception.
Philosophy and Phenomenological
Research, vol. V, 1944, pp.1-36.

Spatial order is merely
a matter of mind;
if there is no mind
it doesn't matter.

A.T.

CONTENTS.

Part II: Differential spatial displacement discrimination in the human visual system.

GENERAL INTRODUCTION AND SUMMARY.

Every visual system must build an internal representation of the spatial structure of its visual environment using the signals transmitted by its individual photoreceptors. Ideal photoreceptors transform the spatial distribution of an environmental intensity pattern into a set of flux measurements. This thesis deals with the question how a neural system may obtain a whole consistent percept from a myriad of seemingly unconnected input signals.

In the human visual system the fibers of the optic nerve reach the visual cortex in an orderly fashion such that neighbouring points on the retina are projected to neighbouring points on the cortex. As a result the electrochemical activity patterns in the brain are to a large extent isomorphic to the retinal image. This seems to support the so-called "inner screen" theories. Descartes' (1963) notion of the projection on the pineal body was perhaps the first clear statement of such a projection theory. However, these theories require an external observer (homunculus) to appreciate the spatial lay-out of the neural activity patterns. As this leads to an infinite regress these models are clearly of no avail to explain the concept of spatial vision.

The philosopher Lotze (1884; III.2.) realized that only the functional relations between neural elements are relevant to a neural system. Whereas the geometrical order is only available for external observers, the functional order is objectively available to the system itself. He introduced the "Lokalzeichen" ("translated" into English by the Germanism "local sign") which is a label residing in the signal activity of the optic nerve fibers stating from which part of the sensorium each signal originates. It is obvious that a label or local sign residing in the activity of any single fiber is of no avail. This would still require an external observer to appreciate the spatial order of the activity patterns in the neural net. Therefore, such a label has to be in the constraints on the relative simultaneous signal activity of a collection of fibers.

In Lotze's view the local signs were some kind of extra information transmitted by the fibers of the optic nerve. Carnap (1979) demonstrated how the constraints on the possible simultaneous/successive order of the total signal activity in a collection of fibers may be used to constitute a functional order that is topologically equivalent to the spatial order of the underlying sensorium. For instance, when the activity on two wires is correlated a "proximity" may be assumed. Thus, there is no need to assume the existence of extra signals that indicate the relative spatial position of the detector from which any signal originates. In this view the constraints on the possible signal activities are the "key" to the functional structure of the neural net (i.e. the local sign). These constraints are partly determined by the hardware (the spatial structure of the sensorium). This key can only be obtained by monitoring the activity in the neural net and noting which patterns can and which patterns cannot occur.

The first part of this thesis presents two simulation models that integrate the input signals presented to a neural system by its sensorium into a whole consistent "percept". The second part presents the results of some experiments that were performed to test the limits of the spatial localization capability (i.e. the tolerance of the abovementioned integration process) for the human visual system.

PART I: The construction of a simultaneous functional order in nervous systems.

Introduction to Part I.

Coincidences in the signal activity in a neural net that occur frequently do so because they result from some causal connections residing either in the spatial lay-out of the sensorium or in the spatial structure of the environment. A neural system is sometimes thought to function as a gifted detective, noting suspicious coincidences in its afferent input and encoding these (e.g. by selective stabilization or competitive

disconnection of certain neural interconnections) in the constraints on its functional structure (Barlow, 1985). Because of the huge number of neural elements involved, the problem of detecting such coincidences is an immense one. However, there are indications that the global functional order is genetically determined (e.g. Jeffery, 1985) whereas the local functional order may be modified by experience in an early stage of postnatal development (for an overview see Movshon and van Sluyters, 1981). This implies that the detection of signal coincidences is only applied at a local scale, which means an enormous reduction of the number of relations that have to be monitored.

Since two nearby detector units are frequently activated together they are apt to be mapped on "neighbouring" individuals in the functional order. On the other hand, distant units are activated relatively seldom at the same time so that they may be mapped on different regions of the neural system. When the neural net has sufficient internal coherence the resulting functional order may be homeomorphic with the underlying detector array.

This section presents two models that construct a simultaneous functional order in a collection of nervous elements by monitoring their signal activity over a certain time span. The results of simulation experiments show the possibility to encode the topological information on the afferent input signals of the neural elements in their simultaneous functional order.

Only one-dimensional sensoria were used in the simulation experiments. It is indicated how the models can be extended for more-dimensional detector arrays. However, the mathematical analysis becomes much more difficult because the topology of for instance two-dimensional detector arrays (e.g. the retina) is far richer than the simple one-dimensional topology.

Summary of Part I.

Chapter I.1 presents two algorithms that construct a simultaneous functional order in a collection of neural elements using purely functional relations. The input of the first algorithm is a matrix describing the total of covariances of signals carried by the members of the neural collection. The second algorithm proceeds from a matrix describing a primitive functional inclusion relation among the members of the neural collection that can be determined from coincidences in their signal activity. From this information both algorithms compute a partial functional order in the collection of neural elements. As noted before, such an order has an objective existence for the system itself and not only for an external observer. By either merging individual neurons or recruiting previously unspecified ones the partial order is thereafter locally transformed into a lattice order. Simulation experiments are presented that were performed to study the number of individuals in the resulting lattice order as a function of the number of individuals in the underlying partially ordered set.

Chapter I.2 shows how the resulting functional order in a nervous net can be related to the geometry of the underlying detector array. In particular, an algorithm is presented to construct an abstract geometrical complex from this functional order. The algebraic structure of this complex reflects the topological and geometrical structure of the underlying detector array. It is shown how the activated subcomplexes of a complex can be related to segments of the detector array that are activated by the projection of a stimulus pattern. The homology of an abstract complex (and therefore of all of its subcomplexes) can be obtained from simple combinatorial operations on its coincidence scheme. Thus, both the geometry of a detector array and the topology of projections of stimulus patterns may have an objective existence for the neural system itself.

The signal activity in a neural net will be constrained both by its physical restrictions and by environmental constraints. By monitoring its signal activity a neural system can build up a simultaneous functional order that encodes these constraints. Chapter I.3 presents the results of

simulation experiments that were performed to study the influence of the physical constraints of a neural system on the simultaneous functional order produced by both models that were introduced in Chapter I.1. A one-dimensional detector array was used in these experiments. The physical constraints are delineated which such an array has to satisfy in order to induce a functional order relation that allows an isomorphism with a geometrical order. It is shown that for an appropriate choice of the system parameters both models can produce a simultaneous functional order with sufficient internal coherence to allow isomorphisms with a triangulation. In this case the dimensionality and the coherence of the detector array are objectively available to the system itself.

Chapter I.4 presents the results of simulation experiments that were performed to study the influence of environmental constraints on the resulting functional order in a set of neural elements corresponding to a one-dimensional detector array. It is shown that the coincidence-model produces a functional order that encodes the physical constraints of the environment. Moreover, it is demonstrated that the signal activity in the neural net (the "perceptions") can be related to events in the outer world. Thus it is possible to study to what extent experience contributes toward shaping the notion of space. Some examples are provided to demonstrate that these models may prove useful to gain insight into certain developmental disorders.

PART II: Differential spatial displacement discrimination in the human visual system.

Introduction to Part II.

The subject of the second part of this thesis is an experimental study of the ability of the human visual system to **relate spatial positions** of different features that are simultaneously present in the visual field. Knowledge of this ability may help in gaining an understanding of the wider problem mentioned in the first part, namely how the unitary and apparently continuous visual space we experience can arise from a myriad of separate inputs. At some stage in the visual system every signal line must be linked to every other because we can appreciate the spatial relation between any two visual objects that stimulate the retina together. By studying the limits of this localization ability we may find out how the relations between different signal lines are established in the visual pathways.

The human visual system can detect changes in the relative spatial position of features in the visual field which are an order of magnitude below the diameter of a foveal photoreceptor and nearly two orders of magnitude smaller than the smallest receptive fields (Volkmann, 1863; Wülfing, 1892; Westheimer and McKee, 1977; Levi and Klein, 1985). This precision is far higher than the accuracy obtained in standard spatial resolution tasks. Because of its extremely high precision this ability is sometimes called "hyperacuity" (Westheimer, 1975). Visual acuity or the precision with which two stimulus features can be resolved is limited by the precision with which the illumination in the image plane can be determined (Harris, 1964). However, the question probed in hyperacuity tasks is not "Are there one or two features?", but rather "Where is this feature with respect to the other?" (Westheimer, 1976). It has been suggested that this involves the computation and comparison of place tags or local signs for the different stimulus features (Hering, 1899). In this view, the lower limit of accuracy for the retinal local signs is obviously set by the diameter of the retinal photoreceptors. However, it is in principle possible to compute place tags for the mean or centroid of a

collection of simultaneously activated retinal photoreceptors with an accuracy that exceeds the spatial dimensions of the photoreceptors themselves. It has been noted that the stimulus features have to be clearly resolved in order to attain an optimal hyperacuity performance (Westheimer, 1976). The differences in acuity and hyperacuity processing show up clearly in the effects of stimulus blur: hyperacuity thresholds are far less affected by stimulus blur than acuity thresholds (Hartridge, 1923; Stigmar, 1971; Foley-Fisher, 1977; Westheimer, 1979; Enoch and Williams, 1983; Watt and Morgan, 1983; Williams et al., 1984). In summary, it appears that (i) changes in the relative spatial position of stimulus features can be discriminated extremely accurately and (ii) the accuracy with which a location can be attributed to a single stimulus feature depends on its resolvedness.

An impressive feature of the human visual system is its scale-invariance: the perceived shape of a scene does not change with changes in the viewing distance (e.g. Jamar and Koenderink, 1983). If you walk towards a scene it will simply get larger; it does not significantly distort. The absolute size of the retinal image is only important when parts of the scene are too small to be resolved or too large to be seen in a single glance. The notion of scale-invariance has resulted in models in which the retina is depicted as a self-similar detector array, graded with respect to aperture size (Koenderink, 1977; Koenderink and van Doorn, 1978; Hartmann, 1982; Hirsch and Hylton, 1982; 1985; Burton et al., 1986). The principle of scale-invariance has also been successfully applied in many modern (hierarchical) multi-resolution image processing techniques (Tanimoto and Pavlidis, 1975; Burt et al., 1981).

The notion of scale-invariance in the perception of spatial intensity patterns suggests that the visual system may use a single strategy to assign a location tag to stimulus features independent of their spatial scale parameter. However, the accuracy with which such a tag can be computed will depend on the prevailing aperture size of the sampling units in the applied detector array (i.e. on the coarseness of the spatial quantization). Therefore, we expect that the accuracy with which the visual system can determine the relative spatial position of near detection threshold stimulus features will scale with their blur parameter

(i.e. for geometrically similar stimuli). We chose to study the spatial localization ability of the human visual system by means of differential spatial displacement discrimination tasks, as these clearly explore the limits of the accuracy of this capacity.

Summary of Part II.

Chapter II.1 presents the differential spatial displacement discrimination thresholds for a three-blob alignment task as a function of the spatial scale parameter of the stimuli. The results show that the thresholds are a constant fraction of the blur parameter of the blobs for a constant ratio of the blur parameter and the separation of the outer two blobs (i.e. for geometrically similar stimuli at different levels of resolution) and over a range of at least two decades.

Chapter II.2 describes an experiment that was performed to determine the differential spatial displacement discrimination thresholds for a three-blob alignment- and a three-blob bisection-task as a function of both the blur parameter and the spatial separation of the blobs. At all levels of resolution there appear to be two blob-separation regimes in which different strategies are used to compute differential spatial displacements. Independent of the level of resolution, transition between those regimes occurs when the separation of the outer two blobs is a constant multiple (approximately 25) of their blur parameter.

Chapter II.3 deals with an experiment that was devised to test the ability of the human visual system to resolve two points presented at threshold luminance contrast. Discrimination thresholds were determined as a function of the blur parameter of the stimulus pattern. The results show that the discrimination thresholds are a constant fraction of the blur parameter over a range of at least two decades. It is argued that there is no direct need to invoke separate mechanisms mediating spatial separation discrimination for resolved and unresolved stimulus features.

The different processing regimes found in Chapter II.2 may reflect the existence of spatial regions or processing modules mediating differential spatial displacement discrimination. Chapter II.4 describes

an experiment that was performed to test this hypothesis. If these processing modules really exist it seems likely that the simultaneous presence of interfering stimuli within their processing area will have a detrimental effect on their performance on target stimuli. The results show that the mechanisms that compute differential spatial displacements for the three-blob alignment task are not disturbed by the presence of interfering stimuli even when these enter the region over which the computations are performed. It is argued that the so-called crowding effect, found for hyperacuity tasks, is no substantial evidence for the existence of modules specialized in the performance of differential spatial displacement discrimination. Crowding most probably reflects the introduction of a zero-offset by the presence of the interfering stimuli.

Chapter II.5 deals with an experiment designed to manifest the existence of a bright/dark dichotomy in the human visual system. If the mechanisms that signal increment/decrement luminance changes form two separate systems one would expect the differential spatial displacement discrimination accuracy to be higher for tasks that require comparison of the relative spatial position of stimulus features represented within the same system than for tasks that involve the comparison of the spatial position of features represented in different systems. The results show that the differential spatial displacement discrimination thresholds are identical for stimuli with features of equal or opposite contrast polarity. Thus, this experiment provides no evidence in favor of the existence of a bright/dark dichotomy.

Chapter II.6 presents the differential spatial displacement discrimination thresholds for three-Gabor blob alignment- and bisection-tasks. The results of the foregoing chapters demonstrate that the accuracy with which location can be assigned to stimulus features depends on their level of resolution. Therefore, it seems likely that the alignment discrimination thresholds for three Gabor patches, presented at threshold luminance contrast, will depend on their spatial frequency content. However, the results of these experiments show that the three-blob alignment- and bisection-discrimination thresholds are a constant fraction of the spatial scale parameter of the Gaussian envelope of the sinusoidal grating patches and are independent of the spatial frequency of the

modulated grating. Thus, it seems likely that the visual system assigns a single location tag to an entire Gaussian modulated patch of sinusoidal grating.

Chapter II.7 deals with the effects of stimulus resolution and retinal eccentricity on differential spatial displacement discrimination thresholds. For a two-blob separation discrimination task and a three-blob alignment acuity task thresholds were determined as a function of eccentricity along the horizontal meridian of the visual field (from 45° nasal to 65° temporal) with the spatial spread or blur parameter of the blobs as a scale parameter. The results show that the performance of the visual system in differential spatial displacement discrimination tasks becomes progressively more homogeneous for a progressive increase in the blur parameter of the stimuli. Scaling (i) the three-blob alignment results with estimates of the cortical magnification factor and (ii) the two-blob separation discrimination results with their corresponding neural blur parameter shows an impressive isotropy and blur scale-invariance for the mechanisms mediating differential spatial displacement discrimination across the visual field. These results are interpreted in terms of a scaled sampling lattice model of the visual system in combination with an automatic scale-selection mechanism.

Chapter II.8 describes an attempt to identify the nature of the spatial primitives that are involved in the visual coding of spatial location. This was done by performing Vernier acuity, three-line interval bisection and line-width discrimination experiments for a target bar stimulus with an asymmetrical orthoaxial contrast profile. The results of these experiments are compared with the outcome of a numerical simulation model. We conclude that both the zero-crossings and the centroid or extremum of the zero-bounded region of the neural activity distribution that is elicited by the presentation of the target bar are in principle available to perception. It probably depends on the spatial characteristics of the applied stimulus pattern and the adopted strategy which features are actually used in different localization tasks.

References.

Barlow, H.B. (1985) Cerebral cortex as a model builder. In: Models of the visual cortex. Eds. D. Rose and V.G. Dobson. John Wiley and Sons Ltd., New York, London.

Burt, P.J., Hong,Tsai-Hong and Rosenfeld, A. (1981) Segmentation and estimation of image region properties through hierarchical computation. IEEE Tr. Systems, Man and Cybern. SMC-11, 802-825.

Burton, G.J., Haig, N.D. and Moorhead, I.R. (1986) A self-similar stack model for human and machine vision. Biol. Cybern. 53, 397-403.

Carnap, R. (1979) Der logische Aufbau der Welt. Ullstein, Frankfurt.

Descartes, R. (1963) Le traité de l'homme. In: Oeuvres philosophiques (1618-1637), Tome I, ed. F. Alquié, pp. 305-480. Garnier Frères, Paris.

Enoch, J.M. and Williams, R.A. (1983) Development of clinical tests of vision: initial data on two hyperacuity paradigms. Percept. & Psychophys. 33, 314-322.

Foley-Fisher, J.A. (1977) Contrast, edge-gradient, and target line width as a factor in Vernier acuity. Optica Acta 24, 179-186.

Harris, J.L. (1964) Resolving power and decision theory. J. Opt. Soc. Am. 54, 606-611.

Hartmann, G. (1982) Recursive features of circular receptive fields. Biol. Cybern. 43, 199-208.

Hartridge, H. (1923) Visual acuity and the resolving power of the eye. J. Physiol. 57, 52-67.

Hering, E. (1899) Über die Grenzen der Sehschärfe. Ber. Math.-phys. Cl. d. Königl. Sächs. Gesell. Wiss. Leipzig. Naturwiss. Teil 16-24.

Hirsch, J. and Hylton, R. (1982) Limits of spatial-frequency discrimination as evidence of neural interpolation. J. Opt. Soc. Am. 72, 1367-1374.

Hirsch, J. and Hylton, R. (1985) Spatial-frequency discrimination at low frequencies: evidence for position quantization by receptive fields. J. Opt. Soc. Am. A2, 128-135.

Jamar, J.H.T. and Koenderink, J.J. (1983) Sine-wave gratings: scale-invariance and spatial summation at suprathreshold contrast. Vision Res. 23, 805-810.

Jeffry, G. (1985) Retinotopic order appears before ocular separation in developing visual pathways. Nature 313, 575-576.

Koenderink, J.J. (1977) Current models of contrast processing. In: Spatial Contrast, Report of a workshop held in Amsterdam, 1976. Spekreijse, H. and Tweel, L.H. eds. Amsterdam-Oxford-New York: North Holland.

Koenderink, J.J. and Doorn, A.J. van (1978) Visual detection of spatial contrast; influence of location in the visual field, target extent and illuminance level. Biol. Cybern. 30, 157-167.

Koenderink, J.J. and Doorn, A.J. van (1982) Invariant features of contrast detection: an explanation in terms of self-similar detector arrays. J. Opt. Soc. Am. 72, 83-87.

Lotze, H. (1884) Mikrokosmos. Hirzel, Leipzig.

Movshon, J.A. and van Sluyters, R.C. (1981) Visual neural development. Ann. Rev. Psychol. 32, 477-522.

Stigmar, G. (1971) Blurred visual stimuli. II: The effect of blurred visual stimuli on Vernier and stereo acuity. Acta Ophthal. 49, 364-379.

Tanimoto, S. and Pavlidis, T. (1975) A hierarchical data structure for picture processing. Comp. Graph. and Im. Proc. 4, 104-119.

Hering, E. (1899) Über die Grenzen der Sehschärfe. Ber. Math.-phys. Cl.d. Königl. Sächs. Gesell. Wiss. Leipzig. Naturwiss. Teil 16-24.

Watt, R.J. and Morgan, M.J. (1984) Spatial filters and the localization of luminance changes in human vision. Vision Res. 24, 1387-1397.

Watt, R.J., Morgan, M.J. and Ward, R.M. (1983) The use of different cues in Vernier acuity. Vision Res. 23, 991-995.

Westheimer, G. (1975) Visual acuity and hyperacuity. Invest. Ophthal. Visual Sci. 14, 570-572.

Westheimer, G. (1976) Diffraction theory and visual hyperacuity. Am. J. Optom. & Physiol. Optics 53, 362-364.

Westheimer, G. (1979) The spatial sense of the eye. Invest. Ophthal. Vis. Sci. 18, 893-912.

Westheimer, G. (1982) The spatial grain of the perifoveal visual field. Vision Res. 22, 157-162.

Westheimer, G. and McKee, S.P. (1977) Integration regions for visual hyperacuity. Vision Res. 17, 89-93.

Williams, R.A., Enoch, J.M. and Essock, E.A. (1984) The resistence of selected hyperacuity configurations to retinal image degradation. Invest. Ophthalmol. Vis. Sci. 25, 389-399.

CHAPTER I.1.

The construction of a simultaneous functional order in nervous systems.

I. Relevance of signal covariances and signal coincidences in the construction of a functional order.

Abstract.

The anatomical geometrical order of a nervous net exists only for external observers. However, the functional order of a collection of nervous elements is available to the system itself. We have developed two algorithms that construct a simultaneous functional order in a collection of neural elements using purely functional relations. The input of the first algorithm is a matrix describing the total of covariances of signals carried by the members of the neural collection. The second algorithm proceeds from a matrix describing a primitive inclusion relation among the members of the neural collection that can be determined from coincidences in their signal activity. From this information both algorithms compute a partial functional order in the collection of neural elements. Such an order has an objective existence for the system itself and not only for an external observer. By either merging individual neurons or recruiting previously unspecified ones the partial order is locally transformed into a lattice order. Thus, the simultaneous functional order in a nervous net may become isomorphic with a geometrical order if the system has enough internal coherence. Simulation experiments were done, both for the neuron-merging and the neuron-recruitment routines, to study the number of individuals in the resulting lattice order as a function of the number of individuals in the underlying partially ordered set.

1. Introduction.

Electrophysiology has shown that the spatial distribution of the electrochemical activity in the visual cortex is to a large extent isomorphic with the geometry of the visual image. However, the spatial layout of this activity can only have meaning for an external observer. For instance, an external observer can mark neural elements with their spatial coordinates. The neural system itself can only distinguish its elements on account of their activity. Clearly a label or "local sign" (Lotze, 1884) which is encoded in the activity of a single element is of no avail. The system can only compute the simultaneous functional order of a collection of neural elements (i.e. their relative functional position) when the total of their causal connections is encoded in the relations between their simultaneous activities.

Koenderink has recently argued how relative place tags may be assigned to a collection of nervous elements by the constraints imposed on the correlation structure of their simultaneous signal activity (Koenderink, 1984a,c). As these constraints cannot be known to the system a priori they have to be established during a tuning stage. Both the structure of the outside world and the geometrical layout of the detector array will impose restrictions on the possible simultaneous neural activity. Therefore, it seems a priori likely that the resulting functional structure will depend both on the topological structure of the outside world and on that of the sensory modality (Koenderink, 1984b).

There is a growing amount of psychophysical evidence for the fact that the visual system computes relative place tags for stimulus features. The results of differential spatial displacement discrimination tasks have shown that the brain can discriminate changes in the relative spatial position of features in the visual field which are an order of magnitude below the size of a foveal photoreceptor and nearly two orders of magnitude smaller than the smallest receptive fields (Westheimer and McKee, 1977b). This astonishing precision is often attributed to computational processes that assign differential place tags with sub-sample accuracy (Hering, 1899; Westheimer and McKee, 1977a).

There is a rapidly growing body of evidence that the postnatal development of the nervous system is determined by the interaction of the innate genetic program and environmental factors (Imbert and Buisseret, 1975; Blakemore and van Sluyters, 1975; Buisseret and Imbert, 1976; Fregnac and Imbert, 1977, 1978). For instance, developmental functional disorders of vision can be generated by modifying the visual experience of young animals (Blakemore and Cooper, 1970; Cleland et al., 1982; Crewther et al., 1985; von Grunau and Singer, 1980; Ikeda, 1980; Jacobson and Ikeda, 1979; Rauschecker and Singer, 1981).

As it seems, not the connections between specific cells are preprogrammed, only an algorithm is given genetically to select functionally relevant system connections. A global topographic mapping between areas of the nervous system might be preprogrammed (Hubel and Wiesel, 1970, 1974; Jeffery, 1985), whereas activity dependent self organizing mechanisms may be responsible for the precise fine tuning of the mappings.

In this view a neat somatotopical mapping is no prerequisite. It merely economizes on hardware and is computationally efficient. For instance, with sufficient regularity at both the retina and the cortex, the structural development at both sides could initially evolve independently. In a later (tuning) stage functional homology may be achieved. This would only require the optic nerve to maintain nearest neighbour relationships. This is far simpler than requiring each fiber to separately seek appropriate end points, or postulating a cortical mechanism capable of an arbitrarily complicated unscrambling procedure. A logical consequence of this argument is that the cortical mechanisms that process the information from the two dimensional retina should also reflect the two dimensional organization of the photoreceptor lattice. This seems confirmed by recent experiments of Hirsch and Hylton (1984) who reported that the orientation dependence of differential spatial displacement discrimination judgements contains a component with hexagonal symmetry. This suggests that the hexagonal packing of photoreceptors is preserved in the functional cortical representation of their relative spatial position.

Modifications in the functional behaviour of the nervous system may correspond to a combination of

(i) A structural change due to the alteration of synaptic connections (Innocenti, 1981; Rakic and Riley, 1983; Price and Blakemore, 1985).

(ii) The modification of synaptic strength (efficacy) of the individual synapses of the principally fixed network. This could be caused by increasing the strength of response over synaptic connections that are frequently used, thereby causing a relative weakening of unused connections (e.g. Hebb, 1949; Erdi and Barna, 1984).

(iii) Cell death, which appears to contribute to the specification of a cortical neuron's functional identity (Finlay and Slatterly, 1983).

(iv) The recruitment of newly generated neurons into functional circuits. There is evidence that this process can occur in a vertebrate brain well after it has achieved its full adult size (Paton and Nottebohm, 1984).

In this paper we present two algorithms, that construct a simultaneous functional order in a collection of neural elements. The algorithms proceed from purely functional relations (a cross-correlation- or coincidence-relation structure) which are objectively available to the neural system. For instance, in case of the optic nerve, signal correlations or coincidences may be induced by the overlap of dendritic trees of ganglion cells. Thus, the spatial coordinates of the ganglion cells in the retina are irrelevant; what counts is their overlap structure.

In our models we assume that the neural system has enough plasticity to retract existing or grow new neural interconnections (synapses) in the process of establishing a simultaneous functional order. In one case we even assume that the system is capable of recruiting new neurons into a functional circuit. With regard to the forementioned neurophysiological data we feel that these assumptions are not unnatural or far fetched.

2. The construction of a partial functional order.

2.1. Using signal covariances to construct a partial functional order.

Consider an ensemble of neural elements $E = \{\alpha, \beta, \gamma, \ldots\}$. We assume that the geometrical (spatial) order of the elements is unknown and that there exists no further inherent order in the ensemble. If we think of the retina, the elements of the ensemble correspond to the retinal ganglion cells that transmit the signals from the retinal detectors (receptive fields) to the visual cortex. We now want to establish a simultaneous order in this collection using only the functional relations that exist between its constituent elements. An obvious approach is to use the covariances of the signals carried by the individuals of E. The required hardware consists of a matrix or "association network" of multipliers and time averagers to monitor signal correlations over time. The output of this network is a subset D of $E \times E$, defined in such a way that, for two elements $\alpha, \beta \in E$, $(\alpha,\beta) \in D$ iff (if and only if) the covariances of the signals carried by α and β exceeds some given level. Clearly, if $(\alpha,\beta) \in D$ then you must have $(\beta,\alpha) \in D$. Moreover, for any $\alpha \in E$ you have that $(\alpha,\alpha) \in D$. Thus D is reflexive and symmetrical. The set (E,D) represents the objective functional correlation structure that can be established in the ensemble E over a certain temporal interval. D clearly depends on the history of the observed inputs (learning process) and may slowly change over time.

In this study we are only interested in those correlations in the signals carried by the neural elements that arise due to the structure of the detector network (i.e. have functional relevance). In case of retinal ganglion cells we think of correlations in their signal activity that are induced by the geometrical overlap of their corresponding receptive fields. However, the signals of the neural elements may also be correlated due to their accidental simultaneous activation. Therefore, we require that the system makes a distinction between correlations occuring due to accidental coincidences and those that have functional relevance. This discrimination will generally not be absolutely correct, as the frequency of the accidental simultaneous activations will depend on the signal to

noise ratio of the applied stimuli. A simple discrimination power can be implemented by introducing a detection threshold for the covariances of the signals carried by the neural elements.

For stimuli with low feature density, neural elements that correspond to detectors with large aperture sizes and no causal connections will be more frequently activated simultaneously than unrelated elements corresponding with detectors with small aperture sizes. This is due to the fact that detectors with large aperture sizes will be simultaneously activated by many different stimulus configurations with low feature density, whereas detectors with small aperture sizes will only be simultaneously activated by a small number of different stimuli. Therefore we expect that the covariance-detection threshold will depend on the relative aperture size of the detectors corresponding to the neural elements.

The number of different stimulus patterns that simultaneously activate a number of small sized detector units that have no causal interconnections will increase with increasing feature density. In order to discriminate these accidental correlations from functional relevant ones the system has to raise its correlation detection threshold in this case. Thus, the correlation detection threshold also has to be a function of the feature density in a stimulus pattern.

If the activation threshold is the same for all neural elements (absolute threshold) and independent of the feature density in the stimulus pattern, neurons corresponding to detectors with large aperture sizes will be activated more frequently than those corresponding to detectors with small aperture sizes. This is a result of the fact that detectors with large aperture sizes cover a larger part of the stimulus pattern and have therefore a bigger chance of detecting stimulus features. In this case the activation frequency of a neural element is a measure for the aperture size of its corresponding detector unit. If the activation threshold of a neural element is a function of the feature density or the aperture size of its corresponding detector unit (relative threshold) there is no obvious mechanism for the system to obtain information about this aperture size.

We did not want to make any assumptions about the mechanisms a neural network might use to tune its **covariance-detection** thresholds. In our model the covariances between the signals carried by the neural elements are therefore directly computed from the geometrical overlap of their corresponding detector units. Whenever the ratio of the geometrical overlap of two detectors and the square root of the product of their aperture sizes was above some predetermined threshold value T_v it was assumed that the signals carried by their corresponding neural elements were correlated;

$(\alpha,\beta) \in E : D(\alpha,\beta) = D(\beta,\alpha) = 1$ iff

$$Cov(\alpha,\beta) = \frac{\text{area } (\alpha \cap \beta)}{\sqrt{\text{area } (\alpha).\text{area } (\beta)}} \geq T_v$$

were T_v denotes the covariance detection threshold. We thereby explicitly introduce an external observer. However, this external observer may at any time be traded for a mechanism that allows the system to tune its covariance-detection thresholds. Therefore, at this stage, the introduction of knowledge about the spatial order of the physiological substrate is no serious restriction to our model.

We will proceed to show how the set (E,D) can be given a **partial order** (Grätzer, 1978). Thus, we have to transform the reflexive and symmetrical relation D between the elements of E into a reflexive, antisymmetrical and transitive relation between subsets of elements of E.

First a binary relation Q, subset of $E \times E$, is defined so that if $\alpha, \beta \in E$ then $(\alpha,\beta) \in Q$ iff (if and only if) for any $\gamma \in E$ such that $(\alpha,\gamma) \in D$ it is also the case that $(\gamma,\beta) \in D$. Therefore Q is a transitive subset of D. The reflexivity of D is transmitted to Q. However, the symmetry of D is not transmitted to Q. Q is neither symmetric nor antisymmetric. Only pairs of elements of E which both have the same D-relation with all other elements of E will also have a symmetrical Q-relation. The relation Q removes pairs of elements from the set (E,D) for which no functional order relation exists.

Antisymmetry can then be obtained by forming subsets of E, called "blocks", so that all elements of a block have a symmetrical Q-relation with all other elements of the same block. This implies that all elements of E that have a symmetrical Q-relation with one of the elements of a block (and because of the transitivity of Q with all other elements of

that block) are incorporated in that block. This means that we lump all elements of E that have the same D-relation with all other elements of E and that are therefore functionally equivalent. Different blocks can only have empty intersections. An element in the intersection of two different blocks would be functionally equivalent to all elements of both blocks, thereby causing all elements of one block to be functionally equivalent to all other elements of the other block. But the blocks are by definition functionally different, therefore their intersection has to be empty.

Let I be the set of blocks. We define a relation R, subset of $I \times I$, between blocks as follows: if a, b $\in$ I then (a,b) $\in$ R iff $(\alpha,\beta) \in Q$ for some (and thus for all) $\alpha \in a$, $\beta \in b$. Because of the construction of the blocks, the relation R is antisymmetric ((a,b) $\in$ R and (b,a) $\in$ R implies the equality of a and b). The relation R is reflexive, antisymmetric and transitive, and therefore defines a partial order on the set I.

This completes the description of the algorithm that transforms an unordered set of elements E, with a given covariance relation D, into a set of individuals I, with a partial order relation R. As all blocks are functionally different the set I will be regarded as a set of individuals in the sequel.

2.2. Using signal coincidences to construct a partial functional order.

Consider again an ensemble of neural elements $E = \{\alpha, \beta, \gamma, \ldots\}$. Assume that the neural system has no knowledge of the geometrical order (spatial lay-out) of the elements of E and that there exists no further inherent order in the ensemble. A (simultaneous) functional inclusion order can be established in this collection using coincidences in the signal activity of the individuals of E. The required hardware is a binary matrix Q' or "association network", consisting of logical (bistable) memory elements. For two neural elements $\alpha, \beta \in E$ we will write $Q'_{\alpha,\beta} = 1$ (0) iff α is (not) functionally included in β. Initially $Q'_{\alpha,\beta} = Q'_{\beta,\alpha} = 1$ for all $\alpha, \beta \in E$. This fact represents the assumption that the neural system has no a priori knowledge of the functional order of the neural elements. Thus, in the initial state of the system each element may be

functionally included in any other element. During a learning stage an inclusion relation is falsified (i.e. the corresponding matrix element is set to zero) once a neural element is activated without a simultaneous activation of the element in which it is supposed to be included. The learning stage may be ended when no inclusion relations have been falsified during a prescribed number of stimulus presentations. Thereafter Q' is explicitly made anti-symmetrical by resetting all symmetrical elements of Q' to zero. Note that no relevant information is lost as symmetrical Q'-relations present no information about the relative functional position the members of the symmetrical pairs have with respect to eachother. There is no need for two symmetrical elements to be functionally equivalent. Moreover, when they are functionally equivalent they may represent detector units that are geometrically separated and which have not had a chance to establish their separate identity (e.g. because they were always simultaneously stimulated, or because they were never stimulated at all). In this case, the resulting functional order will give an incorrect representation of the geometrical order of the detector array when the two functional equivalent elements are merged into one functional individual. The annihilation of symmetrical Q'-relations seems therefore the most sensible way to proceed. Thus, the final output of the association network is a subset Q' of $E \times E$, defined in such a way that, for any two elements $\alpha, \beta \in E$, $Q'_{\alpha,\beta} = 1$ or, equivalently, $(\alpha,\beta) \in Q'$ iff the activation of α implies the activation of β (i.e. the situation in which α is activated and β is not activated has never occurred during the learning stage). The set (E,Q') represents the objective functional inclusion structure that can be established in the ensemble E during some time span (learning stage). Thus, Q' depends on the history of the observed inputs and may be refined over time. Due to the activation thresholds of the neural elements, geometrical inclusion relations between detectors of different aperture sizes need not be reflected in the (pairwise established) functional inclusion relation Q' (in Part II we will present some examples). As a result Q' is generally not transitive. Therefore, we will call this inclusion relation a "primitive" one.

During the learning stage the neural system is presented with a large number of randomly structured binary stimulus patterns. These stimuli have

the same spatial extent as the detector array. The resolution of the neural system is determined by the neurons corresponding to the detectors with the smallest aperture size. As a result, a large number of stimulus configurations which differ only in the small scale arrangement of segments that are smaller than the smallest aperture size may give rise to the same output of the detector array. Therefore, the speed of the learning process will increase if the smallest segments of a stimulus pattern are not much smaller than the detectors with the smallest aperture size. However, situations in which most neurons are activated (due to the presentation of binary stimulus patterns that are almost everywhere non-zero), provide little or no information about the functional order among these neural elements. We wanted to speed up the learning process by decreasing the number of different stimuli needed in the learning stage while still providing stimulus patterns with sufficient information content (i.e. enough inherent structure) to allow the system to find out its physical constraints (to decode its own physical structure). To fulfill the first condition we used stimulus patterns which were composed of segments with an area that was 0.5 times the area of the detectors with the smallest aperture size. (The choice of the ratio 0.5 was based on the results of some simulation experiments and is rather arbitrary. In fact, any ratio between 0.5 and 1.0 would serve our purpose.) We satisfied the second condition by introducing an upper limit for the number of segments of the stimulus pattern that have a non-zero value. This limit was chosen such that 25% of the area of a stimulus pattern was covered with non-zero valued segments. Note that this upper limit for the number of non-zero valued segments is merely imposed to quicken the learning process in our simulation experiments and does not reflect any physical constraints of the neural system itself.

In a companion paper (Part III) we will report an extensive series of simulation experiments that were done to study the dependence of the resulting functional order in a neural network on different values of the system parameters (e.g. the geometrical properties of the underlying collection of neural detectors and different values of their activation thresholds). These kind of studies may provide insight into the way a neural system might encode its physical constraints in its simultaneous

functional order. We extended our algorithm with the option to skip the learning stage and compute the primitive functional inclusion relation Q' of the neural elements directly from the geometrical overlap of their corresponding detector units. This was done to rule out external ("environmental") influences and to enable a comparison of the influence of the system parameters on the functional orders produced by respectively the coincidence- and the covariance-model. (An additional advantage is that this option is computationally slightly more efficient than the simulation of a learning stage in which the system has to analyse a large number of randomly generated binary stimulus patterns.) The coincidence detection threshold we adopted is equivalent to the correlation detection threshold as defined in section 2.1. We assume that there is a **coincidence relation** (and therefore, there may exist a primitive functional inclusion relation) between any two neural elements for which the ratio of the geometrical overlap of their corresponding detector units and the square root of the product of their aperture sizes was above some predetermined threshold value T_i. (Note that this definition of the coincidence detection threshold is equivalent to the definition of the covariance detection threshold T_v in section 2.1). Two neural elements can only have a primitive (antisymmetrical) inclusion relation when they are distinguishable by their signal activity. The functional identity of the neural elements reflects both the spatial lay-out and the geometrical properties of their corresponding detector units. Therefore, we checked the geometrical overlap structure of pairs of detector units corresponding to pairs of neural elements for which a coincidence relation could be established (on the basis of the forementioned geometrical considerations). As noted before, the neural system can only distinguish its elements by their signal activity. We will now present a geometrical analogue for the notion of functional distinctness. Let $\alpha, \beta \in E$ be two neural elements that have a coincidence relation and that correspond to detector units with an area A_α and A_β respectively. The overlap area of both detector units will be denoted by $A_{\alpha \, n \, \beta}$. We now define α and β as **functionally distinct**, when

(i) $A_\alpha - A_{\alpha \, n \, \beta} < A_t$ and $A_\beta - A_{\alpha \, n \, \beta} > A_t$ or (ii) $A_\alpha - A_{\alpha \, n \, \beta} > A_t$ and $A_\beta - A_{\alpha \, n \, \beta} < A_t$, where A_t represents a certain threshold area. If one of

these conditions is satisfied we assume that there exists a **functional inclusion relation** between α and β. If (i) holds, we say that α is functionally included in β, for (ii) we have that β is included in α. (Note that the external observer we have introduced here may at any time be traded for the forementioned learning process.)

The relation Q' (either established during a learning process or resulting from geometrical calculations) is antisymmetric. It is explicitly made reflexive by postulating that each neural element is functionally included in itself (which is merely a formal requirement). As we noted before, this primitive inclusion relation is generally not transitive, due to the existence of the coincidence detection threshold. A partial order relation Q" can be obtained by constructing a transitive extension of Q' as follows. We define Q": $(\alpha,\beta) \in Q''$ iff there exists an ordered set $\{\pi_1, \ldots, \pi_k\}$ with $\pi_i \in E$ $(i = 1,\ldots, k)$ such that $\alpha = \pi_1$, $\beta = \pi_k$, and $(\pi_i, \pi_{i+1}) \in Q'$ for $i = 1,\ldots, k-1$. Then you have (trivially) that $(\alpha,\beta) \in Q''$ and $(\beta,\gamma) \in Q''$ imply $(\alpha,\gamma) \in Q''$. Thus, Q" is a transitive extension of Q'.

Because Q" is reflexive, antisymmetric and transitive it defines a partial order. However, because of its construction, it may occur that two neural elements that are incomparable have identical Q"-relations with all other neural elements. As these elements are therefore functionally indistinguishable it is obviously of no avail to maintain their separate status. Therefore, our algorithm lumps these "functionally equivalent" elements in so-called "blocks". We will write $Q''_{\alpha,\beta} = 1$ iff $(\alpha,\beta) \in Q''$, and $Q''_{\alpha,\beta} = 0$ iff $(\alpha,\beta) \notin Q''$. A block is a subset of E with the following properties: a is a block iff $a \neq 0$ and for $\alpha, \beta \in a$ and any $\gamma \in E/\{\alpha,\beta\}$ we have that $Q''_{\alpha,\gamma} = Q''_{\beta,\gamma}$ and $Q''_{\gamma,\alpha} = Q''_{\gamma,\beta}$. As an example, Figure 1a shows the geometrical lay-out of the detector array corresponding to a neural system with two functionally equivalent, incomparable, neural elements (ζ,η; Fig. 1b). Figure 1c shows how these two functionally equivalent elements may be lumped in a block structure.

Let I' be the set of blocks. We define a relation R', subset of $I' \times I'$, between blocks as follows: if $a, b \in I'$ then $(a,b) \in R'$ iff $(\alpha,\beta) \in Q''$ for some (and thus for all) $\alpha \in a$, $\beta \in b$. The partial order defined by Q" is transmitted to the relation R'. Thus, we have presented

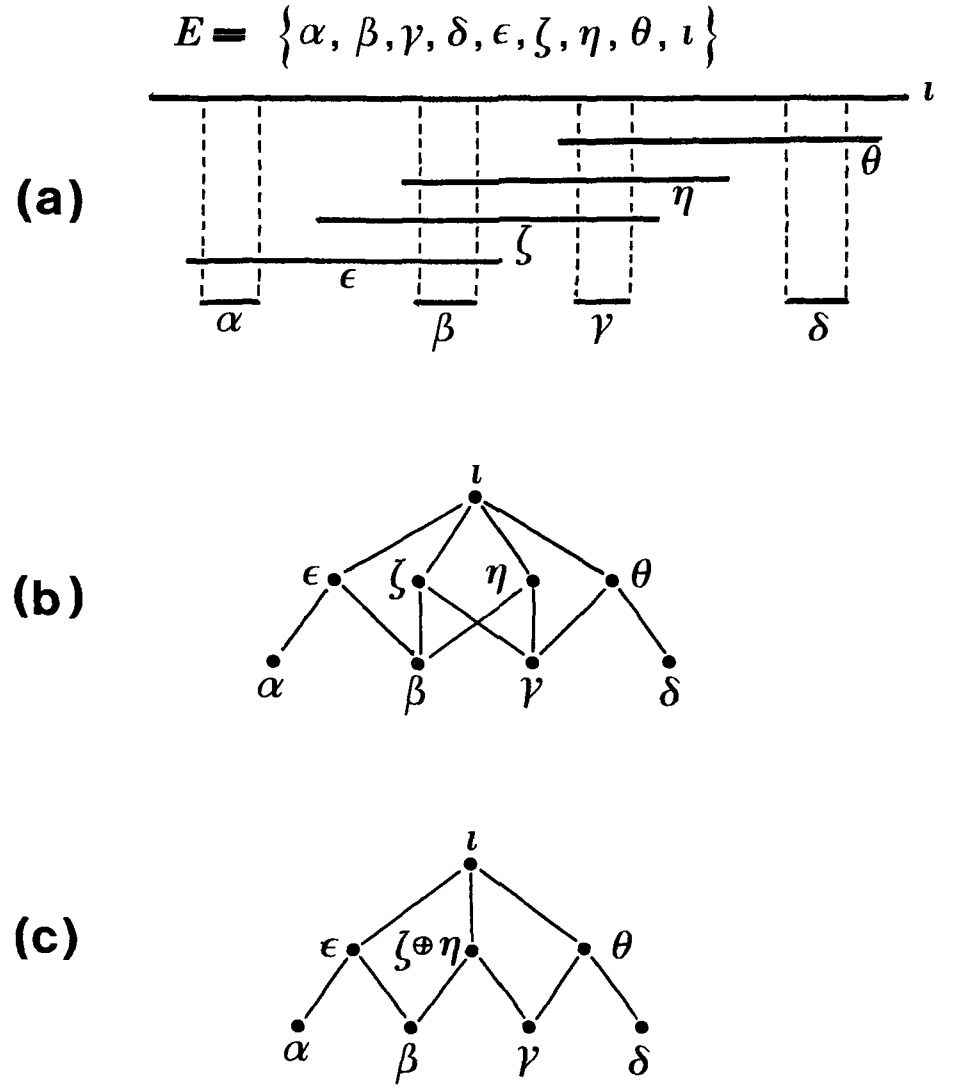

Figure 1. An example of the forming of blocks of functionally equivalent elements in the coincidence-model. **a.** The geometrical lay-out of the detector distribution corresponding with a set of neural elements E. Each detector unit is labelled with its corresponding neural element. **b.** The Hasse-diagram of the coincidence relation of individuals of E. **c.** The Hasse-diagram that results when ζ and η are lumped in a block.

an algorithm that transforms an unordered set of elements E with a given coincidence relation Q' into a partially ordered set I'. As all blocks of the set I' are functionally different the set I' will be regarded as the set of individuals in the sequel.

3. Some special individuals and subsets of I: definitions and terminology.

In section 2 we showed how an unordered set of elements E can be transformed into a partially ordered set. The individuals of this partially ordered set are blocks of elements of E which are functionally equivalent because they have either the same covariance relation D (I), or the same extended coincidence relation Q" (I') with all other elements of E. In the sequel we will define some special individuals and subsets of the resulting partially ordered set. As these definitions apply to partial order relations in general we will restrict our definitions to the partial order relation (I,R), i.e. to the unprimed case. The results can simply be applied to the set (I', R') by substituting the primed symbols for the unprimed ones.

The binary relation R defines the partially ordered set or "poset" {I,R}, subset of $I \times I$. The elements of this poset are ordered pairs {a,b}, with $a,b \in I$ and a and b related by R, denoted as aRb. As the relation R defines the poset and as this set in turn determines the relation R, we may regard the relation R identical with this set. The binary relation R is usually denoted by $\leq$. Therefore, we can write $a \leq b$ when the ordered pair (a,b) is a member of R. Also, $a \leq b$ (pronounced as "a precedes b") will mean $b \geq a$ (pronounced as "b dominates a"). Two elements $a,b \in I$ are called **comparable** if $a \leq b$ or $b \leq a$. Otherwise, a and b are incomparable.

If R is linear (i.e. $a \leq b$ or $b \leq a$ for all $a,b \in I$; any two elements are comparable) then I is fully or linearly ordered. Such sets are often called **chains**. When we think in terms of receptive fields, a set of mutually nested receptive fields covering some smallest one could lead to a chain. If any pair of individuals is incomparable then I is unordered.

A poset {I,R} is often represented by its "Hasse diagram" (Grätzer, 1978). In such a diagram each individual is represented with a node. If (a,b) $\in$ R and b is the smallest element of I for which b $\geq$ a is valid (i.e. if b $\leq$ c then a $\leq$ c) then the node representing b is drawn above the node representing a and both nodes are connected with a straight line. In our computer model the relation {I,R} exists in the form of a two-dimensional binary array.

When studying the Hasse diagram of the poset {I,R} we immediately notice two singular types of individuals: **minimal elements** for which there are no elements that strictly precede them and **maximal elements** that are not strictly dominated by any other elements. For example, in Fig. 5a there are 6 minimal elements (a to f) and 3 maximal elements (m,n,o).

Let J be a subset of I with a partial order that is naturally induced by the binary relation R. Then {J, $\leq$ } is a subposet of {I, $\leq$ }. An element a in I that precedes every element in J is called a **lower bound** of J. Similarly, an element b in I that dominates every other element in J is called an **upper bound** of J. We are only interested in the extremal elements of the sets of lower and upper bounds. In the sequel these will be denoted respectively by **minub (min**imal **u**pper **b**ound) and **maxlob (max**imum **l**ower **b**ound). If J has more than one maximal or minimal elements the minub or maxlob need not exist. Therefore, J may have any number (less than, or equal to, the total number of elements in I) of minubs and maxlobs, including zero. If an upper bound of J precedes every other upper bound of J (i.e. if J has an unique minub) then it is called the least upper bound or **supremum** (sup) of J. If a lower bound of J dominates every other lower bound of J (i.e. if J has an unique maxlob) then it is called the greatest lower bound or **infimum** (inf) of J. By their definition, the infimum and supremum are unique.

Note that it is not necessary that the infimum and supremum exist for each pair of elements of I. Consider for example the poset of Fig. 5a. In this example sup{m,n} is the smallest receptive field containing both m and n (which does not exist) and inf{m,n} is the largest receptive field contained in both m and n (in this case k). For a set I representing neural elements it is clear that there is no reason to expect the existence of a supremum or infimum for each pair of individuals. Pairs of

individuals that have no supremum may be called "functionally remote"; those that have no infimum "functionally disjunct".

We will now present definitions of some entities that will be frequently used in the sequel. The **inclusion** a_* of an individual a is the subset of all individuals of I that precede a. The **exclusion** a^* of an individual a is the subset of all individuals of I that dominate a. If $a < b$ then a_* is a subset of b_* and b^* is a subset of a^*. Thus, the partial order of $\{I, <\}$ is transmitted to I_* and I^*.

The inclusion of a maximal element will be called a **district.** A district is a subset of I. The minimal elements of a district will be called the **atoms** of that district. Elements in different districts are functionally remote (have no common upper bound). The set of individuals I is the union of its districts. Subsets corresponding to disjunct subdiagrams in the Hasse diagram of the set $\{I, <\}$ will be called **modalities.** For example, the poset represented in the Hasse diagram in Fig. 5c consists of two modalities. There is no functional order among modalities. A functional order among districts within a modality can be established by using their intersections. Let $D_1, \ldots, D_k$ be the districts of I; i.e. $I = D_1 \cup D_2 \cup \ldots \cup D_k$. Then for any D_i, D_j there is a sequence $D_{\mu_1}, \ldots, D_{\mu_1}$ so that $D_{\mu_1} = D_i$, $D_{\mu_1} = D_j$, $D_{\mu_p} \cap D_{\mu_{p+1}} \neq 0$ for $p = 1, \ldots, l-1$. If $D_{\mu_p} \cap D_{\mu_{p+q}}$ exists for any q between 2 and l-p, then $D_{\mu_p} \cap D_{\mu_{p+1}} > D_{\mu_p} \cap D_{\mu_{p+q}}$.

A **region** in a set $\{I,R\}$ is defined as the intersection or sum of any number of regions and the inclusion of an individual is also a region. Note that the atoms of a district form the smallest possible regions. A region is called **connected** if for any two individuals a and b belonging to the region there exists a sequence $p_1, \ldots, p_k$, such that $a = p_1$, $b = p_k$, and $(p_i, p_{i+1}) \in \{I,R\}$ for $i=1,\ldots, k-1$.

We define the **hull** of a subset J of I, denoted as [J], as the intersection of the inclusions of all minubs of J: $[J] = \{\{\text{minubs}\{J\}\}_*\}_n$. This is again a subset of I. If J has only one minub the hull of J equals the inclusion of this minub (i.e. the inclusion of an individual of I). If J has more than one minub the intersection of the inclusion of those minubs defines a subset of I that is not equal to the inclusion of an element of I. Therefore, the set H of all hulls generated by the poset

$\{I,<\}$ consists of all elements of I_*, augmented by the hulls of those subsets of I that have more than one minub. As an example consider Figure 5a. This Figure shows the Hasse diagram of a poset consisting of three districts and generated by a one-dimensional detector array. All possible hulls of this poset are:

$a_*, \ldots, o_*$

$[b,c] = \{\{i,j\}_*\}_n = \{b,c\}$

$[d,e] = \{\{j,k,l\}_*\}_n = \{d,e\}$

$[c,e] = \{\{j,k\}_*\}_n = \{c,d,e\}$

$[d,h] = \{\{l,n\}_*\}_n = \{d,e,h\}$

$[h,k] = \{\{n,o\}_*\}_n = \{c,d,e,h,k\}$

These are all different hulls generated by the poset from Fig. 5a. All other hulls are either equal to one of the forementioned hulls or *do not* exist. For instance:

$[a,b,c] = [a,c] = [a,g] = [c,g] = [i]$

$[k,l] = [o]$

$[f,j]$ does not exist

$[c,d] = [c,d,e] = [c,e]$

4. The construction of districts with a lattice order.

A **lattice** is a poset $\{L, \leq\}$ for which $\sup\{a,b\}$ and $\inf\{a,b\}$ exist for all $a,b \in L$. Under certain constraints a lattice may become isomorphic with a geometry (Blumenthal and Menger, 1970). Then it becomes possible to define functional equivalents for geometrical notions as the neighbourhood, proximity, distance and the spatial order of individuals.

A partial order can be transformed into a lattice order, either by merging existing functional individuals, or by creating new ones. We implicitly assume the existence of an infimum of the poset $\{I,<\}$. This is no serious restriction as the empty subset can always be adopted as an infimum. Each district has a supremum. Thus, it is in principle possible that the functional order in a nervous net is (at least at a local scale or within districts) isomorphic with the abstract geometry of the physiological substrate.

4.1. Neuron merging.

In Figs. 2 and 3 we give examples of the transformation of a partially ordered set $\{I, \leq\}$ into a lattice order L by the process of merging individuals of a poset I. Two elements a and b of the partially ordered set I are merged into one element, which we will denote as a•b, if they have more than one minub. This new element a•b (which is an individual of L) has of course only itself as a minub. a•b dominates any element that is dominated either by a or by b. a•b precedes those elements that are preceded by both a and b. Note that, in case of neural elements, the underlying detectors remain unmodified (they still form geometrical distinct entities), only their corresponding neurons are merged.

In Fig. 2 we demonstrate that the result of the merging process depends on the order in which the elements are merged. When a and b are merged first we get a poset that differs from the result we get when we first merge b and c.

In general, a poset will have less structure when some of its elements have been merged. A **chain** is a subset for which all elements are comparable. We define the **order** of an element of a poset as the number of elements in the largest chain of which this element is a maximal element. The loss of structure depends on the order of the elements that are to be merged. Fig. 3a shows the Hasse diagram of a poset. The elements d and e have two minubs, namely f and g of order 3. Fig. 3b shows the Hasse diagram of the poset that results after merging the elements d and e. We could also decide to merge the elements a and c of order 1, as these have the same two minubs f and g. However, after merging a and c, d and e still have the same two minubs f and g. Therefore, d and e still have to be merged, together with a•c, in order to obtain a lattice relation. The result of merging a and c followed by merging a•c, d and e is shown in Fig. 3c. When we start with merging a and c we end up with a poset that has less structure than the poset we get when we start with merging d and e. In general, more coherence will be preserved when the merging process starts with elements of high order than when it starts with elements of low order.

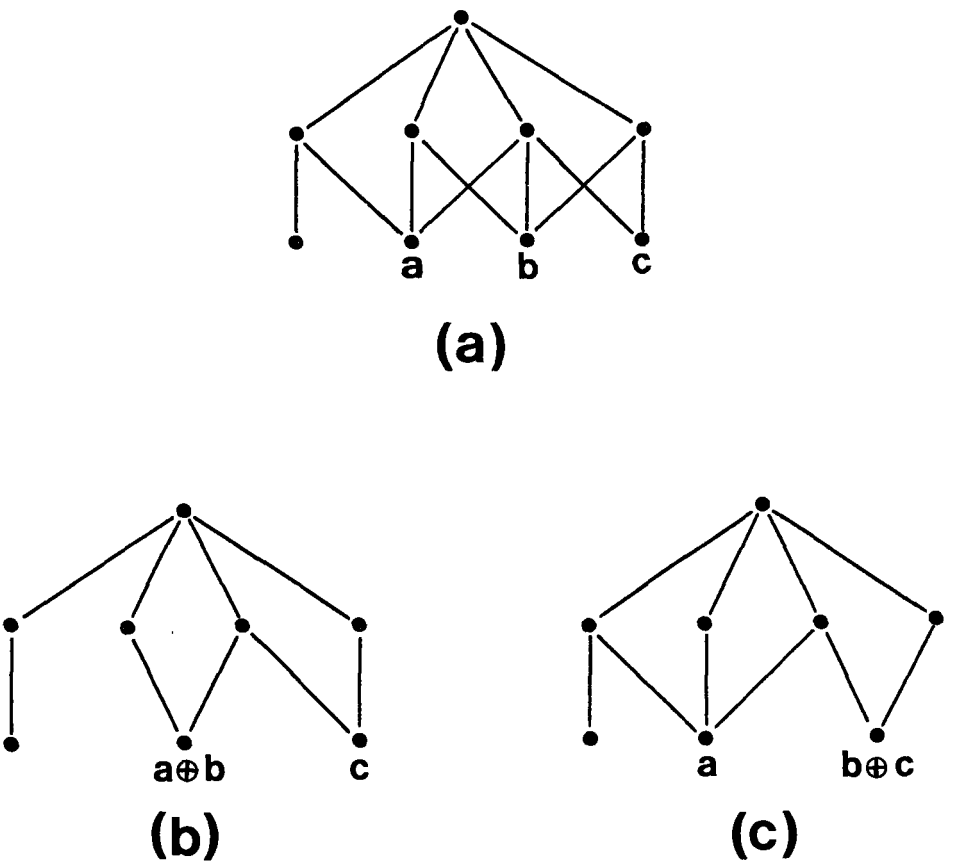

Figure 2. a. The Hasse-diagram for a partially ordered set of individuals. b. The Hasse-diagram that results when a and b are merged. c. The Hasse-diagram that results when b and c are merged.

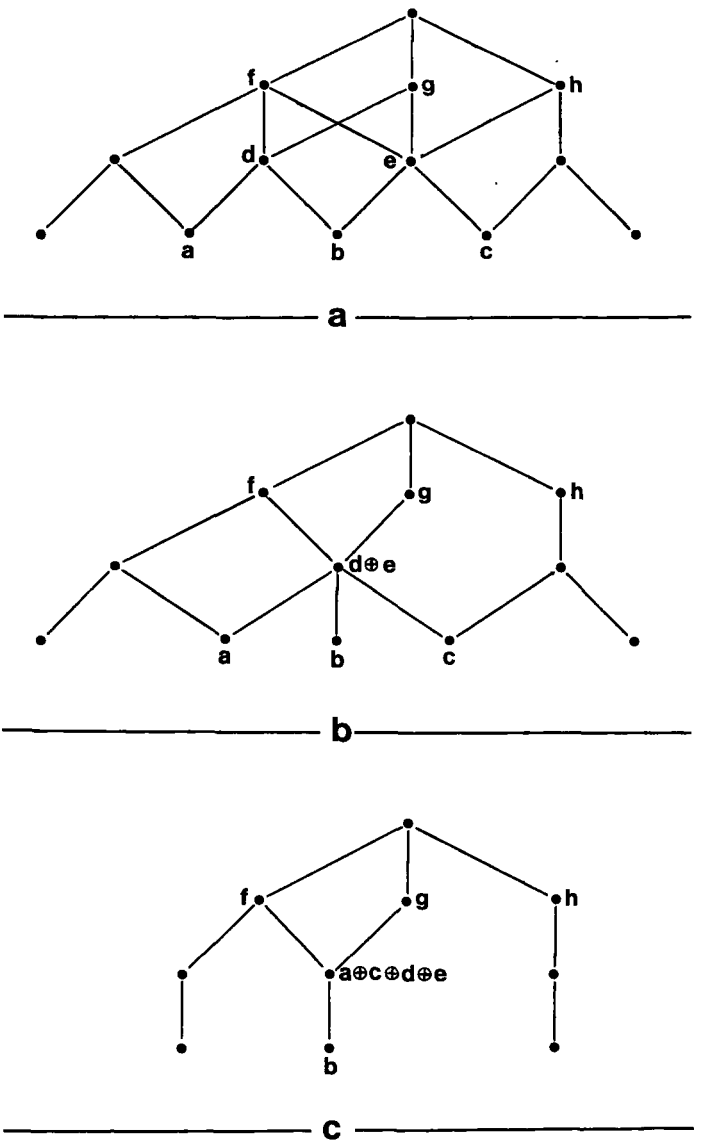

Figure 3. a. The Hasse-diagram for a partially ordered set of individuals. **b.** The Hasse-diagram that results when d and e are merged first. **c.** The Hasse-diagram that results when a and c are merged first.

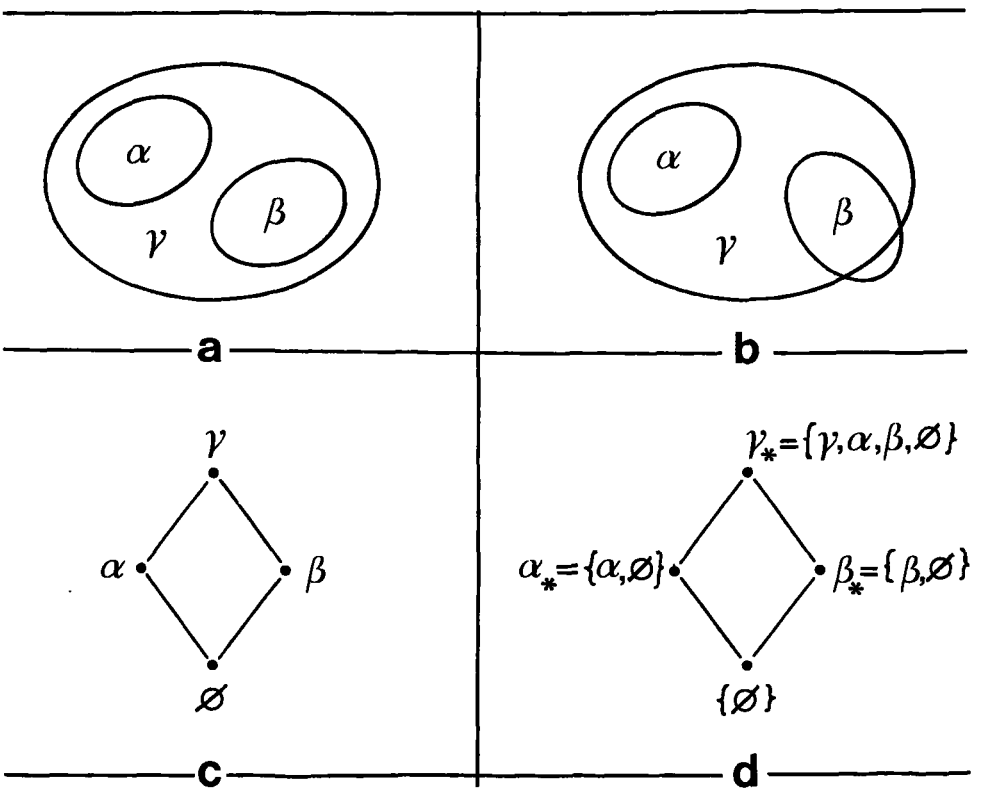

Figure 4. The two geometrical situations **a** and **b** may (depending on the value of the detection thresholds) give rise to the same functional lattice order **c**. **d.** The lattice order describing the set of inclusions of the neural elements is a correct functional representation of both geometrical situations **a** and **b.**

On implementing the merging process we chose for a procedure that preserved as much coherence in the poset as possible. Our algorithm checks for pairs of elements {i,j} if they have to be merged. We start checking for elements of the lowest order and thereafter increase the order. For an element i it is checked for all elements j (starting with those of the lowest order), residing in different chains (i.e. for all elements j that are not comparable to i), but within the same district, if the pair {i,j} has more than one minub. If this condition is satisfied we test whether the subset {i,j} is a subset of the set of maxlobs of the set of minubs of {i,j}. If this is the case, the elements i and j may be merged. The latter condition guarantees that the elements that are picked from the collection of elements that are available for merging will be those which have highest order.

Note that the lattice order L thus obtained need not be a correct representation of the geometrical inclusion relations of the underlying detector units. Figures 4a and 4b show two geometrical situations that give rise to the same lattice order (shown in Fig. 4c). This lattice order is a correct representation of the geometrical inclusion situation as depicted in Figure 4a. In case of the situation as represented in Figure 4b a stimulus presented to the part of the corresponding detector unit of β that extends outside that of γ may activate β but not γ, although β is functionally included in γ. To prevent error situations like this, we will use the fact that there are natural isomorphisms of a lattice order L on the set of inclusions of all elements of L. The set L_* can be naturally ordered under set inclusion. If $a < b$ $(a,b \in L)$ then $a_* \subseteq b_*$. L_* is a lattice with its order inherited from $\{L, < \}$. Because L is a lattice L_* is equal to the set H of all hulls generated by L (both L_* and H ordered under set inclusion). In our simulation model the signal activity of the hull of an individual is represented as the binary sum of the signal activities of its elements. Thus, an individual of H will always be activated when there is at least one activated individual that precedes it (or, equivalently, when one of its constituting elements is activated).

The merging process and the construction of the hulls have no priviliged temporal order. In our algorithm the order was such that merging precedes the construction of hulls. This order was merely chosen

because it is computationally efficient.

4.2. Neuron recruitment.

In this section we will present an algorithm that transforms the districts of a partially ordered set $\{I, \leq\}$ into lattice orders by augmenting the set I_* with the hulls of those subsets of I that have more than one minub. In the sequel we will call this augmentation process "neuron recruitment". The set H, thus obtained, is the set of all hulls generated by the poset $\{I, \leq\}$. In somatotopical terms, the hull of a set of neural elements defines the smallest connected region containing their corresponding receptive fields. It will be shown that the districts of H (ordered under set inclusion) have a lattice structure.

The algorithm starts with the construction of the subset I_* of H. As we already mentioned, there are natural isomorphisms of I on the set I_*. I_* ordered under set inclusion is a poset with its partial order inherited from $\{I, \leq\}$. Thereafter the algorithm checks for all subsets of I whether there are more than one minubs. If a subset has only one minub, the hull of this subset is already a member of H (as this hull equals the inclusion of the forementioned minub, which is an individual of I_*). In case there are more than one minubs, the hull of the subset is obtained by determining the intersection of the inclusion of all minubs. H is then augmented with this hull. Thus we obtain the set H of all hulls generated by the poset of individuals $\{I, \leq\}$. In general, repeated application of the hull addition or "neuron recruitment" process transforms the districts of I_* into (districts of H that are) semi-modular lattice orders (or pre-geometries; see Crapo and Rota, 1970).

Note that the complexity of the elements of H increases after repeated application of the neuron recruitment process. At first the hulls are subsets of I. After a second application they are sets of subsets of I. (In Part II we will define an abstract dimension of a poset. It will appear that only one application of the hull addition process is sufficient to transform the districts of a poset with a one-dimensional character into lattice orders. For posets with a higher dimensional

character the neural recruitment process may have to be applied more than once. The reason for this becomes clear when we relate the hulls to abstract geometrical structures, as we will do in Part II. In the sequel we will only consider posets with a one-dimensional character.)

Repeated application of the neural recruitment process will always result in the construction of districts with a lattice order. This is due to the fact that the hulls which are generated by pairs of elements of H that initially have more than one minub precede the inclusions of these minubs either directly or via chains.

An example of the tranformation of a poset into a lattice order, both by means of the neuron recruitment and the neuron merging routine, is shown in Figure 5. When the hulls, generated by all possible subsets of the poset from Fig. 5a, are ordered under set inclusion, all districts have a lattice order, as shown in Fig. 5b. Next to the inclusions of all individuals of the poset, the hulls of {b,c}, {d,e}, {c,e}, {d,h} and {h,k} were added to obtain this lattice order. In Fig. 5c we show the result we get when neuron merging is used to transform the poset from Fig. 5a into a lattice. It is obvious that the neural network we get after neuron recruitment has more structure than a network that is produced by neuron merging.

5. Simulation experiments.

The algorithms we presented in section 2 construct a simultaneous functional order in a collection of neural elements using either covariances or coincidences in their corresponding signal activities. In the sequel we will refer to these models as respectively the covariance- or coincidence-model.

Our algorithms transform a partially ordered set of elements (I_* or $I_\sharp$) into a lattice order by either merging existing elements or by recruiting previously unspecified ones. As a result the total number of elements in the resulting lattice order will generally differ from the initial number of elements in the partially ordered set (only when this partial order is already a lattice order will both numbers be equal). We

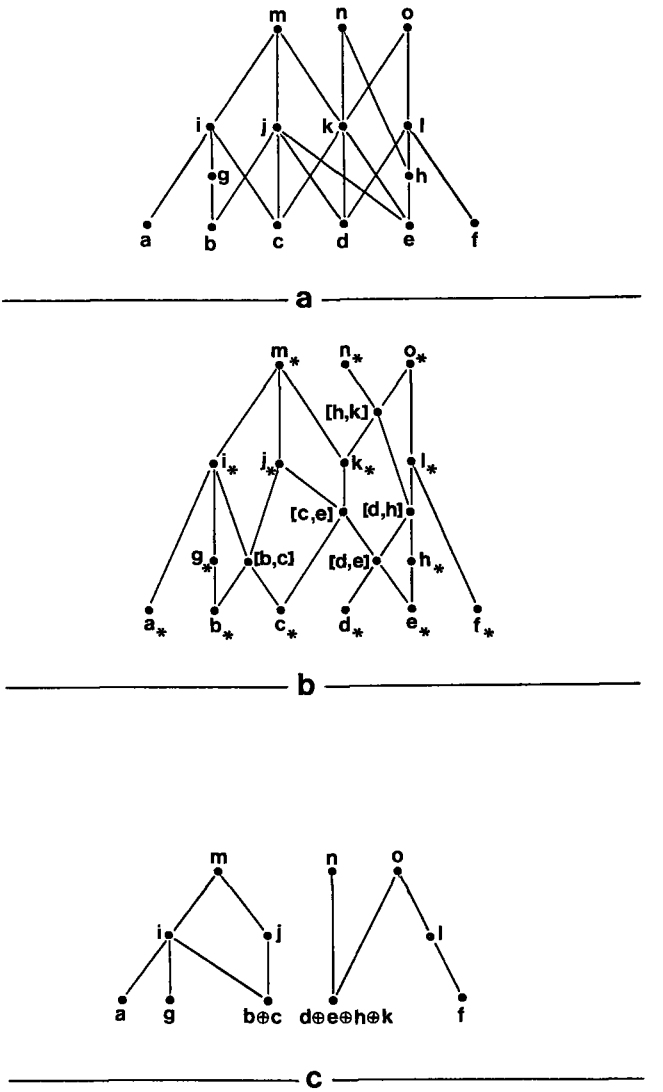

Figure 5. **a.** The Hasse-diagram of a partially ordered set of individuals. **b.** The Hasse-diagram of the resulting lattice order after neuron-recruitment. **c.** The Hasse-diagram of the resulting lattice order after neuron-merging.

wanted to study the difference between these numbers as a function of the initial number of individuals in the underlying partially ordered set. For this simulation study we used the coincidence-model and one-dimensional detector arrays.

We adopted a distribution for the position and aperture size of the one-dimensional detectors that is compatible with the known neuroanatomy of the retina and the geniculostriate system (Koenderink and van Doorn, 1978). The aperture area radius length is exponentially distributed between a minimum (r_1) and maximum (r_N) value and is quantized in N intervals: $r_i = a.e^{b.i}$ (a and b proportionality constants; i = 1, ... ,N). The density function according to which the detectors with an aperture area of radius r_i were distributed was chosen inversely proportional to this radius length. As we wanted to produce many different partially ordered sets of individuals, a certain degree of randomness in the spatial structure of the detector array was required. The adopted distribution function provides a detector array that has sufficient spatial structure to yield a well-developed simultaneous functional order, whereas its actual structure is not trivial. An additional advantage is its analogy to receptive field distributions found in neuroanatomy and electrophysiology.

In this particular experiment both the actual choice of the model (covariance or coincidence) and the values of the parameters of the detector array are irrelevant, as we are merely interested in the creation of a partially ordered set which can serve as a datum for the neuron-merge- and neuron-recruitment routines. Therefore, we want a (geometrical and thus functional) structure which is as rich as possible within the limited space available. This was partly achieved by regarding the detector array as periodically extended. In this case there are no restrictions on the possible positions of the larger detector units. To prevent two-sided overlap of the detector units in our model, the radius of the largest detector units was always chosen smaller than 1/4 of the smallest dimension of the detector array. The actual choice of the system parameters was based on the results of an extensive series of simulation experiments (which will be reported in a companion paper) and was such as to guarantee well developed functional structures. We were restricted to the use of one-dimensional detector arrays. The study of higher

dimensional systems proved not feasible at the moment, because of (i) the large amount of memory space needed, due to the large number of individuals that is needed to obtain a system with enough internal coherence to allow an unambiguous interpretation as a triangulation (see Part II of this series) and (ii) the difficulties in visualizing the results.

Figure 6 shows the total number of elements in the lattice order that results after applying the neuron-merging or the neuron-recruitment routine to a partially ordered set, as a function of the initial number of individuals in this set. Just for the sake of completeness we will now present the adopted system parameters. The minimum detector radius value was 10 (arbitrary) units, the maximum radius value 400 units. Radius values were quantized in 8 intervals. The length of the detector array was 1600 units. The smallest detector units were distributed without any spatial overlap. Therefore the detector array is completely covered by the smallest detector units when their number is 80. Because a poset of n+1 elements was created from a poset of n elements by adding (according to the forementioned distribution function) one or more detectors to an initial distribution, the final functional order will depend on this particular distribution and the exact location of these randomly added detectors. However, simulations starting with different initial distributions yielded results which were almost identical (i.e. show no significant differences) to those of Fig. 6. Thus, the results from Fig. 6 will serve as a general example.

In case of the merging process, Figure 6 shows that the number of elements in the resulting lattice order increases with the number of individuals in the poset to which merging is applied, up to about 110 individuals in this poset. Thereafter, the number of elements in the lattice order remains nearly independent of the number of individuals in the initial poset. For a detector array which is completely covered by the smallest detectors (which is the case when their number is 80), the final lattice order has only a few more elements than the number of these smallest detectors (87 in this example). Thus, the geometrical inclusion- or overlap-structure of the detectors in an array that is densily covered, is not very well represented in the functional representation of the

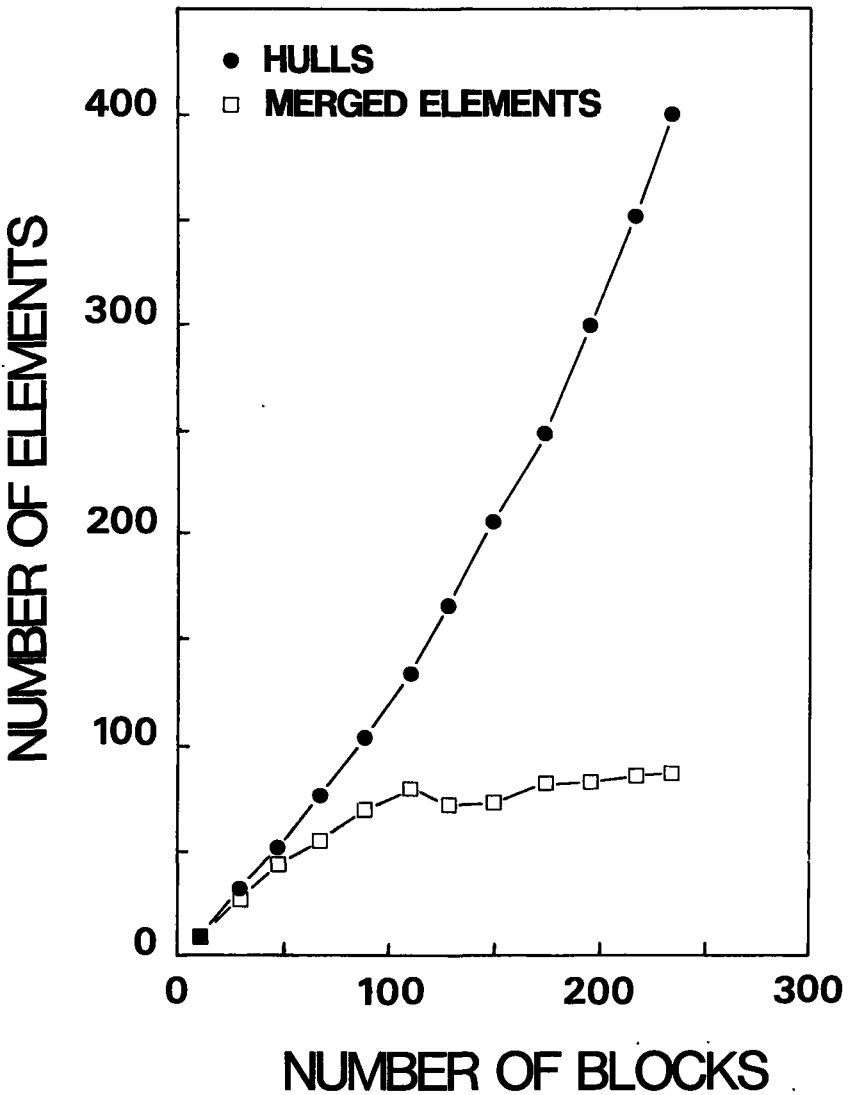

Figure 6. The total number of elements in the resulting lattice order after applying neuron-merging of neuron-recruitment to a partially ordered set of neural individuals, as a function of the initial number of individuals in this set.

neural system after the merging process.

A steady increase of the number of lattice elements with the number of poset individuals is found when neuron-recruitment is applied to transform the poset into a lattice order. Over the same range where the resulting number of lattice elements remains constant after merging the number of elements that remains after neuron-recruitment strongly increases. This means that there is a significant increase of internal coherence in the functional structure over this range. Thus, as might be expected, neuron-recruitment produces a functional order with more internal coherence than neuron-merging (and may therefore provide a more faithful representation of the geometry of the underlying detector distribution).

6. Conclusions.

We have presented two algorithms that compute the simultaneous functional order in a nervous net. The algorithms proceed from respectively a cross-correlation or coincidence-structure which is objectively available to the neural system itself. This cross-correlation or coincidence-structure is transformed into a partially ordered set. By either merging existing neural interconnections, or growing new ones, this partial order is locally transformed into a lattice order. Geometrical entities as "regions" or "districts" can then be defined in a purely functional manner. We presented functional analogues for physical concepts like sensory modalities and the cohesion ("connectivity") within modalities (e.g. the visual field).

In this first of a series of four companion papers we have shown that it is in principle possible for a nervous net to build up a simultaneous order using purely functional relations. Such an order has an objective existence for the system itself and is independent of an external observer's description of the spatial lay-out of the network. In three companion papers we will

(i) show how functional analogues for a geometrical "betweenness" relation and for the notion of "dimension", and even a triangulation, can be computed from the resulting lattice order (Part II)

(ii) study the resulting simultaneous functional order as a function of the physical constraints of the neural system (Part III)

(iii) study the resulting simultaneous functional order as a function of constraints on the spatial structure of the stimulus patterns presented to the neural network during a learning stage (Part IV).

References.

Blakemore, C. and Cooper, G.F. (1970) Development of the brain depends on the visual environment. Nature 228, 477-478.

Blakemore, C. and Van Sluyters, R.C. (1975) Innate and environmental factors in the development of the kitten's visual cortex. J. Physiol. 248, 663-716.

Blumenthal, L.M. and Menger, K. (1970) Studies in geometry. San Francisco: Freeman.

Buisseret, P. and Imbert, M. (1976) Visual cortical cells: their developmental properties in normal and dark reared kittens. J. Physiol. 255, 511-525.

Cleland, B.G., Crewther, D.P., Crewther, S.G. and Mitchell, D.E. (1982) Normality of spatial resolution of retinal ganglion cells in cats with strabismic amblyopia. J. Physiol. 326, 235-249.

Cowan, W.M., Fawcett, J.W., O'Leary, D.D.M. and Stanfield, B.B. (1984) Regressive events in neurogenesis. Science 225, 1258-1265.

Crapo, H.H. and Rota, G.C. (1970) On the foundation of combinatorial theory: combinatorial geometries. Cambridge, Mass.: MIT Press.

Crewther, D.P., Crewther, S.G. and Cleland, B.G. (1985) Is the retina sensitive to the effects of prolonged blur? Exp. Brain Res. 58, 427-434.

Erdi, P. and Barna, Gy. (1984) Self-organizing mechanism for the formation of ordered neural mappings. Biol. Cybern. 51, 93-101.

Finlay, B.L. and Slattery, M. (1983) Local differences in the amount of early cell death in neocortex predict adult local specializations. Science 219, 1349-1351.

Fregnac, Y. and Imbert, M. (1977) Cinetique de development des cellules du cortex visuel. J. Physiol. (Paris) 6, T.73.

Fregnac, Y. and Imbert, M. (1978) Early development of visual cortical cells in normal and dark-reared kittens: relationship between orientation selectivity and ocular dominance. J. Physiol. 278, 27-44.

Grätzer, G. (1978) General lattice theory. New York, San Fransisco: Academic Press (A Subsidiary of Harcourt Brace Jovanovich, Publishers).

Grunau, M.W. von and Singer, W. (1980) Functional amblyopia in kittens with unilateral exotropia. II. Correspondence between behavioural and electrophysiological assessment. Exp. Brain Res. 40, 305-310.

Hebb, D.O. (1949) The organization of behaviour. New York: John Wiley.

Hering, E. (1899) Über die Grenzen der Sehschärfe. Ber. Math.-phys. Cl.d. Königl. Sächs. Gesell. Wiss. Leipzig. Naturwiss. Teil 16-24.

Hirsch, J. and Hylton, R. (1984) Orientation dependence of visual hyperacuity contains a component with hexagonal symmetry. J. Opt. Soc. Am. A1, 300-308.

Hubel, D.H. and Wiesel, T.N. (1970) The period of susceptibility to the physiological effects of unilateral eye closure in kittens. J. Physiol. 206, 419-436.

Hubel, D.H. and Wiesel, T.N. (1974) Ordered arrangement of orientation columns in monkeys lacking visual experience. J. Comp. Neurol. 158, 307-318.

Huntington, E.V. (1913) A set of postulates for abstract geometry, expressed in terms of the simple relation of inclusion. Math. Ann. 73, 522-559.

Innocenti, G.M. (1981) Growth and reshaping of axons in the establishment of visual callosal connections. Science 212, 824-827.

Ikeda, H. (1980) Visual acuity, its development and amblyopia. J. R. Soc. Med. 73. 546-555.

Imbert, M. and Buisseret, P. (1975) Receptive field characteristics and plastic properties of visual cortical cells in kittens reared with or without visual experience. Exp. Brain Res. 22, 25-36.

Jacobson, S.G. and Ikeda, H. (1979) Behavioural studies of spatial vision in cats reared with convergent squint: is amblyopia due to arrest in development? Exp. Brain Res. 34, 11-26.

Jeffery, G. (1985) Retinotopic order appears before ocular separation in developing visual pathways. Nature 313, 575-576.

Koenderink, J.J. (1984a) Simultaneous order in nervous nets from a functional standpoint. Biol. Cybern. 50, 35-41.

Koenderink, J.J. (1984b) Geometrical structures determined by the functional order in nervous nets. Biol. Cybern. 50, 43-50.

Koenderink, J.J. (1984c) The concept of local sign. In: Limits in perception. Eds. Doorn, A.J. van, Grind, W.A. van de and Koenderink, J.J. VNU Science Press, Utrecht, 495-547.

Lotze, H. (1884) Mikrokosmos. Leipzig: Hirzel.

Lundell, A.T. and Weingram, S. (1969) The topology of CW complexes. New York, Cincinnati, Toronto, London, Melbourne: Van Nostrand Reinhold Company.

Paton, J.A. and Nottebohm, F.N. (1984) Neurons generated in adult brain are recruited into functional circuits. Science 225, 1046-1048.

Price, D.J. and Blakemore, C. (1985) Regressive events in the postnatal development of association projections in the visual cortex. Nature 316, 721-724.

Rakic, P. and Riley, K.P. (1983) Overproduction and elimination of retinal axons in the fetal rhesus monkey. Science 219, 1441-1444.

Rauschecker, J.P. and Singer, W. (1981) The effects of early visual experience on the cat's visual cortex and their possible explanation by Hebb synapses. J. Physiol. 310, 215-239.

Westheimer, G. and McKee, S.P. (1977a) Integration regions for visual hyperacuity. Vision Res. 17, 89-93.

Westheimer, G. and McKee, S.P. (1977b) Spatial configurations for visual hyperacuity. Vision Res. 17, 941-947.

CHAPTER I.2.

The construction of a simultaneous functional order in nervous systems.

II. Computing geometrical structures.

Abstract.

The functional order of a collection of nervous elements is available to the system itself, as opposed to the anatomical geometrical order which exists only for external observers. It has been shown before (Part I) that covariances or coincidences in the signal activity of a neural net can be used in the construction of a simultaneous functional order in which a modality is represented as a concatenation of districts with a lattice structure. In this paper we will show how the resulting functional order in a nervous net can be related to the geometry of the underlying detector array. In particular, we will present an algorithm to construct an abstract geometrical complex from this functional order. The algebraic structure of this complex reflects the topological and geometrical structure of the underlying detector array. We will show how the activated subcomplexes of a complex can be related to segments of the detector array that are activated by the projection of a stimulus pattern. The homology of an abstract complex (and therefore of all of its subcomplexes) can be obtained from simple combinatorial operations on its coincidence scheme. Thus, both the geometry of a detector array and the topology of projections of stimulus patterns may have an objective existence for the neural system itself.

1. Introduction.

In a previous paper (Part I) we showed how the signal- covariances and signal- coincidences in a neural net can be used in the construction of a simultaneous functional order among the neural elements. In the present paper we study the relations between the resulting functional order in a nervous net and the geometry of its underlying detector array. In particular, we will show how the activity patterns in a neural net can be considered to be isomorphic to projections of stimulus patterns on the underlying detector array. We will study the constraints the functional order has to meet to allow isomorphisms with abstract geometrical entities such as CW-complexes or triangulations. These abstract geometrical complexes are combinatorial entities that describe the construction of a topological space as the union of a collection of elementary cell structures. If a neural net has enough internal coherence, the algebraic structure of the complex with which it can be identified will reflect the topological and geometrical structure of the underlying detector array. Hence it is conceivable that the cohesion and the dimensionality of a certain modality may have an objective existence in the simultaneous functional order of the collection of nervous elements that define that particular modality. For instance, it is possible that the cohesion and two-dimensionality of the visual field result from the constraints put by the anatomy on the simultaneous activity in the neural net. If the functional order in a modality can be identified with an abstract geometrical complex, it becomes possible to identify regions of the modality with abstract geometrical subcomplexes. Projections of stimulus patterns on a detector array may cause the activation of certain subsets of segments of this array. These segments correspond to activated regions in the functional order. As these regions can in turn be identified with subcomplexes of the abstract geometrical complex, the topology of projections of stimulus patterns on a detector array may have an objective representation in the simultaneous activity in its corresponding neural net. Hence there would be no need to look for a "reconstruction" of stimulus patterns in the central nervous system. Note that such "reconstructions" have no intrinsic meaning (inherent order) for the

neural system anyway, as they are only available to external observers.

2. Dependency, independency and dimension.

In a previous paper (Part I) we defined the **hull** of a subset J of a partially ordered set I as the intersection of the inclusion of all minubs (minimal upper bounds) of J: $[J] = \{\{\text{minubs}\{J\}\}_*\}_n$. This is again a subset of I. A **lattice** is a poset $\{L,\leq\}$ for which sub $\{a,b\}$ exists for all $a,b \in L$, or, equivalently, for all subsets of L (for terminology, see Part I). Thus, the hull of a subset J of a lattice order L is simply the inclusion of its supremum.

The hull of an atomic set $\{a_0,\ldots, a_p\}$ will be called a **p-tope**. In a lattice structure, the hull of an atomic set is the smallest connected region containing the atoms of that set. A tope a is called a **sub-tope** of a tope b, if the set of atoms generating tope a is a real subset of the set of atoms generating tope b. A tope is called **dependent** if it is equal to the union of all of its sub-topes. A tope is called **independent** if the union of all of its sub-topes is a real subset of the tope. These definitions can in turn be used in the following definition for an abstract geometrical **dimension**. The dimension of a district is defined to be n, if n+1 is the largest number of atoms that uniquely define an independent tope. Thus, in a district of dimension n, the maximal number of atoms that generates an independent connected region is n+1. Therefore, the abstract dimension of a district in the functional representation of a neural network can directly be related to the geometrical dimension of the underlying sensor array. As an example, consider Figure 1. It is easily verified that, according to our definition, the districts g_*, h_*, and i_* are respectively two, one and zero dimensional.

Note that, in case of a lattice order, the definition of the abstract dimension is restricted to districts. This is a result of the fact that, for a lattice order, the hull of an atomic set is only guaranteed to exist within a district. The dimension-definition can also be applied to atomic sub-sets of a partial order for which a hull exists (i.e. for atoms located within the same district). Our definition of the abstract

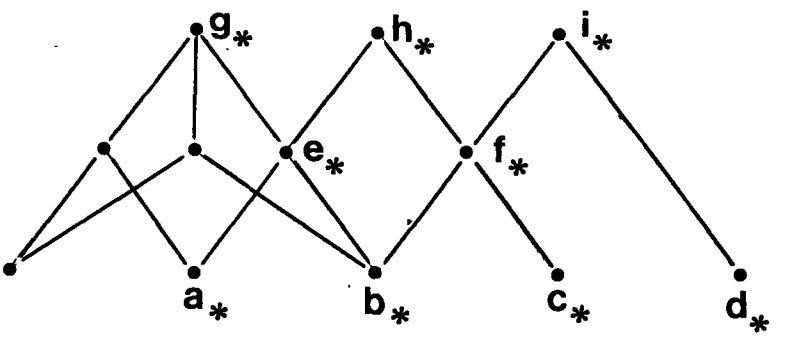

Figure 1. The Hasse-diagram of a poset with three districts g_*, h_* and i_*.

dimension is only valid for lattices that are isomorphic with triangulations (Koenderink, 1984b: see also section 4). In practice, a dimension-definition based on the theory of CW-complexes (Lundell and Weingram, 1969) is more universally valid. However, we used only geometrically one-dimensional detector arrays for our simulation experiments (which will be presented in a companion paper). CW-complexes that represent zero- or one-dimensional convex sets are equal to triangulations.

In our simulation model the dimension of a district is determined by the following procedure. All 0-topes are always independent and unique. 1-Topes are also independent, but need not be unique. If a 1-tope is found that contains exactly two atoms (and is therefore unique), the algorithm continues looking for independent and unique 2-topes. To test the dependency of a p-tope it is sufficient to determine the union of its subset of (p-1)-topes. If the p-tope is equal to this union it is dependent, otherwise it is independent. Let there be an independent and unique n-tope. If all (n+1)-topes are dependent or independent but not unique, then there can be no independent and unique (n+i)-topes for $i > 1$. In this case, the dimension of the lattice is n.

3. Local geometrical order.

3.1. A functional representation of geometrical order.

One of the most important concepts in geometry is the relation that one point q may have with respect to two points p,r and which is usually described by saying that the point q is between the points p and r. In the most general sense in which the notion is used a betweenness relation has to be a ternary (three place) relation R(a,b,c) defined for ordered triples of elements of an abstract set S which (i) is symmetric with respect to the outer points (i.e. R(a,b,c) holds iff R(c,b,a) holds) and (ii) has a special inner point (i.e. R(a,b,c) and R(a,c,b) imply b=c).

We will now present a functional representation for this metrical betweenness relation based on the hull-construction. Let {B,S} be a partially ordered set of dimension n. Let $p, b_0, \ldots, b_n$ be individuals of B

that are located within the same district of B (because of the hull construction a betweenness relation can only be established within districts). The element p of B is now defined to be <u>within</u> the n-dimensional region defined by the individuals $b_0,\ldots,b_n$ if $[b_0,\ldots,b_{i-1},b_{i+1},\ldots,b_n,p] < [b_0,\ldots,b_n]$ for i = 0, ...,n. In the case that {B,S} is a lattice an element p of B is defined to be <u>within</u> the n-dimensional region defined by the individuals $b_0, \ldots ,b_n$ if the supremum of the set $\{b_0,\ldots,b_{i-1},b_{i+1},\ldots,b_n,p\}$ precedes the supremum of the set $\{b_0,\ldots,b_n\}$, for i=0,...,n.

As an example, consider the district defined by h_* in Figure 1. We may ask whether the individual b is located between a and c. Both the hull of {a,b} (={a,b,e}) and the hull of {b,c,} (={b,c,f}) are real subsets of the hull of {a,c} (={a,b,c,e,f,h}). Therefore, according to our definition, b is indeed located between a and c.

As a result of our definition the relative position of an individual in the functional order is determined by its relations to other individuals. If an individual lacks enough functional relations with other individuals it may not be possible to determine a betweenness relation. For instance, we fail to reach a conclusion when we try to establish a betweenness relation for the individuals b,c and d in Fig. 1. This is a result of the fact that the hulls of {b,d} and {c,d} are equal ({b,c,d,f,i}). Therefore, the system can not determine the functional position of the "interval" defined by the individuals b and c relative to the interval defined by b and d. A betweenness relation for individual c cannot be determined, because it has not enough functional relations with other individuals to impose sufficient restrictions on its relative functional position.

3.2. Relating the geometrical order to its functional representation.

It is impossible to define a functional equivalent for all geometrical concepts (Koenderink, 1984 b,c). For instance, "functionally convex" can never be equivalent to "geometrically convex". Suppose you have a geometrically convex set of individuals. After projection on a

warped space these elements may become geometrically anything but convex while their overlap (and therefore, the correlations in their signal activities or their functional-) relations are conserved. Thus, a set of individuals which is geometrically not convex may still be functionally convex. The functional order of individuals that are not geometrically convex may also differ from the geometrical order of their corresponding detector units. Consider for instance the geometrical lay- out of the detector array depicted in Figure 2a. A possible functional representation of the structure of this array, determined from either the covariance- or coincidence-relations in the signal activities of the neural elements to which it reports, is shown in Figure 2b. Note that b is functionally in between a and c, although c is geometrically (as judged by an external observer) in between a and b. We assumed that the individuals in our models were open hyperspheres (Koenderink, 1984b). For instance, Huntington (1913) has shown that a "discgeometry" is isomorphic with the Euclidian plane. Thus, it is in our model in principle possible for a neural net to obtain a correct functional representation of the geometrical order of its underlying detector array.

In case of the covariance- or coincidence-models (described in Part I of this series), the correlation- or coincidence-detection thresholds may cause the functional inclusion order for the functional individuals to differ from the partial order that is induced by the geometrical inclusion or overlap relation for their corresponding detector units.

We will now consider the spatial lay-out of a set of detectors for which the covariance model will not produce a correct functional representation of their geometrical configuration. If we have three individuals α, β and γ, each one geometrically including its successor, the signal activity of α need not be correlated with that of γ due to the **covariance detection threshold.** Thus, we may have $(\alpha,\beta) \in D$, $(\beta,\gamma) \in D$ but $(\alpha,\gamma) \notin D$. Therefore, $(\beta,\gamma) \notin Q$. The result is that both α and γ are functionally included in β, whereas β is geometrically included in γ. Thus, the degree in which the functional order is a faithful representation of the geometrical order depends on the value of the correlation detection threshold.

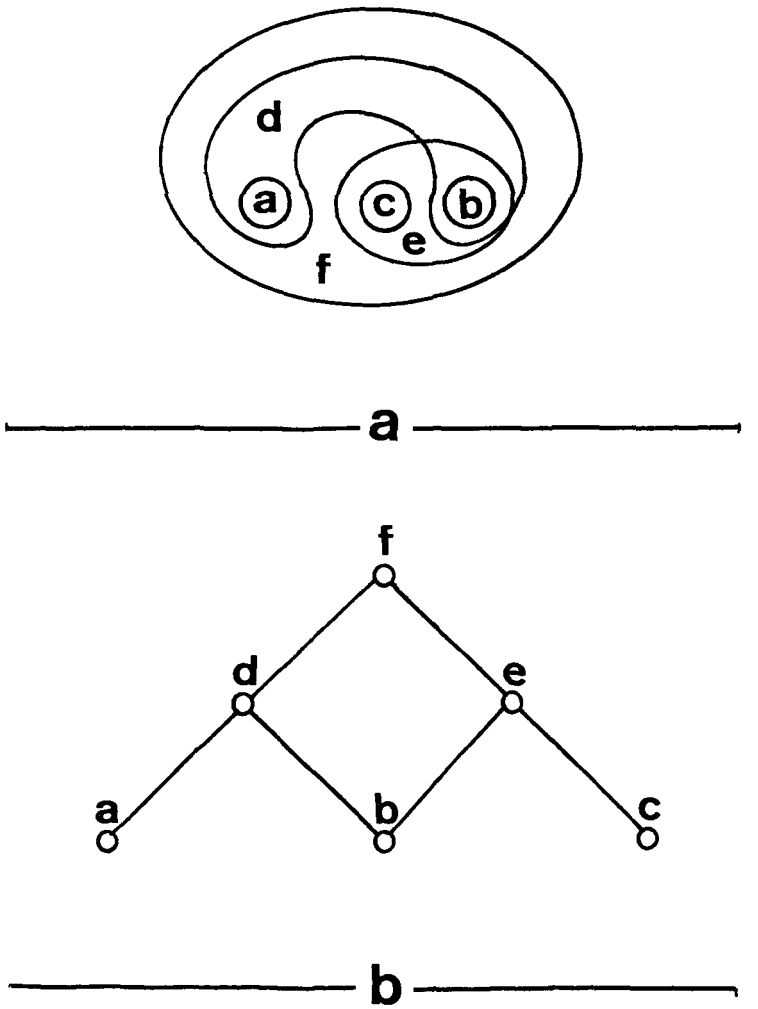

Figure 2. **a** The spatial lay-out of a detector array and **b** the Hasse-diagram representing the functional order in its corresponding neural network.

A further example of a spatial detector distribution that has no correct functional representation in the covariance model is shown in Figure 3. Figure 3a shows the spatial layout of a (part of a) detector array. It is assumed that the correlation between α and θ is below the covariance detection threshold. The relation D is defined by

D	α	β	γ	δ	ε	ζ	η	θ	ι
α	1	0	0	0	0	1	0	0	0
β	0	1	1	0	0	1	1	1	1
γ	0	1	1	0	0	1	1	1	1
δ	0	0	0	1	0	0	1	1	1
ε	0	0	0	0	1	0	0	0	1
ζ	1	1	1	0	0	1	1	1	1
η	0	1	1	1	0	1	1	1	1
θ	0	1	1	1	0	1	1	1	1
ι	0	1	1	1	1	1	1	1	1

The relation Q is given by

Q	α	β	γ	δ	ε	ζ	η	θ	ι
α	1	0	0	0	0	1	0	0	0
β	0	1	1	0	0	1	1	1	1
γ	0	1	1	0	0	1	1	1	1
δ	0	0	0	1	0	0	1	1	1
ε	0	0	0	0	1	0	0	0	1
ζ	0	0	0	0	0	1	0	0	0
η	0	0	0	0	0	0	1	1	1
θ	0	0	0	0	0	0	1	1	1
ι	0	0	0	0	0	0	0	0	1

From Q we see that the individuals β and γ are functionally equivalent as they are related and have the same relations with all other individuals.

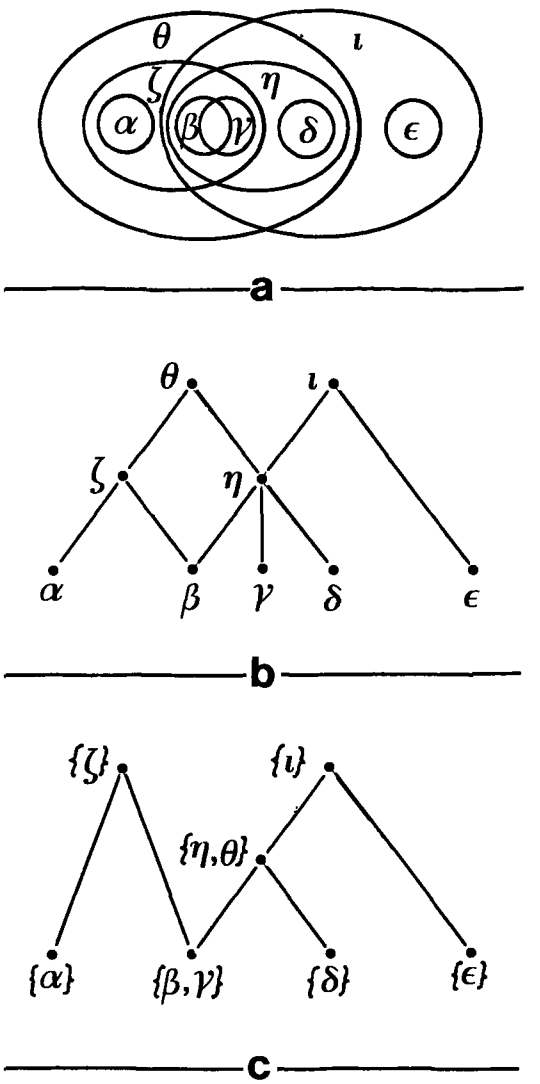

Figure 3. **a** The spatial lay-out of a collection of detector units that are labelled with their corresponding neural elements. **b** The Hasse-diagram representing the geometrical inclusion order in the collection of detector units from **a.** **c** The functional inclusion order between blocks of neural elements as produced by the covariance model.

The same holds true for the individuals η and θ. After lumping functionally equivalent individuals in blocks we get the partial order relation R:

R	α	$\{\beta,\gamma\}$	δ	ε	ζ	$\{\eta,\theta\}$	i
α	1	0	0	0	1	0	0
$\{\beta,\gamma\}$	0	1	0	0	1	1	1
δ	0	0	1	0	0	1	1
ε	0	0	0	1	0	0	0
ζ	0	0	0	0	1	0	0
$\{\eta,\theta\}$	0	0	0	0	0	1	1
i	0	0	0	0	0	0	1

Figs. 3b and 3c show the Hasse diagrams of respectively the geometrical and functional inclusion relations. Notice that ζ is geometrically included in θ, whereas it is functionally outside θ. The opposite is the case for θ and i: functionally θ is included in i, whereas geometrically both individuals are merely overlapping (i is functionally distinct from θ, because i is related to ε whereas θ is not related to ε).

With the coincidence model we performed some simulation experiments to study the resulting functional order in a collection of neural elements (after a learning stage) as a function of different values of their **activation thresholds.** In these studies (which will be reported in Part III of this series) we used randomly structured binary stimulus patterns. To simulate the functioning of physiological detectors at low stimulus intensity levels we assumed that a neural element is activated when at least a certain absolute (threshold) area of its corresponding detector unit is covered with non-zero valued image segments. This threshold area was assumed to be independent of the detector aperture area (i.e. the same absolute threshold area was valid for all detectors). To simulate a high stimulus intensity level condition the activation threshold of the neural elements was assumed to be a constant fraction of the aperture area of

their corresponding detector units. In case of a relative activation threshold area, a small detector unit may be covered with enough non-zero valued segments of the stimulus pattern to activate its corresponding neural element, while this need not be the case for a larger detector unit in which the former is geometrically included. Thus, in case of a relative activation threshold, the geometrical inclusion relations of detector units may not be represented in the functional order of their corresponding neural elements. This is not the case for an absolute activation threshold.

Besides the (covariance- or coincidence-) detection thresholds a neural system has more physical constraints which may result in a functional order that is no correct representation of its geometrical structure. This may happen when the distribution of the detectors is **sparse**. Then there is not enough geometrical overlap (or inclusion) between the detector units to induce a functional order in the set of neural elements with enough internal coherence to provide a correct representation of their geometrical situation. When the **aperture size intervals** are too widely spaced (which is the case when there are only a few different discrete aperture sizes) and if there is not much geometrical overlap between their corresponding detector units, many neural elements (particularly those corresponding to detector units of smaller sizes) will either be functionally equivalent (coincidence model) or will have not enough functional relations with other individuals to determine their relative functional position (covariance model). An extreme value for the **threshold area** A_t, as used in the definition of functional distinctness for individuals in the coincidence model, may result in functional inclusion relations that do not reflect geometrical inclusion. Figure 4 shows an example of the geometrical situation of three detector units corresponding with the neural elements α, β, and γ. The coincidence model starts with checking the existence of a coincidence relation between α, β and γ. Suppose a primitive inclusion relation Q' has been established (either during a learning stage or, if the learning stage is skipped and the geometrical option is chosen, after the assessment of the functional distinctness of the individuals) so that α is functionally included in β and β is included in γ. The transitive extension Q" of Q'

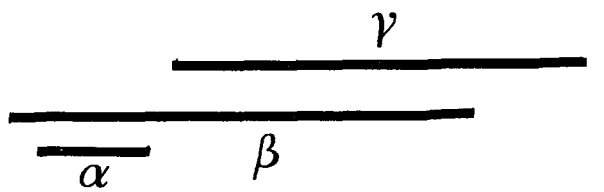

$$Q'(\alpha,\gamma) = 0$$

$$Q'(\alpha,\beta) = Q'(\beta,\gamma) = 1$$

$$Q''(\alpha,\gamma) = 1$$

Figure 4. Schematic representation of the spatial lay-out of three detector units that are labelled with their corresponding neural elements. Because of the transitive extension of the primitive inclusion relation in the coincidence model the neural element α is functionally included in γ, although the detector unit corresponding with α is located outside the detector unit corresponding with γ.

will then cause α to be functionally included in γ, whereas there need not exist any geometrical overlap (let alone inclusion) between their corresponding detector units. In the coincidence model functional equivalent individuals that have no geometrical overlap may be lumped in a block structure. Figure 5a represents the spatial lay-out of the detector units corresponding with a set of five neural elements ($\{\alpha, \beta, \gamma, \delta, \varepsilon\}$). The relative functional position (e.g. a betweenness relation) of the individuals α, β and γ is undefined before the construction of blocks of functional equivalent elements (Fig. 5b). After this construction process α and γ are regarded as one functional individual. However, their corresponding detector units are spatially separated by the one corresponding to β. Situations like this can only arise in systems with low detector densities; a more dense detector distribution will result in a functional order with enough internal coherence to allow the assessment of the functional identity of most individuals.

The resulting covariance- or coincidence-structure of the neural net not only reflects the physical limitations of the detector array, but will also depend on the constraints of the **environment** in which this array resides. A neural net that organizes itself according to either of the two models can to a certain extent (limited by its physical constraints) encode (learn from) the topological information in its sensory signals. Thus, a deficient training, due to certain correlations which may be invariably present in the stimulus patterns presented to a neural system during its learning stage, may prevent the development of a correct functional representation of the geometry of the detector array. For instance, in case of the retina blurred eye optics could produce a functional overlap in the signal activities of neural elements that correspond to receptive fields that have no (significant) geometrical overlap. An extreme case would be a system left to mature in a "Ganzfeld". In this case all detectors are always stimulated simultaneously. In this situation the system would have no way of telling the individuals apart (it would never get the opportunity to establish their functional identity). Thus, the resulting functional order would certainly be zero-dimensional. In a companion paper (Part IV) we will study the influence of the environmental constraints on the resulting functional order.

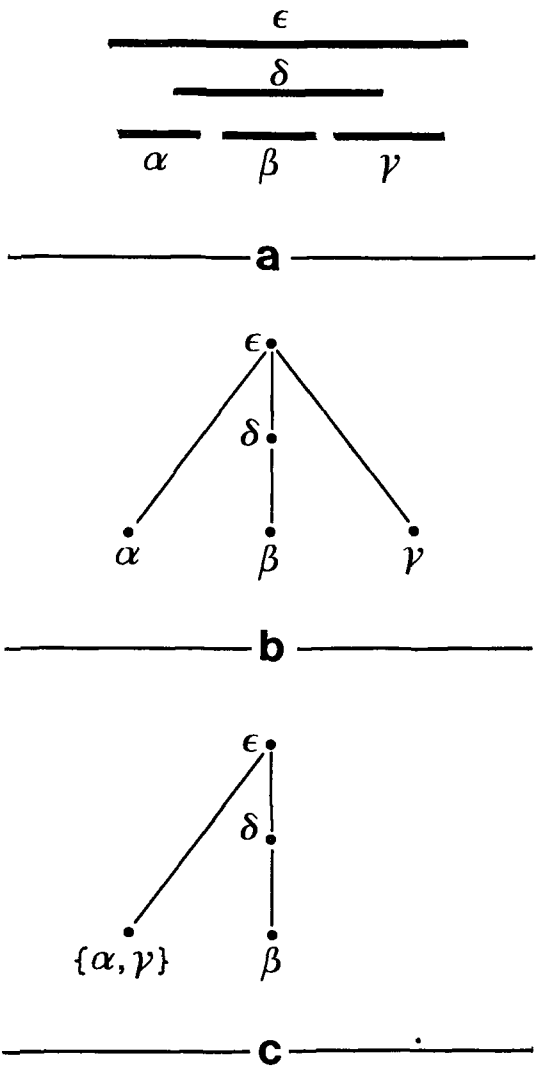

Figure 5. **a** Schematic representation of the spatial lay-out of 5 detector units that are labelled with their corresponding neural elements. **b** The Hasse-diagram before and **c** after the forming of blocks of neural elements in the coincidence model. Although α and γ are disconnected and separated by β they are still lumped in the same block.

4. The abstract geometry determined by the simultaneous functional order in a neural net.

In a previous paper (Part I) we showed how the hull construction can be used to construct a lattice order from the simultaneous activity in a neural net. In this section we will show how certain subsets of this lattice order can be identified with an **abstract geometrical complex.** The algebraic structure (the "homology groups"; Alexandroff, 1935; Hilton and Wylie, 1965) of an abstract complex reflects the topological and geometric structure of the underlying space. Thus, it is in principle possible that the geometry of the detector array has an objective existence for the neural system itself.

The aim of combinatorial or algebraic topology (e.g. Henle, 1977) is to characterize geometrical objects in terms of properties of finite subsets. Objects that can be constructed from simple **cells** by joining these along their edges are called **complexes.** In general the cells are topologically equivalent to n-dimensional hyperspheres. In the sequel we will study complexes that are at most two-dimensional. In case of surfaces the cells are topologically equivalent to discs. The cells are called **polygons** when a finite number of points on their boundary are chosen as **vertices.** The sections of their boundaries in between two vertices are called **edges.** Thus, a complex is a topological space plus a combinatorial structure that describes how the space is created (proper joining rules for the cells). The same topological surface can give rise to many different homologous complexes (the cell decomposition is not unique). Homology of complexes is reflected in the existence of combinatorial invariants like the Betti numbers and the Euler characteristic. These can be obtained from the application of simple combinatorial operations to the incidence coefficient scheme of a complex (which indicates whether a frame of dimension k appears in a frame of dimension k+1; Agoston, 1976; Henle, 1977).

Algebraic topology describes the structure of a topological space by associating it with an algebraic system, usually a group. The algebraic structure of a group has to reflect the topological and geometrical structures of the underlying space with which it is associated. Homology

theory (e.g. Hilton and Wylie,1965) is a method to associate a group with a space. The group thus associated with any space is a topological invariant of that space (homeomorphic spaces have isomorphic groups). Once a space has been associated with a group each object in that space can be associated with its abstract counterpart. The abstract representation of a cell will be called a **frame**. The union of all frames will be called an **abstract geometrical complex.**

We will now indicate how an abstract geometrical complex K can be constructed from a lattice order H. We assume that H is obtained after application of the "neuron merging" or "neuron recruitment" routine to the inclusion I_* of a certain set of neural individuals I. The individuals of H are therefore subsets of the set of neural individuals I. H is ordered under set inclusion. (For a detailed description of the structure and the construction of H, see Part I). A subset of individuals of H (which are subsets of I) will be identified with the **frames** of K. K must satisfy the following conditions:

1. Each individual is a frame.
2. An individual belongs to only a finite number of frames.
3. The intersection of two frames is either empty or also a frame.

To each frame can then be associated a new geometrical object: the cell spanned by the frame. The general dimension of the frame is called the dimension of the cell. The dimension of the complex K is defined as the least upper bound of the dimensions of its frames. The cells spanned by sub-frames of a certain frame are called the **faces** of the cell spanned by that frame. The union of the cells spanned by all frames of a complex K will be called the **underlying polyhedron** of K.

In the sequel we will restrict our discussion to complexes which are at most two-dimensional. If the conditions for the construction of K are supplemented with the condition that any subset of a frame should also be a frame then K is sometimes called a **simplicial complex.** Pilot experiments showed that the number of individuals required to produce enough internal functional coherence in a neural net to allow the construction of a simplicial complex is approximately an order of magnitude larger for a random detector distribution (as used in our simulation experiments; see

Part I) than for a regular one. Because we wanted as much functional structure as possible in our simulated neural nets while keeping the number of individuals within practical limits we adopted an abstract geometrical complex which is a restriction of a so-called **CW-complex** (Lundell and Weingram, 1969; Jänich, 1980). In the sequel we will call this geometrical complex a **PCW-complex** (Polygonal, Closure finite, Weak topology). The **vertices** in a PCW-complex are the individuals of the set H. The one-dimensional frames correspond to straight **edges**, connecting two vertices. Thus, zero- and one-dimensional PCW-complexes are equal to simplicial complexes. The two-dimensional frames correspond to **polygonal cells**. The intersection of two such elements is either a vertex or a collection of connected edges of both cells.

Let X be a topological space. If there is an abstract simplicial complex K whose underlying polyhedron is homeomorphic to X, then X is said to be a triangulable space and the complex K is called a **triangulation of X**. We will now present an algorithm that computes a triangulation from a periodically extended modality consisting of districts with a one-dimensional lattice order. The algorithm starts with the determination of a subset C_1 of the set of individuals H such that all members of C_1 are **connected** with at least two other elements of H which must themselves be members of C_1. Two elements are called connected when they are not comparable and when their infimum exists and is not equal to the empty subset. The infimum of two members of C_1 will be called a **candidate vertex**. The algorithm thereafter selects those elements of C_1 that have the lowest functional order. The resulting set of elements of C_1 together with their vertices is called the triangulation of the lattice order. As any element of C_1 is the supremum of two candidate vertices we will call these elements *the* **candidate edges** *of the triangulation*.

Figure 6 shows the triangulation (indicated by the fat edges) determined from a one-dimensional lattice order by the forementioned procedure. The indices c and v indicate elements of the lattice order that belong respectively to C_1 (candidate edges) or to the set of candidate vertices. Because individual d is not the infimum of two other individuals of C_1, individual k cannot be an edge and individual c is therefore not available as a vertex in the triangulation. In this case, the structure

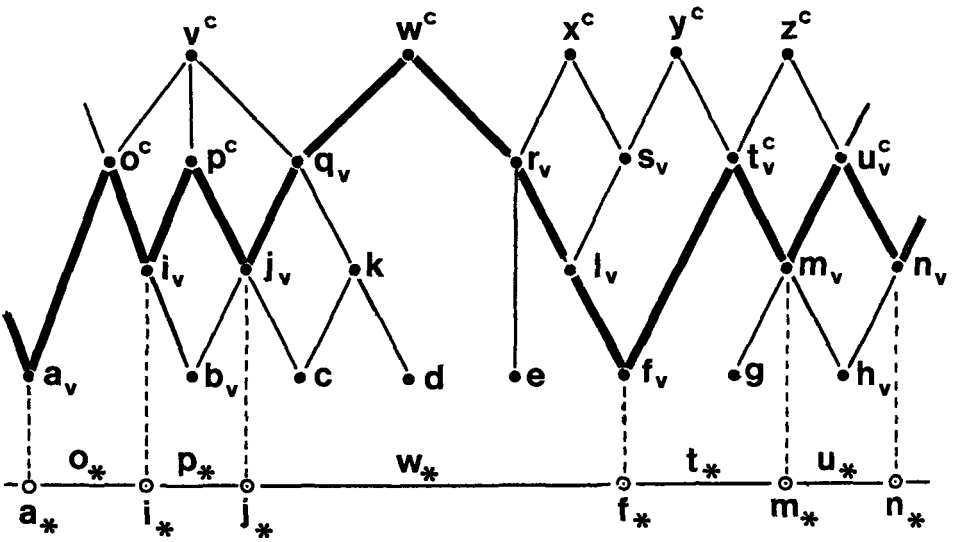

Figure 6. The Hasse-diagram of a one-dimensional closed lattice structure. The triangulation is indicated by the fat edges. One-dimensional simplices are:o, p, w, t and u with vertices: a, i, j, f, m and n.

defined by individuals of low functional order has not enough coherence to allow the representation of the functional order as a triangulation. Thus, vertices and edges are recruited from individuals of higher functional order. When there are several possibilities for the construction of a triangulation our definition is such that the simplices (edges) in the triangulation will be formed by those individuals of C_1 that have the lowest functional order. For example, individual x in Fig. 6 is not selected as an edge. Because edge- (and vertex-) candidate t precedes edge candidate y the former is selected as an edge. Thus, element s is no longer a vertex candidate. As a result, individual x is no longer connected with two edge candidates and is therefore no longer an edge candidate itself. The motivation for the selection of edges of the lowest functional order is that this process generally preserves more resolution than any other choice.

In our simulation experiments we used periodically extended detector arrays (see Part I). The triangulations of these arrays will therefore have no boundaries. This is no serious restriction, as our algorithm can be adapted to triangulate non-periodic detector arrays by the proper choice of a boundary definition.

The algorithm that constructs a PCW-complex from a modality with two-dimensional districts is similar to the algorithm for the one-dimensional case. This algorithm starts with the determination of the subset C_1 of connected individuals of H. This set contains the candidates for zero- and one-dimensional frames of an abstract geometrical complex K. The determination of the subset of two-dimensional connected frames C_2 is analoguous to the determination of the set C_1. An individual of C_2 is called connected when it is a member of a subset of C_2 consisting of at least four individuals that are mutually incomparable and if the infima of all combinations of two elements of this subset are (i) not mutually comparable and (ii) not equal to the empty subset. Thus, an individual of C_2 should be properly connected (or joined) with at least three other individuals of C_2. The elements joining the individuals of C_2 are the sub-frames (edges) of the frames (polygons) of C_2 and are therefore elements of C_1. As the one-dimensional boundary of the two-dimensional cells has to be closed, the zero-dimensional boundary of the one-dimensional edges is

always zero.

Thus, we have completed the description of an algorithm that constructs an abstract geometrical (PCW-) complex using certain subsets of a series of concatenated lattice orders (districts) within a modality.

5. Abstract geometrical structures determined by the functional order in a set of simultaneously activated neural elements.

In the previous paragraph we demonstrated how the functional order in a neural network can sometimes (i.e. when the system has sufficient internal coherence) be identified with an abstract geometrical complex. In this section we will show explicitly how the activity patterns in a neural net can be considered in geometrical terms, that is how such patterns can be considered to be isomorphic to projections of stimulus patterns on the underlying detector array.

The homology groups (i.e. the combinatorial invariants) of an N-dimensional abstract geometrical complex can be computed from its incidence schemes $E^0 \ldots E^{n-1}$ (e.g. Agoston, 1976). The algebraic properties of these homology groups reflect the topological properties of the N-dimensional array of detectors that correspond with the neural individuals. When the homology of a complex is known, it is also known for all of its algebraic subcomplexes. When a complex can be identified with the functional order in a neural net, its subcomplexes represent regions of this neural network which correspond to segments of the underlying detector array. Thus, it is in principle possible that a neural system determines the homology of simultaneously activated regions in a neural net in order to determine the topological structure of the corresponding activated segments in the underlying detector array. These segments are in turn activated as a result of the projection of a stimulus pattern on the detector array. Thus, the topology of stimulus patterns may be objectively represented in the simultaneous activity in a neural net.

We assume that the neural system has enough internal coherence for the construction of an abstract geometrical complex whose underlying polyhedron is homeomorphic (topologic equivalent) to the detector array.

We will now present a way to determine the homology of those subcomplexes that represent regions in a neural net that have been activated due to the presentation of a stimulus pattern. The activated detectors stimulate subsets of neural individuals that correspond to frames in the abstract complex. After localizing the activated N-dimensional frames in an N-dimensional complex, the homology of the activated N-dimensional subcomplexes can be determined. The homology groups of a complex describe the arrangement of the frames in the complex, thereby telling us about the "holes" in and the number of disjunct components of the underlying polyhedron.

We will first consider a one-dimensional PCW-complex. In this case, the triangulation is completely determined by the incidence scheme E^0. Let $(E^0)^A$ be the incidence scheme of the activated one-dimensional simplices of the triangulation. According to homology theory the rank of the zeroth homology group (i.e. the zeroth-Betti number) is equal to the Euler number in the one-dimensional case. In this case the Euler number is the difference between the number of zero-dimensional simplices and the number of one-dimensional simplices which can easily be determined from $(E^0)^A$.

As an example consider Figure 7. The lattice order H obtained after applying either neuron-merging or neuron-recruitment to the initial poset I_* from Figure 7b (representing the simultaneous functional order in a set of neural individuals corresponding to the one-dimensional spatial distribution of detector units depicted in Fig. 7a) is shown in respectively Figures 7c and 7d. The triangulation of H is indicated by the fat edges in Figs. 7c and 7d. Both $(i \bullet j)_*$ and [i,j] (both equal to {b,c,e,f,i,j}) are one-dimensional simplices of the triangulation. We have a pathological geometric situation if the gapwidth D > 0. This situation may occur when the distribution of the smallest detector units (corresponding to the atomic elements in the functional representation of the detector array) is sparse. If D > 0 Figure 7a represents a detector array that is not completely covered by the smallest detector units (there is a segment D where no smallest detector unit is present). For this situation the triangulation would not notice the projection of a stimulus located in the area D, while the large detector units l and m may be activated (depending on the activation thresholds). Figures 7b and 7c show

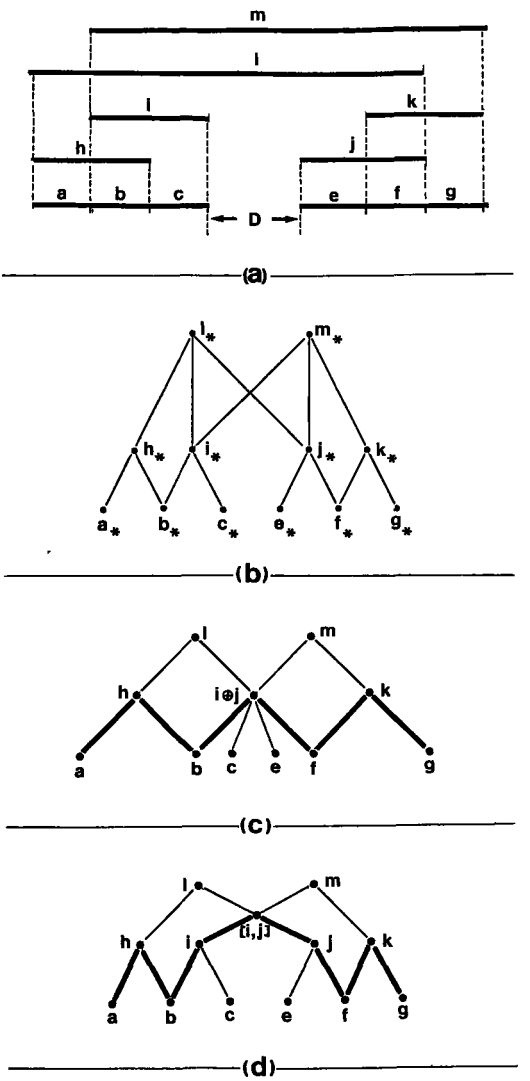

Figure 7. **a** Schematic representation of the spatial lay-out of a detector array. D represents an area that is not covered with the smallest detector units. **b** The Hasse-diagram representing the functional order in the neural net. **c** The Hasse-diagram representing the functional order in the neural net after neuron-merging and **d** after neuron-recruitment. The fat edges indicate a triangulation of the neural net.

that the processes of merging and recruiting neural elements are both of no avail to deal with this situation. In this case $(i \bullet j)_*$ and [i,j] correspond to segments of the underlying detector space that are not connected. The activation of b and e implies the activation of respectively $(i \bullet j)_*$ or [i,j]. The presentation of a stimulus projection located within D (which is in turn located **between** b and e) may activate l and m without the simultaneous activation of $(i \bullet j)_*$ or [i,j]. To preclude pathological geometrical situations like the one presented in Figure 7a (and for D>0) we performed our simulation experiments with systems in which the detector array was completely covered by the smallest detector units. In the rest of this discussion we will therefore assume that D=0.

TABLE I.

IMAGE SEGMENTS						ACTIVATED SIMPLICES		
a	b	c	e	f	g	h_*	s	k_*
*	-	-	-	-	-	*	-	-
-	*	-	-	-	-	*	*	-
-	-	*	-	-	-	-	*	-
-	-	-	*	-	-	-	*	-
-	-	-	-	*	-	-	*	*
-	-	-	-	-	*	-	-	*

S = $(i \bullet j)_*$ or [i,j]

* = NON-ZERO VALUED IMAGE SEGMENT OR ACTIVATED 1-D SIMPLEX

- = ZERO VALUED IMAGE SEGMENT or INACTIVE 1-D SIMPLEX

We will now consider the activity in the neural net of Figure 7 that arises due to the projections of stimuli on its corresponding detector array. The segments constituting these projections are assumed to coincide

with the smallest detector units. The stimulus projections (their segments labelled by the detector units with which they coincide and which are assumed to be activated by these segments) together with the one-dimensional simplices in the triangulation they activate are listed in Table I. The boundaries of these one-dimensional activated simplices can be calculated from the incidence-scheme E^0. Note that all segments except c and e coincide with a vertex of the triangulation. Due to its small number of neural individuals (low resolution) the system can only distinguish two topologically different kinds of stimulus projections: (i) two disconnected line segments and (ii) a single (connected) line segment. A stimulus projection consisting of segments a and g activates the one-dimensional simplices h_* and k_* without the simultaneous activation of s and is therefore classified as a stimulus projection of the first kind (i.e. two disconnected line segments). All stimulus projections consisting of other combinations of the segments a to g are classified as projections of the second kind (are connected line segments).

We proceed with the study of a two-dimensional PCW-complex K. In this case K is completely determined by the incidence schemes E^0 and E^1. Homology theory can only provide the number of connected components and the number of "holes" of the activated subcomplex K^A. Figure 8 shows two different activated subcomplexes K^A and L^A of a two-dimensional PCW-complex K. Both subcomplexes consist of two components (again subcomplexes) that are not connected and that have a different number of "holes". The zeroth and the first homology groups of the complex K^A are equal to respectively the zeroth and the first homology groups of L^A (respectively $H_0(K^*) = H_0(L^*) = Z_2 \oplus Z_2$ and $H_1(K^*) = H_1(L^*) = Z_2 \oplus Z_2 \oplus Z_2 \oplus Z_2$). However, it is possible to distinguish K^A from L^A because the first homology groups of their disconnected subcomplexes are different: $H_1(K_1^*) = Z_2$, $H_1(K_2^*) = Z_2 \oplus Z_2 \oplus Z_2$ and $H_1(L_1^*) = Z_2 \oplus Z_2$, $H_1(L_2^*) = Z_2 \oplus Z_2$. Let K^A be an activated subcomplex of a complex K. Suppose K^A consists of n disconnected subcomplexes K_i^A, i=1, ... ,n (that are again subcomplexes of K^A). A classification of K^A can be obtained from the study of the homology groups of its disconnected components. Because K_i^A is closed in K^A (and thus in K) these components

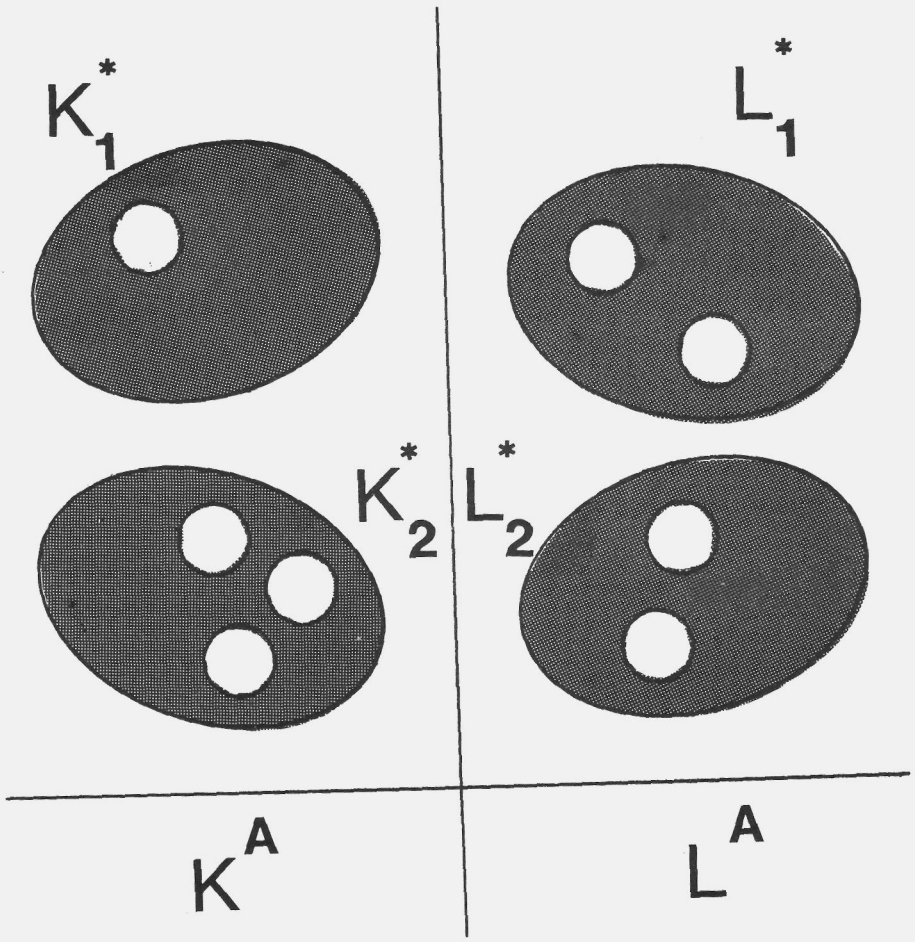

Figure 8. Example of two subcomplexes that can be distinguished by the first homology groups of their disconnected components.

can easily be computed from the incidence schemes $(E^0)^A$ and $(E^1)^A$. For an arbitrary frame of K_i^A the incidence schemes $(E^0)^A$ and $(E^1)^A$ yield all 0-, 1- and 2-dimensional frames that are connected with this particular frame. Together all these frames constitute K_i^A. For the Euler number χ of K_i^A we have $\chi(K_i^A) = n_0(K_i^A) - n_1(K_i^A) + n_2(K_i^A)$ where $n_j(K_i^A)$ denotes the number of j-dimensional frames (j = 0,1,2) of K_i^A. The rank of the first homology group of K_i^A yields the number of "holes" in the underlying polyhedron of K_i^A and can easily be determined from the Euler number with the use of the Euler-Poincaré formula (in the 2-dimensional case it is equal to $1-\chi(K_i^A)$).

Homology theory provides no information about the geometrical inclusion relations of the subcomplexes of a complex K. Figure 9 shows two activated subcomplexes M^A and N^A. The rank of the zeroth and first homology groups of M^A and N^A are equal (respectively 2 and 1). The ranks of the zeroth and first homology groups of the disconnected subcomplexes $M_1{}^A$ (1 and 1 respectively) and $M_2{}^A$ (1 and 0 respectively) are equal to those of respectively $N_1{}^A$ (1 and 1 respectively) and $N_2{}^A$ (1 and 0 respectively). Thus, homology theory alone cannot provide a complete description of the geometry of the underlying polyhedron of a PCW-complex. More information about the geometry of this polyhedron can be obtained from a closer inspection of the PCW-complex. For instance, in the triangulation depicted in Figure 7 the 1-dimensional simplex w_* is located **between** the 1-dimensional simplices o_* and t_* because w_* is met after o_* and before t_* on a sequential scanning operation starting at o_* and ending at t_* (thus a sequential scanning process can attribute a "geometrical order" to this triple).

6. Conclusions.

In a previous paper (Part II) we presented two algorithms that construct a simultaneous functional lattice order in the districts of a nervous net (i.e. at a local scale) using purely functional relations. In this paper we studied how the functional order in a nervous net is related to the geometry of the underlying detector array, both at a local (i.e. within districts) and at a global (i.e. within a single modality or the

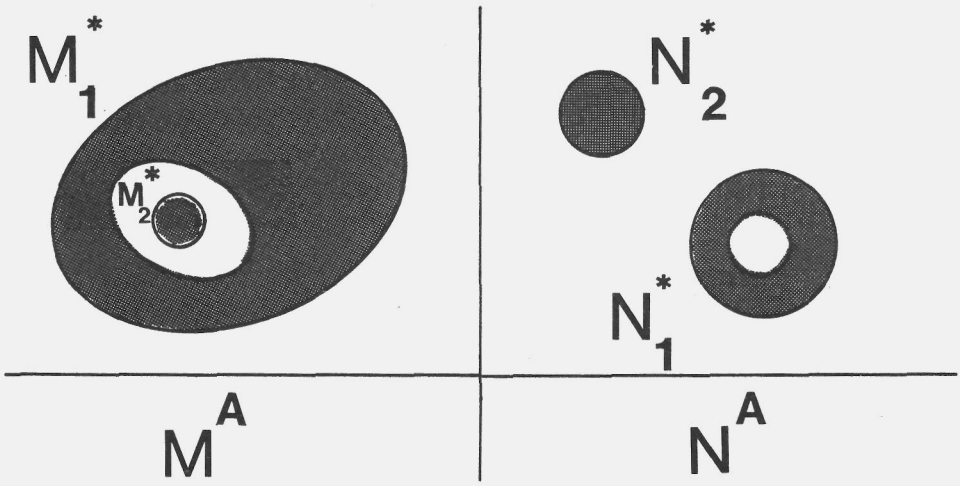

Figure 9. Example of two subcomplexes that cannot be distinguished by their homology alone.

concatenation of several districts) scale.

First we studied the simultaneous functional order in a district as a representation of the local geometrical order in the underlying detector array. We showed how a natural dimension can be computed for a district with a lattice order. It was found that a partial order relation was sufficient to define a functional analogue of the metrical betweenness relation. A functional betweenness relation for a set of three neural individuals is easily computed from the functional (partial) order by checking the (set) inclusion relations of the hulls of the three different pairs of individuals that can be formed from this set. We demonstrated that the existence of detection-thresholds and certain characteristics of the spatial- and aperture size-distributions of the detectors may give rise to a simultaneous functional order in a nervous net that is (at least at a local scale) no correct representation of the geometry of the underlying detector array. We indicated that the resulting functional order in a nervous net will also depend on the constraints of the environment in which the underlying detector array resides. This environmental dependency will be extensively studied in a companion paper (Part IV).

We presented an algorithm that constructs an abstract geometrical (PCW-) complex using certain subsets of a series of concatenated lattice orders (districts) within a modality. The algebraic structure of such a complex reflects the topological and geometrical structure of the underlying detector space. Combinatorial invariants that specify the homology of a complex can be obtained from simple operations on its coincidence scheme. Thus, it is in principle possible that the geometry of the detector array has an objective existence for the neural system itself.

When the functional order in a nervous net has been identified with an abstract geometrical complex it is possible to relate its subcomplexes to regions of the neural network that correspond to segments of the underlying detector array. When a stimulus pattern is projected on the detector array (the detectors contained in) certain segments of this array will activate their corresponding subcomplexes. We showed how the homology of the activated subcomplexes can be computed from their coincidence

schemes by simple combinatorial operations. Thus, the topology of stimulus projections may be objectively represented in the simultaneous activity in a neural net.

The algorithms we used to construct a simultaneous functional order in a nervous net proceed from purely functional (covariance- or concidence-) relations that are objectively present in the signal activities of the neural elements. In this view a diffuse somatotopy cannot destroy the functional order in the nervous net. Our results demonstrate that the dimension and the cohesion of a modality, and even the homology of regions of simultaneous activity within a modality, may have an objective existence in the simultaneous functional order of the collection of nervous elements that define that modality. Thus there is no need to resort to "reconstructions" of stimulus projections in the central nervous system. Moreover, such "reconstructions" or somatotopic mappings can only be noted by external observers but have no intrinsic meaning (inherent order) to the neural system itself.

The resulting functional order in a nervous net encodes the constraints on its simultaneous signal actvity. As far as the system is concerned these constraints are a datum. However, an external observer can point out causes for the constraints. In two companion papers we will study the resulting simultaneous functional order in a nervous net both as a function of the physical constraints of the neural system (Part III) and as a function of environmental constraints (Part IV).

References.

Agoston, M.K. (1976) Algebraic topology (A first course). Marcel Dekker. New York, Basel.

Alexandroff, P. (1935) Topologie. Verlag von Julius Springer. Berlin.

Henle, M. (1977) A combinatorial introduction to topology. W.H.Freeman and Company. San Francisco.

Hilton, P.J. and Wylie, S. (1965) Homology theory. An introduction to algebraic topology. Cambridge University Press. London, New York.

Huntington, E.V. (1913) A set of postulates for abstract geometry, expressed in terms of the simple relation of inclusion. Math. Ann. 73, 522-559.

Jänich, K. (1980) Topologie. Springer Verlag. Berlin, New York.

Koenderink, J.J. (1984a) Simultaneous order in nervous nets from a functional standpoint. Biol. Cybern. 50, 35-41.

Koenderink, J.J. (1984b) Geometrical structures determined by the functional order in nervous nets. Biol. Cybern. 50, 43-50.

Koenderink, J.J. (1984c) The concept of local sign. In: Limits in perception. Eds. Doorn, A.J. van, Grind, W.A. van de and Koenderink, J.J. VNU Science Press, Utrecht, 495-547.

Lundell, A.T. and Weingram, S. (1969) The topology of CW complexes. New York, Cincinnati, Toronto, London, Melbourne: Van Nostrand Reinhold Company.

Toet, A., Blom, J. and Koenderink, J.J. (1987) The construction of a simultaneous functional order in nervous systems. I. Relevance of signal covariances and signal coincidences in the construction of a functional order. Submitted to Biol. Cybern.

CHAPTER I.3.

The construction of a simultaneous functional order in nervous systems.

III. The influence of physical constraints on the resulting functional order.

Abstract.

The signal activity in a neural net will be constrained both by its physical structure and by environmental constraints. By monitoring its signal activity a neural system can build up a simultaneous functional order that encodes these constraints. We have previously (Part I) presented two models that construct a simultaneous functional order in a collection of neural elements using either signal-covariances or signal-coincidences. In this paper we present the results of simulation experiments that were performed to study the influence of the physical constraints of a neural system on the simultaneous functional order produced by both models. In the simulation experiments we used a one-dimensional detector array. We delineate the physical constraints such an array has to satisfy in order to induce a functional order relation that allows an isomorphism with a geometrical order. We show that for an appropriate choice of the system parameters both models can produce a simultaneous functional order with sufficient internal coherence to allow isomorphisms with a triangulation. In this case the dimensionality and the coherence of the detector array are objectively available to the system itself.

1. Introduction.

In a previous paper (Part I) we presented two models for the construction of a simultaneous functional order in nervous nets. The algorithms proceed from respectively the signal-covariances or signal-coincidences in a neural net. This cross-correlation- or coincidence-structure is objectively available to the neural system itself. We have previously (Part II) shown how the resulting functional order in a nervous net may be related to the geometry of the underlying detector array. In particular, we presented an algorithm to construct an abstract geometrical complex from this functional order (Part II). If the neural net has sufficient internal coherence the algebraic structure of such an abstract complex reflects the topological and geometrical structure of the underlying detector array. In this view the cohesion and the dimensionality of a modality result from the constraints put by the anatomy on the simultaneous activity in the neural net. One may say that the functional order encodes the physical constraints (e.g. the geometry of the detector distribution, detector-activation thresholds, correlation- or coincidence- detection thresholds etc.) of the neural system. As far as the system is concerned its constraints are a datum (which it can only assess by monitoring its signal activity). However, an external observer can point out causes for the constraints. In this paper we study for both (coincidence- and covariance-) models how the resulting simultaneous functional order depends on the physical constraints of the neural system.

2. The geometry of the detector array.

For the moment we will assume that the signal-covariances or signal-coincidences in a neural net are solely induced by the geometrical structure of its underlying detector array. (In Part IV of this series we will study constraints on the signal activity that arise due to constraints on the inherent structure of the stimulus patterns.) Both in the covariance- and in the coincidence-model we assume that there is a relevant functional relation between two neural elements (i.e. their

signal activities are assumed to have a significant correlation- or coincidence-relation) when the ratio of the geometrical overlap of their corresponding detector units and the square root of the product of their aperture sizes exceeds some predetermined fraction or threshold value.

We demand that the resulting simultaneous order presents a correct functional representation (see Part II) of the geometry of the detector array. This can only be achieved when the detector units themselves and their intersections are connected regions. We therefore demand that the detector units in $\mathbf{R}^n$ form compact, convex subsets of $\mathbf{R}^n$. An obvious choice is to adopt the hyperspheres of $\mathbf{R}^n$ together with their overlap relations as a model for the detector array (Koenderink, 1984). Huntington (1913) has shown that in two dimensions such a (disc) model is isomorphic with the Euclidian plane. Since nervous systems are inherently discrete and finite we have to use a discrete approximation of the continuous hypersphere model. A finite and discrete model with an overlap structure similar to the hypersphere model can be obtained by defining the individuals as equivalence classes of hyperspheres, containing the same subsets of a discrete collection of points in $\mathbf{R}^n$ (Koenderink, 1984).

We adopted a distribution for the position and size of detector units that is compatible with the known neuroanatomy of the retina and the geniculostriate system (Koenderink and van Doorn, 1978). In our model, detector units are n-dimensional hyperspheres. The radius of the hyperspheres is exponentially distributed between a minimum ($r_{min}=r_1$) and maximum ($r_{max}= r_N$) value and is quantized in N intervals:

$r_i = a.e^{b.i}$ (a and b proportionality constants, i = 1, ... , N).

The density function according to which the hyperspheres of radius r_i were distributed was chosen proportional to r_i^{-n}. The finite dimensions (or outer scale) of the detector array, as represented in our simulation program, necessarily introduce inhomogenities in the distribution of the radii of the hyperspheres. Because they cannot extend over the boundaries of the detector array, larger spheres have to be located nearer to the centre of this array. We are mainly interested in the dependency of the internal coherence of the resulting simultaneous functional order in the neural network on the inner scale parameters of the underlying detector array (namely the spatial- and aperture scale-distribution of the detector

units). Therefore, we eliminated the outer scale dependency by regarding the detector array as periodically extended. In this case, there are no restrictions on the possible positions of the larger detector units. To prevent two-sided overlap of detector units the radius length of the largest hypersphere in our model was always chosen smaller than 1/4 of the smallest dimension of the detector array.

Our particular choice of the distribution functions for the radius length and the density of the hyperspheres, together with the adoption of a periodically extended detector array, result in a distribution with the following properties:

(i) At any location in the detector array many sizes of the detector units are to be found.

(ii) The overlap factor for detector units of the same radius length, defined as detector unit density times detector unit area, is (a) independent of the size of the detector units and (b) everywhere the same.

For the simulation studies we used one dimensional detector arrays. The study of higher dimensional systems proved not feasible at the moment because of (i) the large amount of memory space needed due to the large number of individuals that is needed to produce a system with sufficient internal coherence and (ii) the difficulties in visualizing the results. In case of a one-dimensional system distributions of detector units with a high degree of regularity would have resulted in outcomes of our algorithm that are relatively easy to predict. As we wanted to study the outcome of the algorithm as a function of many different input distributions, a certain degree of randomness in the spatial structure of the input detector array was required. On the other hand, a detector unit distribution was required with enough spatial structure to yield a well-developed simultaneous functional order (i.e. one with sufficient internal coherence). The distribution function we have chosen fulfills all these demands. An additional advantage is its analogy to receptive field distributions found in neuroanatomy and electrophysiology.

2.1. Influence of detector density on the resulting simultaneous functional order.

Figure 1 shows the number of individuals in the posets I_* (produced by the covariance model; Fig. 1a) and I_*' (produced by the coincidence model; Fig. 1b) and the number of functional individuals in the lattice orders resulting after applying neuron-merging or neuron-recruitment to both posets, as a function of the detector unit density and for a one-dimensional periodical detector array. In the coincidence model we used the option to compute the coincidence relations from the geometrical lay-out of the detector array. The reader is referred to Part I for matters of terminology and method.

In this simulation experiment the following parameter values were adopted. The minimum radius value was 10 (arbitrary) units, the maximum radius value 400 units. Radius values were quantized in 8 intervals. The length of the detector array was 1600 units. The smallest detector units were distributed without any spatial overlap and such that the detector array is completely covered (i.e. each point in the detector space coincides with exactly one detector unit) by the smallest detector units when their number is 80. As the length of the detector array remained constant, the number of detector units is a measure for their spatial density. The covariance detection threshold T_v and the coincidence detection threshold T_i were both chosen equal to 0. The threshold area A_t used in the assessment of functional distinctness in the coincidence model was chosen equal to 4 (arbitrary) units. (The motivation for this choice will become apparent in section 3.2.)

The spatial detector configurations used were generated according to the forementioned detector distribution function. A denser distribution was generated from a less dense one by adding (according to the distribution function) additional detector units. To enable the comparison of both models they were always applied to the same (spatial) detector configurations.

When there are only a few detector units both the covariance- and the coincidence-model produce a poset (respectively I_* and I_*') with not much internal coherence. Because of the lack of structure (i.e. of geometrical

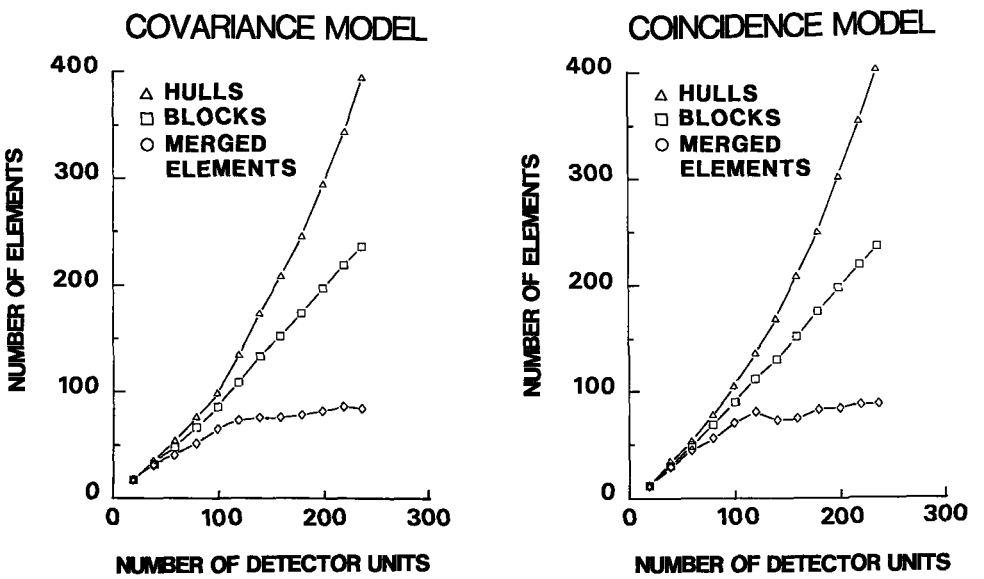

Figure 1. The number of elements in the initial poset I_* **(a)** or I'_* **(b)** and the number of lattice individuals after application of the neuron-merging and the neuron-recruitment routine are shown for both the covariance-model **(a)** and the coincidence-model **(b)**.

overlap) in the detector array many individuals will be functionally equivalent in the coincidence model. These elements are therefore lumped in blocks. Thus the coincidence model produces only a small number of different blocks when the total number of detector units is small. The covariance model can only lump elements that correspond to detector units that have a mutual geometrical overlap. As the detector units with the smallest radius length have no mutual geometrical overlap in our models, no two individuals corresponding to these smallest units will be lumped in the same block by the covariance model. For instance, when there are 39 detector units in the distribution from Figure 1, there are 36 blocks (functional individuals) in the covariance model (Fig. 1a) and 30 in the coincidence model (Fig. 1b).

For an increasing number of detector units the number of functional individuals produced by both models will generally also increase. This is due to the fact that the increasing complexity of the geometrical overlap situation of the detector units results in an increased complexity of the correlation- or coincidence-structure in the signal activities of the neural elements corresponding with these units. Thus, the mean number of interrelations per individual (the coherence) in the resulting poset I_* or I_*' will increase with the number of detector units. The system will therefore have a larger chance to establish the functional identity of (to differentiate between) its constituting elements. For instance, consider the detector distribution used in Figure 1. The distribution consists of 236 detector units. The detector array was completely covered with the detector units of the smallest radius length. In this case Figs. 1a and 1b show that both models produce posets consisting of respectively 236 and 235 blocks of functional individuals.

Because their internal coherence increases with an increase in the number of detector units, the structure of the posets produced by both models will generally get further removed from a lattice structure. Figure 1 shows that the neuron merging procedure reacts to this situation by lumping so many individuals of the poset that the number of individuals in the resulting lattice order is nearly independent of the number of detector units for distributions consisting of more than approximately 120 detector units. In case of the distribution used in the experiment that

results in Figure 1, the number of lattice individuals is approximately 80 when there are more than 120 detector units. Therefore, the total number of individuals in the resulting lattice order is nearly equal to the maximum number of smallest detector units (which is 80 in this case). This means that a lot of structure is lost in the functional order; many elements of the poset have been merged in this case.

The neuron recruitment routine reacts differently to an increasing number of detector units (to increasing detector unit density). As the total number of interrelations in a poset increases, the total number of hulls will also increase. The neuron recruitment routine will restore a lattice order by adding those hulls which are not yet represented in the poset as an individual. Therefore, the structure of the lattice will increase markedly with an increasing number of detector units. In Figure 1a and 1b we see that the number of hulls increases steadily with the number of detector units for distributions consisting of more than 120 detector units. Thus the coherence of the poset increases markedly over the same range. (As we noted before, the number of individuals that remain after the neuron-merging process is nearly constant over this range.)

In the sequel we will only study lattice orders obtained with the neuron recruitment routine. This routine provides a functional order with more internal coherence than the merging routine. Thus, there is a larger chance that the resulting functional order will be a correct representation of the geometrical order in the underlying detector array (i.e. that isomorphisms can be constructed between the activity in a neural net and the geometry of the detector array or the geometry of projections of stimulus patterns on the detector array; see Part II for an extensive discussion on this subject).

2.2. Influence of the range of aperture sizes on the resulting simultaneous functional order.

Figure 2 shows the influence of variation of the number of discrete values for the radius length of the detector units on the resulting simultaneous functional order produced by both models. In this experiment

the following parameter values were adopted. The minimum and maximum radius length values were respectively 10 and 300 units. The length of the detector array was 1200 units. A distribution was rejected when the detector array was completely covered by units with a radius length other than the minimal radius length before it had been covered completely by the smallest units themselves (as such a distribution induces a functional order which is an incorrect representation of the geometry of the underlying detector array; see Part II). We used the option to calculate the coincidence structure from the geometrical overlap situation of the detector units. The covariance detection threshold T_v and the coincidence detection threshold T_i were both chosen equal to zero. The threshold area A_t used in the assessment of the functional idenitity of individuals in the coincidence model was chosen equal to 4 units. From the results of the simulation experiments described in section 3.2 it will become apparent that this is a reasonable choice. The results shown in Figure 2 are the mean of a series of 5 different detector unit distributions. As fluctuations in the total number of receptive fields in a distribution might confuse the issue, the number of resulting individuals in the simultaneous functional order is displayed relative to the total number of detector units.

In the **covariance model** "blocks" of functionally identical individuals contain only related individuals (i.e. neural elements that correspond to detector units that have sufficient geometrical overlap). In our model, the smallest detector units (corresponding to the functionally "smallest" individuals or atoms) are distributed so that they have no mutual geometrical overlap. Therefore, the atoms in a district are not related to each other. As a result, a block of functionally identical individuals cannot contain more than one atom. This explains why the relative number of blocks in Figure 2a starts at 1 when the number of intervals for the radius length of the detector units equals 2 (i.e. when there are only two different values possible for the radius length). When there are more than 8 intervals for the radius length, the relative number of blocks drops below 1. This is a result from the fact that the absolute difference between the radius length in two consecutive intervals will decrease with an increasing number of intervals (and for a fixed upper and

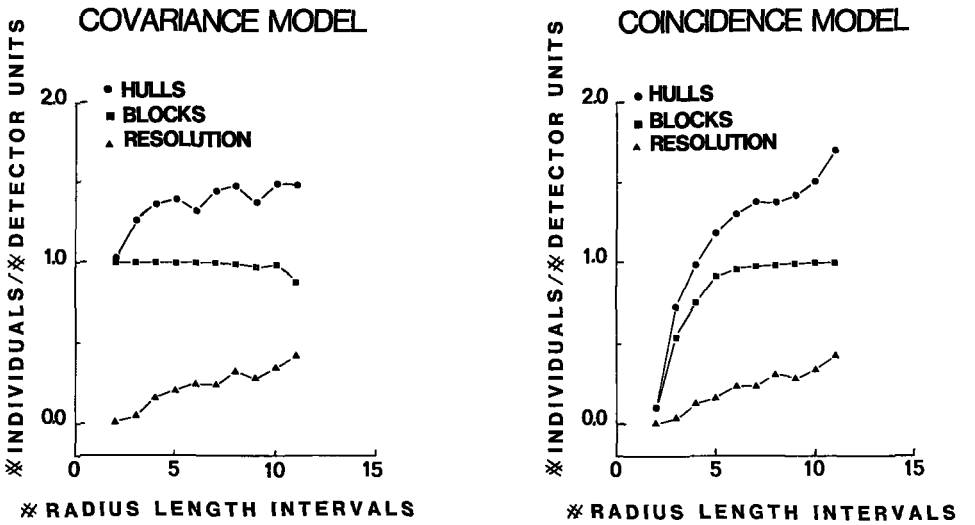

Figure 2. The relative number of poset individuals, the relative number of lattice individuals that remain after application of the neuron-recruitment routine and the resolution measure as a function of the number of radius length intervals used in the detector distribution. The numbers of individuals were taken relative to the number of detector units. **a** shows the results of the covariance-model and **b** for the coincidence-model. The results shown are the mean of a series of 5 different detector unit distributions.

lower bound on the radius length value). Therefore, it will occur more frequently that two detectors from two consecutive intervals (and therefore nearly equal in aperture size) have the same (co-) relations with all other individuals. As a result, more elements will become functionally indistinguisable and will therefore be lumped in blocks. In this case, the total number of blocks may remain fairly constant as the number of detector elements increases. Therefore, the relative number of blocks may even decrease.

When there are only a few discrete radius length intervals the relative number of blocks in the poset relation produced by the **coincidence model** is small (Figure 2b). Suppose there are only detector units of two (largely) different radius values r_{min} and r_{max}. Then the only possible functional inclusion relation that can occur in the coincidence model is that the neural elements corresponding with detector units with a radius length r_{min} are functionally included in those elements that correspond to detector units with a radius length r_{max}. In this case, many elements of low functional order (corresponding to small detector units) may be directly included in one element of higher functional order (corresponding to a large detector unit). Thus, many of the elements of low functional order will be functionally equivalent and will therefore be lumped in a block structure. For a larger number of radius length intervals there is a pronounced drop in the number of functional equivalent elements. This is a result from the increased number of interrelations in the poset or, equivalently, the increased spatial overlap structure in the detector array.

*) Actually, one should study the number of hulls relative to the number of blocks of functional individuals, as we did in Part I. However, the number of blocks is almost equal to the number of detector units in well developed functional orders. This validates the adoption of the number of hulls relative to the number of detector units as an indicator for the internal coherence of the poset. Moreover, this relative standard enables the comparison of the number of hulls and the number of blocks of functional individuals as a function of the number of radius length intervals.

In section 2.1 we noted that the number of hulls increased with the number of detector units for systems consisting of more than 120 detector units (while the number of individuals that results after neuron-merging was nearly constant over the same range). We argued that this increase reflects the increase in the number of interrelations or, equivalently, the increased coherence in the resulting poset. Thus, the number of hulls relative to the number of detector units will be a good indication for the internal coherence of the functional (poset- and lattice-) structure.*). From Figure 2 we see that the relative number of hulls generally increases with an increasing number of intervals for the radius length value. This increase is more pronounced for the coincidence model than for the covariance model. Figure 2b shows a sharp increase in the relative number of hulls produced by the coincidence model up to a number of 7 different radius length intervals. This sharp increase is mainly due to the increase in the relative number of blocks of functional equivalent elements. The less pronounced increase of the relative number of hulls produced by the covariance model (Figure 2a) is partly due to the constancy of the relative number of blocks in this case.

Figure 2 also shows the "resolution" of the simulated neural system as a function of the number of aperture size (radius length) intervals. The "resolution" measure was determined as follows. In each district all possible combinations of three activated atoms were studied. For each of these triples the system had to determine which of the three activated atoms was "in between" the two other activated atoms (see Part II for the definition of the functional betweenness relation). The resolution is now defined as the fraction of the total number of different configurations of three activated atoms for which a "middle atom" could be determined. From Figure 2 we see that the resolution generally increases with an increasing number of aperture size intervals, both for the covariance- and for the coincidence-model. The maximal resolution is about 45% in both models. Note that only a detector array of an extreme regularity may give rise to a functional order that has a resolution of 100%. For the randomly generated detector distributions used in our simulation experiments we cannot expect our models to produce a functional order with a resolution approaching 100%.

As shown in Figure 3, the number of one-dimensional simplices that can be obtained from the functional lattice order produced by both models generally increases as a function of the number of intervals for the radius length of the detector units. The results shown are the mean of 5 different detector distributions. All lattice orders that were produced had 60 atoms. The large standard errors reflect the sensitivity of the triangulation for small variations in the (random) distribution of individuals of low functional order. This is a direct result of the construction of the triangulation, which is such that it selects connected individuals of the lowest functional order in order to preserve as much resolution as possible. For the forementioned distribution conditions and for both models the maximum number of one-dimensional simplices is approximately 70% of the number of atoms. When the number of one-dimensional simplices is equal to the number of atoms we will call the system **optimally connected.**

3. Influence of detection thresholds on the resulting simultaneous functional order.

In Part II we argued that the existence of detection thresholds may result in a functional order of the neural individuals that is not isomorphic to the partial order induced by the geometrical inclusion relation of their corresponding detector units. In this section we will study the resulting functional order in a nervous net for different definitions and as a function of different values of the detection thresholds. We will first compare the covariance model with the coincidence model. To enable this comparison we will use the option to compute the coincidence structure directly from the geometrical overlap structure of the receptive fields. Finally we will study the coincidence structure resulting after a learning stage as a function of different values and for different definitions of the activation thresholds of the detector units.

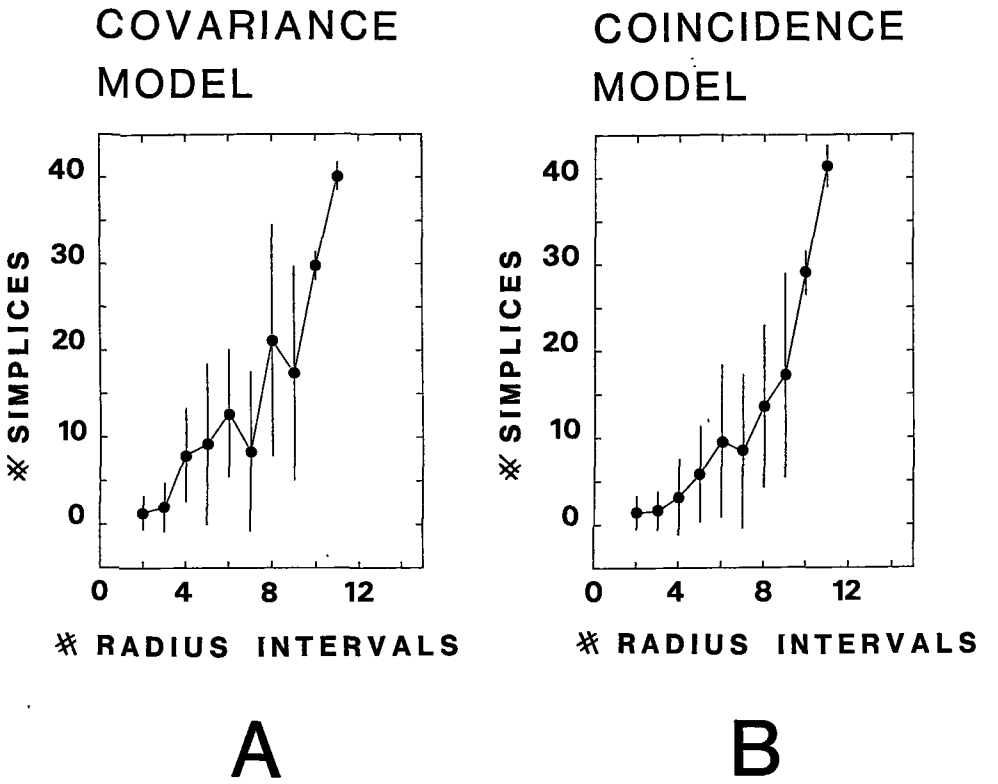

Figure 3. The number of one-dimensional simplices that can be computed from the functional order produced by the covariance-model (a) and the coincidence-model (b) as a function of the number of radius length intervals used in the detector distribution. The results shown are the mean of 5 different detector distributions.

All of the following studies were performed with one particular detector distribution. The following distribution parameter values were adopted. The minimum and maximum radius length values were respectively 10 and 400 units. The radius length values were quantized in 8 intervals. The length of the detector array was 1600 units. These parameters resulted in a distribution with a total number of 186 detector units. In this case the detector array was completely covered by the detector units with the smallest radius length. In each case the neuron-recruitment routine was used.

3.1. Comparison of the influence of the covariance- and the coincidence-detection thresholds in both models.

From the definition of the covariance- (T_v) and coincidence- (T_i) detection thresholds as presented in Part I it follows that we have a "critical" value T_c for these thresholds when they are equal to the root of the ratio of the radii of the smallest and largest detector units that are present in a certain detector distribution, i.e. $T_c = (r_{min}/r_{max})^{\frac{1}{2}}$.

The importance of this critical value is different for both models. We will first consider the coincidence model. For values of T_i smaller than T_c, small variations in the value of T_i will not result in significant changes in the resulting functional inclusion structure. This is a result of the combined effect of the coincidence detection threshold T_i and the threshold area A_t used in the assessment of the functional distinctness of the neural elements (see Part I). Only those neural elements with a coincidence relation that are also functionally distinct will have a functional inclusion (Q'; see Part I) relation. For values of A_t that are not too large compared to the smallest detector units (i.e. not more than approximately $0.5*r_{min}$) the geometrical overlap of two detector units corresponding with two neural elements with a functional inclusion relation Q' yields a value for T_i that is larger than T_c, due to the functional distinctness condition. In this case there is generally more geometrical overlap between the detector units than minimally needed for the existence of a coincidence relation between their corresponding

neural units. As a result small variations in the value of the coincidence detection threshold will have practically no influence on the resulting functional order. If $T > T_c$ the neural elements corresponding with the smallest detector units can no longer have a coincidence relation with those corresponding to the largest units. In this case a geometrical inclusion relation between two detector units no longer guarantees the existence of a coincidence relation between their corresponding neural elements. Therefore, the resulting primitive functional inclusion order Q' may differ from the geometrical inclusion order. In general Q' is not transitive. Transitivity is produced in the coincidence model by the construction of the transitive extension Q" of Q' (see Part I). When $T_i > T_c$ this transitive extension restores a certain fraction of the functional inclusion relations (corresponding to geometrical ones) that are lost due to this coincidence detection threshold.

In the covariance model the critical value of the covariance detection threshold has a less special status. In this model there can also be no covariance relation between the neural elements corresponding with respectively the smallest and the largest detector units when $T_v > T_c$. However, in this model there is a continuous decrease of the number of covariance relations for a continuous increase in the covariance detection threshold (i.e. also over the range of values of T_v below T_c). Because any covariance relation between two neural elements is of importance for the functional order that is produced by this model, any variation in the covariance detection threshold may be reflected in this functional order. Partly because of the use of the transitive extension in the coincidence model, the discrepancy between the two order relations will increase with an increasing value of the covariance- and coincidence-detection thresholds.

The influence of the correlation detection threshold T_v and the coincidence detection threshold T_i on the resulting simultaneous functional order is shown in Figure 4. A_t was chosen equal to 4 in the coincidence model. In the sequel we will show that this is a reasonable choice. In stead of the covariance detection threshold T_v and the coincidence detection threshold T_i we will use the **relative detection threshold** T_r. In case of the covariance model $T_r = T_v/T_c$ and for the

coincidence model $T_r = T_i/T_c$. Figure 4a shows the number of blocks and hulls produced by both models as a function of the value of the relative detection threshold T_r. To show the influence of the transitive extension and the critical character of T_c (i.e. for $T_r = 1$) Figure 4a also shows the number of blocks and hulls before the construction of the transitive extension. Figure 4b represents the number of one-dimensional simplices that can be determined in the lattice order produced by both models. The number of simplices that can be determined before the construction of this extension are also shown in this Figure in order to emphasize the influence of the transitive extension. The number of districts produced by both models is depicted in Figure 4c as a function of the relative detection threshold. Figure 4d shows how the resolution of the functional order produced by both models depends on the relative detection threshold.

Figure 4 shows that the functional order produced by the coincidence model remains unchanged when T_r varies from 0 to 1.25. The covariance model is sensitive for changes in T_r for values of T_r larger than 0.1. As we already noticed, this is a result of the fact that each covariance relation between two neural elements in the covariance-model is of importance for the final functional order relation. The pairwise determined primitive inclusion relations between two neural elements in the coincidence-model are generally attended with so much geometrical overlap between their corresponding detector units that the coincidence detection threshold is amply surpassed. Small variations in this detection threshold may therefore pass unnoticed in the coincidence model.

Figure 4a shows that the number of blocks produced by both models is not sensitive for variations in the relative detection threshold. Only for $T_r = 2.99$ we notice a sharp decrease in the number of blocks produced by the coincidence model. In this case a considerable number of primitive inclusion relations is lost. As a result the number of functionally equivalent elements increases. Thus, the number of blocks decreases in this case. The decreasing number of hulls for larger values of T_r also reflects a progressive loss of functional inclusion relations in the posets I and I'.

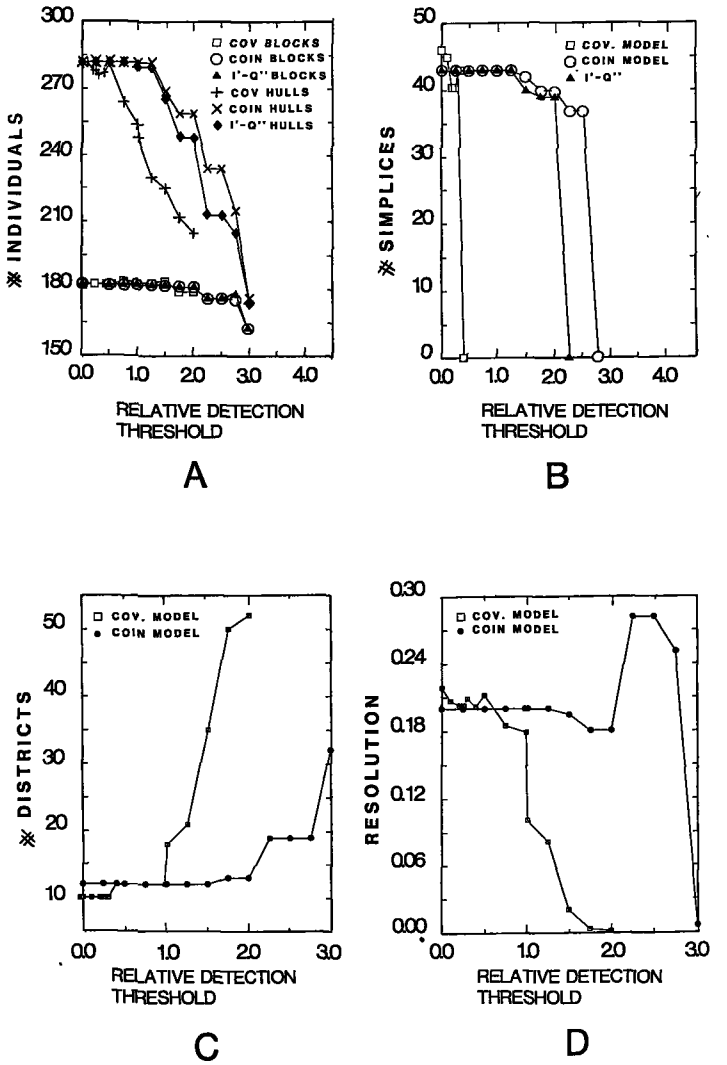

Figure 4. The number of poset- and lattice-individuals (**a**), the number of simplices (**b**), the number of districts (**c**) and the resolution (**d**) of the functional order produced by both models as a function of the relative detection threshold. In all cases the neural recruitment routine was used to produce a lattice order. To indicate the influence of the transitive extension used in the coincidence model, Figures **a** and **b** also show the results that are produced by this model without the use of this extension.

Figure 4a clearly demonstrates the influence of the transitive extension on the resulting functional order produced by the coincidence model. For values of T_r up to 0.99 the number of hulls that can be determined from the functional order, both before and after the construction of the transitive extension, are the same. (Note that the resulting functional order R' is no poset without the construction of the transitive extension Q" as R' need not be transitive in this case.) For values of T_r larger than 1.0 the transitive extension procedure starts reconstructing the functional inclusion relations that are lost due to this detection threshold. As the number of interrelations in the poset increases the number of hulls in the lattice order will generally also increase.

The internal coherence of the resulting functional order relations produced by both models varies with the relative detection threshold. This is reflected in the variation of the number of one-dimensional simplices that can be determined from these relations, as shown in Figure 4b. For the covariance model this decrease is very pronounced. For $T_r = 0.4$ the lack of coherence is already such that no triangulation can be determined. The influence of the transitive extension in the coincidence model is only noticeable for values of T_r larger than 1.25. This is due to the fact that for increasing T_r the first functional inclusion relations to disappear are those between neural elements corresponding with the smallest and the largest detector units. As these relations are generally not used in the construction of the triangulation their disappearance will not be reflected in the number of simplices.

Figure 4c shows a sharp increase in the number of districts produced by the covariance model when the correlation detection threshold value is just above the critical value ($T_r = 1$). As mentioned before, for values of the correlation detection threshold larger than the critical value the functional inclusion relation is no longer a faithful representation of (i.e. is not isomorphic to) the geometrical inclusion relation. In this case, geometrical inclusions between the smallest and largest detector units can no longer be represented as functional inclusions between their corresponding neural elements. This causes the sharp increase in the number of districts near $T_r = 1$. For increasing values of T_r (> 1) the

number of districts produced by the covariance model generally increases (Figure 4c) whereas the resolution generally decreases (for $T_r > 0.5$; Figure 4d). This is a direct result of the decreasing internal coherence of the resulting functional order. When there are fewer functional inclusion relations more elements of lower functional order may become maximal elements. Therefore, the number of districts increases. As a result, the resolution (defined as the total number of different configurations of three activated atoms for which a "middle atom" can be determined; see section 2.2) decreases. The sudden increase in resolution for the coincidence model near $T_r = 2.25$ is merely a result from a change in the local lattice structure and is not typical. For correlation detection threshold values smaller than the critical value there is hardly any variation of the resolution with the relative detection threshold value. For this range of threshold values a geometrical inclusion relation between the smallest and largest detectors in a distribution may result in a functional inclusion relation. Over this range a small variation in the correlation detection threshold value will not affect the resolution. This is due to the fact that the number of districts is constant over this range and the functional inclusion relations between neural elements corresponding to detector units of different sizes and with geometrical inclusion relations are all maintained. Only those functional interrelations that are induced by large detector units with a mutual overlap area that is so small that the induced correlation in their signal activities is near detection threshold may disappear when the value of this threshold increases. As these interrelations were not relevant for the determination of the resolution measure anyway (see the definition of this measure in Part II), the resolution will not be affected by their elimination.

3.2. Influence of the functional distinctness condition on the resulting functional order produced by the coincidence model.

Figure 5 shows the number of blocks and hulls (Fig. 5a), the number of simplices (Fig. 5b), the number of districts (Fig. 5c) and the resolution (Fig. 5d) of the simultaneous functional order produced by the coincidence model as a function of the threshold area A_t that is used in the computational assessment of the functional distinctness of the neural elements.

From Figure 5a we see that the number of hulls for $A_t = 1$ is much smaller than for $2 \leq A_t \leq 6$. Figure 5b shows that no triangulation can be computed when $A_t = 1$, while there are 43 one-dimensional simplices for $2 \leq A_t \leq 6$. Figure 5d shows that the resolution of the functional order is also lower for $A_t = 1$ than for $2 \leq A_t \leq 6$. This lack of internal coherence of the functional order for $A_t = 1$ is due to the fact that the geometrical tolerance corresponding with the functional distinctness criterium is less than one unit of length (or one-dimensional area) in the detector space. For example, when $A_t = 1$ there can be no functional inclusion between a large and a small detector unit when the smaller one protrudes one or more length units outside the larger one.

From Figure 5 the functional order appears to be nearly independent for variations in A_t for $2 \leq A_t \leq 6$. For $6 < A_t \leq 10$ the number of blocks and hulls decreases with increasing A_t (Fig. 5a). This can partly be explained as follows. In our distribution the radius length of the smallest detector units is 10 length units and the radius length of the next larger detector units is 17 length units. Thus, when the centers of a smallest detector unit and one of the class of next larger ones coincide and when $A_t > 7$ a primitive inclusion relation cannot be determined for these elements. When the neural elements corresponding with these two detector units have the same relations with all other elements (and are therefore functionally equivalent) they will be lumped in a block. Thus, the number of blocks decreases. In general it will be the case that progressively less geometrical inclusion relations will be represented as functional inclusion relations for progressively larger values of A_t.

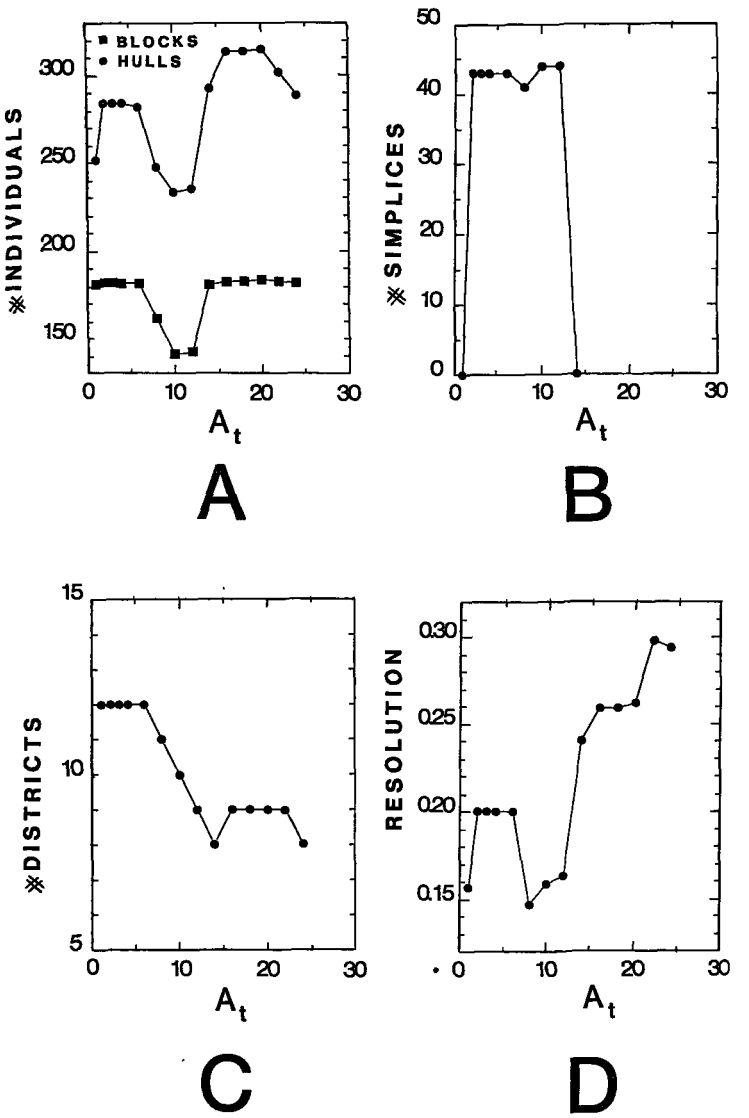

Figure 5. The number of poset- and lattice-individuals (**a**), the number of simplices (**b**), the number of districts (**c**) and the resolution (**d**) of the functional order produced by the coincidence-model as a function of the threshold area A_t used in the geometrical assessment of the functional distinctness of the neural elements. In all cases the neural recruitment routine was used to produce a lattice order.

The number of blocks and hulls increases with increasing A_t for $12 < A_t < 16$ (Fig. 5a). In the sequel we will speak of a **geometrical overlap situation** when two detectors have a certain area in common, while it is not the case that one is geometrically included in the other. For $A_t = 16$ the number of hulls is larger than the number that is found over the range $2 < A_t < 6$. For progressively larger values of A_t the primitive functional inclusion relation will represent progressively more geometrical overlap situations and progressively less geometrical inclusion relations as functional inclusion relations. For $A_t > 20$ the number of hulls decreases. This reflects the fact that progressively less geometrical inclusion- and overlap-relations between detector units can give rise to functional inclusion relations between neural elements.

Figure 5b shows the number of one-dimensional simplices as a function of A_t. For $2 < A_t < 12$ the functional order has sufficient internal coherence for the construction of a triangulation. The fact that progressively more geometrical overlap situations and progressively less geometrical inclusion relations are represented as functional inclusion relations for larger values of A_t (thereby yielding an incorrect functional representation of the geometrical order of the underlying detector array) is also reflected in the fact that no triangulation can be determined for $A_t > 13$.

Figure 5c represents the number of districts as a function of A_t. The decrease in the number of districts for $8 < A_t < 14$ is due to the increased number of geometrical overlap relations that give rise to functional inclusion relations. Because of this increase in the number of functional inclusion relations there is a decrease in the number of maximal elements (or districts). For $14 < A_t < 22$ there is no further decrease because the number of geometrical inclusion relations that can no longer give rise to functional inclusion relations increases over this range.

Because of the decrease in the number of blocks and hulls for $6 < A_t < 8$ the resolution also decreases over this range (Figure 5d). For $A_t > 8$ the resolution increases. However, this is merely a quasi-resolution, as the functional order in the neural net can no longer be a correct representation of the geometrical order of the underlying detector array.

Note that Figures 5a-d merely represent a single detector distribution. As demonstrated in this section the resulting functional order is highly dependent on the specific geometrical overlap situation in the underlying detector array. However, our simulation experiments showed that detector distributions that are different from the one used here all have the same global characteristics. Thus, we may regard the results that are presented in this section as representative for the influence of the threshold A_t on the functional order produced by the coincidence model.

3.3. Influence of the detector excitation thresholds on the resulting functional order produced by the coincidence model.

In this section we will study the influence of the detector excitation thresholds on the primitive inclusion relation Q' that is established during a learning stage. The stimuli presented to the detector array in its learning phase consisted of non-zero valued segments with a diameter of 10 units (i.e. a radius length of 5 units). The maximum fraction of the detector array that was covered by these segments (i.e. the segment density) was 0.25. The learning stage was ended when the primitive (pairwise-determined) inclusion relation Q' remains unaltered for 750 consecutive stimulus presentations. (For matters of terminology and details of the method we refer to Part I section 2.2.)

From neurophysiology it is known that most detectors have an absolute detection threshold for low levels of stimulus intensity, whereas they show a relative detection threshold for high levels of stimulus intensity. For reasons of simplicity we will assume that all detectors in our model have either an absolute detection threshold A_a or a relative detection threshold A_r. In reality some parts of a detector array may function according to an absolute detection threshold while other parts perform with a relative detection threshold due to local stimulus intensity differences. Moreover, in practice there will be an intermediary stage of transition between the absolute and relative detection thresholds.

First we will consider the number of blocks, hulls, simplices, districts and the resolution as a function of the absolute detection

threshold A_a (Figure 6). In our model the absolute detection threshold is represented by a certain minimal area of a detector unit that has to be covered with non-zero valued image segments in order to activate this detector unit. In this study the upper limit of A_a will be 10 length units. For larger values of A_a the system can no longer detect isolated image segments (which were of length 10 in this case). This will severely impair the learning process.

We can not expect large variations in the entities represented in Figure 6 as a function of A_a for values of A_a smaller than 10 length units. For this range of A_a values a detector unit may still be activated by isolated image segments that extend over its boundary (that are not geometrically included in this unit). Thus, a number of geometrical overlap situations (that are not equal to geometrical inclusion relations) will give rise to functional inclusion relations. Therefore, small variations in the value of A_a may result in minor changes in the primitive functional inclusion relation due to changes in the functional representation of certain geometrical overlap situations. Figures 6a-d show that there is indeed no large variation in the depicted entities as a function of A_a for $A_a < 6$. For $7 < A_a < 9$ only the resolution decreases markedly while the other entities do not change much. For these values of the absolute detection threshold the resulting functional order will generally be no longer a correct representation of the geometrical inclusion order. For instance, in the example of Figure 6 the model produces a district that contains 75 of the total number of 80 atoms, which is geometrically impossible. In this case there are only 2000 correct determinations of a betweenness relation for 67000 presented test-patterns. Thus, in this case absolute threshold values in the range $7 < A_a < 9$ cause a large decrease of the resolution of the system. For $A_a = 10$ we notice a large decrease of the number of hulls (Fig. 6a) and the number of one-dimensional simplices (Fig. 6b). This reflects the decreasing similarity between the functional inclusion relation of the neural elements and the geometrical inclusion relation of the detector units.

Figure 7 shows the number of blocks, hulls, simplices, districts and the resolution as a function of the relative detection threshold A_r. In our model a relative detection threshold corresponds to a certain constant

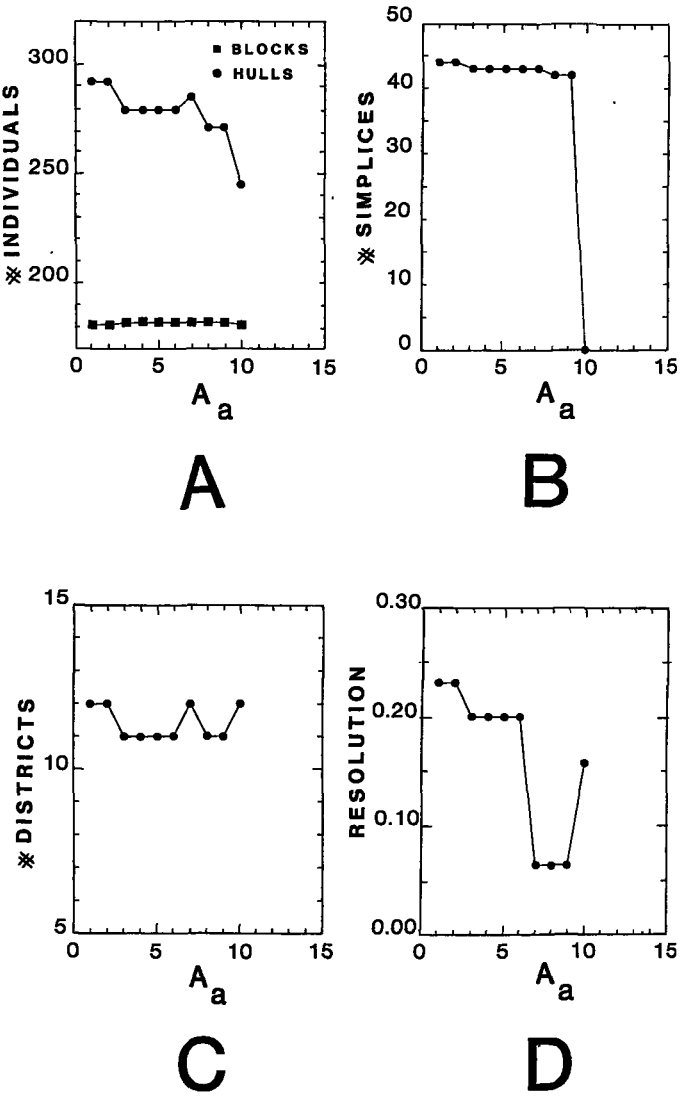

Figure 6. The number of poset- and lattice-individuals (**a**), the number of simplices (**b**), the number of districts (**c**) and the resolution (**d**) of the functional order produced by the coincidence-model as a function of the absolute detection threshold area A_a. In all cases the neural recruitment routine was used to produce a lattice order.

fraction of a detector unit that has to be covered by non-zero valued image segments in order to elicit a response. We assume that this fraction is independent of the radius length of the detector units.

In case of a relative activation threshold a small detector unit may be activated without the simultaneous activation of a larger detector in which the former is geometrically included. Thus, a relative activation threshold can give rise to a large discrepancy between the geometrical inclusion order of the detector units and the functional inclusion order of their corresponding neural elements. In fact, we expect that the functional order shows a dependency on the relative activation threshold of the detectors that is similar to its dependency on the coincidence-detection threshold as used in the geometrical computation of the functional order (see section 3.1). For $A_r = 0.0125$ an isolated image segment can no longer activate the largest detector units (with a radius length of 400). Thus, we expect a loss of internal coherence in the functional order for values of A_r near to 0.0125.

The results depicted in Figure 7 show indeed some similarities with those of the coincidence model represented in Figure 4. The functional order is indeed independent of A_r for $A_r \leq 0.010$. This corresponds well with the theoretical critical value of 0.0125. The results indicate a loss of internal coherence in the functional order for larger values of A_r. The changes in the functional order due to variations in the relative activation threshold occur rather sudden. It appears that small changes in A_r can cause large changes in the functional order. The low number of one-dimensional simplices for $0.021 \leq A_r \leq 0.025$ is due to the low degree of internal coherence of the largest district (i.e. the district with the largest number of atoms). The maximal element that determines this district also acts as a one-dimensional simplex.

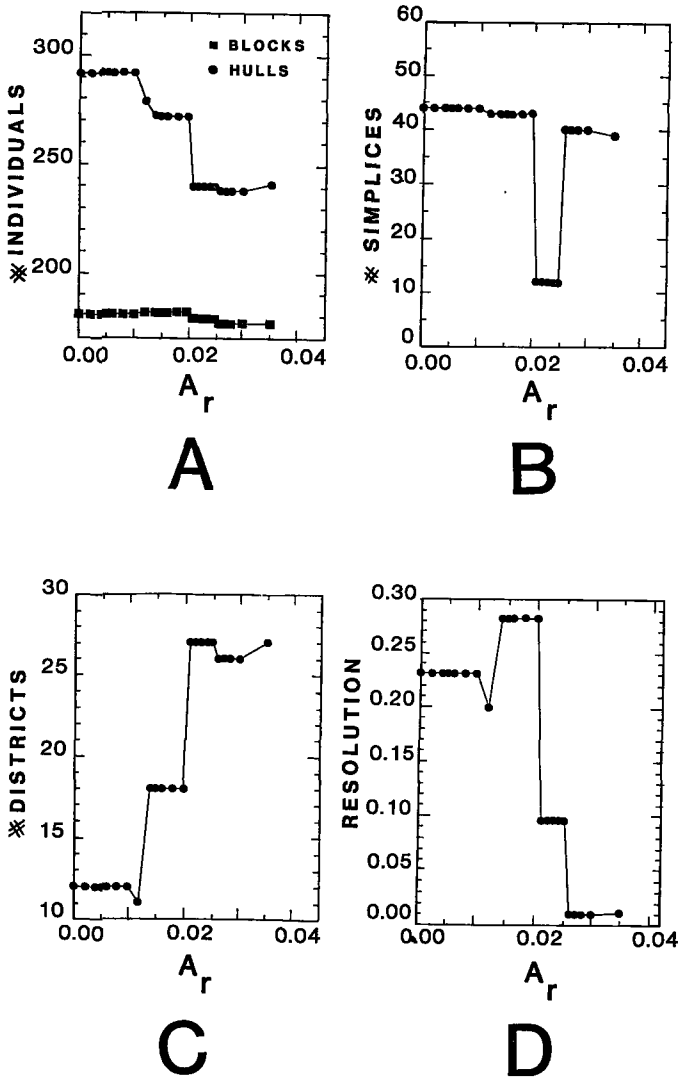

Figure 7. The number of poset- and lattice-individuals (**a**), the number of simplices (**b**), the number of districts (**c**) and the resolution (**d**) of the functional order produced by the coincidence-model after a learning stage as a function of the relative detection threshold area A_r. In all cases the neural recruitment routine was used to produce a lattice order.

4. Conclusions.

We have previously argued (Part I) that the simultaneous functional order in a nervous net encodes the constraints on its simultaneous signal activity. In this paper we have studied the functional order that can be produced in a collection of neural elements by respectively the covariance- and the coincidence-model. In particular, we studied the influence the physical constraints of a neural system have on the resulting functional order produced by these models. To rule out the influence of environmental constraints (which will be subjected to an extensive study in Part IV), we assumed that there is no systematic inherent order in the spatial structure of the stimulus patterns. In our simulation experiments we used a one dimensional detector array that was periodically extended. We chose a detector distribution that is compatible with the known neuroanatomy of the retina and the geniculostriate system.

The results of our simulation experiments show that both models generally produce a functional order relation with a large degree of internal coherence when:

(i) the detector distribution is relatively dense, or, equivalently, when
there is a reasonable number of intervals for the radius length of the detector units

(ii) the signal correlation detection thresholds and the activation thresholds have appropriate values.

The coincidence model is relatively stable for (i.e. there are no significant changes in the studied entities with) small variations in (i) the relative coincidence detection threshold T_r (up to $T_r = 1.25$) and (ii) the threshold area A_t (for $2 \leq A_t \leq 6$). The covariance model is nearly always sensitive to small changes in the relative covariance detection threshold. For $T_r = 0$ the functional order relations produced by both models are very similar. For $T_r \gg 1$ both models produce relations with a low degree of internal coherence. However, this loss of structure in the functional order relation does not introduce extra incorrect functional representations of the underlying geometry. This is due to the fact that an increase in the detection threshold in this range only causes

the elimination of existing functional interrelations, and not the creation of new ones. There is an optimum range of values for the threshold area A_t that is used in the geometrical assessment of the functional distinctness condition in the coincidence model. Both small and large values of this threshold area give rise to functional order relations which are an incorrect representation of the geometry of the underlying detector array.

The functional order produced by the coincidence model after a learning stage is sensitive for variations in the absolute or relative detection thresholds. This is largely due to the fact that this model determines a pairwise primitive functional inclusion relation on the basis of single stimulus presentations. A learning-procedure that uses the mean of a number of consecutive stimulus presentations to determine this relation will yield results that reflect the relative size of the aperture area of the detector units. Thus, the adoption of such a procedure will probably produce results that are comparable to those that were obtained with the option to compute the functional inclusion relation from the geometrical overlap structure of the detector array (and that were less sensitive to changes in the physical constraints of the neural net).

In this paper we have shown that the covariance- and the coincidence-model are both perfectly capable of producing a simultaneous functional order in a collection of neural elements proceeding from purely functional relations which are objectively available to the neural system itself. We have delineated the physical constraints a one-dimensional detector array has to satisfy in order to induce a functional order relation that allows an isomorphism with a geometrical order. Moreover, we have shown that it is perfectly feasible to compute triangulations from the resulting functional order when it has a sufficient degree of internal coherence. Thus, the dimensionality and the cohesion of the detector array is objectively present in the signal activity in the neural net and it exists independently of an external observer's description of the spatial lay-out of this array. The degree to which the functional order is a faithful representation of the geometry of the underlying detector array depends on the exact choice of the system parameters.

References.

Huntington, E.V. (1913) A set of postulates for abstract geometry, expressed in terms of the simple relation of inclusion. Math. Ann. 73, 522-559.

Koenderink, J.J. (1984) Geometrical structures determined by the functional order in nervous nets. Biol. Cybern. 50, 43-50.

Koenderink, J.J. and van Doorn, A.J. (1978) Visual detection of spatial contrast; influence of location in the visual field, target extent and illuminance level. Biol. Cybern. 30, 157-167.

Toet, A., Blom, J. and Koenderink, J.J. (1987) The construction of a simultaneous functional order in nervous systems. I. Relevance of signal covariances and signal coincidences in the construction of a functional order. Submitted to Biol. Cybern.

Toet, A., Blom, J. and Koenderink, J.J. (1987) The construction of a simultaneous functional order in nervous systems. II. Computing geometrical structures. Submitted to Biol. Cybern.

CHAPTER I.4.

The construction of a simultaneous functional order in nervous systems.

IV. The influence of environmental constraints on the resulting functional order.

Abstract.

In a previous paper (Part I) we introduced a model that constructs a simultaneous functional order in a set of neural elements by monitoring the coincidences in their signal activities (the so-called **coincidence-model**). The simultaneous signal activity in a neural net will be constrained both by its physical restrictions and by environmental constraints. We have previously studied the influence of the physical constraints of a neural net on the resulting functional order (Part III). In this paper we present the results of simulation experiments that were performed to study the influence of environmental constraints on the resulting functional order in a set of neural elements corresponding to a one-dimensional detector array. We show that the coincidence-model produces a functional order that encodes the physical constraints of the environment. Moreover, we demonstrate that the signal activity in the neural net (the "perceptions") can be related to events in the outer world. We provide some examples to demonstrate that our model may prove useful to gain insight into certain developmental disorders.

1. Introduction.

Although the brain is to an important degree specified by genetic and developmental processes, there is a substantial amount of evidence that the patterns of interconnections between neurons also depend upon experience (i.e. E.R.Kandel, 1985a,b). For instance, it has been shown that innate mechanisms endow the vertebrate visual system with highly specific connections, while visual experience is necessary for their maintenance and full development (e.g. Hirsch and Leventhal, 1978; Wiesel, 1982).

It appears that the development of the vertebrate nervous system consists of both progressive and regressive events. The progressive phenomena (so termed because of their essentially additive character) include the proliferation of cells and their interconnections. The regressive events include cell death and the selective elimination of synaptic connections, which are both widespread and substantial during vertebrate neurogenesis (Cowan et al., 1984). Thus, it is at least feasible that modifications in the structure of the environment may be reflected in the brain structure by changes in the number of its neural elements and the number or efficacy of their corresponding synapses.

The influence of the environment on the brain varies with age. The period of highest susceptibility is probably different for each specific psychophysical function (Harwerth et al., 1986). Abnormal environmental experience or patterns of stimulation usually have more pronounced effects at early stages of development than at later ones. For instance, deprivation experiments demonstrate that neural connections can be modulated by environmental influences during a critical period of postnatal development (e.g. Blakemore and Cooper, 1970; Hirsch and Spinelli, 1970; Pettigrew and Freeman, 1973; Stryker et al., 1978; for a comprehensive review of the literature see Movshon and van Sluyters, 1982). However, it has been demonstrated that even well into adult life the vertebrate brain retains sufficient plasticity to modify its structure in response to changes in nutrition or environmental stimulation (e.g. Bedi, 1986; Paton and Nottebohm, 1984).

The plasticity or modifiability of neural connections together with electrophysiologically determined retinotopic, somatotopic and tonotopic projections in the primary sensory areas has led to the development of self-organizing neural networks that produce topologically correct maps of structured signal distributions in the outside world (e.g. Amari, 1985; Kohonen, 1982). However, it has been argued that such orders can only be noted by external observers and have therefore no objective existence for the neural system itself (Koenderink, 1984).

In a previous paper (Part I; Toet et al., 1987) we introduced two models for the construction of a simultaneous functional order in nervous systems. The models proceed from the signal-covariances or signal-coincidences in a neural net. These relations are purely functional and therefore objectively available to the system itself. We showed how the resulting functional order can be related to the geometry of a detector array and to the topology of projections of stimulus patterns on that array (Part II). Simulation experiments have yielded the physical constraints a neural net has to satisfy in order to induce a functional order relation that has sufficient internal coherence to allow an isomorphism with a geometrical order (Part III).

The coincidence model proceeds from a neural net with a connection structure which is initially overdetermined and thereafter selectively thinned out. The updating process (corresponding to the abovementioned regressive events) is such that only those interconnections remain that represent significant functional inclusion relations (that relate neural elements with a significant coincidence rate in their signal activity). Thereafter the algorithm proceeds by transforming the thus obtained partial order into a lattice order (corresponding to the aforementioned progressive phenomena; for an extensive description of the algorithm the reader is referred to Part I.).

In this paper we study the influence of stimulus constraints on the resulting functional order produced by the coincidence-model. The results of this study may provide some insight into developmental disorders like monocular diplopia or amblyopia (e.g. Hess, 1982; Ikeda, 1980; Ikeda and Wright, 1974; Mitchell et al., 1973).

2. Simulation experiments.

A neural net obtains information about the external world by monitoring the patterns of activity in its underlying detector array. The constraints on the environment will be reflected in constraints on the spatial order of the projections of this environment on the detector array (i.e. in constraints on the spatial structure of the stimulus patterns). These will in turn put constraints on the simultaneous activity in the neural net. The simultaneous functional order produced by the coincidence-model encodes the restrictions on the simultaneous signal activity in the neural net. In this model these limitations are assessed during a learning stage. By presenting the coincidence-model in its learning stage with stimulus patterns that have systematic spatial constraints we simulated the effects of a constrained environment on the functional development of a simple nervous system. The following sections (2.1 to 2.5) deal with the influence of different spatial constraints on the functional order produced by the coincidence-model. Each section starts with a simple example. Thereafter we present the results of computer simulation experiments.

Our experiments were performed for a one-dimensional (periodically extended) detector array. In all experiments we assumed that the (contrast) detection thresholds were equal to zero. To increase the speed of the learning process, the smallest segments of the stimulus patterns were always chosen equal to the radius length of the smallest detector units. The maximum fraction of the detector array that was covered by these segments (i.e. the segment density) was 0.25. The learning stage was ended when the primitive (pairwise determined) functional inclusion relation Q' remained unaltered for 750 consecutive stimulus presentations.

To determine the influence of the environmental constraints on the resulting functional order in the neural net we study the one-dimensional triangulations (or PCW-complexes; see Part II) that can be determined from this order. From these triangulations we can deduct how the system perceives the topological structure of different stimulus patterns.

2.1. Experiment I: An unconstrained environment.

2.1.1. Example.

In this section we present a simple example that demonstrates how the coincidence-model produces a functional inclusion order in a set of neural elements when there are no restrictions on the stimulus patterns.

Figure 1a shows the spatial lay-out of a set of detector units. The units are labelled with their corresponding neural elements (i.e. the neurons to which they project their output). The detector array is periodically extended. Figure 1b shows the Hasse diagram representing the geometrical inclusion relation of the detector units. It is assumed that the segments of the stimulus pattern (1 ... 6) are of the same size as the smallest detector units (α ... ζ) and that each segment coincides with one particular smallest detector unit. Moreover, we assume that a non-zero valued stimulus pattern segment will activate all detector units that have a (non-zero) spatial overlap with this segment (i.e. we assume a zero-valued detection threshold).

To stimulate the development of this neural system in an unconstrained environment we present it in its learning stage with stimulus patterns consisting of a random number and combination of non-zero valued image segments. In case of the absence of a detection threshold (which was chosen equal to zero in this case), the number of training patterns needed for the assessment of the functional order in the system is minimal when each pattern contains only one non-zero valued segment. This is due to the fact that the coincidence model proceeds from a-priori assumed coincidence relations which are falsified during the learning process. More coincidence relations can be simultaneously falsified when less elements are simultaneously activated. Thus, a series of training patterns that successively activate the smallest detector units will shorten the learning stage.

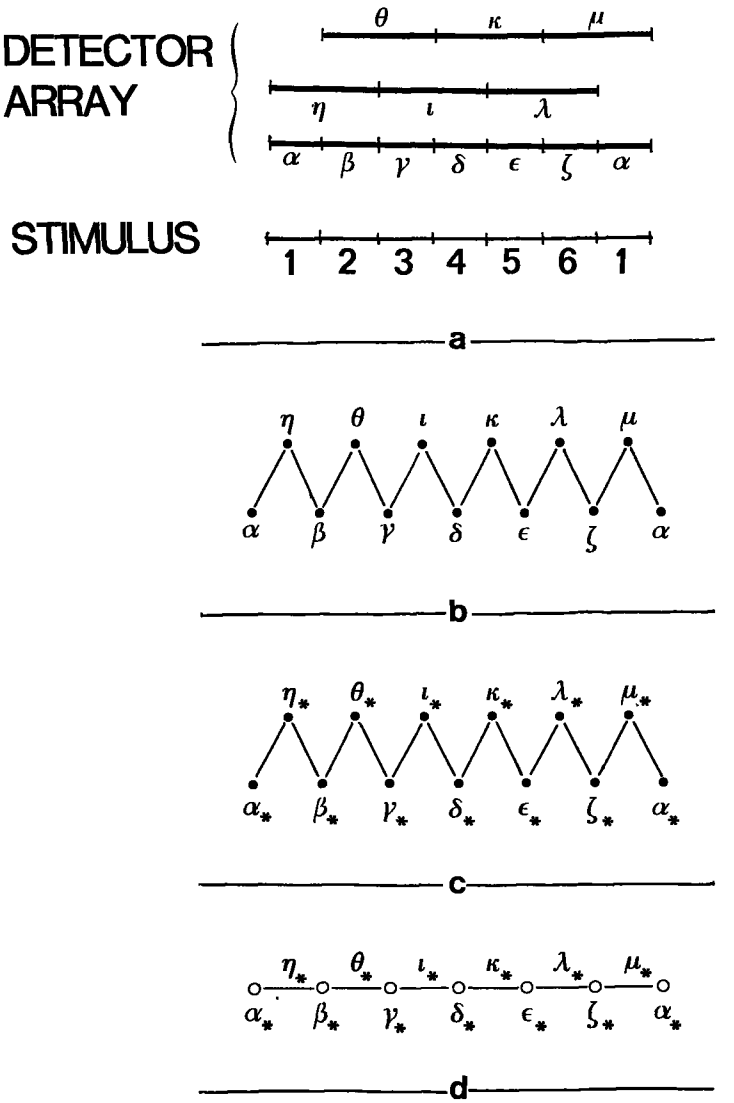

Figure 1. **a** The spatial lay-out of a set of detector units that coincides with the projection of a stimulus pattern consisting of 6 segments. **b** The Hasse diagram representing the geometrical inclusion relation between the detectors of **a**. **c** The Hasse diagram representing the triangulation of the resulting functional order in the set of neural elements corresponding with the detectors of **a** and **d** a schematical representation of its underlying polyhedron.

TABLE I.

Non-zero valued image segment	Activated detector units
1	α, η, μ
2	β, η, θ
3	γ, θ, ι
4	δ, ι, κ
5	$\varepsilon, \kappa, \lambda$
6	$\varepsilon, \lambda, \mu$

From Table I we see which neural elements are activated by the successive presentation of all different stimulus patterns consisting of a single non-zero valued image segment. From these results the coincidence-model can completely determine the primitive functional inclusion relation Q' (see Part I).

As an example of the determination of the relation Q' Table IIa illustrates the consecutive steps that have to be taken to check all primitive functional inclusion relations for neural element α. For two sets of neural elements S_1 and S_2 the notation S_1 ---> (---x-->) S_2 means that any (no) element of S_1 has a Q'- (primitive functional inclusion) relation with any of the elements of S_2. In the initial state of the functional structure all Q'-relations between α and all other neural elements are valid (i.e. α may be functionally included in any other element and any element may still be included in α). For each stimulus presentation the algorithm checks which Q'-relations are falsified. From Table II we see that the presentation of a single pattern segment that coincides with the detector unit corresponding to α allows the algorithm to eliminate all those Q'-relations between α and neural elements that were previously erroneously assumed to contain α. The consecutive presentation of stimulus patterns that selectively activate each of the remaining smallest detector units (β ... ζ) together with the larger detector units in which these are contained, allows the algorithm to successively eliminate all Q'-relations between α and those neurons that

were previously falsely assumed to be contained in α. In this example, the only Q'-relations for α that are not falsified during the learning stage (and that are therefore functionally significant) are respectively $(\alpha,\alpha) \in Q'$, $(\alpha,\eta) \in Q'$ and $(\alpha,\mu) \in Q'$. Table IIb shows the relations that are falsified during the learning stage for i, which corresponds to one of

TABLE II.

A. Checking the Q'-relation for neural element α.

Non-zero valued image segment	Falsified Q'-relations for α
1	α —x—> $\beta, \gamma, \delta, \varepsilon, \zeta, \theta, i, \kappa, \lambda$
2	β, η, θ —x—> α
3	γ, i —x—> α
4	δ, κ —x—> α
5	ε, λ —x—> α
6	ζ, μ —x—> α

B. Checking the Q'-relations for neural element i.

Non-zero valued image segment	Falsified Q'-relations for i
3	i —x—> $\alpha, \beta, \delta, \varepsilon, \zeta, \eta, \kappa, \lambda, \mu$
4	i —x—> γ, θ
1	α, η, μ —x—> i
2	β, θ —x—> i
5	ε, κ, μ —x—> i
6	ζ —x—> i

the larger detector units. From Table IIb we see that the only valid Q'-relations for i are respectively $(i,i) \in Q'$, $(\gamma,i) \in Q'$ and $(\delta,i) \in Q'$. By checking all other Q'-relations the algorithm finally produces a simultaneous functional order Q' that is identical to the geometrical inclusion order presented in Figure 1b (in this case the transitive extension Q" is identical to Q').

The Hasse-diagram representing the triangulation of the resulting functional order is presented in Figure 1c. The vertices are α_*, β_*, γ_*, δ_*, ε_*, ζ_* and the edges are η_*, θ_*, i_*, κ_*, λ_* and μ_*. Figure 1d represents the underlying polyhedron that can be associated with this abstract geometrical complex. The line segments represent the edges or one-dimensional simplices (cells); the dots they connect represent the vertices or zero-dimensional simplices (faces) of this complex. Table III shows the activation that is elicited in the triangulation by different stimulus patterns consisting of a single non-zero valued segment. These results may be interpreted as the consecutive stimulation of adjoining edges when a small stimulus traverses the entire detector array (regard patterns 1 to 6 as a time sequence). This is just the result that may be expected from a normally developed system.

TABLE III.

NR OF PATTERN	STIMULUS PATTERN						TRIANGULATION					
	SEGMENT NR						1-D SIMPLICES					
	1	2	3	4	5	6	η_*	θ_*	i_*	κ_*	λ_*	μ_*
1	*	-	-	-	-	-	*	-	-	-	-	*
2	-	*	-	-	-	-	*	*	-	-	-	-
3	-	-	*	-	-	-	-	*	*	-	-	-
4	-	-	-	*	-	-	-	-	*	*	-	-
5	-	-	-	-	*	-	-	-	-	*	*	-
6	-	-	-	-	-	*	-	-	-	-	*	*

* = NON - ZERO VALUED IMAGE SEGMENT or ACTIVATED SIMPLEX

\- = ZERO " " " or NON-ACTIVATED SIMPLEX

2.1.2. Experiment.

For the sake of completeness we will first present the adopted system parameters (for terminology, see Part I). The minimum detector radius value was 10 (arbitrary) units, the maximum radius value 300 units. Radius values were quantized in 8 intervals. The length of the detector array was 1200 units. The smallest units were distributed without any spatial overlap. Therefore, the detector array was completely covered by the smallest detector units when their number was 60.

First we train this system with patterns consisting of a random number and combination of non-zero valued image segments. In this way we simulate the development of the system in an unconstrained environment. When the learning stage is finished we can study the activity that is elicited in the triangulation by the presentation of a stimulus pattern. We will regard this activity pattern as the "perceived image". The triangulation allows us to determine the topology of this perceived image.

Figure 2a shows the reaction of the (mature) system to all different stimulus patterns consisting of a single non-zero valued image segment. If we regard the series of stimulus patterns as a time-sequence, the non-zero valued segment in these patterns moves systematically from left to right without skipping intermediate positions. In Figure 2a (and in all the following figures of this kind) all one-dimensional simplices in the triangulation have been aligned such that two adjoining simplices have one vertex in common. The results of Fig. 2a show that the activation in the triangulation closely follows the course of the stimulating pattern. When the non-zero valued (stimulating) image segment traverses the detector array once, its perceived image also traverses the perceived detector space once.

In the following sections we want to compare the "normally developed" system to systems that matured in constrained environments. Therefore, we obtained the reaction of this system to a sequence of stimulus patterns representing respectively two and three clearly separated non-zero valued (stimulating) image segments that traverse the detector array while maintaining their relative spatial separation. The rationale for the choice of these stimuli will become apparent in the next sections. The

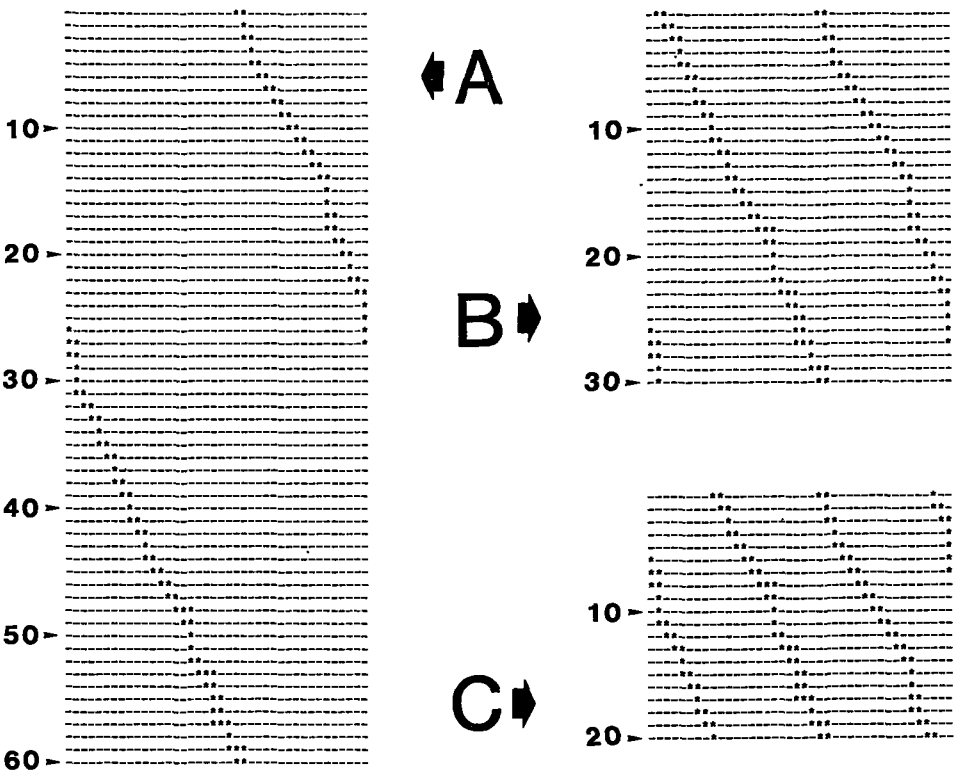

Figure 2. **a** The activation elicited in the triangulation of a system developed in an unconstrained environment for all different images consisting of a single non-zero valued image segment. Each horizontal line indicates the reaction of the system to the presentation of a different stimulus pattern. The - sign indicates a non-activated simplex and a * sign indicates an activated simplex. **b** and **c** represent respectively the reaction of the system from **a** to two or three clearly separated non-zero valued image segments traversing the entire detector array once while maintaining their relative distances.

results are shown in Figures 2b and 2c. As might be expected for a normally developed system, in both cases the perceived image is topologically identical to the presented stimulus pattern. When the stimulus patterns traverse a certain fraction of the detector array (respectively 1/2 in case of Figure 2b and 1/3 in case of Figure 2c), their perceived image is seen to traverse the same fraction of the perceived detector space.

2.2. Experiment II: During the development of the neural system both halves of the detector array are always stimulated with identical patterns.

2.2.1. Example.

TABLE IV.

NON-ZERO VALUED IMAGE SEGMENTS	ACTIVATED DETECTOR UNITS
1 , 4	α , δ , η , ι , κ , μ
2 , 5	β , ε , η , θ , κ , λ
3 , 6	γ , ζ , θ , ι , λ , μ

TABLE V A.

Checking Q'-relations for neural element α.

NON-ZERO VALUED IMAGE SEGMENTS	FALSIFIED Q'-RELATIONS FOR α.		
1 , 4	α	—x—>	$\beta,\gamma,\varepsilon,\zeta,\theta,\lambda$
2 , 5	β, ε, η, θ, κ, λ	--x-->	α
3 , 6	γ, ζ, ι, μ	—x—>	α

TABLE V B.

Checking Q'-relations for neural element i.

NON-ZERO VALUED IMAGE SEGMENTS	FALSIFIED Q'-RELATIONS FOR i.		
1 , 4	i	—x—>	$\beta,\gamma,\varepsilon,\zeta,\theta,\lambda$
3 , 6	i	—x—>	$\alpha,\delta,\eta,\kappa$
2 , 5	$\beta,\ \varepsilon,\ \eta,\ \theta,\ \kappa,\ \lambda$	—x—>	i

In this example we will use the detector distribution represented in Figure 1. During the learning stage we want the stimulus patterns to be such that both halves are identical. Therefore, only the following combinations of non-zero valued image segments are allowed as training patterns: {1,4}, {2,5}, {3,6} and all combinations of these three sets. Table IV presents the minimal number of stimulus patterns needed for a complete assesment of the functional order in this case, together with the neural elements activated by each of these patterns. Table Va shows the Q'-relations for element α that can be falsified on the basis of the information from Table IV. From Table Va we can conclude that $\{\delta\}$ —> $\{\alpha\}$ —> $\{\delta,\eta,i,\kappa,\mu\}$. The algorithm proceeds with removing the symmetrical relations $(\alpha,\delta) \in Q'$ and $(\delta,\alpha) \in Q'$. The result is therefore $\{\alpha\}$ —> $\{\eta,i,\kappa,\mu\}$. Similarly, we can derive the following relations from Table Vb for element i: $\{\alpha,\gamma,\delta,\zeta,\mu\}$ —> $\{i\}$ —> $\{\mu\}$. The algorithm thereafter removes the symmetrical relations $(i,\mu) \in Q'$ and $(\mu,i) \in Q'$. The result is $\{\alpha,\gamma,\delta,\zeta\}$ —> $\{i\}$. All other Q'-relations are checked in a similar way. Table VI presents the order relation Q' when the learning stage has been completed and all Q'-relations have been checked. For the sake of clarity we separated Table VI in two parts: Table VIa and VIb present the Q'-relations for respectively the smallest detector units (α ... ζ) and the largest ones (η ... μ). As a result each Q'-relation is mentioned two times in Table VI.

When the Q'-relation has been established the algorithm proceeds by lumping those neural elements that have identical Q'-relations with all other elements (and that are therefore functionally equivalent). In this

example the algorithm produces the following blocks of functional individuals: a={α,δ}, b={β,ε}, c={γ,ζ}, d={η,κ}, e={θ,λ} and f={i,μ}. The relation R' between blocks is a lattice order. Figure 3a shows the triangulation that can be determined from this lattice order and Figure 3b

TABLE VI The Q'-relation.

α , δ	---->	η , i , κ , μ
β , ε	---->	η , θ , κ , λ
γ , ζ	---->	θ , i , λ , μ
.....		
α, β, δ, ε	---->	η , κ
β, γ, ε, ζ	---->	θ, λ
α, γ, δ, ζ	---->	i, μ

a schematical representation of its underlying polyhedron. The vertices of this triangulation are a_*, b_*, c_* and the edges are d_*, e_* and f_*.

TABLE VII.

	STIMULUS PATTERN						TRIANGULATION		
PATTERN	SEGMENT NUMBER						1-D SIMPLICES		
	1	2	3	4	5	6	d_*	e_*	f_*
1	*	-	-	-	-	-	*	-	*
2	-	*	-	-	-	-	*	*	-
3	-	-	*	-	-	-	-	*	*
4	-	-	-	*	-	-	*	-	*
5	-	-	-	-	*	-	*	*	-
6	-	-	-	-	-	*	-	*	*

* = NON-ZERO VALUED IMAGE SEGMENT or ACTIVATED SIMPLEX

\- = ZERO " " " or NON-ACTIVATED SIMPLEX

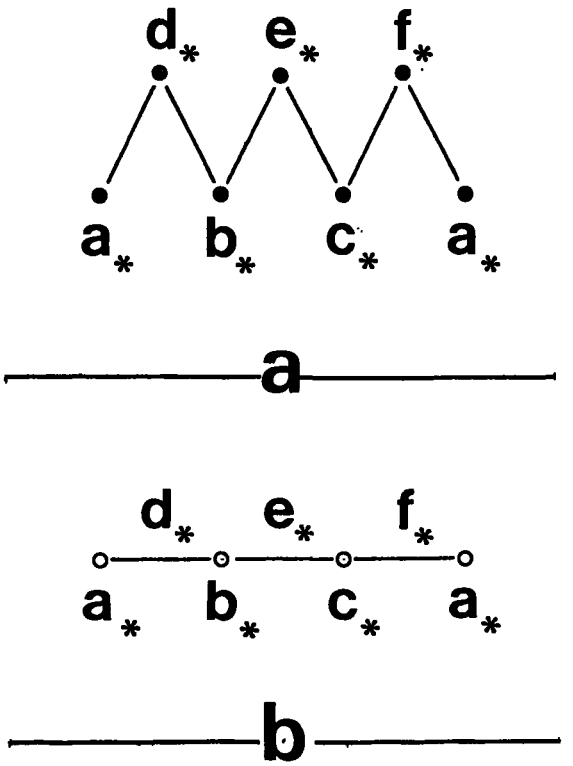

Figure 3. **a** The Hasse diagram representing the triangulation of the system from Figure 1 after completion of a learning stage in which both halves of the detector array were always stimulated with identical patterns. **b** A schematical representation of the underlying polyhedron of the triangulation from **a**.

Table VII shows the activation that is elicited in the triangulation by different stimulus patterns consisting of a single non-zero valued segment. Note that such patterns always activate a single vertex and two adjoining edges (which have that vertex in common) in the triangulation. (In this case the triangulation has no boundaries because of the choice of a periodically extended detector array. As already argued in Part II, this is no restriction to our theory.) From Table VII we see that the system cannot distinguish the stimuli from the pairs 1 and 4; 2 and 5; 3 and 6 because for each of these pairs both elements elicit identical activity patterns in the triangulation. This is due to the fact that the system has never had the chance to establish the separate identity of the neural elements corresponding to the detector units on which these stimuli are projected: the members of these pairs of patterns were always presented simultaneously during the learning stage, thereby always activating the corresponding detector units (and neurons) in synchrony.

We may regard the patterns 1 to 6 in Table VII as a time sequence depicting a small stimulus traversing the detector array from α to ζ. When the small stimulus traverses the entire detector array once its perceived image traverses the entire triangulation (corresponding to the perceived extent of the detector array) twice. This is a result of the fact that both halves of the detector array have become functionally equivalent.

An analogue is found in the well known example (due to Helmholtz) that patients with toothache often cannot indicate which of a pair of upper and lower molars is the affected one. Helmholtz explains this through pointing out that the nerves serving the molars are always excited in synchrony. If the neural system indeed produces an internal representation of the outside world by studying the coincidences in the signal activities of its neural elements, it must necessarily come up with a representation in which the molars are at a single place.

2.2.2. Experiment.

The adopted system parameters were the same as in Experiment I.

The system we will study in this section was only presented during its learning stage with stimulus patterns consisting of two identical halves. Figure 4a shows the activation elicited in the triangulation of this system by a single non-zero valued image segment that traverses the detector space only once. This result shows that the perceived image of this stimulus pattern traverses the triangulation (or perceived detector space) twice. This is a result of the fact that both halves of the detector array were always stimulated in synchrony during the learning stage of the system. Therefore, these halves have become functionally identical. To the system they are therefore no longer distinguishable. One might say that they are at the same perceived location.

Figure 4b shows the activation elicited in the triangulation by stimulus patterns consisting of two non-zero valued image segments which are separated by a distance that is exactly one half of the length of the detector array. The results show that these stimulus patterns are perceived as a single (contiguous) image segment. When this stimulus traverses one half of the detector array its perceived image traverses the entire triangulation.

Figure 4c shows the reaction of the system to stimulus patterns that consist of three isolated image segments which are exactly 1/3 of the length of the detector array apart. When such a pattern traverses 1/3 of the detector array its perceived image traverses 2/3 of the extent of the perceived detector space.

The foregoing results may be compared to those of the "normally developed" system of section 2.1. In both cases the same underlying detector distribution was used. In case of the unconstrained environment (section 2.1) the coincidence-model produces a functional order that is isomorphic with the geometry of the detector array. The functional order that is produced in the restricted environment used in this section is isomorphic to the geometry of either half of the detector array. Both halves of the detector array have become functionally equivalent due to the fact that they were always simultaneously stimulated with identical

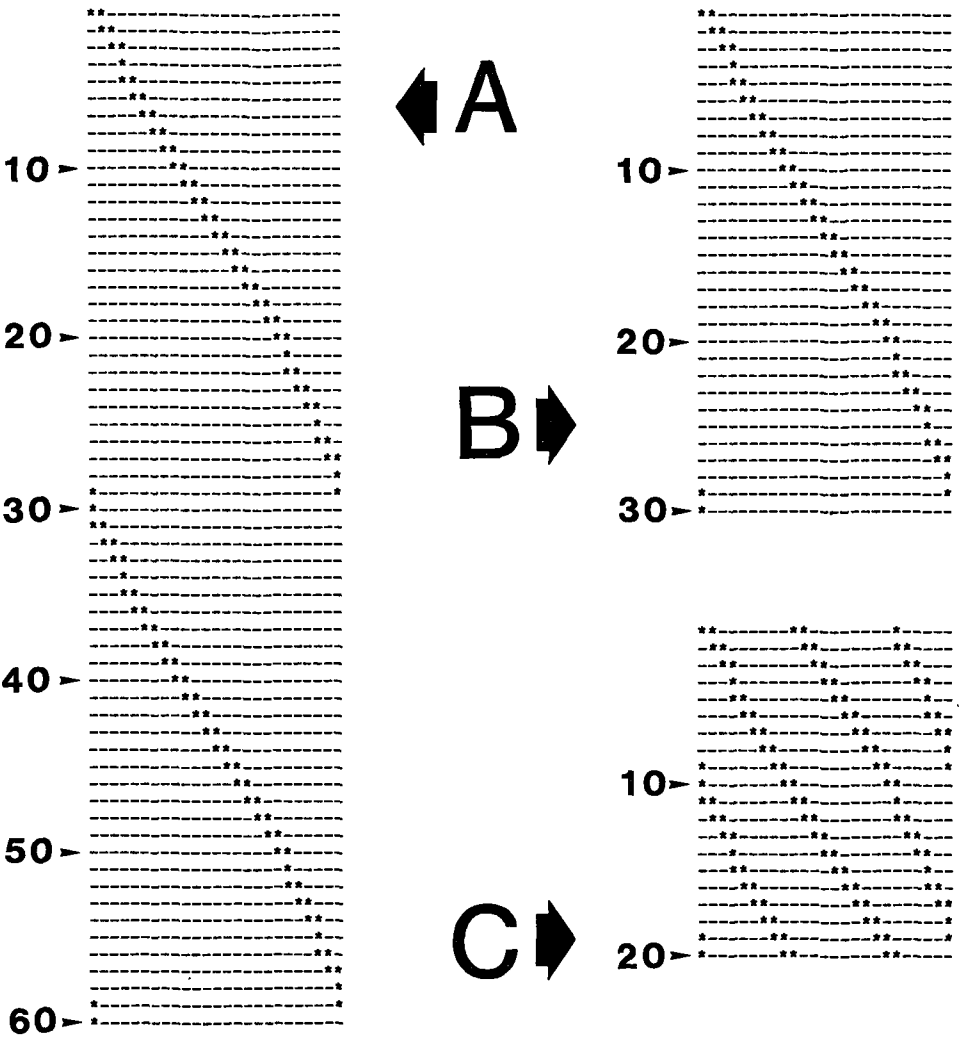

Figure 4. As Figure 2 but for a system for which both halves of the detector array were always stimulated with identical patterns during its development.

patterns during their learning stage. Thus, one might say that the functional order in the nervous net encodes the restrictions of its environment.

2.3. Experiment III: During the development of the neural system the stimulus pattern presented to the first half of the detector array is always a subset of the pattern presented to the second half.

2.3.1. Example.

In this example we will again use the detector distribution represented in Figure 1. During the learning stage we want the stimulus patterns to be such that their first half is always a subset of their second half. Therefore, only the following combinations of non-zero valued image segments are allowed as training patterns: {1,4}, {2,5}, {3,6}, {4}, {5}, {6} and all combinations of these six sets. Table VIII presents the minimal number of stimulus patterns needed for a complete assessment of the functional order in this case, together with the neural elements activated by each of these patterns.

TABLE VIII.

NON-ZERO VALUED IMAGE SEGMENTS	ACTIVATED DETECTOR UNITS
1 , 4	α , δ , η , ι , κ , μ
2 , 5	β , ε , η , θ , κ , λ
3 , 6	γ , ζ , θ , ι , λ , μ
4	δ , ι , κ
5	ε , κ , λ
6	ζ , λ , μ

Table IX presents the order relation Q' when the learning stage has been completed and all Q'-relations have been checked. In this case the relation Q' is identical to the relation R' as there are no functionally equivalent elements. In Figure 5a the relation R' is represented by its Hasse diagram. Figure 5b shows the Hasse diagram of the lattice order resulting after the application of the neuron-recruitment routine. In this case the hull element $[\alpha, \gamma]$ was added to produce a lattice order. The fat lines in this diagram represent the triangulation that can be determined from this lattice order. The individuals α_*, β_*, γ_* are the vertices and η_*, θ_*, $[\alpha,\gamma]$ are the edges of this one-dimensional complex. Figure 5c shows a schematical representation of the underlying polyhedron of this triangulation.

Table X shows the activation that is elicited in the triangulation by different stimulus patterns consisting of a single non-zero valued segment. Consider the patterns 1 to 6 as a time sequence. In this case we see that when a small stimulus traverses the detector array from α to γ (i.e. the first half of the detector array) its perceived image traverses the entire triangulation. The patterns 4 to 6 are not noted by the system.

TABLE IX. The Q'-relation.

	→	α →	δ , η , ι , κ , μ
	→	β →	ε , η , θ , κ , λ
	→	γ →	ζ , θ , ι , λ , μ
α	→	δ →	ι , κ
β	→	ε →	κ , λ
γ	→	ζ →	λ , μ
α,β	→	η →	κ
β,γ	→	θ →	λ
α,γ,δ	→	ι →	
α,β,δ,ε,η	→	κ →	
β,γ,ε,ζ,θ	→	λ →	
α,γ,ζ	→	μ →	

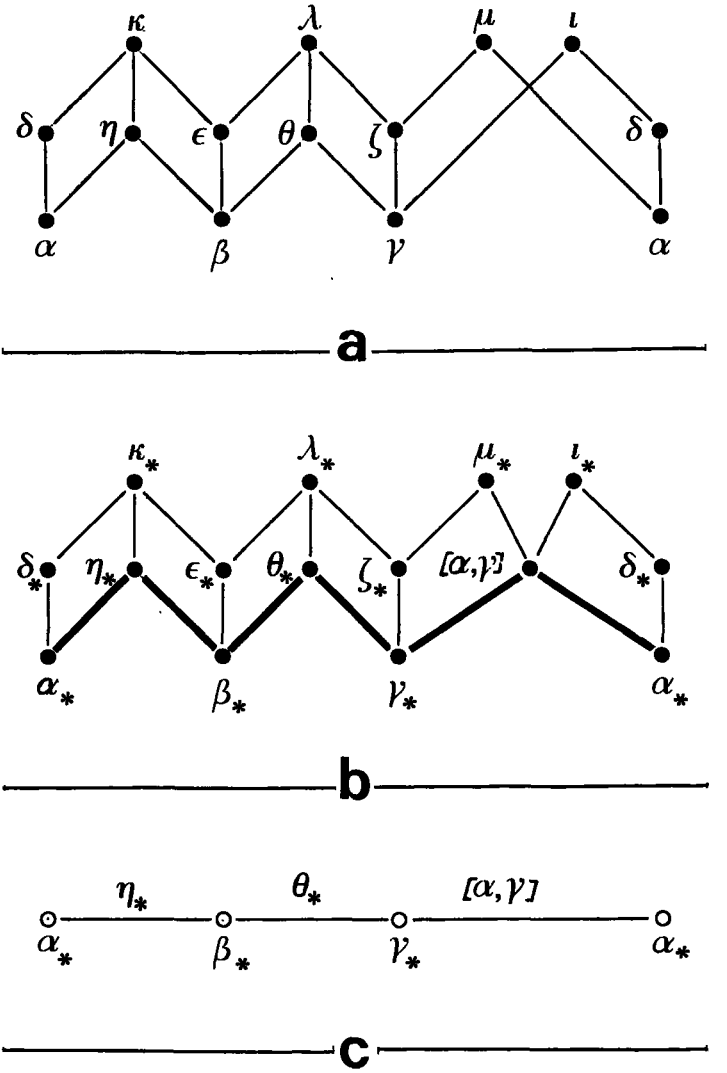

Figure 5. **a** The Hasse diagram representing the relation R' for the system from Figure 1 after completion of a learning stage in which it was only stimulated with patterns that were such that their first half was always a subset of their second half. **b** The Hasse diagram representing the lattice order after the application of the neuron recruitment routine to the poset from **a**. The fat lines indicate the triangulation that can be determined from this lattice order. **c** A schematical representation of the underlying polyhedron of the triangulation of **b**.

TABLE X.

PATTERN	STIMULUS PATTERN SEGMENT NUMBER						TRIANGULATION 1-D SIMPLICES		
	1	2	3	4	5	6	η_*	θ_*	$[\alpha,\gamma]$
1	*	-	-	-	-	-	*	-	*
2	-	*	-	-	-	-	*	*	-
3	-	-	*	-	-	-	-	*	*
4	-	-	-	*	-	-	-	-	-
5	-	-	-	-	*	-	-	-	-
6	-	-	-	-	-	*	-	-	-

* = NON-ZERO VALUED IMAGE SEGMENT or ACTIVATED SIMPLEX

- = ZERO " " " or NON-ACTIVATED SIMPLEX

Note that the one-dimensional simplex $[\alpha,\gamma]$ corresponds to a part of the detector array that is not geometrically convex. Because the patterns 4 to 6 do not activate the triangulation $[\alpha,\gamma]$ is still functionally convex.

2.3.2. Experiment.

The adopted system parameters were as follows. The minimum detector radius value was 5 (arbitrary) units, the maximum radius value 200 units. Radius values were quantized in 5 intervals. The length of the detector array was 800 units. The smallest units were distributed without any spatial overlap. Therefore, the detector array was completely covered by the smallest detector units when their number was 40.

In its learning stage the system was only stimulated with patterns that were such that the first half of each pattern was always a subset of its second half. In this case the coincidence model could not produce a closed triangulation for systems with a maximum radius length value of 300. This is a result of the fact that a neural element corresponding to a detector unit located in the second half of the detector array need not be located in between two individuals in the resulting functional order (as

opposed to our Example, in which this condition is neatly fulfilled). It may be the case that it has arbitrary connections with other individuals. This precludes the construction of a closed triangulation. For the maximum radius value we adopted (200) the algorithm produces a triangulation in about 50% of all cases (i.e. for 50% of all different detector distributions). Figure 6 shows that the reaction of the system to a small stimulus traversing the entire detector array is essentially identical to the behaviour of the system in the above mentioned Example.

2.4. Experiment IV: During the development of the neural system the stimulus pattern presented to the first two-third part of the detector array is always reduced with a factor two and projected on the remaining third part of the detector array.

2.4.1. Example.

TABLE XI.

NON-ZERO VALUED IMAGE SEGMENTS	ACTIVATED DETECTOR UNITS
1 , 5	α , ε , η , κ , λ , μ
2 , 5	β , ε , η , θ , κ , λ
3 , 6	γ , ζ , θ , ι , λ , μ
4 , 6	δ , ζ , ι , κ , λ , μ

In this example we will also use the detector distribution represented in Figure 1. During the learning stage we want the stimulus patterns to be such that their first two-third part reduced in size by a factor two is identical to their remaining (third) part. Therefore, only the following combinations of non-zero valued image segments are allowed as training patterns: {1,5}, {2,5}, {3,6}, {4,6} and all combinations of these four sets. Table XI presents the minimal number of stimulus patterns needed for a complete assessment of the functional order in this case, together with the neural elements activated by each of these patterns.

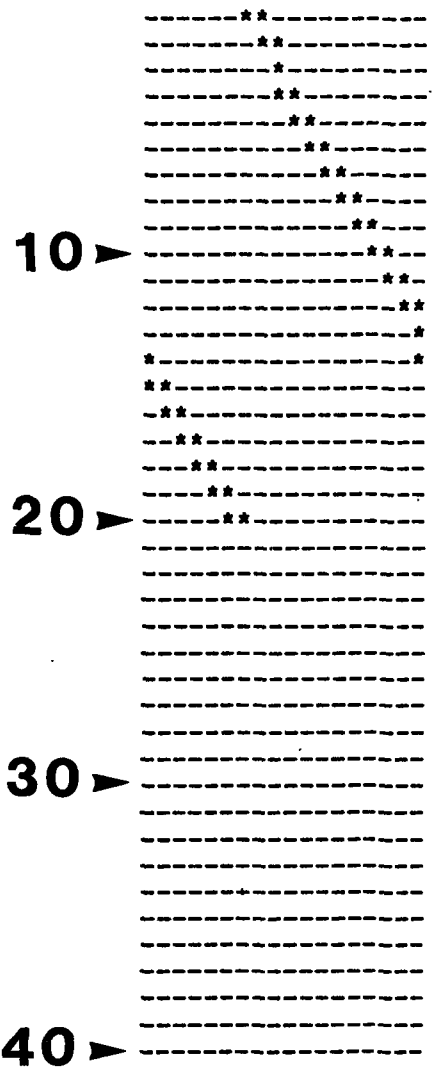

Figure 6. A schematical representation of the activation elicited in the triangulation of a system by a single non-zero valued image segment traversing the entire detector array once. This particular system was stimulated during its development with patterns that were such that their first half was always a subset of their second half.

TABLE XII. The Q'-relation.

	→ α	→	ε, η, κ, λ, μ
	→ β	→	ε, η, θ, κ, λ
	→ γ	→	ζ, θ, i, λ, μ
	→ δ	→	ζ, i, κ, λ, μ
α,β,~~η~~	→ ε	→	~~η~~, κ, λ
γ,δ,~~i~~	→ ζ	→	~~i~~, λ, μ
α,β,~~ε~~	→ η	→	~~ε~~, κ, λ
β,γ	→ θ	→	λ
γ,δ,~~ζ~~	→ i	→	~~ζ~~, λ, μ
α,β,δ,ε,η	→ κ	→	λ
α,β,γ,δ,ε,ζ,η,θ,i,κ,λ,μ	→ λ	→	
α,γ,δ,ζ,i	→ μ	→	λ

Table XII presents the order relation Q' when the learning stage has been completed and all Q'-relations have been checked. The algorithm proceeds with the elimination of symmetrical Q'-relations. In Table XII these symmetrical relations are represented by the scratched elements. Thereafter the algorithm detects two sets of functional equivalent elements and lumps the elements of each set in a single block: a = {ζ,η} and b = {ζ,i}. All other blocks contain only one neural element. In Figure 7a the relation R' is represented by its Hasse diagram. Figure 7b shows the Hasse diagram of the lattice order resulting after the application of the neuron-recruitment routine. In this case the hull element [α,δ] was added to produce a lattice order. The fat lines in this diagram represent the triangulation that can be determined from this lattice order. The individuals α_*, β_*, γ_*, δ_* are the vertices and a_*, θ_*, b_*, [α,δ] are the edges of this one-dimensional complex. Figure 7c shows a schematical representation of the underlying polyhedron of this triangulation.

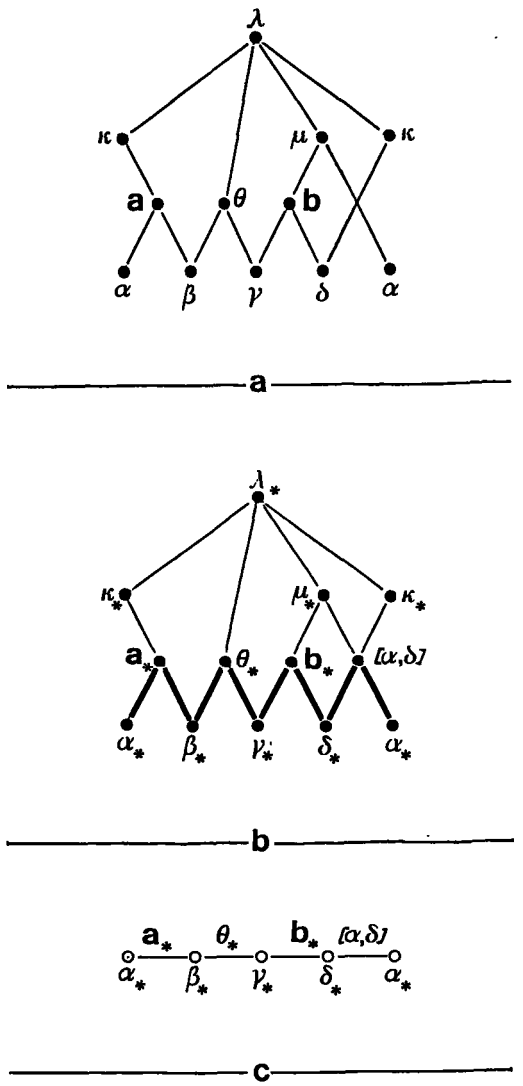

Figure 7. As Figure 5 but for a learning stage in which the system from Figure 1 was stimulated with patterns that were such that their first two-third part is always reduced with a factor two and projected on the remaining third part of the detector array.

Table XIII.

	STIMULUS PATTERN SEGMENT NR.						TRIANGULATION 1-D SIMPLICES.			
PATTERN	1	2	3	4	5	6	a_*	θ_*	b_*	$[\alpha,\delta]$
1	*	-	-	-	-	-	*	-	-	*
2	-	*	-	-	-	-	*	*	-	-
3	-	-	*	-	-	-	-	*	*	-
4	-	-	-	*	-	-	-	-	*	*
5	-	-	-	-	*	-	*	-	-	-
6	-	-	-	-	-	*	-	-	*	-

* = NON-ZERO VALUED IMAGE SEGMENT OR ACTIVATED SIMPLEX.
- = ZERO-VALUED " " OR NON-ACTIVATED SIMPLEX.

Table XIII shows the activation that is elicited in the triangulation by different stimulus patterns consisting of a single non-zero valued stimulus segment. Consider again the patterns 1 to 6 as a time sequence. In this case we see that when a small stimulus traverses the detector array from α to δ (i.e. the first two-third of the detector array; patterns 1 to 4) its perceived image traverses the entire triangulation. When the stimulus traverses from ε to ζ its perceived image goes from a_* to b_*, thereby skipping θ_*. This is due to the reduction factor 2 which causes ε to be included in a_* and ζ in b_*, which are in turn separated by θ_*.

2.4.2. Experiment.

In this experiment we adopted 7 intervals for the radius value of the detector units. The other system parameters were chosen equal to those that were used in Experiment I. In this case the algorithm was able to produce a triangulation for about 40% of all different detector distributions.

Figure 8a shows the activation that is elicited in the triangulation by a series of different stimulus patterns, each one consisting of a single non-zero valued image segment. The results are in agreement with those of the above mentioned Example. When a small stimulus traverses the first 2/3 part of the detector array its perceived image traverses the entire triangulation. The same holds true for the last 1/3 part of the detector array. Thus, when a small stimulus traverses the detector array once its perceived image traverses the entire extent of the perceived detector array twice. This is essentially the same result as the one we obtained in section 2.2. As we already noted in that section, both parts of the detector array have become functionally indistinguishable to the system.

Note that some one-dimensional simplices are not activated when the small stimulus traverses the last third part of the detector array. This is a result of the fact that both parts of the detector array are subserved by the same neural network, due to the fact that they have become functionally equivalent. Because these parts differ in their spatial extent they contain different numbers of detector units. The functional individuals corresponding to the detector units in the smaller part of the detector array are therefore more widely spaced over the functional order than the ones corresponding with the larger part, which are adjacent. As a result, the continuous movement of a small stimulus pattern across the first 2/3 part of the detector array will be perceived as a fluent motion (a consecutive stimulation of adjacent simplices) whereas a continuous movement across the last 1/3 part will be seen as a jerky movement (a consecutive stimulation of separated simplices).

Figure 8b shows the activation that is elicited in the triangulation by the presentation of stimulus patterns consisting of three non-zero valued image segments with a mutual separation equal to 1/3 of the length of the detector array. When a stimulus pattern of this kind traverses the detector array once its perceived image traverses the entire extent of the perceived detector space twice.

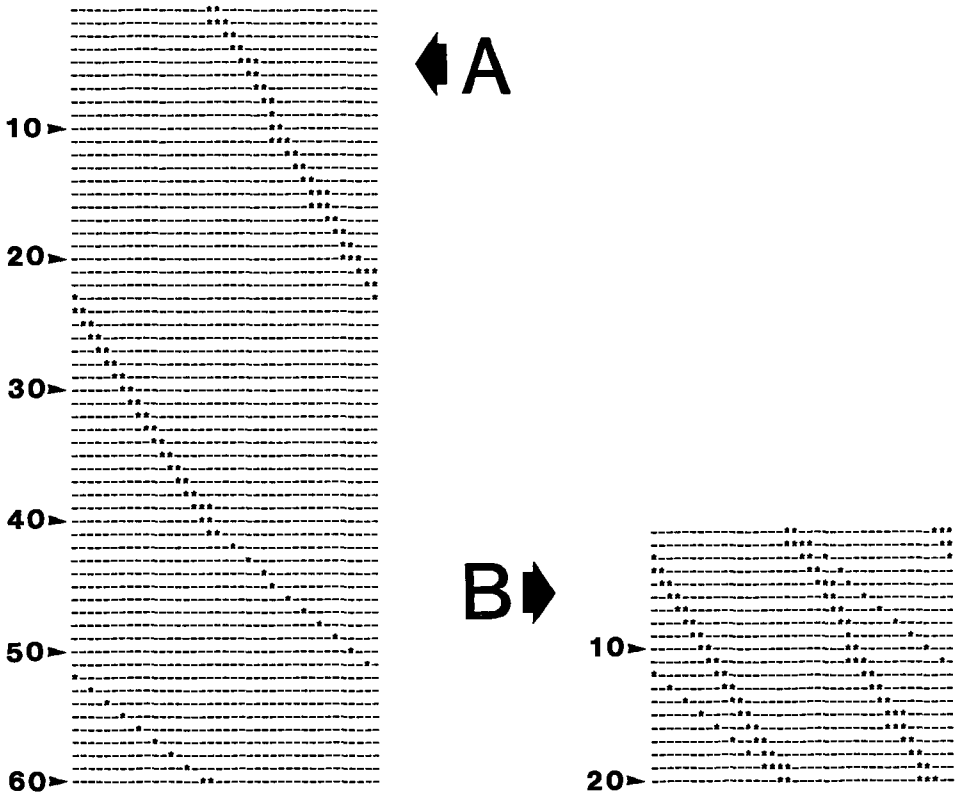

Figure 8. A schematical representation of the activation elicited in the triangulation of a system that was stimulated during its development with patterns that were such that their first two-third part is always reduced with a factor two and projected on the remaining third part of the detector array. **a** shows the reaction of the system to a single non-zero valued image segment and **b** shows its reaction to three non-zero valued image segments with a mutual separation equal to 1/3 of the length of the detector array. Both patterns traverse the entire detector array once.

2.5. Experiment V: A part of the detector array is occluded during the development of the neural system.

2.5.1. Example.

In this example we will use the detector distribution represented in Figure 1, extended with an extra unit υ. This unit coincides with the smallest detector units α, δ, ε and ζ. As will become apparent in the sequel, the element υ was merely added to obtain a closed lattice order in this example. During the learning stage we want to simulate an occlusion of the image segments 5 and 6. Therefore, we only present training patterns to the system that have zero-valued segments 5 and 6. As a result, the detector units that coincide with the segments 5 and 6 (i.e. the units corresponding to the neural elements ε, ζ and λ) will never be stimulated during the learning stage. Table XIV presents the minimal number of stimulus patterns needed for a complete assessment of the functional order in this case together with the neural elements activated by each of these patterns.

As a result of the fact that the neural elements corresponding to the detector units ε, ζ and λ (with which the patterns 5 and 6 coincide) have never been activated during the learning stage there has never been a falsification of the a priori assumed inclusion relations between these elements and all other elements. As a result, ε, ζ and λ have the same functional inclusion relations with all other neural elements and are therefore functionally equivalent. The algorithm proceeds by lumping the functionally equivalent elements in blocks. In this particular example the blocks consisting of more than one neural element are respectively $a=\{\alpha,\mu\}$, $b=\{\delta,\kappa\}$ and $c=\{\varepsilon,\zeta,\lambda\}$. All other blocks contain only one neural element (and will be labelled by that element).

TABLE XIV.

NON-ZERO VALUED IMAGE SEGMENTS	ACTIVATED DETECTOR UNITS
1	$\alpha, \eta, \mu, \upsilon$
2	β, η, θ
3	γ, θ, ι
4	$\delta, \iota, \kappa, \upsilon$

Figure 9a shows the Hasse diagram of the resulting lattice order. The fat lines in this diagram represent the triangulation that can be determined from this lattice order. The individuals a_*, β_*, γ_*, b_* are the vertices and η_*, θ_*, ι_*, υ_* are the edges of this one-dimensional complex. Figure 9b shows a schematical representation of the underlying polyhedron of this triangulation. Note that the one-dimensional simplex υ_* (that corresponds to the detector unit that geometrically includes the occluded part of the detector array) joins the vertices a_* and b_*.

TABLE XV.

	STIMULUS PATTERN SEGMENT NR.						TRIANGULATION 1-D SIMPLICES			
PATTERN	1	2	3	4	5	6	η_*	θ_*	ι_*	υ_*
1	*	-	-	-	-	-	*	-	-	*
2	-	*	-	-	-	-	*	*	-	-
3	-	-	*	-	-	-	-	*	*	-
4	-	-	-	*	-	-	-	-	*	*
5	-	-	-	-	*	-	*	*	*	*
6	-	-	-	-	-	*	*	*	*	*

Table XV shows the activation that is elicited in the triangulation by different stimulus patterns consisting of a single non-zero valued segment. Consider again the patterns 1 to 6 as a time sequence. In this

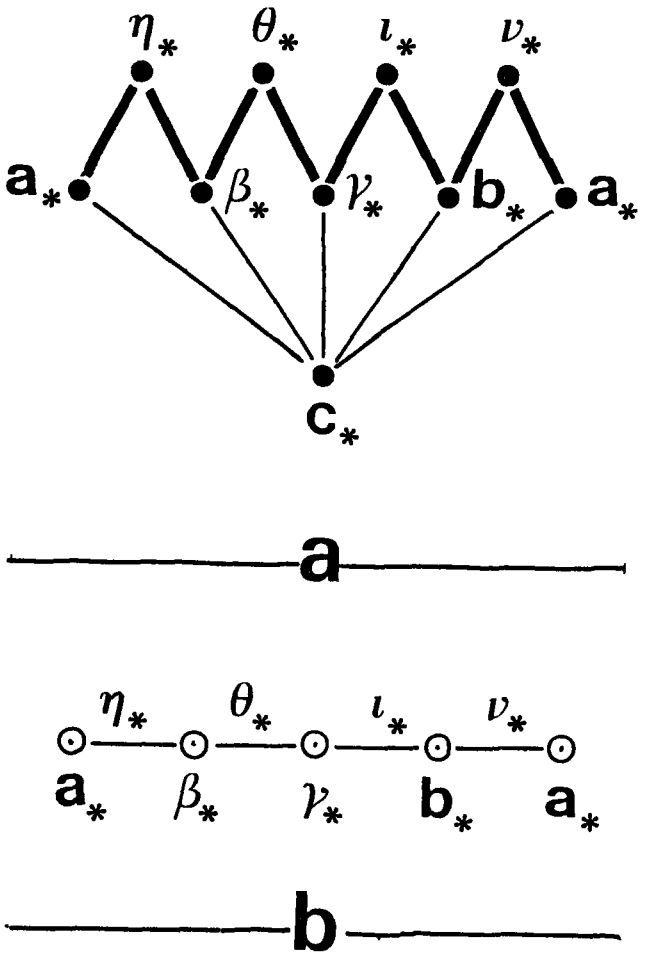

Figure 9. **a** The Hasse diagram representing the lattice order for the system from Figure 1 extended with an extra detector unit ν and after a learning stage in which a part of the detector array was never stimulated. **b** A schematical representation of the underlying polyhedron of the triangulation of the lattice order from (indicated by the fat lines in) **a**.

case we see that when a small stimulus traverses the detector array from α to δ (i.e. the first two-third of the detector array) its perceived image traverses the entire triangulation. The stimulus patterns 5 and 6 activate the entire triangulation. This is a direct result of the imposed constraints on the spatial structure of the stimulus patterns that were presented during the learning stage. Due to a lack of information in these patterns the system has not been able to assess the functional identity and the relative functional position of the neural elements ε, ζ and λ. Because their identity remains unspecified these elements are lumped in a block and because their relative functional position cannot be determined this block may be located anywhere within the functional order; a fact that is represented by its status of infimum in the lattice order of Figure 9a.

2.5.2. Experiment.

The adopted detector distribution was identical to the one that was used in the Experiments I and II. During the development of the system a certain extent of the detecor array was never stimulated. The training patterns used in the learning stage had no inherent restrictions. We will now present the results of two neural systems N_1 and N_2. These systems merely differ in the extent of the part of the detector array that was occluded during the learning stage. In N_1 the last 100 units of the detector array were occluded, whereas the last 200 units were covered in N_2.

Figures 10a and 10b show the activation elicited in the triangulations of respectively N_1 and N_2 by a small stimulus pattern (corresponding to a single non-zero valued image segment) that traverses the entire detector array. From Figure 10 we see that a small stimulus that is located inside the area that was covered during the learning stage activates the entire triangulation. The occluded parts correspond to 5 detector units in N_1 and 10 in N_2. Note that we chose the image segments such that they coincided with the smallest detector units. As a result we find that the last 5 stimulus patterns in Figure 10a and the last 10 in

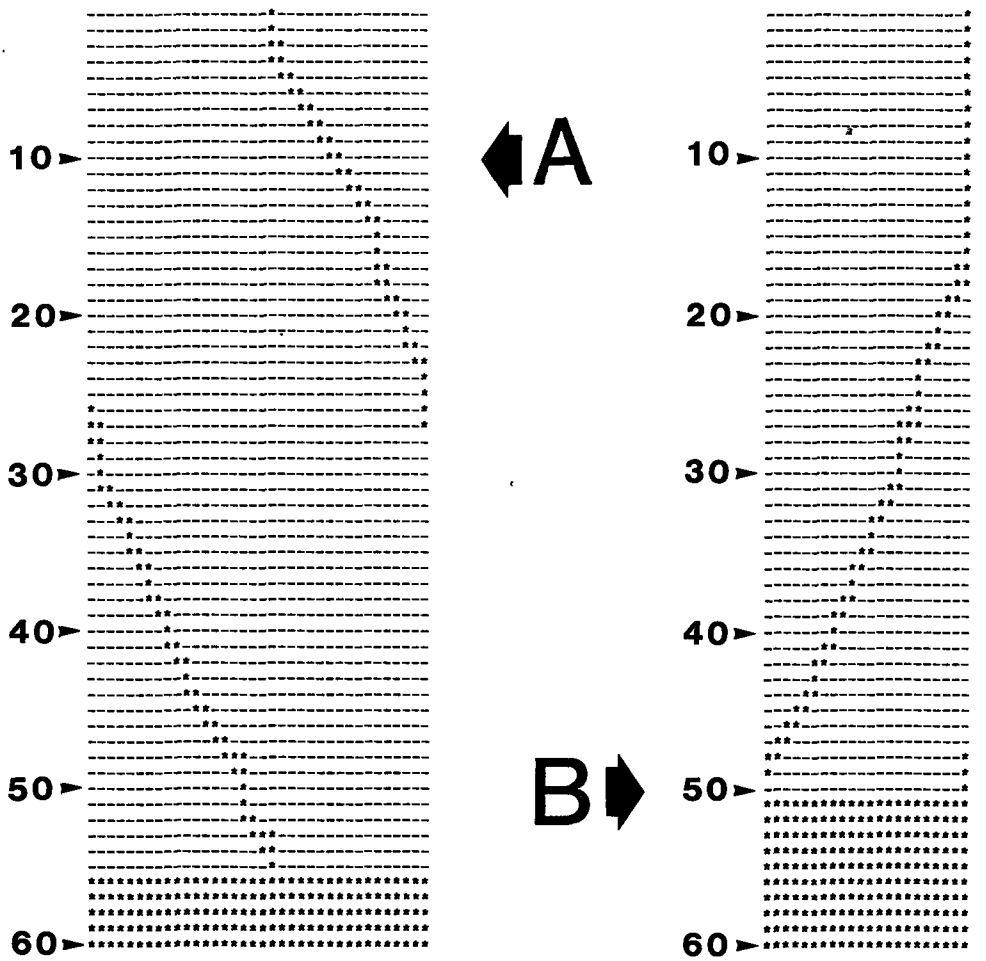

Figure 10. Schematical representation of the activation elicited in the triangulations of systems for which a part of the detector array was never stimulated during their development. **a** and **b** represent the reaction of systems with an occluded part consisting of respectively 100 and 200 smallest detector units to all different images consisting of a single non-zero valued image segment.

Figure 10b activate those vertices that are functionally included in all edges of the triangulation. This is the same effect as we demonstrated in the above mentioned Example.

We will now compare these results to the results of the neural system from Experiment I (which we will sometimes indicate with N in the sequel). Comparing Figs. 2a and 10a we see that N and N_1 show identical reactions to stimulus patterns 5 to 54. To produce a closed triangulation the algorithm has to connect the neural elements of N_1 that correspond to the detector units that coincide with image segments 55 and 1. The neural element that serves to bring this connection about corresponds to a detector unit that geometrically includes the entire occluded part of the detector array. As the occluded part in N_2 is twice as large as that in N_1 we expect the range of stimulus patterns for which N and N_2 show comparable reactions to be smaller than the range found for N_1. Figure 10b shows that this is indeed the case. N and N_2 show identical reactions to stimulus patterns 15 to 50.

3. Conclusions.

In this paper we presented some simulation experiments that were performed to study the influence of a constrained environment on the simultaneous functional order produced by the coincidence model. The results of these experiments show analogies to some neurophysiological facts. For instance, neural elements which are always stimulated in synchrony during the learning stage will be located at the same (functional) position to the system. This may be compared to the aforementioned example of a patient which cannot indicate which of a pair of upper and lower molars is the affected one (Helmholtz's example). Neural elements which have never been activated during the learning process cannot be located within the perceived detector space. This result may be compared to the visual defects found in patients that suddenly regain their vision after a long period of blindness. These patients often show a loss of form-vision and in some cases even a separation of form- and color-vision. These defects may be a direct result of the lack of

internal coherence in the neural network due to a lack of visual experience.

As we already mentioned in the introduction, it seems that global topographic mappings between areas of the nervous system might be preprogrammed (Hubel and Wiesel, 1970, 1974; Jeffery, 1985), whereas activity dependent self organizing mechanisms may be responsible for the precise fine tuning of these mappings. This notion can easily be incorporated into our model by restricting the monitoring of signal coincidences to nearest neighbours only. In this view local developmental disorders like amblyopia or monocular diplopia may result from impairments of the mechanisms responsible for the development of the functional order at a small scale.

References.

Amari, S. (1985) Formation of retinotopy and columnar microstructures by self-organization: a mathematical model. In: Models of the visual cortex, 157-163. Eds. Rose, D. and Dobson, V.G. John Wiley and Sons Ltd. New York, London.

Bedi, K.S. (1986) Nutrition, environment and brain development. Sci. Prog. 70, 555-570.

Blakemore, C. and Cooper,G.F. (1970) Development of the brain depends on the visual environment. Nature 228, 477-478.

Cowan, W.M., Fawcett, J.W., O'Leary, D.D.M. and Stanfield, B.B. (1984) Regressive events in neurogenesis. Science 225, 1258-1265.

Harwerth, R.S., Smith, E.L., Duncan, G.C., Crawford, M.L.J. and Noorden, G.K. von (1986) Multiple sensitive periods in the development of the primate visual system. Science 232, 235-238.

Hess, R.F. (1982) Developmental sensory impairment: amblyopia or tarachopia? Human Neurobiology 1, 17-29.

Hirsch, H.V.B. and Leventhal, A.G. (1978) Functional modification of the developing visual system. In: Handbook of sensory physiology IX, 279-335. Ed. Jacobson, M. Springer Verlag. Berlin-New York.

Hirsch, H.V.B. and Spinelli, D.N. (1970) Visual experience modifies distribution of horizontally and vertically oriented receptive fields in cats. Science 168, 869-871.

Hubel, D.H. and Wiesel, T.N. (1970) The period of susceptibility to the physiological effects of unilateral eye closure in kittens. J. Physiol. 206, 419-436.

Hubel, D.H. and Wiesel, T.N. (1974) Ordered arrangement of orientation columns in monkeys lacking visual experience. J. Comp. Neurol. 158, 307-318.

Ikeda, H. (1980) Visual acuity, its development and amblyopia. J. R. Soc. Med. 73, 546-555.

Ikeda, H. and Wright, M.J. (1974) Is amblyopia due to inappropriate stimulation of the "sustained" pathway during development? Brit. J. Ophthal. 58, 165-175.

Jeffery,G. (1985) Retinotopic order appears before ocular separation in developing visual pathways. Nature 313, 575-576.

Kandel, E.R. (1985a) Early experience, critical periods, and developmental fine tuning of brain architecture. In: Principles of neural science, 2nd ed. Eds. Kandel, E.R. and Schwartz, J.H. Elsevier, New York-Amsterdam-Oxford.

Kandel, E.R. (1985b) Cellular mechanisms of learning and the biological basis of individuality. In: Principles of neural science, 2nd ed. Eds. Kandel, E.R. and Schwartz, J.H. Elsevier, New York-Amsterdam-Oxford.

Koenderink, J.J. (1984) Simultaneous order in nervous nets from a functional standpoint. Biol. Cybern. 50, 35-41.

Kohonen, T. (1982) Self-organized formation of topologically correct feature maps. Biol. Cybern. 43, 59-69.

Mitchell, D.E., Freeman, R.D., Millodot, M. and Haegerstrom, G. (1973) Meridional amblyopia: evidence for modification of the human visual system by early visual experience. Vision Res. 13, 535-558.

Movshon, J.A. and Sluyters, R.C. van (1982) Visual neural development. Ann. Rev. Psychol. 32, 477-522.

Paton, J.A. and Nottebohm, F.N. (1984) Neurons generated in the adult brain are recruited into functional circuits. Science 225, 1046-1048.

Pettigrew, J.D. and Freeman, R.D. (1973) Visual experience without lines: effect on developing cortical neurons. Science 182, 599-601.

Stryker, M.P., Sherk, H., Leventhal, A.G. and Hirsch, H.V.B. (1978) Physiological consequences for the cat's visual cortex of effectively restricting early visual experience with oriented contours. J. of Neurophysiol. 41, 896-909.

Toet, A., Blom, J. and Koenderink, J.J. (1987a) The construction of a simultaneous functional order in nervous systems.I. Relevance of signal covariances and signal coincidences in the construction of a functional order. Submitted to Biol. Cybern.

Toet, A., Blom, J. and Koenderink, J.J. (1987b) The construction of a simultaneous functional order in nervous systems. II. Computing geometrical structures. Submitted to Biol. Cybern.

Toet, A., Blom, J. and Koenderink, J.J. (1987c) The construction of a simultaneous functional order in nervous systems. III. The influence of physical constraints on the resulting functional order. Submitted to Biol. Cybern.

Wiesel, T.N. (1982) Postnatal developments of the visual cortex and the influence of environment. Nature 299, 583-591.

CHAPTER II.1.

Differential spatial displacement discrimination at low resolution.

ABSTRACT.

Similar to the three-dot alignment hyperacuity task, differential (orthoaxial) spatial displacement discrimination thresholds were determined for three blobs with Gaussian spatial contrast profiles at threshold luminance contrast. Stimulus size was varied by varying the viewing distance. The results show that the differential orthoaxial spatial displacement discrimination thresholds scale linearly with the stimulus size over at least two decades. We conclude that at all levels of resolution a similar mechanism is used to detect differential (orthoaxial) spatial displacement.

key-words: hyperacuity 3-dot alignment task resolution threshold contrast

INTRODUCTION.

The human visual system can determine changes in the relative spatial position of features in the visual field with an extremely high accuracy (Volkmann, 1863; Wülfing, 1892; Westheimer and McKee, 1977b). This precision, coined "hyperacuity" by Westheimer (1975), is possible for a variety of spatial localization tasks (Westheimer and McKee, 1977b) and remains unaffected by movement of the stimuli across the retina over several min of arc (Westheimer and McKee, 1975, 1977a). Thresholds for the accuracy obtained in these tasks are typically a few seconds of arc. Klein and Levi (1985) have recently shown that under optimal conditions observers could correctly discriminate the relative spatial position of a line with an accuracy of less than 1 arc sec.

The astonishing precision of this performance becomes clear when the optical properties of the human eye are considered. Estimates of the size of foveal photoreceptors vary from 20"-30" and the width of the Gaussian core of the optical point spread function of the human eye is about 1.5', corresponding to a spatial-frequency cutoff of about 60 cy/deg. According to signal theory the spatial rate at which the intensity distribution falling on the retina is sampled by the retinal photoreceptors is sufficient to obtain a unique (i.e. free of aliasing effects) continuous reconstruction of the retinal intensity distribution (Barlow, 1979).

"Neural blurring" due to the retinal ganglion cells that transmit retinal signals to the cortex causes a further degradation of the higher spatial frequencies present in the retinal intensity distribution. Ganglion cells compute the weighted mean of the activity in a collection of photoreceptors. The area over which this mean signal value is calculated (receptive field) has a center excitatory area with a diameter of at least 1'.

Hyperacuity thresholds show that the brain can discriminate changes in the relative spatial position of features in the visual field which are an order of magnitude below the size of a foveal photoreceptor and nearly two orders of magnitude smaller than the smallest receptive fields. Although the exact nature of the processing subserving hyperacuity is unknown the site of this processing is assumed to be cortical (Barlow, 1979). The most direct evidence for this assumption are the facts that (i) Vernier acuity for one eye is affected by the simultaneous presentation of an interfering stimulus to the other eye (Westheimer and Hauske, 1975; Levi et al., 1985) and (ii) that functionally monocular subjects have significantly higher Vernier acuity than functionally binocular subjects (Freeman and Bradley, 1980). Moreover, an electrophysiological response to a horizontal displacement of one of a pair of vertical lines arranged one above the other (Vernier task) has been recorded from the visual cortices of both humans (Levi et al., 1983; Zak and Berkley, 1985) and cats (Swindale and Cynader, 1986). The amplitude of the visually evoked potentials elicited by the appearance of a Vernier offset varied systematically with the magnitude of the offset. Thresholds obtained for these potentials were similar to the observer's psychophysical thresholds.

In addition it was found that the elevation of Vernier acuity thresholds in the presence of interfering flanking lines (Westheimer and Hauske, 1975) has an electrophysiological analog (Klein, 1984).

Invariant features of contrast detection and frequency discrimination tasks have resulted in models in which the retina is depicted as a self-similar detector array graded with respect to aperture size (Koenderink, 1977; Koenderink and van Doorn, 1978, 1982; Hartmann, 1982; Hirsch and Hylton, 1982, 1985; Burton et al., 1986). If these descriptions of the visual system have any validity it is a priori likely that the mechanisms that compute differential spatial displacement are also scale invariant (i.e. do not depend on the level of resolution at which the stimulus features used in the differential spatial displacement computation process are present). Therefore, it seems possible that the notion of hyperacuity can be generalized to low resolution tasks in which differential spatial displacement is computed from the output of detectors with large aperture sizes (large receptive field sizes).

Judgements based on relative spatial location of stimulus features are known to be less affected by optical blur than judgements based on resolution of stimulus features (Hartridge, 1923; Stigmar, 1971; Foley-Fisher, 1977; Westheimer, 1979; Enoch and Williams, 1983; Watt et al., 1983a; Watt and Morgan, 1984; Williams et al., 1984). This is attributed to the relative attenuation of the high spatial frequency components of the stimulus pattern. Blurring of a stimulus changes the relative contribution of channels tuned to different spatial frequencies (with different widths of spatial weighting functions) but it does not provide a precise control over the levels of resolution at which the stimulus features are present. In a study designed to investigate the differential sensitivity of spatial channels to relative position Schor and Badcock (1985) used DOG stimuli in an attempt to selectively stimulate size-tuned channels. However, no attempt was made to study the relation between the differential spatial displacement discrimination thresholds and the levels of resolution at which the stimulus features are present.

In order to investigate this relationship we designed an experiment to determine whether differential spatial displacement discrimination thresholds for low-resolution features scale with feature size, i.e.

whether the mechanisms involved in the detection of differential spatial displacements are scale invariant. In this case one may assume that the visual system uses the same strategy to compute relative spatial position on all levels of resolution. If different mechanisms are active at different levels of resolution one would expect to find indications for regions of transition in resolution space where a mechanism at a higher level of resolution starts to dominate the previous one active at a lower level of resolution. The relative spatial localization task we devised is equivalent to the three-dot alignment acuity task which is well documented in the literature (Ludvigh, 1953; Ludvigh and McKinnon, 1967; Andrews et al., 1973; Andrews and Miller, 1978; Beck and Schwartz, 1979; Watt, 1984).

METHODS.

Subjects.

Three male subjects, aged between 22 and 29, served in the experiment. Subject A.T. was highly practised with corrected myopic vision. Subjects H.S. and M.E. each underwent several weeks of practice before making the threshold measurements reported below. Both are emmetropic and have 20/15 Snellen acuity.

Apparatus.

A PDP 11/34 minicomputer in combination with a Gould deAnza IP8500 image array processor was used to generate, process and present the stimuli, record the responses and analyze the data.

The stimulus was displayed on a Philips LDH2123 monochrome monitor. The CRT was driven in an interlaced mode with a frame rate of 60 Hz. The display consisted of 512 × 512 pixels with the luminance value of each pixel quantized to 8 bits. A 512 × 512 correction matrix was added to the deAnza frame buffer to compensate for the inhomogeneity of the display.

The display was placed in an optical tunnel with nonreflecting black walls. Observers were seated with their heads supported by a chin rest, adjusted in height and position so that their dominant eye was on the line perpendicular to the center of the monitor screen. The use of a forehead rest prevented tilting of the head. Viewing was monocular with the subject's dominant eye. The unused eye was covered with an eye cap. Viewing distance varied from 12.5 cm to 16 m. Except for viewing distances of 12.5 cm and 25 cm viewing was through a 2 mm artificial pupil. At 12.5 cm and 25 cm the natural pupil was used in order to avoid vignetting effects. At these distances variations of accomodation had no influence on our results as the spread of the optical blur function of the eye is more than two orders of magnitude smaller than the spread of the spatial contrast profile of the stimuli that were presented.

Stimuli.

The stimuli comprised three blobs arranged one above the other at equal spatial intervals. The blobs had identical Gaussian spatial contrast profiles and were temporally modulated with a Gaussian envelope. Their luminance is given by

$$L(x,y,t) = L_b\,[1 + cw(x,y,t)]$$

where L_b denotes the background luminance and c is the threshold contrast value as determined for a single blob. The window function w(x,y,t) is given by

$$w(x,y,t) = \exp[-(x^2 + y^2)/(2s_s^2) - (t^2/(2s_t^2)]$$

We adopt the term spread for the distance over which a normalized Gaussian falls from 1 to $e^{-1/2}$, corresponding to the standard deviation measure as defined in statistics. (A spatial region with radius $2s_t$ and centered on (x,y) = (0,0) contains 92% of the total energy; a temporal interval of width $2s_t$ centered on t = 0 contains 96% of the total stimulus energy). The window function is the product of spatial and temporal

Gaussians with spreads of s_s and s_t respectively. Both the temporal and the spatial windows were truncated at plus and minus four times their spread (containing respectively 99.994% and 99.990% of the total stimulus energy). The threshold contrast c is defined as $(L - L_b)/L_b$, where L denotes the threshold luminance level.

Watt and Morgan (1983b) showed that the differential spatial displacement discrimination threshold for Gaussian blurred edges at 80% luminance contrast as a function of the stimulus extent reaches an asymptote when the extent of the displayed fraction of the blurred edge is at least 6 times the spread of the Gaussian blurring function. At threshold luminance contrast (typically 10%) we assume that an extent of 4 times the spread (containing 99.99% of the total stimulus energy) will serve to approximate optimum performance.

The spread of the Gaussian temporal profile was 0.2 sec (therefore the stimulus was above one half of its peak value for 0.47 sec). The frame rate was 60 Hz and interlaced. Intermediate presentations lasted for 0.08 sec, corresponding to 5 frames. This was found to be short enough to present a perceptually smooth temporal contrast profile. The total duration of the stimulus presentation was eight times the spread of its Gaussian temporal contrast profile (i.e. if T is the moment at which the stimulus attained its maximum contrast and s_t represents the spread of the Gaussian temporal contrast profile the presentation lasted from $T - 4s_t$ to $T + 4s_t$). The angular dimensions of the stimulus pattern were scaled by varying the viewing distance. Thus all stimuli were geometrically similar.

If we define the bandwidth of a Gaussian signal as the distance between the (negative and positive) frequency components for which the amplitude has dropped to one half of the value of the frequency component with maximum amplitude (which is at zero frequency for a Gaussian signal) we find that the temporal bandwidth is given by $(2 * \ln 2)^{1/2}/(\pi * s_t)$. In our case the temporal frequency bandwidth is 1.87 Hz and the spatial frequency bandwidth is between 0.1 cy/deg and 53.6 cy/deg.

We also used sharp edged (disc-like) circular stimuli. The results obtained with Gaussian blobs for a certain value of their spread were compared with the results obtained with discs with a radius of the same value.

Motivation of the stimulus choice.

Campbell and Robson (1968) proposed the existence in the human visual system of a set of independent spatial frequency selective mechanisms for the processing of spatially varying luminance distributions. Their proposal received support from a variety of psychophysical and physiological experiments (Campbell, 1974). Various techniques have also been used to measure the temporal properties of spatial frequency selective mechanisms (Watson and Nachmias, 1977; Breitmeyer and Ganz, 1977; Breitmeyer et al., 1981). There appear to be two distinct mechanisms termed sustained and transient after possible neural processes. The transient mechanisms respond best to rapid temporal changes whereas the sustained mechanisms respond best to steady or slowly varying stimuli. Kulikowsky and Tolhurst (1973) have found that transient mechanisms have a low-pass spatial frequency characteristic but a band-pass temporal characteristic. However, later results (Furchner et al., 1977; Arend and Lange, 1979; Stromeyer et al., 1982) indicate that there are mechanisms that are selectively sensitive to low spatial frequencies and Furchner et al. (1977) and Stromeyer et al. (1982) demonstrated (by using grating stimuli that were gradually turned on and off) that the sustained mechanisms are more narrowly tuned to low spatial frequency bands than the more broadly tuned transient mechanisms. Stromeyer et al. (1982) and Arend and Lange (1979) convincingly argued that there may not be a simple analogy between electrophysiologically defined "sustained" and "transient" neurons and psychophysical mechanisms. The dichotomy between transient motion sensitive channels and sustained spatial form-sensitive channels may therefore be the result of an unrealistic simplification.

An alternative formulation for a multiple channel model can be obtained by Fourier-transforming the spatial frequency tuning curves. This yields a set of weighting functions or "receptive fields" which represent the space-domain sensitivity of the spatial frequency channels (Thomas, 1970; MacLeod et al., 1974; Legge, 1976, 1978; Shapley, 1985; Kelly, 1985). It is assumed that the response of a single channel is proportional to the convolution of its corresponding receptive field weighting function and the stimulus luminance distribution. Schade (1956) postulated that the

receptive field weighting function could be described by the algebraic sum of two concentric Gaussian distributions. This is now often called a DOG (Difference of Gaussians) function (Wilson and Bergen, 1979) and has previously been used to fit the sensitivity profiles of retinal ganglion cells in the cat (Rodieck, 1965; Enroth-Cugell and Robson, 1966).

We adopted a smooth (Gaussian) spatial stimulus contrast profile and a smooth (Gaussian) temporal stimulus contrast profile in an attempt to stimulate only a small number (narrow range) of low-frequency selective (sustained) mechanisms. Both a sharp edged spatial stimulus contrast profile and an abrupt on- and off-set of the temporal stimulus contrast profile would have resulted in the activation of high spatial frequency sensitive transient mechanisms. These might in turn interfere with the operation of the low spatial frequency selective mechanisms under study. The smooth temporal on- and off-set also served to minimize the possibility that subjects compare the relative spatial location of temporal contrast gradients (Arend, 1976a). The short exposure duration (small spread of the Gaussian temporal profile) ensured that slow drifting eye movements, which could provide subjects with information about the relative position of the three blobs (e.g. by comparing the location of contrast gradients in the spatial contrast distribution), can make no significant contribution to the differential spatial displacement detection threshold.

Although it seems a priori reasonable to assume that the most detectable signal for a given detector must match the spatial weighting function of that detector (as can be inferred from the Schwarz-inequality) it is very illustrative to explicitly compute the response of receptive fields to a given stimulus. We therefore assumed a DOG-like spatial weighting function for the receptive fields. This weighting function was obtained by taking the Laplacian of a two dimensional Gaussian. The DOG-like weighting function thus obtained has the advantage that it can be characterized by only one parameter, namely the spread of the underlying Gaussian. Moreover, it has a zero spatial integral*. The response of a

*It can be shown that a DOG-function, with spread s of its center excitatory part and r.s of its surrounding inhibitory part, attains minimal bandwidth, and approaches the Laplacian of a Gaussian function

receptive field to a stimulus was obtained by taking the integral of the product of the receptive field weighting function and the luminance distribution of the stimulus pattern.

To illustrate that the retinal response to a retinal Gaussian intensity distribution is rather well localized in the retinal image plane we calculated the response of a receptive field to a Gaussian intensity distribution as a function of the distance of the receptive field centre from the centre of the forementioned distribution. As shown in Fig. 1 this response is maximal when the receptive field is centered on the Gaussian intensity distribution. For a receptive field with a spread equal to that of the Gaussian intensity distribution the response drops to about 60% of the maximum response over a distance equal to the spread of the Gaussian intensity distribution. For a receptive field with a spread that differs a factor 5 from the spread of the intensity distribution the response is nowhere more than 18% of the response of a receptive field with a spread equal to the spread of the Gaussian intensity distribution and it falls off to zero fast over distances larger than the spread of the Gaussian intensity distribution.

We calculated the response of receptive fields centered on a Gaussian intensity distribution as a function of their spreads (expressed as a fraction of the spread of the Gaussian intensity distribution, see Fig. 2) in order to illustrate that the response to a retinal Gaussian intensity distribution is rather well localized in resolution space. It appears that receptive fields with spreads equal to that of the Gaussian intensity distribution have maximum response. For receptive fields with spreads that differ a factor 5 from the spread of the applied Gaussian intensity distribution the response has dropped to 10% of the value of the response of a receptive field with a spread equal to that of the intensity distribution.

Because the receptive fields in the retina overlap and interact we also computed the response of a whole layer of (continuously distributed) receptive fields of the same spread as a function of the spread of the receptive fields (Fig. 3). We therefore applied spatial probability

with spread s, in the limit of r approaching 1.)

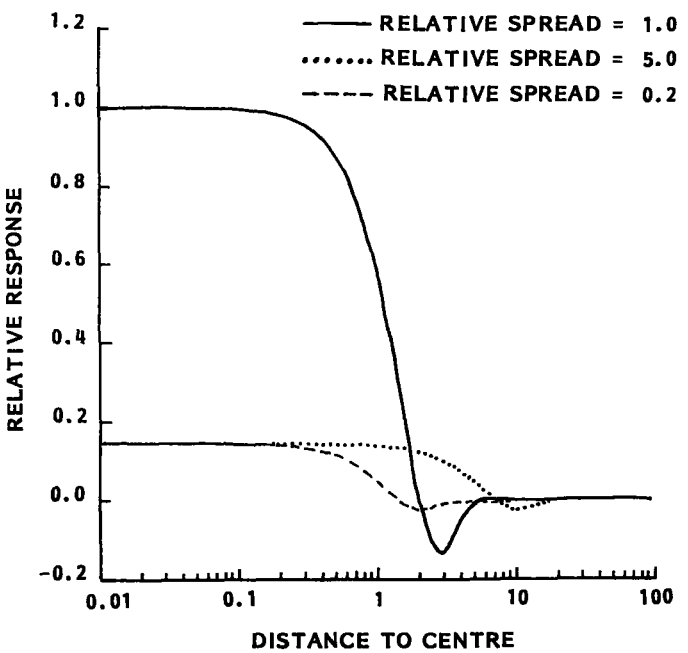

Figure 1. The response of receptive fields with DOG-like weighting functions to a Gaussian intensity distribution. The responses are shown as a function of the distance of the receptive field centers from the centre of the intensity distribution. The response values are normalized for the response of a receptive field with a spread equal to that of the Gaussian intensity distribution and centered on this distribution. The response functions are shown for spatial weighting functions with 0.2, 1 and 5 times the spread of the Gaussian intensity distribution. This figure illustrates that the response falls off to zero fast over distances larger than the spread of the intensity distribution.

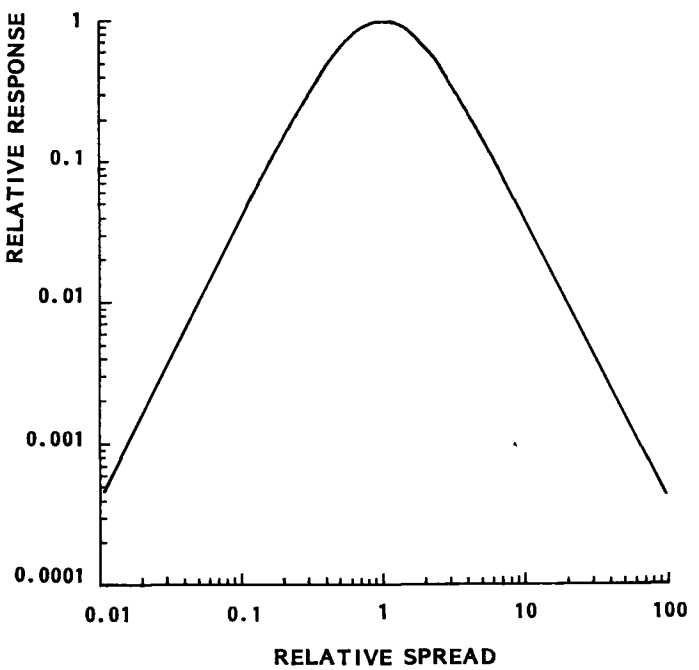

Figure 2. The response of receptive fields with DOG-like weighting functions, centered on a Gaussian intensity distribution. The response is shown as a function of the spread of the weighting function, relative to the spread of the intensity distribution. The response values are normalized for the response of a receptive field with a spread equal to that of the Gaussian intensity distribution. This figure illustrates that the response falls off fast for weighting functions with a spread differing a factor more than two from the spread of the Gaussian intensity distribution.

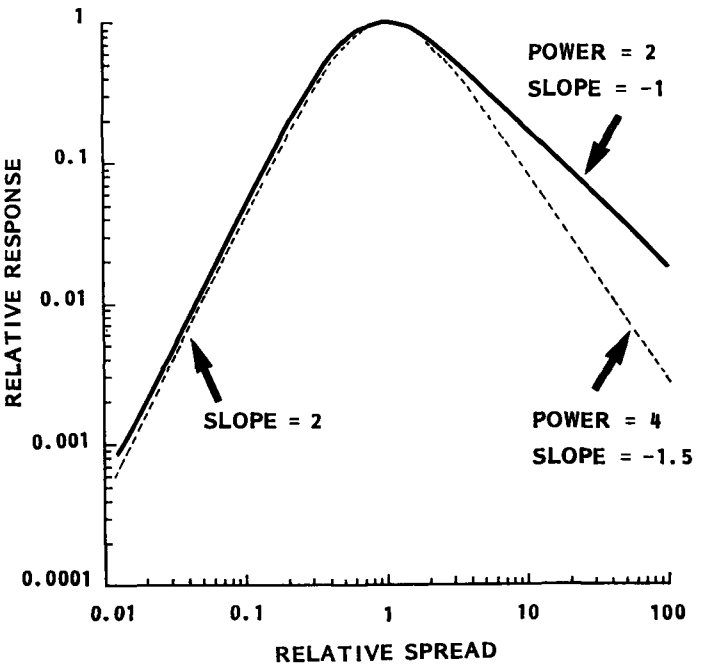

Figure 3. The response of layers of continuously distributed receptive fields with DOG-like weighting functions to a Gaussian intensity distribution. It was assumed that the spread of the weighting functions is constant within a layer. Spatial probability summation was used to compute the total response of a layer. The relative contribution of each receptive field was computed, using two different powers in the summation process. A power of 2, resulting in the squared mean of the response of all receptive fields within a layer and a power of 4 as propagated by Wilson and Bergen (1979) The response of the layers is shown as a function of the spread of their corresponding weighting functions relative to the spread of the weighting function corresponding to the layer with maximum response. The spread of the weighting functions in the layer with maximum response is given by $(N/(N-1))^{1/2}s_b$, in which N denotes the power used in the spatial probability summation and s_b denotes the spread of the Gaussian intensity distribution. This figure illustrates that the response to a Gaussian intensity distribution is rather well localized in resolution space.

summation. We used two powers in the calculation of the mean relative contribution of each receptive field. A power of 2, resulting in the squared mean of the response of all receptive fields within a layer, and a power of 4, as propagated by Wilson and Bergen (1979). If N is the power used in the spatial probability summation the response is maximal for a layer with receptive fields that have a spread equal to $(N/(N-1))^{1/2}$ times the spread of the Gaussian spatial intensity distribution. The response of layers with receptive field spreads differing by a factor 10 or more from the spread of the Gaussian intensity distribution have an overall response of nearly 10% of the response of the layer in which the receptive field spread is equal to that of the Gaussian intensity distribution.

According to the multiple channel models a decrease of the stimulus contrast level may cause the stimulus contrast to drop below the detection threshold of one or more of the channels that were previously operating at higher contrast levels (Woodward et al., 1985). Because we were interested in the three-blob alignment discrimination threshold as a function of the resolution (spatial frequency) of the blobs we wanted our stimuli to activate as few spatial frequency channels as possible. Therefore the experiment was performed at the detection threshold contrast level as determined for a single blob.

The vertical distance between the centres of the outer two blobs was 10 times the spread of the Gaussian spatial contrast profile of the blobs. The blobs appeared clearly resolved at this distance. The center blob appeared on one of 15 different horizontal positions relative to the axis defined by the outer two blobs: 0, ±1/64, ±2/64, ±3,64, ±4/64, ±6/64, ±8/64 and ±12/64 times the spread of the Gaussian spatial blob contrast profile. These positions were determined in an extensive series of practice trials designed to ensure that their corresponding response levels spanned the psychometric function.

The continued response of the visual system following the termination (offset) of briefly presented stimuli is known to generate so-called after-images, even at threshold luminance contrast (Bowen et al., 1974; Bowling and Lovegrove, 1980). This visual persistence has been shown to increase with decreasing stimulus contrast (Bowling et al., 1979). To avoid the possibility that the presence of after-images or memory effects

would introduce (false) cues in the relative spatial localization task the stimulus pattern as a whole appeared at random on one of 9 different horizontal positions, symmetrical with regard to the centre of the screen (0, ±3/16, ±6/16, ±9/16, ±12/16 times the size of the spread of the Gaussian blob profile). If the stimulus pattern had appeared in the same position in each trial comparison (using either the presence of after-images or memory effects) of successive displacements of the middle blob relative to the axis through the outer two blobs would have introduced a (false) cue for the localization judgement.

The stimulus was superposed on a 100 cd/m^2 (300 Td for the 2 mm pupil) luminance background level. The luminance level of the background was chosen such as to operate in the photopic domain.

Procedure.

The determination of the contrast threshold.

After adaptation of the subject to the background luminance level, the contrast detection threshold for a single Gaussian blob was determined. This was done by means of a staircase method. The Gaussian blob was presented on the centre of the monitor screen and appeared according to the forementioned Gaussian temporal contrast envelope. Subjects were instructed to fixate on the centre of the monitor screen. No fixation mark was used. A continuously present fixation mark on the centre of the monitor screen would severely impair the determination of the contrast detection threshold because it would cover the area of maximum contrast of the blobs. Due to the large spatial extent of the stimuli that were used a continuously present fixation mark outside the range of the spatial stimulus contrast profile would cause extrafoveal perception of the blobs over the complete range of spatial stimulus extents used. A discontinuously present fixation mark (e.g. a light spot turned on in the intervals between two consecutive stimulus presentations and interrupted on presentation of the stimuli) could activate transient mechanisms which might in turn interfere with the low-frequency selective mechanisms under

study and thereby influence the contrast detection thresholds that are to be determined.

The onset of a stimulus presentation was announced by a buzzer signal. By pressing the appropriate response buttons the subject had to respond "yes" if he had seen the blob and "no" if he could not detect it. A new presentation was started immediately after the subject had responded (the length of the time interval between two consecutive presentations depended on the subject's response time). On a negative response the maximum contrast level reached during the next presentation was increased, on a positive response it was decreased. The stepsize with which the maximum contrast level reached during a presentation was changed decreased on each turning point. A total of 11 turning points were measured of which the first three were discarded. The mean of the resulting 8 turning points was taken as the threshold luminance contrast level or the level at which 50% of the presentations is seen.

The contrast detection thresholds for the Gaussian blobs were determined at the start of each session and between separate runs.

The determination of the differential spatial displacement discrimination thresholds.

For the three-blob acuity task no use was made of a fixation mark either because it would have presented a cue for the task to be performed. Therefore the subjects were instructed to fixate on the centre of the monitor screen.

The method of constant stimuli was used. The 15 stimulus levels used were determined during an extensive series of practice trials. These levels were chosen in such a way that they were evenly distributed over the corresponding psychometric curve. The sequence of presentation of the different stimulus levels was random. At the onset of each presentation a buzzer signal sounded. After completion of the presentation the subject had to choose (forced choice) between a left or right displacement of the middle blob relative to the axis defined by the outer two blobs. Immediately after the subject had responded to a trial a new presentation

was started. By withholding his answer for a while the subject was able to take a short rest. In case no decision could be made because one or more blobs were not detected (and in that case only) the subject could skip his obligation to answer and go on to the next presentation. In this case the missed presentation was randomly incorporated into the sequence of remaining trials. This situation occurred in about half of the number of presentations.

For each of the 15 possible positions of the centre blob 100 answers were obtained in 10 runs of 10 answers per position each. Each session consisted of three to four runs preceded by one test run.

The resulting psychometric function was determined by Probit analysis (Finney, 1971). The standard deviation of the subject's error response distribution serves as a measure of threshold sensitivity and corresponds to the difference between the 50% and 83% points on the psychometric function.

RESULTS.

For a large range of angular dimensions of the Gaussian blobs (spanning two decades) we measured their contrast detection thresholds. The angular dimensions of the blobs were varied by varying the viewing distance. Blobs with spread values below 1.5 min of arc were obtained by reducing the blob dimensions on the monitor screen. Except for blobs with spreads larger than 55 min of arc viewing was through a 2 mm artificial pupil. The blobs were temporally modulated with a Gaussian envelope with a spread of 0.2 sec. The results, represented in Fig. 4, show that the contrast detection thresholds of the Gaussian blobs are independent of their angular dimensions.

As a comparison we measured the contrast detection thresholds for sharp-edged circular discs. The discs had the same temporal modulation as the Gaussian blobs. In Fig. 4 the contrast detection thresholds obtained for discs of a certain radius are compared with the detection thresholds of blobs with a spread of the same value. This comparison is of course rather arbitrary as one cannot be sure what fraction of the spatial

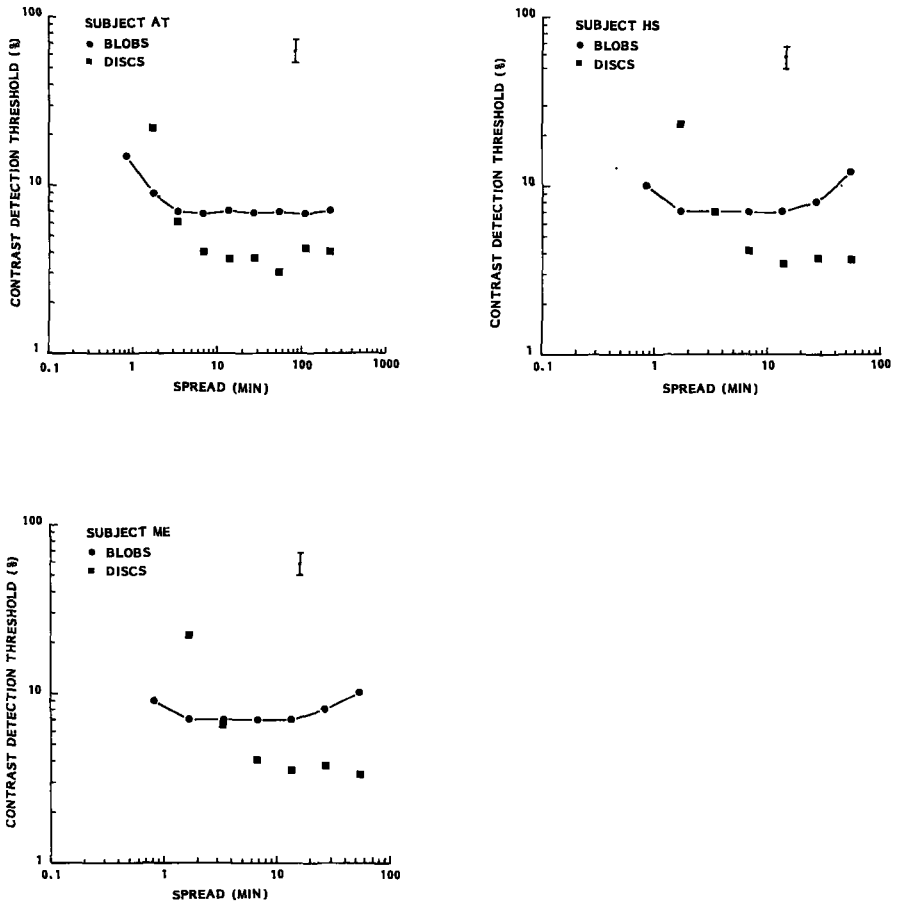

Figure 4. Contrast detection thresholds for Gaussian blobs and (sharp-edged) circular discs as a function of their spatial scale parameters (respectively spread and radius) are shown for three subjects. All stimuli were temporally modulated with a Gaussian envelope with a spread of 0.2 sec. The error bar represents two standard errors.

contrast profile of the Gaussian blobs actually contributes to their detection. Therefore there is no simple equivalence relation between the spread of the Gaussian blobs and the radius of the circular discs. Our results show that the contrast detection thresholds for discs larger than $2'$ are always below the (constant) contrast detection thresholds for the Gaussian blobs and decrease with increasing angular dimensions.

Contrast detection thresholds were measured at the start of each run of the three-blob differential spatial displacement discrimination task. We found that the detection thresholds remained constant during the sessions and were reproduced in separate sessions.

The differential spatial displacement discrimination thresholds for the three-blob task as a function of the angular dimensions of the blobs are shown in Fig. 5. The thresholds were defined as those displacements which resulted in a fraction of 83% correct localization judgements. The stimuli were temporally modulated with a Gaussian envelope with a spread of 0.2 sec. We computed a least-square fit of an exponential curve to our data points. Only data points for spreads larger than 1.5 min of arc were used in the calculation of the regression lines. The least-square curves thus obtained closely fit the data points. The correlation coefficients (r^2) range in value between 0.99 and 1.00. The powers obtained for the exponential curves range between 0.98 and 1.00. We may therefore conclude that the differential spatial displacement discrimination threshold is a constant fraction of the angular dimensions of the blobs, at least for blobs with spreads larger than approximately 1.5 min of arc.

For blobs with spreads smaller than 1.5 min of arc the differential spatial displacement discrimination thresholds rise. This is probably a result of the fact that the blobs can no longer be resolved by the subjects.

For two subjects we measured the differential spatial displacement discrimination thresholds for sharp edged circular discs. In Fig. 5 the results of these measurements are shown as a function of the angular dimension of the radius of the discs. If the differential spatial displacement discrimination thresholds for discs of a certain radius are compared with the thresholds obtained for Gaussian blobs with a spread of the same value we see that for radius values larger than 1.5 min of arc

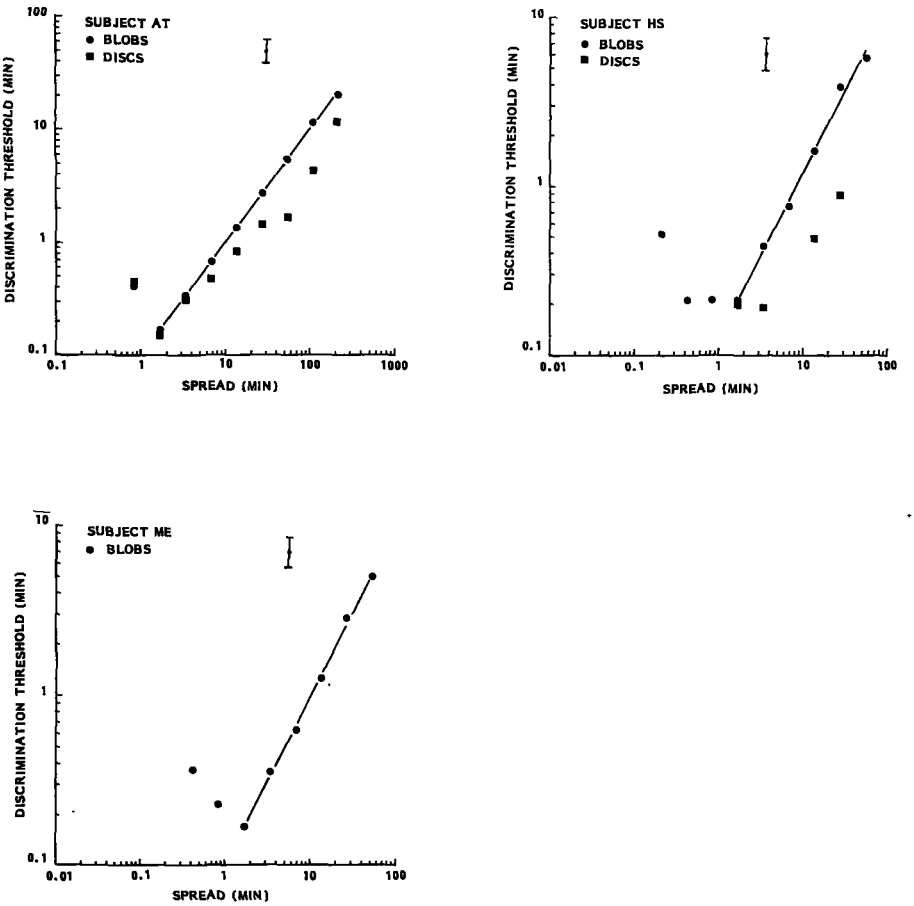

Figure 5. Differential spatial displacement discrimination thresholds for Gaussian blobs (all subjects) and circular discs (subjects AT and HS) as a function of stimulus scale represented by the spread of the Gaussian blobs (respectively the radius of the circular discs). All stimuli were temporally modulated with a Gaussian envelope with a spread of 0.2 sec. The solid line indicates the result from a least square fit of an exponential curve to the data points. The error bar represents two standard errors.

the thresholds for discs are lower than those for blobs. For increasing radius width of the discs the discrepancy between the differential spatial displacement discrimination thresholds for discs and for blobs increases.

DISCUSSION.

The constancy of the measured contrast detection threshold values for the Gaussian blobs as function of their angular dimensions is in agreement with the results of Arend (1976a, 1976b) who found that low frequency selective spatial channels are equal in sensitivity when the temporal changes of retinal illuminance are equal. This result seems to indicate that we have succeeded in stimulating only a small range of low spatial frequency selective mechanisms. In terms of a layered sampling lattice model of spatial vision in which the lattice spacing is proportional to the detector aperture size (Koenderink, 1977; Koenderink and van Doorn, 1978, 1982; Hirsch and Hylton, 1985) this result implies (i) that only a small and approximately constant number of receptive fields with spatial dimensions of the order of the retinal projections of the Gaussian blobs contributes to their detection, thereby causing their detection thresholds to remain constant, whereas (ii) an increasing number of high frequency selective mechanisms contributes to the detection of the sharp edged discs on increasing their radius (and thus their sharp edged circumference), thereby lowering their respective detection threshold.

For stationary stimuli the rate of local temporal illuminance change on the retina, dL/dt, is the product of the rate of movement of the stimulus pattern with respect to the retina, ds/dt, and the spatial rate of change of illuminance at that locus in the retinal image, dL/ds. At high spatial frequencies even the limited eye movements of fixation will produce rapid temporal changes which will lower the detection threshold. This may explain the difference found between the detection thresholds for sharp and blurred stimuli on prolonged presentations (Shapley, 1974) and the equality of those thresholds for short presentation durations (Hood, 1973).

Also in our case small involuntary eye movements may explain the difference found between the detection thresholds of the Gaussian blobs and the discs as a function of their angular dimensions. Due to the presence of the sharp edges of the spatial contrast profile of the discs small involuntary eye movements may activate high spatial frequency sensitive mechanisms. For increasing angular dimensions of the discs the number of activated high frequency selective mechanisms will increase. For increasing angular dimensions of the Gaussian blobs the activation of high spatial frequency selective mechanisms due to small involuntary eye movements will decrease because of the decreasing spatial rate of change of the stimulus contrast profile.

The results show that differential spatial (orthoaxial) displacement discrimination thresholds for the three-blob alignment task scale linearly with stimulus size over a range of at least two decades. The differential spatial displacement discrimination threshold is always an order of magnitude smaller than the spread of the Gaussian blobs. For angular dimensions of the stimuli smaller than 1.5 min of arc the blurring (point spread) function of the eye causes the thresholds to rise, probably because the stimuli can no longer be resolved.

Due to the fact that the relative localization experiment was performed at threshold luminance contrast (the contrast level at which 50% of the presentations is seen) in about half of the presentations no answer could be obtained. A number of stimulus presentations is probably missed due to the uncertainty in the spatial position in which the stimulus pattern as a whole appeared (Cohn and Lasley, 1974; Cohn and Wardlaw, 1985). The subjects had the impression that they were able to reach a conclusion on presentations in which they could not resolve the blobs by determining the global orientation or curvature of the observed (unresolved) stimulus pattern as whole. The criterium that was actually used (curvature or orientation) probably depends on the fraction of the pattern that was actually observed. Observation of all three blobs permits the use of both an orientation and a curvature criterium. When one of the outer two blobs is missed only the orientation criterium can be used (orientation of the axis defined by the remaining two blobs relative to a subjective vertical). When the blob in the middle, two, or all three blobs

are missed the subject is unable to reach a conclusion. In a large fraction of the presentations the subjects had the impression that the lower blob was displaced relative to the axis through the upper two (which appeared to be vertically oriented in that case); in those instances an orientation or curvature criterium also proved helpful to obtain an answer.

Sullivan et al. (1972) have compared the thresholds obtained for five different hyperacuity tasks, namely (i) the Vernier alignment threshold as a function of the vertical separation between the lines, (ii) the threshold for detection of the tilt of a single line from the vertical as a function of line length, (iii) the threshold of the three-dot alignment task as a function of dot separation, (iv) the threshold for the detection of curvature as a function of arc length and (v) the threshold for displacement detection for the lower of two dots relative to the vertical through the upper dot. Assuming specific orientation cues for each task they were able to express these thresholds as an angle of rotation about the vertical. They claim that the thresholds as a function of the separation between the orientation cues in the stimulus coincide for the various tasks. Especially in the case of the two-dot hyperacuity task (Sullivan et al., 1972; Westheimer and McKee, 1977b; Beck and Schwartz, 1979; Beck and Halloran, 1985) no other cue than orientation of the axis through the two dots relative to the vertical seems to be present. Using an ideal detector to determine the efficiency of their subjects Andrews et al. (1973) concluded that curvature cannot solely be detected according to differences in orientation signals. Watt and Andrews (1982) and Watt (1984) argued that straight and curved lines are processed in parallel by different mechanisms. In a recent paper Wilson (1985) provides evidence that curvature discrimination is based on the responses of spatial frequency- and orientation selective-mechanisms. In any case we assume that in our experiment the nature of the detection task remains the same whether the subject sees the blobs resolved or as a curved global pattern.

Because it is known for the three-dot alignment task that the differential spatial displacement discrimination threshold has an optimum as a function of the distance between the outer two dots (Ludvigh, 1953; Sullivan et al., 1972; Beck and Schwartz, 1979; Watt, 1984; Beck and

Halloran, 1985) an experiment was performed to determine the variation of the differential spatial displacement discrimination threshold with the distance between the outer two blobs. For separations between the outer two blobs from 4 to 24 times the spread of the Gaussian spatial contrast profiles (the maximum separation allowed by the finite dimensions of the monitor screen) no variation of the differential spatial displacement acuity threshold was found. We therefore concluded that (at least over the range of spatial separations between the outer two blobs that was admitted by the finite dimensions of the monitor screen) there was no "optimum" distance between the outer two blobs.

The differential spatial displacement discrimination thresholds rose for spatial separations between the outer two blobs smaller than 3 times the spread of the Gaussian spatial contrast profiles. For these separations the blobs appeared no longer resolved which considerably impaired the detection task.

The overall orientation of the stimulus pattern has been shown to exert a (small) effect on relative location judgement tasks (Leibowitz, 1953) and on the three-dot alignment task in particular (Ludvigh and McKinnon, 1967). We measured the differential spatial displacement discrimination thresholds for the three-blob task with a horizontal orientation of the line joining the centres of the outer two blobs. Differential spatial displacement discrimination thresholds thus obtained did not differ from those obtained from the measurements with a vertical orientation of the stimulus pattern. These results agree with those of McKee and Westheimer (1978) for the three-dot alignment task. Because McKee and Westheimer (1978) found that the thresholds obtained for oblique orientations of the stimulus pattern depend strongly on practice and that both the sign and the dependence on practice of the observed differences varied strongly between different subjects we did not determine thresholds for oblique stimulus orientations.

We measured the ability of the subjects to maintain their voluntary fixation during a stimulus presentation. The electro-oculograms obtained showed no evidence of saccadic eye-movements larger than 0.5 deg (corresponding to the limit set by the resolution of our set-up) for the duration of the stimulus presentation. Therefore, we may conclude that the

subjects performed in the relative spatial localization judgement tasks without the help of information obtained from saccadic eye-movements introduced by the lack of a fixation stimulus.

We will now discuss what strategy the visual system might use to perform relative spatial localization judgements. Hering (1899) postulated the theory of mean local sign. According to this theory the visual system can perform relative spatial localization tasks with an accuracy of a fraction of a retinal receptor diameter by taking the mean of the place tags of a collection of retinal receptors. The increase in differential spatial displacement discrimination thresholds found for two- and three-dot tasks with increasing interdot separation (Beck and Halloran, 1985) indicates that the visual system is unable to access and compare the absolute retinal position of activated retinal receptors. Koenderink (1984a, 1984b) has recently argued how relative place tags may be assigned to a collection of nervous elements by the (physiologically imposed) constraints on the simultaneous/successive order of their total activity.

Now we have to consider to what features of a stimulus that are objectively present in the retinal image a place tag could be assigned by the visual system. We found that the differential spatial displacement discrimination thresholds for the three-blob task were almost constant as a function of the separation between the centers of the outer two blobs (at least for separations larger than three blob spreads and over the range of separations the finite display dimensions allowed) and that they scaled linearly with the angular dimensions of the blobs. The computation of place tags for peaks in the retinal intensity distribution would involve a comparison of the activity of receptive fields with angular dimensions that are at least an order of magnitude smaller than the angular dimensions of the stimuli. The activity of adjoining small receptive fields coinciding with the retinal projections of blobs with large spatial spreads will vary very slowly over the retinal image plane. One would therefore expect the accuracy with which the location of the peak in a Gaussian retinal intensity distribution can be determined to be inversely related to the spread of that distribution if the visual system uses the strategy of comparing the activity of neighbouring receptive fields. This expectation seems confirmed by our results. However, we have

argued that the retinal response to a retinal Gaussian intensity distribution is rather sharply localized in resolution space. It seems very unlikely that the visual system would base its localization judgements on the response of the least active detectors instead of using the output of the most active ones. One may object that the decreasing differential spatial displacement discrimination thresholds for increasing spread of the Gaussian blobs may be a demonstration of increasing inhibition as the surround of a peak increases on increasing the spread of the Gaussian blobs, thereby maybe raising the detection threshold for the peak. We therefore measured the differential spatial displacement discrimination thresholds for the three-blob task at 30% stimulus contrast and found that all threshold values decreased (their value was typically 0.7 times the values found for the experiments performed at threshold luminance contrast, which was typically 7%). If inhibition had been involved one would expect this effect to become stronger on increasing stimulus contrast, thereby raising the differential spatial displacement discrimination thresholds. We conclude that it is not very likely that the visual system computes the relative spatial position of peaks in the retinal light distribution. This conclusion is in agreement with that of Watt and Morgan (1983a) who explicitly verified that the location of a peak was not available for relative location judgements.

If the visual system is able to compare the relative spatial position of spatial gradients in the retinal light distribution one would expect the differential spatial displacement discrimination thresholds to remain constant for a constant ratio between blob spread and luminance contrast (i.e. for geometrically similar spatial contrast profiles). The foremen-tioned measurements at 30% luminance contrast demonstrate that this is not the case. For a constant ratio between the blob spread and the luminance contrast value we found that the differential spatial displacement acuity thresholds were approximately 6 times higher for a luminance contrast of 7% than for a luminance contrast of 30%. These results agree with those of Watt et al. (1983b) who ruled out gradient detection as a mechanism for detection of Gaussian edge blur on the same argument.

Psychophysical data have been presented (Watt and Morgan, 1983a, 1983b) supporting the hypothesis that the visual system may use the zero-

crossings or stationary points in the second derivative of the retinal light distribution as features on which relative localization judgements might be based. These features may be available to the visual system after the convolution of the retinal image with the spatial (DOG-like) weighting function of the receptive fields corresponding with the retinal ganglion cells (Marr et al., 1980).

Location may also be assigned to some spatially weighted mean of the retinal light distribution. By using stimuli that are subthreshold, devoid of contours and even of contrary information content, Westheimer and McKee (1977a) have shown that differential local signs can be integrated over regions extending several minutes of arc and may be still be used to elaborate differential spatial localization tasks precise to a fraction of a receptor diameter. Experiments of Watt and Morgan (1983a), Watt et al. (1983b) and Zeevi and Mangoubi (1984) have demonstrated that the visual system assigns the relative spatial location of stimulus features to the first moment of the retinal intensity distribution corresponding to those features.

We have argued that it is likely that our stimuli will only stimulate a small range of spatial frequency selective mechanisms (only receptive fields with spatial dimensions of the order of those of the retinal projection of the Gaussian blobs will contribute to their detection) when the Gaussian blobs are at their respective detection threshold contrast level. Assuming that we have indeed succeeded in stimulating only a small number of receptive fields within a narrow range of receptive field widths and noting from our results that differential spatial displacement discrimination thresholds scale linearly with blobsize we may conclude that differential spatial displacement discrimination thresholds scale linearly with the level of resolution at which the stimulus features are present. If the visual system uses different strategies to encode relative location at different levels of resolution one would expect to find indications for regions of transition between the ranges in resolution space in which the different mechanisms are active. However, our data, as well as those of Hirsch and Hylton (1982, 1985), provide no indication for the existence of different mechanisms to encode relative spatial position. Even the ratio between the spread of the Gaussian blobs (which is, as we

have argued before, a measure for the width of the receptive fields most actively responding to stimulation with those blobs) and the corresponding differential spatial displacement discrimination thresholds (typically 0.1) is close to the ratio of the differential spatial displacement discrimination thresholds obtained for the three-dot alignment task (Ludvigh, 1953; Ludvigh and McKinnon, 1967; Andrews et al., 1973; Andrews and Miller, 1978; Beck and Schwartz, 1979; Watt, 1984) and the spread of the optical blur function of the eye. Therefore it seems that the visual system assigns relative location tags to receptive fields on all levels of resolution. These can then in turn be used to compute the differential spatial displacement of stimulus features at a certain level of resolution to an accuracy which is small and constant fraction of the prevailing receptive field width at that level of resolution. These place tags may be encoded in the constraints imposed on the simultaneous activity in the ganglion cell network (Koenderink, 1984a, 1984b).

The same conclusion was reached by Hirsch and Hylton (1982, 1985), who reported that the ability of human observers to discriminate between different spatial frequencies was not a smooth function of frequency but had a definite segmented structure. They interpreted this structure as being due to the existence of a class retinal receptive fields that perform a dual function of neural blurring and spatial sampling. They propose a scaled lattice model of spatial vison that allows apparently scale-free spatial processing. This model is similar to Koenderink's model (1978, 1982) in which the retina is depicted as a self-similar detector array graded with respect to aperture size. They speculate that hyperacuity is the result of a general strategy for encoding positional information and that the difference between high and low resolution is determined by whether differential spatial displacement computations are performed on the output of a receptor lattice on a level of high or low resolution.

Our result that differential spatial displacement discrimination thresholds scale with stimulus size suggests that there is a general strategy for differential spatial displacement discrimination. Therefore, we conclude that (at least in the specific differential orthoaxial spatial displacement task used in this study) the human visual system uses one

strategy to detect differential spatial displacements independent of the level of resolution at which the stimulus features are present.

Acknowledgement - This work was supported by the Dutch Foundation for the Advancement of Pure Research (ZWO).

REFERENCES.

Andrews D.P., Butcher A.K. and Buckley B.R. (1973) Acuities for spatial arrangement in line figures: human and ideal observers compared. Vision Res. 13, 599-620.

Andrews D.P. and Miller D.T. (1978) Acuity for spatial separation as a function of stimulus size. Vision Res. 18, 615-619.

Arend L.E. (1976a) Temporal determinants of the form of the spatial contrast thresholds MTF. Vision Res. 16, 1035-1042.

Arend L.E. (1976b) Response of the human eye to spatially sinusoidal gratings at various exposure durations. Vision Res. 16, 1311-1315.

Arend L.E. and Lange R.V. (1979) Influence of exposure duration on the tuning of spatial channels. Vision Res. 19, 195-199.

Barlow H.B. (1979) Reconstructing the visual image in space and time. Nature 279, 189-190.

Beck J. and Halloran T. (1985) Effects of spatial separation and retinal eccentricity on two-dot Vernier discrimination. Vision Res. 25, 1105-1111.

Beck J and Schwartz T. (1979) Vernier discrimination with dot test objects. Vision Res. 19, 313-319.

Bowen R.W., Pola J. and Matin L. (1974) Visual persistence: effects of flash luminance, duration and energy. Vision Res. 14, 295-303.

Bowling A. and Lovegrove W. (1980) The effect of stimulus duration on the persistance of gratings. Percept. & Psychophys. 27, 574-578.

Bowling A., Lovegrove W. and Mapperson B. (1979) The effect of spatial frequency and contrast on visual persistence. Perception 8, 529-539.

Breitmeyer B.G. and Ganz L. (1977) Temporal studies with flashed gratings: inferences about human transient and sustained channels. Vision Res. 17, 861-866.

Breitmeyer B.G., Levi D.M. and Hartwerth R.S. (1981) Flicker masking in spatial vision. Vision Res. 21, 1377-1385.

Burton G.J., Haig N.D. and Moorhead I.R. (1986) A self-similar stack model for human and machine vision. Biol. Cybern. 53, 397-403.

Campbell F.W. (1974) The transmission of spatial information through the visual system. In: The Neurosciences Third Study Program (ed. Schmitt F.O. and Worden F.G.), 95-103. MIT Press, Cambridge, Mass.

Campbell F.W. and Robson J. (1968) Application of Fourier analysis to the visibility of gratings. J. Physiol. 197, 551-566.

Cohn T.E. and Lasley D.J. (1974) Detectability of a luminance increment: effect of spatial uncertainty. J. Opt. Soc. Am. 64, 1715-1719.

Cohn T.E. and Wardlaw J.C. (1985) Effect of large spatial uncertainty on foveal luminance increment detectability. J. Opt. Soc. Am. A2, 820-825.

Enoch J.M. And Williams R.A. (1983) Development of clinical tests of vision: initial data on two hyperacuity paradigms. Percept. & Psychophys. 33, 314-322.

Enroth-Cugell C. and Robson J.G. (1966) The contrast sensitivity of retinal ganglion cells of the cat. J. Physiol. 187, 517-522.

Finney D.J. (1971) Probit Analysis, 3rd edn. Cambridge Univ. Press.

Foley-Fisher J.A. (1977) Contrast, edge-gradient, and target line width as a factor in Vernier discrimination. Optica Acta 24, 179-186.

Freeman R.D. and Bradley A. (1980) Monocularly deprived humans: non-deprived eye has supernormal Vernier discrimination. J. Neurophysiol. 43, 1645-1653.

Furchner C.S., Thomas, J.P. and Campbell F.W. (1977) Detection and discrimination of simple and complex patterns at low spatial frequencies. Vision Res. 17, 827-836.

Hartmann G. (1982) Recursive features of circular receptive fields. Biol. Cybern. 43, 199-208.

Hartridge H. (1923) Visual discrimination and the resolving power of the eye. J. Physiol. 57, 52-67.

Hering E. (1899) Über die Grenzen der Sehschärfe. Ber. Math.-phys. Cl.d. Königl. Sächs. Gesell. Wiss. Leipzig. Naturwiss. Teil 16-24.

Hirsch J. and Hylton R. (1982) Limits of spatial-frequency discrimination as evidence of neural interpolation. J. Opt. Soc. Am. 72, 1367-1374.

Hirsch J. and Hylton R. (1985) Spatial-frequency discrimination at low frequencies: evidence for position quantization by receptive fields. J. Opt. Soc. Am. A2, 128-135.

Hood D.C. (1973) The effects of edge sharpness and exposure duration on detection threshold. Vision Res. 13, 759-766.

Kelly D.H. (1985) Receptive-field-like function inferred from large-area psychophysical measurements. Vision Res. 25, 1895-1900.

Klein S.A. (1984) Spatial interference with cortical potentials evoked by Vernier offsets. Invest. Opht. visual Sci. 25, 144 (A)

Klein S.A. and Levi D.M. (1985) Hyperacuity thresholds of 1 sec: theoretical predictions and empirical validation. J. Opt. Soc. Am. A, 2, 1170-1190.

Koenderink J.J. (1977) Current models of contrast processing. In: Spatial Contrast, Report of a workshop held in Amsterdam, 1976. Spekreijse H. and Tweel L.H. eds. Amsterdam-Oxford-New York: North Holland.

Koenderink J.J. (1984a) Simultaneous order in nervous nets from a functional standpoint. Biol. Cybern. 50, 35-41.

Koenderink J.J. (1984b) The concept of local sign. In: Limits in Perception. Eds. Doorn A.J. van, Grind W.A. van de and Koenderink J.J., VNU Science Press, Utrecht, 495-547.

Koenderink J.J. and Doorn A.J. van (1978) Visual detection of spatial contrast; influence of location in the visual field, target extent and illuminance level. Biol. Cybern. 30, 157-167.

Koenderink J.J. and Doorn A.J. van (1982) Invariant features of contrast detection: an explanation in terms of self-similar detector arrays. J. Opt. Soc. Am. 72, 83-87.

Kulikowsky J.J. and Tolhurst D.J. (1973) Psychophysical evidence for sustained and transient detectors in human vision. J. Physiol. 232, 149-162.

Legge G.E. (1976) Adaptation to spatial impulse: implication for Fourier transform models of visual processing. Vision Res. 16, 1407-1418.

Legge G.E. (1978) Sustained and transient mechanisms in human vision: temporal and spatial properties. Vision Res. 18, 69-81.

Leibowitz H. (1953) Some observations and theory on the variation of visual acuity with the orientation of the test object. J. Opt. Soc. Am. 43, 902-905.

Levi D.M., Klein S.A. and Aitsebaomo A.P. (1985) Vernier acuity, crowding and cortical magnification. Vision Res. 25, 963-977.

Levi D.M., Manny R.E., Klein S.A. and Steinman S.B. (1983) Electrophysiological correlates of hyperacuity in the human visual cortex. Nature 306, 468-470.

Long G.M. and Kling S.C. (1983) Positive and negative after images from brief target gratings. Vision Res. 23, 959-963.

Ludvigh E. (1953) Direction sense of the eye. Am. J. Ophth. 36, 139-142.

Ludvigh E. and McKinnon P. (1967) The effect of orientation on the three dot alignment test. Am. J. Ophth. 64, 261-265.

MacLeod I.D.G. and Rosenfeld A. (1974) The visibility of gratings: spatial frequency channels or bar detecting units? Vision Res. 14, 909-915.

Marr D. and Hildreth E. (1980) A theory of edge detection. Proc. R. Soc. Lond. B207, 187-217.

Marr D., Poggio T. and Hildreth E. (1980) Smallest channel in early human vision. J. Opt. Soc. Am. 70, 868-870

McKee S.P. and Westheimer G. (1978) Improvement in Vernier acuity with practice. Percept. & Psychophys. 24, 258-262.

Rodieck R.W. (1965) Quantitative analysis of cat retinal ganglion cell response to visual stimuli. Vision Res. 5, 583-601.

Schade D.H. (1956) Optical and photoelectric analog of the eye. J. Opt. Soc. Am. 46, 721-739.

Schor C.M. and Badcock D.R. (1985) A comparison of stereo and Vernier acuity within spatial channels as a function of distance from fixation. Vision Res. 25, 1113-1119.

Shapley R. (1974) Gaussian bars and rectangular bars: the influence of width and gradient on visibility. Vision Res. 14, 1457-1462.

Shapley R. and Lennie P. (1985) Spatial frequency analysis in the visual system. Ann. Rev. Neurosci. 8, 547-583.

Stigmar G. (1971) Blurred visual stimuli. II: The effect of blurred visual stimuli on Vernier and stereo acuity. Acta Ophthal. 49, 364-379.

Stromeyer C.F., Klein S., Dawson B.M. and Spillmann L. (1982) Low spatial-frequency channels in human vision: adaptation and masking. Vision Res. 22, 225-233.

Sullivan G.D., Oatley K. and Sutherland N.S. (1972) Vernier acuity as affected by target length and separation. Percept. Psychophys. 12, 438-444.

Swindale N.V. and Cynader M.S. (1986) Vernier acuity of neurons in cat visual cortex. Nature 319, 591-593.

Thomas J.P. (1970) Model of the function of receptive fields in human vision. Psychol. Rev. 77, 121-134.

Volkmann A.W. (1863) Physiologische Untersuchungen im Gebiete der Optik. Breitkopf & Hartel, Leipzig.

Watson A.B. and Nachmias J. (1977) Patterns of temporal interaction in the detection of gratings. Vision Res. 17, 893-902.

Watt R.J. (1984) Towards a general theory of the visual acuities for shape and spatial arrangement. Vision Res. 24, 1377-1386.

Watt R.J. and Andrews D.P. (1982) Contour curvature analysis: hyper-acuities in the discrimination of detailed shape. Vision Res. 22, 449-460.

Watt R.J. and Morgan M.J. (1983a) Mechanisms responsible for the assesment of visual location: theory and evidence. Vision Res. 23, 97-109.

Watt R.J. and Morgan M.J. (1983b) The recognition and representation of edge blur: evidence for spatial primitives in human vision. Vision Res. 23, 1465-1477.

Watt R.J. and Morgan M.J. (1984) Spatial filters and the localization of luminance changes in human vision. Vision Res. 24, 1387-1397.

Watt R.J., Morgan M.J. and Ward R.M. (1983a) The use of different cues in Vernier acuity. Vision Res. 23, 991-995.

Watt R.J., Morgan M.J. and Ward R.M. (1983b) Stimulus features that determine the visual location of a bright bar. Invest. Ophthalmol. Vis. Sci. 24, 66-71.

Westheimer G. (1975) Visual acuity and hyperacuity. Invest. Ophthal. Visual Sci. 14, 570-572.

Westheimer G. (1979) The spatial sense of the eye. Invest. Ophthal. Vis. Sci. 18, 893-912.

Westheimer G. and Hauske G. (1975) Temporal and spatial interference with Vernier acuity. Vision Res. 15, 1137-1141.

Westheimer G. and McKee S.P. (1975) Visual acuity in the presence of retinal image motion. J. Opt. Soc. Am. 65, 847-850.

Westheimer G. and McKee S.P. (1977a) Integration regions for visual hyperacuity. Vision Res. 17, 89-93.

Westheimer G. and McKee S.P. (1977b) Spatial configurations for visual hyperacuity. Vision Res. 17, 941-947.

Williams R.A., Enoch J.M. and Essock E.A. (1984) The resistence of selected hyperacuity configurations to retinal image degradation. Invest. Ophthal. Vis. Sci. 25, 389-399.

Wilson H.R. (1978) Quantitative characterization of two types of line-spread function near the fovea. Vision Res. 18, 971-981.

Wilson H.R. (1980) Spatiotemporal characterization of a transient mechanism in the human visual system. Vision Res. 20, 443-452.

Wilson H.R. (1985) Discrimination of contour curvature: data and theory. J. Opt. Soc. Am. A2, 1191-1199.

Wilson H.R. and Bergen J.R. (1979) A four mechanism model for threshold spatial vision. Vision Res. 19, 19-32.

Woodward M., Ettinger E.R. and Yager D. (1985) The spatial frequency discrimination function at low contrasts. Spatial Vis. 1, 13-17.

Wülfing E.A. (1892) Über den kleinsten Gesichtswinkel. Z. Biol. 29, 199-202.

Zak R. and Berkley M.A. (1986) Evoked potentials elicited by brief Vernier offsets: estimating Vernier thresholds and properties of the neural substrate. Vision Res. 26, 439-451.

Zeevi Y.Y. and Mangoubi S.S. (1984) Vernier acuity with noisy lines: estimation of relative position uncertainty. Biol. Cybern. 50, 371-376.

CHAPTER II.2.

Scale invariant features of differential spatial displacement discrimination.

ABSTRACT.

For a configuration of three blobs with Gaussian spatial contrast profiles and presented at threshold luminance contrast differential spatial displacement discrimination thresholds were determined. The blobs were arranged one above the other at equal spatial intervals. Thresholds were determined for displacements of the middle blob both orthogonal to and along the axis joining the outer two blobs. Thresholds for both tasks were obtained as a function of both the resolution or "inner scale" and the total extent or "outer scale" of the stimulus patterns.

The thresholds for both tasks increased linearly with increasing inner scale of the stimulus pattern for a constant ratio of outer and inner scales. At all levels of resolution there are two outer scale regimes in which different strategies are used to compute differential spatial displacements. Independent of the level of resolution transition between those regions occurs when the outer scale parameter is a constant multiple (approximately 25) of the inner scale parameter. We interpret these results as further evidence for a scale invariant mechanism for differential spatial displacement computation.

key-words: hyperacuity, 3 dot-alignment task, bisection, resolution, threshold contrast

INTRODUCTION.

Differential spatial displacement discrimination thresholds are known to depend on stimulus feature separation (outer scale) and resolution (inner scale) as well as on stimulus luminance contrast.

Discrimination thresholds as a function of stimulus extent have been obtained for alignment tasks (Beck and Halloran, 1985; Levi et al., 1985; Ludvigh, 1953; Sullivan et al., 1972; Watt, 1984; Watt and Campbell, 1985; Watt and Morgan, 1983; Westheimer, 1982a, 1982b; Westheimer and McKee, 1977b) and for tasks involving spatial interval discrimination or bisection judgements (Andrews and Miller, 1978; Carlson and Klopfenstein, 1985; Fechner, 1858; Klein and Levi, 1985; Levi and Klein, 1983, 1985; Volkmann, 1858, 1863; Watt, 1984; Watt and Morgan, 1983; Westheimer, 1984; Westheimer and McKee, 1977b). For large separation of the stimulus features it was generally found that the discrimination thresholds are a constant fraction of the distance separating the stimulus features (a Weber-law behaviour). For small separations between the stimulus features the spatial displacement discrimination thresholds as a function of the separation between the stimulus features show no uniform behaviour for all different tasks. In this case the discrimination thresholds for the bisection tasks still show a power-law behaviour although they vary less with feature separation whereas the discrimination thresholds obtained from the alignment tasks show almost no variation with feature separation. For very small separations between the stimulus features the differential spatial displacement discrimination thresholds rise sharply for all tasks. This is probably caused by the blur function of the eye which causes the stimulus features to appear no longer clearly resolved when they are too close together.

Several experiments have been performed to study the dependence of the differential spatial displacement discrimination thresholds on the extent of blur of the stimulus (Enoch and Williams, 1983; Hartridge, 1923; Morgan and Ward, 1985; Stigmar, 1971; Watt and Morgan, 1983, 1984; Williams et al., 1984). It was shown that differential spatial displacement acuity generally deteriorates with increasing blur although less than normal Snellen acuity. Stigmar (1971) noticed that a high level

of differential spatial displacement acuity can be maintained in spite of increasing blur if measured in terms of half-widths of the retinal light distribution curves. Anisometropic amblyopes were found to have normal bisection thresholds when the results were scaled with the cutoff spatial frequency (Levi and Klein, 1983).

It is known that the differential spatial displacement discrimination thresholds depend on the prevailing spatial frequency of the stimulus pattern (Hirsch and Hylton, 1982, 1985; Levi and Klein, 1983; Tyler, 1973). For low spatial frequencies it was found that bisection- and orthoaxial displacement-discrimination thresholds were a constant fraction of the spatial period of the prevailing frequency (akin to Weber's law). At high spatial frequencies thresholds rose markedly, probably as a result of the fact that separate periods of the stimuli can no longer be clearly resolved due to the blur function of the eye.

The influence of the retinal location of the stimulus on the differential spatial displacement discrimination thresholds has also been a subject of several investigations (Beck and Halloran, 1985; Bourdon, 1902; Levi et al., 1985; Levi and Klein, 1985; Westheimer, 1982a). It appears that differential spatial displacement discrimination thresholds are as good in the periphery as they are centrally (Levi et al., 1985) when scaled in proportion to recent estimates of the cortical magnification factor (i.e. the linear extent of visual striate cortex to which each degree of the retina projects, see Cowey and Rolls, 1974) .

All forementioned experiments were performed at levels of high stimulus luminance contrast. Only a few studies were done to investigate the dependence of the discrimination thresholds on stimulus contrast (Watt and Morgan, 1983, 1984). It was found that the differential spatial displacement discrimination thresholds increase with decreasing stimulus contrast.

The existence of regions in which different strategies are used to compute differential spatial displacements (Weber-regime for large outer scales and different behaviour for small outer scales) is sometimes attributed to the existence of separate integration regions (Westheimer and McKee, 1977a; Hirsch and Hylton, 1985) or functional processing units. A more direct indication for the existence of such processing modules is

the so-called "crowding-effect" (Levi et al., 1985). This refers to the effect that the process of computing precise relative location tags requires unencumbered use of a zone with an extent of a few minutes of arc (typically 4'). As soon as such a zone is encroached upon by a different (interfering) stimulus a marked reduction is observed in the precision with which differential spatial localization judgements can be performed (Badcock and Westheimer, 1985; Levi et al., 1985; Westheimer and Hauske, 1975; Westheimer et al., 1976). Levi et al. (1985) demonstrated that differential spatial displacement processing modules exist at all eccentricities and that their extent is approximately 60 times the local differential spatial displacement discrimination threshold. Experiments performed with dichoptically presented stimuli (Westheimer and Hauske, 1975; Westheimer et al., 1976) rule out the retina as a possible site of interaction. Therefore the processing modules are often assumed to be located in the visual cortex (Barlow, 1979).

Enoch and Williams (1983) and Williams et al. (1984) performed some experiments in which both the outer- and inner-scales of the stimuli were systematically varied. They studied the differential spatial displacement discrimination thresholds as a function of the outer scale (extent) of the stimulus pattern with the inner scale (resolution) as a parameter. However, both the method of blurring the stimuli and the range of the stimulus luminance contrast values used provided them with no precise control over the range of frequency-selective mechanisms that were activated in the visual system by their stimuli. Therefore, they had to restrict their conclusion to the statement that the differential spatial displacement discrimination thresholds as a function of the outer scale of the stimulus are differently affected in their magnitude for different values of the inner scale of the stimuli although their overall shape is similar. They found the detrimental effect of stimulus blur to be highly dependent on the outer scale of the stimulus. The outer scale at which the differential spatial displacement acuity threshold was minimal increased proportional to the amount of blur. For small values of the outer scale parameter differential displacement discrimination thresholds were found to be a constant fraction of the resolution threshold irrespective of the amount of blur. However, no attempt was made to study the differential

spatial displacement discrimination thresholds as a function of the ratio of the outer and inner scale parameters of the stimuli.

The results from the experiments investigating the influence of the spatial extent, the degree of blur, the spatial frequency and the retinal location of the stimulus on the differential spatial displacement discrimination thresholds all seem to indicate that the mechanisms that compute differential spatial displacements are independent of the level of resolution at which the stimulus features are represented (i.e. are scale-invariant). If these mechanisms are scale-invariant it is a priori likely that the distinction between different processing strategies for small and large separations between the stimulus features as determined for high levels of resolution will be present at all levels of resolution, and that the transition between the different regimes occurs for outer scale parameters which are a constant multiple of the inner scale parameter. Moreover, one would expect the differential spatial displacement discrimination thresholds to be a constant fraction of the inner scale parameter for a constant ratio of outer- and inner-scale parameters.

We devised an experiment to study the differential spatial displacement discrimination thresholds as a function of both the inner- and outer-scale of the observed stimulus pattern. The stimuli we used in this experiment consisted of three blobs with Gaussian spatial contrast profiles and Gaussian temporal envelopes presented at detection threshold luminance contrast. As argued in a previous paper (Toet et al, 1986), these stimuli are likely to activate only a small range of spatial frequency selective mechanisms (i.e. only receptive fields with spatial dimensions of the order of those of the retinal projection of the Gaussian blobs will make a significant contribution to their detection) thereby providing us with a precise measure for the inner scale of the stimuli (namely the spread of the Gaussian blobs). Differential spatial displacement discrimination thresholds were determined for displacements of the middle blob both orthogonal to and along the axis joining the outer two blobs. The separation between the centers of the outer two blobs was adopted as a parameter for the outer scale of the stimulus pattern.

The three-blob alignment task is equivalent to the three-dot alignment hyperacuity task which is well documented in the literature

(Andrews et al., 1973, 1978; Beck and Schwartz, 1979; Ludvigh, 1953; Ludvigh and McKinnon, 1967; Watt, 1984). The three blob bisection task also has its three-dot equivalent in the literature (Levi et al., 1985).

METHODS.

Subjects.

Three male subjects, aged between 22 and 30, served in the experiment. Subject A.T. has corrected myopic vision. Subjects H.S. and M.E. are both emmetropic and have 20/15 Snellen acuity. All subjects were highly practised.

Apparatus.

A PDP 11/34 minicomputer in combination with a Gould deAnza IP8500 image array processor was used to generate, process and present the stimuli, record the responses and analyze the data.

The stimulus was displayed on a Philips LDH2123 monochrome monitor. The CRT was driven in an interlaced mode with a frame rate of 60 Hz. The display consisted of 512 × 512 pixels with the luminance value of each pixel quantized to 8 bits. A 512 × 512 correction matrix was added to the deAnza frame buffer to compensate for the inhomogeneity of the display.

Viewing conditions.

The display was placed in a dark room with nonrèflecting black walls. Observers were seated with their heads supported by a chin rest, adjusted in height and position so that their dominant eye was on the line perpendicular to the center of the monitor screen. The use of a forehead rest prevented tilting of the head. Viewing was monocular with the subject's dominant eye. The unused eye was covered with an eye cap.

The angular dimensions of the blobs were varied by varying the viewing distance. Blobs with spread values below 1.5 min of arc were obtained by reducing the blob dimensions on the monitor screen. Viewing distance varied from 12.5 cm to 16 m. Except for viewing distances of 12.5 cm and 25 cm (i.e. for blobs with spreads larger than 55 min of arc) viewing was through a 2 mm artificial pupil. At 12.5 cm and 25 cm the natural pupil was used in order to avoid vignetting effects. At these distances variations of accomodation had no influence on our results as the spread of the optical blur function of the eye is more than two orders of magnitude smaller than the spread of the spatial contrast profile of the stimuli that were presented.

Stimuli.

The stimuli comprised three blobs arranged one above the other at equal spatial intervals. The blobs had identical Gaussian spatial contrast profiles and were temporally modulated with a Gaussian envelope. Their luminance is given by

$$L(x,y,t) = L_b[1 + cw(x,y,t)]$$

where L_b denotes the background luminance and c is the threshold contrast value as determined for a single blob. The window function w(x,y,t) is given by

$$w(x,y,t) = \exp[-(x^2 + y^2)/(2s_s^2) - t^2/(2s_t^2)]$$

We adopt the term spread for the distance over which a normalized Gaussian falls from 1 to $e^{-1/2}$, corresponding to the standard deviation measure as defined in statistics. (A spatial region with radius $2s_s$ and centered on (x,y) = (0,0) contains 92% of the total energy; a temporal interval of width $2s_t$ centered on t = 0 contains 96% of the total stimulus energy). The window function is the product of spatial and temporal Gaussians with spreads of s_s and s_t respectively. Both the temporal and the spatial

windows were truncated at plus and minus four times their spread (containing respectively 99.994% and 99.990% of the total stimulus energy). The threshold contrast c is defined as $(L - L_b)/L_b$, where L denotes the threshold luminance level.

The spread of the Gaussian temporal profile was 0.2 sec (therefore the stimulus was above one half of its peak value for 0.47 sec). The frame rate was 60 Hz and interlaced. Intermediate presentations lasted for 0.05 sec, corresponding to 3 frames. This was found to be short enough to present a perceptually smooth temporal contrast profile. The total duration of the stimulus presentation was eight times the spread of its Gaussian temporal contrast profile (i.e. if T is the moment at which the stimulus attained its maximum contrast and s_t represents the spread of the Gaussian temporal contrast profile, the presentation lasted from $T-4s_t$ to $T+4s_t$).

If we define the bandwidth of a Gaussian signal as the distance between the (negative and positive) frequency components for which the amplitude has dropped to one half of the value of the frequency component with maximum amplitude (which is at zero frequency for a Gaussian signal), we find that the temporal bandwidth is given by $(2 * \ln 2)^{1/2}/(\pi * s_t)$. In our case the temporal frequency bandwidth is 1.87 Hz and the spatial frequency bandwidth is between 0.1 cy/deg and 53.6 cy/deg.

Because we were interested in the differential spatial displacement discrimination thresholds as a function of the level of resolution (inner scale) of the stimuli we adopted a smooth (Gaussian) spatial stimulus contrast profile and a smooth (Gaussian) temporal stimulus contrast profile in combination with detection threshold luminance contrast (as determined for a single blob) in an attempt to stimulate only a small number (narrow range) of frequency selective mechanisms. An extensive motivation for the exact choice of the stimulus profiles was given in a previous paper (Toet et al., 1987).

We also used sharp edged (disc-like) circular stimuli. The results obtained with Gaussian blobs for a certain value of their spread were compared with the results obtained with discs with a radius of the same value.

The continued response of the visual system following the termination (offset) of briefly presented stimuli is known to generate so-called after-images, even at threshold luminance contrast (Bowen et al., 1974; Bowling et al., 1980). This visual persistence has been shown to increase with decreasing stimulus contrast (Bowling et al., 1979). To avoid the possibility that the presence of after-images or memory effects would introduce (false) cues in the differential spatial displacement discrimination tasks the stimulus pattern as a whole appeared at random on one of 9 different positions, symmetrical with regard to the centre of the screen (0, ±9/16, ±18/16, ±27/16, ±36/16 times the size of the spatial spread of the Gaussian blob profile), both in the horizontal and vertical directions. If the stimulus pattern would appear in the same position in each trial comparison (using either the presence of after-images or memory effects) of successive displacements of the middle blob relative to the axis through the outer two would have introduced a (false) cue for the localization judgement.

The stimulus was superposed on a 100 cd/m^2 (300 Td for the 2 mm pupil) luminance background level. The luminance level of the background was chosen such as to operate in the photopic domain.

Procedure.

After adaptation of the subject to the background luminance level the contrast detection threshold for a single Gaussian blob was determined by means of a staircase method as described in a previous paper (Toet et al., 1987). This was done at the start of each session and in between separate runs. The differential spatial displacement discrimination tasks were performed at detection threshold luminance contrast as determined for a single blob.

For both three-blob acuity tasks no use was made of a fixation mark because it would have presented a cue for the task to be performed. Therefore the subjects were instructed to fixate on the centre of the monitor screen.

At the onset of each stimulus presentation a buzzer signal sounded. After completion of the presentation the subject had to choose (forced choice) between a left or right displacement of the middle blob relative to the axis defined by the outer two blobs in case of the alignment task and between a displacement up- or down-wards relative to the middle of the spatial interval defined by the outer two blobs in case of the bisection task. Immediately after the subject had responded to a trial a new presentation was started. By withholding his answer for a while the subject was able to take a short rest. In case no decision could be made because one or more blobs were not detected (and in that case only), the subject could skip his obligation to answer and go on to the next presentation. In this case the missed presentation was randomly incorporated into the sequence of remaining trials. This situation occurred in about 50% of the presentations.

Adaptive probit estimation (APE: see Watt and Andrews, 1981) was used to measure the differential spatial displacement acuity thresholds. APE is a modified method of constant stimuli that allows bias-free threshold determination with high precision for a relatively small number of trials. Threshold is defined as the standard deviation of the cumulative normal psychometric function (corresponding to half the difference between the 17% and 83% points) and was estimated by Probit analysis (Finney, 1971). Each individual estimate is the standard deviation of the response error distribution from a run of 80 trials preceded by 20 practice trials. Thresholds quoted are the r.m.s. of at least 3 individual estimates. Standard errors for this procedure are typically of the order of 10% of the standard deviation.

The order in which the thresholds were determined was not systematic.

RESULTS.

Contrast detection thresholds were measured at the start of each run of the alignment or bisection task. We found that the detection thresholds remained constant during the sessions and were reproduced in separate sessions. As shown in a previous paper (Toet et al., 1987) the detection

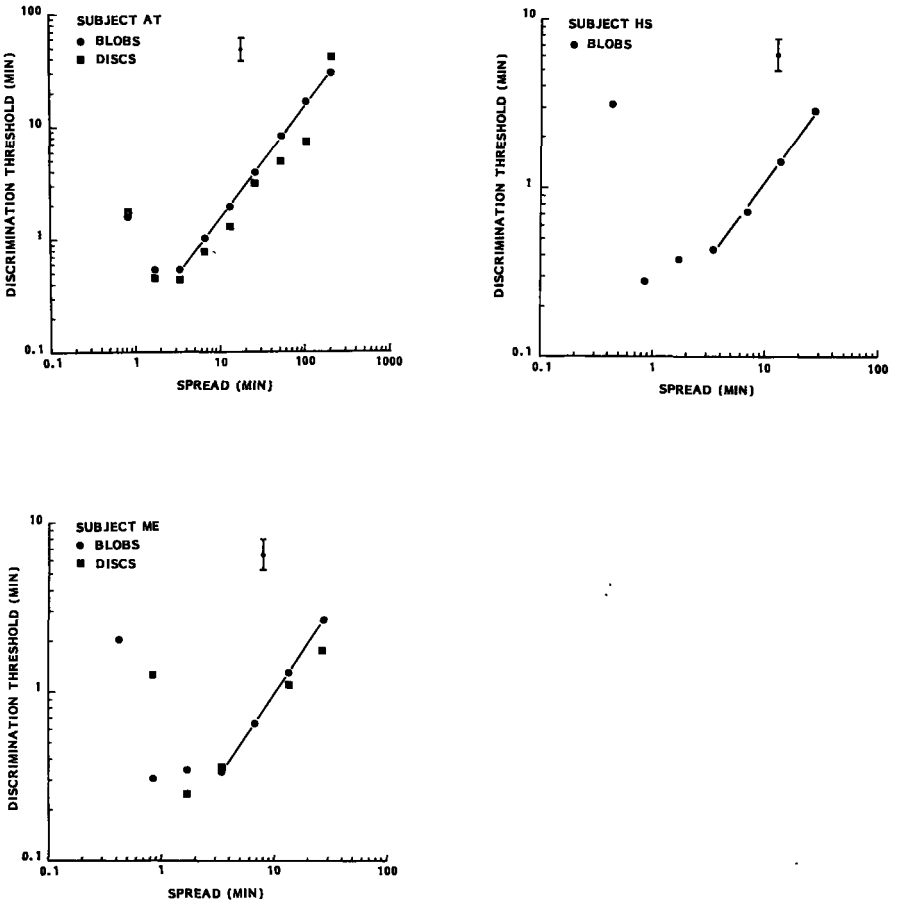

Figure 1. Differential spatial displacement discrimination thresholds for the bisection task as a function of the inner scale of the stimulus patterns represented by the spread of the Gaussian blobs (respectively the radius of the circular discs). All stimuli were temporally modulated with a Gaussian envelope with a spread of 0.2 sec. The solid line indicates the result from a least square fit of an exponential curve to the data points. The error bar represents two standard errors.

contrast thresholds are nearly independent of the angular dimensions of the blobs.

The differential spatial displacement discrimination thresholds for the bisection task are shown in Figure 1 as a function of the angular dimensions of the blobs. The thresholds were defined as those displacements which resulted in a fraction of 83% correct localization judgements. The stimuli were temporally modulated with a Gaussian envelope with a spread of 0.2 sec. The stimuli were scaled by varying the viewing distance. Therefore, the ratio of the outer- and inner-scale parameters was kept constant. We chose for a ratio of 10. This resulted in a stimulus pattern in which blobs with a spread larger than approximately 1.5 min of arc appeared clearly separated. We computed a least-square fit of an exponential curve to our data points. Only data points for spreads larger than 1.5 min of arc were used in the calculation of the regression lines. The least-square curves thus obtained closely fit the data points. The correlation coefficients (r^2) range in value between 0.99 and 1.00. The powers obtained for the exponential curves range between 0.92 and 1.00. We may therefore conclude that the differential spatial displacement discrimination threshold for the bisection task is a constant fraction of the angular dimensions of the blobs, at least for blobs with spreads larger than approximately 1.5 min of arc and for an outer-scale parameter which is 10 times the inner-scale parameter.

For blobs with spreads smaller than 1.5 min of arc the differential spatial displacement discrimination thresholds rise. This is probably a result of the fact that the blobs can no longer be resolved by the subjects.

For two subjects we measured the differential spatial bisection discrimination thresholds for sharp edged circular discs. In Fig. 1 the results of these measurements are shown as a function of the angular dimension of the radius of the discs. If the differential spatial bisection discrimination thresholds for discs of a certain radius are compared with the thresholds obtained for Gaussian blobs with a spread of the same value we see that for radius values larger than 1.5 min of arc the thresholds for discs are lower than for blobs. For increasing radius width of the discs the discrepancy between the differential spatial

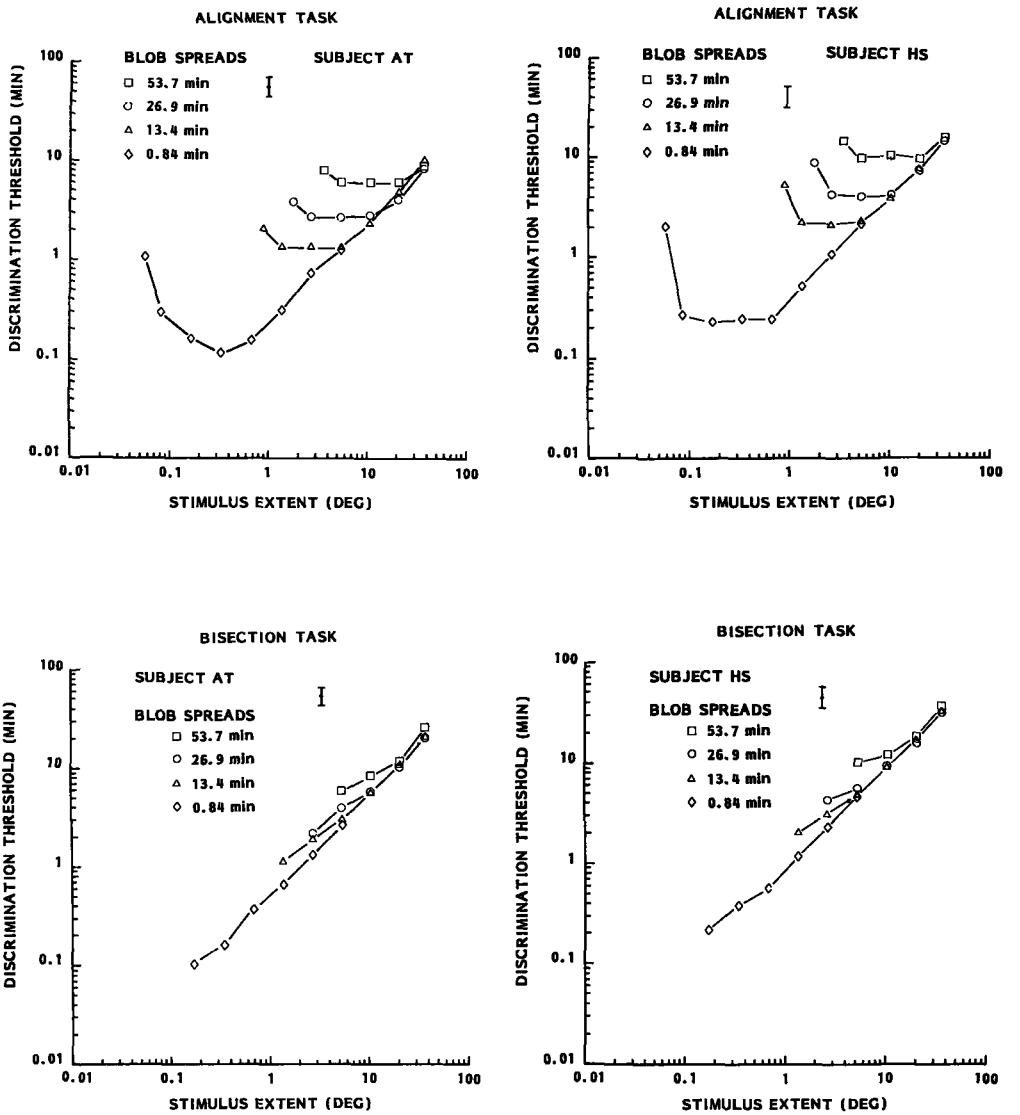

Figure 2. Differential spatial displacement discrimination thresholds for the alignment and the bisection task as a function of the outer scale (extent) of the stimulus pattern. The thresholds were determined for four different values of the inner scale (resolution) parameter. All stimuli were temporally modulated with a Gaussian envelope with a spread of 0.2 sec. The error bar represents two standard errors.

displacement discrimination thresholds for discs and for blobs increases.

Fig. 2 shows the differential spatial displacement discrimination thresholds for the alignment task and for the bisection task as a function of the outer scale of the stimulus pattern with the inner scale as a parameter. As the results of all subjects were similar it suffices to display the results of only two subjects.

In case of the alignment task (Fig. 2a) all curves show a region in which the differential spatial displacement discrimination thresholds are independent of the outer scale of the stimulus pattern, up to a certain extent of the outer scale. In the same region the curves for the bisection task (fig. 2b) show a power law behaviour, i.e. the differential spatial displacement discrimination thresholds vary exponentially with the distance between the outer two blobs with an exponent less than 1.

All curves in Fig. 2 show a Weber-behaviour for large separations between the outer two blobs.

In Fig. 3 we show the results from Fig. 2 when both the differential spatial displacement discrimination thresholds and the outer scale have been scaled with the inner scale parameter. As might be expected from the results for the bisection task as shown in Fig. 1 and from the alignment task as reported in an earlier paper (Toet et al., 1987) the thresholds for geometrically similar stimulus configurations coincide. Note that both in case of the alignment task and the bisection task the transition to the Weber-regime for large ratios between the outer- and inner-scales occurs for ratios larger than approximately 25.

If the ratio between the outer- and inner-scales is less than 25 the thresholds for the bisection task still show a power law-behaviour although the rate at which the thresholds increase with increasing ratio is less than that for ratios larger than 25.

DISCUSSION.

As argued in a previous paper (Toet et al., 1987) the constancy of the measured detection threshold contrast values for the Gaussian blobs as a function of their angular dimensions is an indication for the fact that

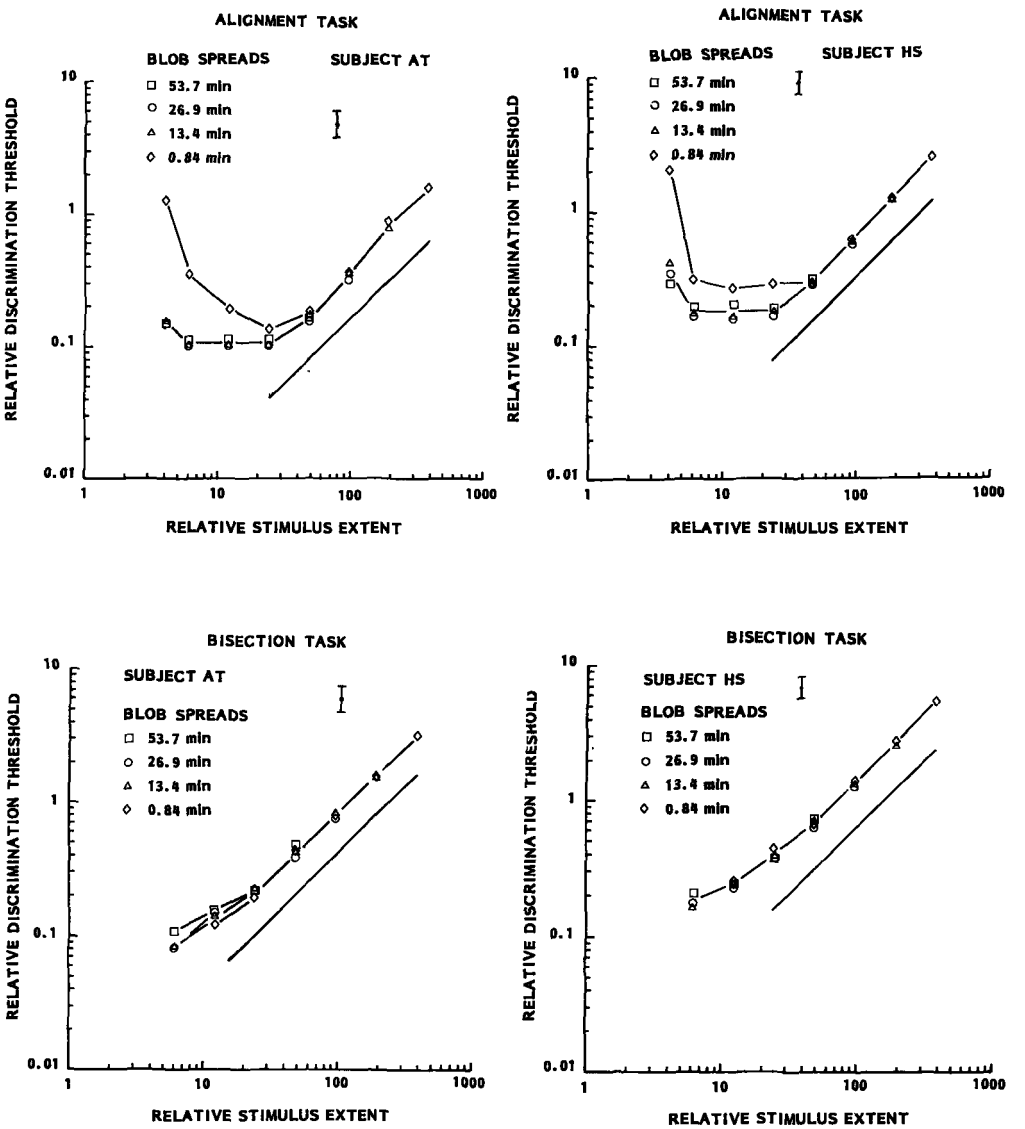

Figure 3. The ratio of the differential spatial displacement discrimination thresholds from Fig. 2 and the corresponding inner scale parameters as a function of the ratio of the outer- and inner- scale parameters of the stimulus pattern. The thresholds were determined for four different values of the inner scale (resolution) parameter. All stimuli were temporally modulated with a Gaussian envelope with a spread of 0.2 sec. The error bar represents two standard errors.

we have indeed succeeded in stimulating only a small range of spatial frequency selective mechanisms.

Due to the fact that the differential spatial localization experiments were performed at threshold luminance contrast (contrast level at which 50% of the presentations is seen) in about half of the presentations no answer could be obtained. An additional number of stimulus presentations is probably missed due to the uncertainty in the spatial position in which the stimulus pattern as a whole appeared (Cohn and Lasley, 1974; Cohn and Wardlaw, 1985).

We have shown that the differential spatial displacement discrimination thresholds for the bisection task increase linearly with increasing inner scale of the stimulus pattern for a constant ratio of outer and inner scales (i.e. for geometrically similar stimuli at decreasing levels of resolution). Previously the same result was obtained for the alignment task (Toet et al., 1987). When scaled with the inner scale parameter the differential spatial displacement discrimination thresholds for both tasks depend only on the ratio of the outer- and inner-scales of the stimulus pattern (i.e. for stimuli with the same ratio of the outer- and inner-scale parameters the discrimination thresholds are the same fraction of the inner-scale parameter). For a constant inner scale and a ratio between the outer- and inner-scale parameters which is less than 25 the differential spatial displacement discrimination thresholds for the bisection task increase with increasing outer scale, whereas the thresholds for the alignment task do not depend on the outer scale. When the ratio of the outer- and inner-scale parameters is more than 25 and the inner scale is kept constant the thresholds for both tasks increase linearly as a function of the outer scale of the stimulus pattern.

For the three-dot alignment hyperacuity task it has been shown that the differential spatial displacement discrimination threshold has an optimum as a function of the distance between the outer two dots (Ludvigh, 1953; Sullivan et al., 1972; Beck and Schwartz, 1979; Watt 1984; Beck and Halloran, 1985). In an earlier paper (Toet et al., 1987) we described an experiment that was performed to determine the variation of the three-blob alignment discrimination thresholds with the distance between the outer

two blobs. For separations between the outer two blobs ranging from 4 two 24 times the spread of the Gaussian spatial contrast profiles of the blobs no variation of the differential spatial displacement discrimination thresholds was found. This is in agreement with our present results which show that the thresholds for the alignment task are constant for separations between the outer two blobs up to two approximately 25 times the spread of the blobs, independent of the value of the spread (inner scale).

If the ratio between the outer- and inner-scale parameters was smaller than three the blobs appeared no longer resolved. This considerably impaired the detection tasks and caused the thresholds to rise markedly.

Our results for the alignment task are similar to those of Enoch and Williams (1983) and Williams et al. (1984) who systematically varied both the inner- and outer-scale parameters for respectively a Vernier- and a two-dot alignment task and to those of Levi et al. (1985) who compared the three-dot alignment task to the three-dot bisection task. A constant discrimination threshold over a range of different stimulus extents as we found for the three-blob alignment task is also found in the literature, for different kinds of alignment tasks (Klein and Levi, 1985); Ludvigh, 1953; Westheimer and McKee, 1977b). A power-law behaviour for the bisection task and for small values of the outer scale parameter was also found by Levi et al. (1985). As for the inner scale, Stigmar (1971) was the first to note that a high level of differential spatial displacement discrimination acuity can be maintained in spite of increasing blur if measured in terms of half-widths of the retinal light distribution curves. Levi and Klein (1983) found that anisometropic amblyopes have normal bisection thresholds when there results are scaled with their cutoff spatial frequency. Watt and Morgan (1983) found a power-law behaviour for edge-blur discrimination.

A Weber-law behaviour for large stimulus extents is generally found in the literature for alignment tasks (Beck and Schwartz, 1979; Beck and Halloran, 1985; Klein and Levi, 1985; Watt, 1984) for bisection tasks (Andrews and Miller, 1978; Klein and Levi, 1985), for spatial interval discrimination tasks (Carlson and Klopfenstein, 1985; Watt and Morgan,

1983; Westheimer and McKee, 19767b) and for spatial frequency discrimination tasks (Hirsch and Hylton, 1983, 1985; Levi and Klein, 1983; Tyler, 1973).

Our results show that at all levels of resolution (for all values of the inner scale parameter) there are two regimes in which different strategies are used to compute differential spatial displacements. Independent of the level of resolution transition between those regions occurs when the outer scale parameter (the stimulus extent) is a constant multiple (approximately 25) of the inner scale parameter (blob size).

In case of the alignment task, we found that the differential spatial displacement discrimination thresholds were typically 0.17 times the inner scale parameter for a ratio between the outer- and inner-scale parameters of 25. Therefore, the transition between the different processing regimes occurs for a stimulus extent of approximately 150 (= 25/0.17) times the differential spatial displacement discrimination threshold, independent of the inner scale of the stimulus.

Levi et al. (1985) found that both in central and in peripheral vision there appear to be psychophysical processing modules with a diameter of their influence sphere of approximately 120 times their corresponding differential spatial displacement discrimination thresholds. Westheimer and McKee (1977a) found integration regions with an extent of approximately 4 min of arc for high resolution differential spatial discrimination tasks. As hyperacuity thresholds of 2 sec of arc are not uncommon for these tasks, this would imply that the integration regions also have an extent of approximately 120 times their corresponding differential spatial displacement discrimination threshold. These data are in close agreement with our results for the alignment task.

A possible explanation for the existence of different processing regimes might be the existence of regions, extending up to 25 times the inner scale parameter, in which differential spatial displacement computations can be performed directly. Differential spatial displacement computations performed on stimuli extending over more than 25 times their inner scale parameter (more than the spatial extent of a single processing module) probably involve an intermediary stage of comparison of the

activity of adjoining regions (i.e. indirect computation modes).

We have argued that it is likely that our stimuli will only stimulate a small range of spatial frequency selective mechanisms (only receptive fields with spatial dimensions of the order of those of the retinal projection of the Gaussian blobs will contribute to their detection) when the Gaussian blobs are at their respective detection threshold contrast level. The constancy of the detection contrast thresholds as a function of the angular dimensions of the blobs justifies the assumption that we have indeed succeeded in stimulating only a small number of receptive fields within a narrow range of receptive field widths. We showed that the differential spatial displacement discrimination thresholds, when scaled with the inner-scale parameter, depend only on the ratio of the outer- and inner-scales of the stimulus pattern (i.e. for stimuli with the same ratio of the outer- and inner-scale parameters the spatial displacement discrimination thresholds are a constant fraction of the inner scale parameter). Furthermore, we found that at all levels of resolution there are two regimes in which different strategies are used to compute differential spatial displacements. The transition between those regions occurs when the outer scale parameter (stimulus extent) is a constant multiple (approximately 25) times the inner scale parameter (blob size) independent of the value of the inner scale parameter. These results suggest that the strategy used by the visual system to compute differential spatial displacements is independent of the level of resolution at which the stimulus features are represented. If the visual system would use different strategies to encode relative location at different levels of resolution one would expect to find indications for regions of transition between the ranges in resolution space in which the different mechanisms are active. However, our data provide no indication for an inner-scale dependency of the mechanisms that are used to encode relative position. Even the ratio between the outer- and inner-scale parameters at which the transition between the two different processing strategies used occurs is in close agreement with values for that ratio found in case of high resolution differential spatial displacement discrimination tasks (Levi et al., 1985); Westheimer and McKee, 1977a). Therefore it seems that the visual system uses a single strategy to assign

relative spatial location tags to receptive fields on all levels of resolution. These tags can then in turn be used to compute the relative spatial displacement of stimulus features at a certain level of resolution to an accuracy which is a small and constant fraction of the prevailing receptive field width at that level of resolution. These place tags may be encoded in the constraints imposed on the simultaneous activity in the ganglion cell network (Koenderink, 1984a, 1984b).

The same conclusion was reached by Hirsch and Hylton (1982, 1985), who reported that the ability of human observers to discriminate between different spatial frequencies was not a smooth function of frequency but had a definite segmented structure. They interpreted this structure as being due to the existence of a class retinal receptive fields that perform a dual function of neural blurring and spatial sampling. They propose a scaled lattice model of spatial vision that allows apparently scale-free spatial processing. This model is similar to Koenderink's model (1978, 1982) in which the retina is depicted as a self-similar detector array graded with respect to aperture size. They speculate that hyperacuity is the result of a general strategy for encoding positional information and that the difference between high and low resolution is determined by whether differential spatial displacement computations are performed on the output of a receptor lattice on a level of high or low resolution.

With regard to our results and those we quoted from the literature we conclude that the human visual system uses a single strategy to detect differential spatial displacement, independent of the level of resolution at which the stimulus features are present.

Acknowledgements - We thank Dr. R.J. Watt and Dr. D.P. Andrews for kindly providing us with a listing of their APE program. We are indebted to Dr. B. Nienhuis for his many valuable suggestions. This work was supported by the Dutch Foundation for the Advancement of Pure Research (ZWO).

REFERENCES.

Andrews D.P., Butcher A.K. and Buckley B.R. (1973) Acuities for spatial arrangement in line figures: human and ideal observers compared. Vision Res. 13, 599-620.

Andrews D.P. and Miller D.T. (1978) Acuity for spatial separation as a function of stimulus size. Vision Res. 18, 615-619.

Badcock D.R. and Westheimer G. (1985) Spatial location and hyperacuity: centre/surround localization contribution function has two substrates. Vision Res. 25, 1259-1267.

Barlow H.B. (1979) Reconstructing the visual image in space and time. Nature 279, 189-190.

Beck J. and Schwartz T. (1979) Vernier acuity with dot test objects. Vision Res. 19, 313-319.

Beck J. and Halloran T. (1985) Effects of spatial separation and retinal eccentricity on two-dot Vernier acuity. Vision Res. 25, 1105-1111.

Bourdon B. (1902) La Perception Visuelle de l'Espace, p. 146. Scheicher, Paris.

Bowen R.W., Pola J. and Matin L. (1974) Visual persistence: effects of flash luminance, duration and energy. Vision Res. 14, 295-303.

Bowling A., Lovegrove W. and Mapperson B. (1979) The effect of spatial frequency and contrast on visual persistence. Perception 8, 529-539.

Bowling A. and Lovegrove W. (1980) The effect of stimulus duration on the persistence of gratings. Percept. & Psychophys. 27, 574-578.

Carlson C.R. and Klopfenstein R.W. (1985) Spatial-frequency model for hyperacuity. J. Opt. Soc. Am. A2, 1747-1751.

Cohn T.E. and Lasley D.J. (1974) Detectability of a luminance increment: effect of spatial uncertainty. J. Opt. Soc. Am. 64, 1715-1719.

Cohn T.E. and Wardlaw J.C. (1985) Effect of large spatial uncertainty on foveal luminance increment detectability. J. Opt. Soc. Am. A2, 820-825.

Cowey A. and Rolls E.T. (1974) Human cortical magnification factor and its relation to visual acuity. Exp. Brain Res. 21, 447-454.

Enoch J.M. and Williams R.A. (1983) Development of clinical tests of vision: initial data on two hyperacuity paradigms. Percept. & Psychophys. 33, 314-322.

Fechner G.T. (1858) Über ein psychophysisches Grundgesetz. Abhandl. d. Leipzig Ges. VI, 457-532.

Finney D.J. (1971) Probit analysis, 3rd edn. Cambridge Univ. Press.

Hartridge H. (1923) Visual acuity and the resolving power of the eye. J. Physiol. 57, 52-67.

Hirsch J. and Hylton R. (1982) Limits of spatial-frequency discrimination as evidence of neural interpolation. J. Opt. Soc. Am. 72, 1367-1374.

Hirsch J. and Hylton R. (1985) Spatial-frequency discrimination at low frequencies: evidence for position quantization by receptive fields. J. Opt. Soc. Am. 2, 128-135.

Klein S.A. and Levi D.M. (1985) Hyperacuity thresholds of 1 sec: theoretical predictions and empirical validation. J. Opt. Soc. Am. A2, 1170-1190.

Koenderink J.J. and Doorn A.J. van (1978) Visual detection of spatial contrast; influence of location in the visual field, target extent and illuminance level. Biol. Cybern. 30, 157-167.

Koenderink J.J. and Doorn A.J. van (1982) Invariant features of contrast detection: an explanation in terms of self-similar detector arrays. J. Opt. Soc. Am. 72, 83-87.

Levi D.M. and Klein S.A. (1983) Spatial localization in normal and amblyopic vision. Vision Res. 23, 1005-1017.

Levi D.M. and Klein S.A. (1985) Vernier acuity and amblyopia. Vision Res. 25, 979-991.

Levi D.M., Klein S.A. and Aitsebaomo A.P. (1985) Vernier acuity, crowding and cortical magnification. Vision Res. 25, 963-977.

Ludvigh E. (1953) Direction sense of the eye. Am. J. Ophth. 36, 139-142.

Ludvigh E. and McKinnon P. (1967) The effect of orientation on the three dot alignment test. Am. J. Ophth. 64, 261-265.

Morgan M.J. and Ward R.M. (1985) Spatial and spatial-frequency primitives in spatial-interval discrimination. J. Opt. Soc. Am. A2, 1205-1210.

Stigmar G. (1971) Blurred visual stimuli. II: The effect of blurred visual stimuli on Vernier and stereo acuity. Acta Ophthal. 49, 364-379.

Sullivan G.D., Oatley K. and Sutherland N.S. (1972) Vernier acuity as affected by target length and separation. Percept. Psychophys. 12, 438-444.

Tyler C.W. (1973) Periodic Vernier acuity. J. Physiol. 228, 637-647.

Volkmann A.W. (1858) Über den Einfluss der Übung auf das Erkennen raumlicher Distanzen. Leipziger Ber. X, 38-69.

Volkmann A.W. (1863) Physiologische Untersuchingen im Gebiete der Optik. Breitkopf & Hartel, Leipzig.

Watt R.J. (1984) Towards a general theory of the visual acuities for shape and spatial arrangement. Vision Res. 24, 1377-1386.

Watt R.J. and Andrews D.P. (1981) APE: Adaptive probit estimation of psychometric function. Curr. Psychol. Rev. 1, 205-214.

Watt R.J. and Campbell F.W. (1985) Vernier acuity: interactions between length effects and gaps when orientation cues are eliminated. Spatial Vision 1, 31-38.

Watt R.J. and Morgan M.J. (1983) The recognition and representation of edge blur: evidence for spatial primitives in human vision. Vision Res. 23, 1465-1477.

Watt R.J. and Morgan M.J. (1984) Spatial filters and the localization of luminance changes in human vision. Vision Res. 24, 1387-1397.

Westheimer G. (1982a) The spatial grain of the perifoveal visual field. Vision Res. 22, 157-162.

Westheimer G. (1982b) Do ocular-dominance columns set spatial limits for hyperacuity processing? Vision Res. 22, 1349-1352.

Westheimer G. (1984) Line-separation discrimination curve in the human fovea: smooth or segmented? J. Opt. Soc. Am. A1, 683-684.

Westheimer G. and Hauske G. (1975) Temporal and spatial interference with Vernier acuity. Vision Res. 15, 1137-1141.

Westheimer G. and McKee S.P. (1977a) Integration regions for visual hyperacuity. Vision Res. 17, 89-93.

Westheimer G. and McKee S.P. (1977b) Spatial configurations for visual hyperacuity. Vision Res. 17, 941-947.

Westheimer G., Shimamura K. and McKee S.P. (1976) Interference with line-orientation sensitivity. J. Opt. Soc. Am. 66, 332-338.

Williams R.A., Enoch J.M. and Essock E.A. (1984) The resistence of selected hyperacuity configurations to retinal image degradation. Invest. Ophthalmol. Vis. Sci. 25, 389-399.

CHAPTER II.3.

Two-point discrimination at low resolution.

ABSTRACT.

Similar to the two-point discrimination task, spatial separation discrimination thresholds were determined for a configuration of two blobs, with overlapping Gaussian spatial contrast profiles, at threshold luminance contrast. It was found that the spatial separation discrimination thresholds scale linearly with stimulus size over a range of at least two decades. It is argued that the same mechanisms that mediate differential displacement detection also perform in so-called resolution tasks. We conclude that the human visual system seems to use one strategy to detect differential spatial displacement, whether the components of a stimulus pattern can be resolved or not, and independent of the level of resolution at which these stimulus features are present. The accuracy that can be obtained for differential spatial displacement discrimination tasks is directly determined by the accuracy with which the stimulus components can be discriminated as spatially resolved, individual features.

INTRODUCTION.

The notion of resolution.

In astronomy there is a long standing interest in the angular separation that is needed to make the duplicity of a double star with components of the same magnitude apparent. Objective resolution is concerned with recognizing as independent two sources with a small angular separation. The construction of criteria for a limit of resolution has proved to be a persistingly vexing problem. Lord Rayleigh[1] produced the criterium that two point sources are resolvable when the maximum of the illuminance distribution of one point coincides with the first minimum in

the illuminance distribution of the other point. This criterium is based on the tacit assumption that the two point sources that are to be resolved are mutually incoherent[2] and corresponds with practical limits. Wolf[3] regards two sources as just resolved when the illuminance at the midpoint of their joint intensity distribution is 26.5% less than the illuminance at either peak; a situation which essentially corresponds to the Rayleigh criterium for a circular aperture.

The criteria of Rayleigh and Wolf were merely intended as an index of relative merit of different optical instruments. A criterium which gives a measure of the actual limit of resolution was given by Sparrow[4]. The Sparrow "undulation" criterium states that two point sources are just resolved if the second derivative of the resultant spatial contrast profile vanishes at the point midway between the respective Gaussian image points. This implies that two point sources are resolved when there exists a minimum (undulation) between two maxima in their joint light distribution. A classification and comparison of various resolution criteria which have been developed is given by Ramsay et al.[5].

While all these resolution criteria can be useful they overlook significant effects that may occur in the imaging process. It should be noted that in case of the image of two points the only measurable quantity is the separation of those two points. Grimes and Thompson[6,7] studied (both theoretically and experimentally) the two-point separation measurement accuracy as a function of the degree of coherence of the illumination. Even in the fully incoherent case they found slight variations in the ratio of the real to the measured separation of the two object points, for separations greater than the Sparrow incoherent limit and in the region of the Rayleigh limit.

It has been noted that, from a mathematical standpoint, the image of two point sources is not identical to the image of a single point source, no matter how closely spaced the pair may be[8]. This would imply that there exists only a practical and not a theoretical limit for two-point resolving power. However, this limit can only be attained if the observer has the (infinite amount of) a priori information that the object consists of either one or two points. Using a decision- or information-theoretical approach it can be shown that the resolution of two point sources is

limited only by the precision with which the flux density in the image plane can be determined[9], or, equivalently, that the two point sources can be distinguished if and only if the power spectrum of the difference of the images is nonzero[10].

The resolution of the human visual system.

With traditional techniques to measure the limits of the spatial differentiation capacity of the eye a given target configuration is spatially changed until a certain discrimination threshold is reached. This involves either recognition of the form of the stimulus pattern that is applied[11], or the detection of changes in the separation between different stimulus features[12],[13]. For instance, in case of a two point target the spatial separation between the points is increased until they appear as double (minimum separable). The separation for which the discrimination threshold is reached is called the minimal angle of resolution. In general, the spatial manipulation required for a stimulus configuration to elicit a criterium response confounds changes in the contrast- and space-parameters. For example, when the distance between two point sources increases not only the separation between the two peaks (assuming they are resolved) in the resulting light distribution changes, but the absolute luminance of the trough between the peaks and the contrast ratio between the peaks and the trough vary also.

It was found by Hooke that two stars can only be resolved by the eye if they are separated by approximately 60". Helmholtz[14] confirmed this observation and introduced a theory to account for the limitation of the resolving power of the eye. He assumed that, in order to see them resolved, the retinal images of two bright point sources should have a perceptibly less stimulated cone in between them. As is well illustrated in double-star resolution, the detection of an intensity dip in the resulting contrast profile is an essential component of the task[15]. This accounts for the influence of factors as adaptation, presentation duration and background- and target-luminances. Ogle[16] studied two-point resolution as a function of the luminance of the background and for different

contrasts between the point sources and the background. His results show that the minimal angle of resolution depends primarily on the contrast, irrespective of the level of adapting luminances. He found that the minimal angle of resolution has an absolute minimum and is constant valued for contrast levels below a certain critical value. A limit of resolution beyond the purely optical one can be determined by the use of interference fringes[17]. Resolution limits found by this method vary between 30" and 35".

It is well known that the human visual system can discriminate changes in the relative spatial position of features in the visual field which are an order of magnitude below the spatial separations needed to see those features as resolved entities[18-20]. This precision, coined "hyperacuity" by Westheimer[21], is possible for a variety of spatial localization tasks[20] and remains unaffected by movement of the stimuli across the retina over several min of arc[22,23]. Thresholds for the accuracy obtained in these hyperacuity tasks are typically a few seconds of arc. Klein and Levy[24] have recently shown that under optimal conditions observers could correctly discriminate the relative position of a line with an accuracy of less than 1 arc sec. Thus, the discriminating power of the eye for differential spatial displacements is much greater than the limit set by the diameter of the foveal cones.

Recently, Geisler and Davila[25] studied two-point resolution and separation acuity using a two-interval forced choice task. They found a two-point resolution threshold of 48". The two-point differential displacement discrimination threshold decreased with increasing intensity and reached a minimum of 11". They compared the results of their subjects with those of ideal discriminator models[26,25]. Their conclusion was that two-point resolution and differential spatial displacement discrimination are essentially equal in terms of relative efficiency. This result was interpreted as an indication for the fundamental equality of the underlying mechanisms determining both acuities.

Possible mechanisms mediating visual resolution.

Hering[27] inferred that the ability to discriminate differential spatial displacements (hyperacuity) was altogether different from the ability to resolve features in the visual field (visual acuity). Tonner[28,29,30] was the first to compare two-point resolution (acuity) and three-point alignment discrimination (hyperacuity) thresholds. He assumed that two points are seen just resolved when the threshold crossings of their corresponding retinal intensity distributions just touch. He argued that differential spatial displacements within the retinal intensity distribution may cause the activation of retinal detectors which were previously sub-threshold. The resolution threshold values he found were approximately 72" [30], and differential spatial displacement discrimination thresholds ranged between 14" and 33" [29]. He assumed that the lower limit of the differential spatial displacement discrimination thresholds was set by the statistical mean of the differential displacements that are needed to activate detectors which were previously near threshold. This limit corresponds to half the retinal detector width. In this view the upper limit was given by the statistical mean of the cone width distribution[29].

Campbell and Robson[31] suggested a multiple-channel model for pattern vision. In this model, a spatial intensity distribution is simultaneously processed by many separate channels each selectively sensitive to a narrow range of spatial frequencies. Nowadays, there is abundant psychophysical[32-34] and neurophysiological[35] evidence consistent with this hypothesis.

The spatial frequency description of the psychophysical channels is equivalent to a description in terms of collections of spatially overlapping detectors with different spatial weighting functions[36]. Thus, a channel can be thought of as an array of detectors each subserving a different part of the visual field but responding to the same range of spatial frequencies. Whether the frequency- or the direct spatial-approach is chosen will partly depend on the type of stimulus that is to be considered. For instance, the response to a periodic stimulus may be easier to understand in terms of its Fourier components whereas a direct spatial approach may be more appropriate for a localized stimulus.

Recent theories generally suppose that a pattern is detected whenever the integrated product of the retinal intensity distribution caused by the presence of a stimulus pattern and the weighting function of a detector plus noise exceeds the threshold value for at least one detector[37-41]. There is still disagreement on the number of detectors with different weighting functions subserving the same retinal area. However, recent evidence suggests that their number may be quite small[37,40,42-44]. It has been suggested that the apparent sharp tuning of the spatial frequency channels may be due to the effects of spatial probability summation of the response of localized detector units at different spatial positions[40,42,45-47].

Psychophysical evidence for the existence of size selective mechanisms, i.e. detectors, maximally sensitive to visual targets with sizes in a particular range, and existing at a single location, was first reported by Pantle and Sekuler[48]. Their results were later confirmed by experiments using selective adaptation[49-51], size discrimination tasks at detection threshold[52,53], and by discrimination experiments with spatially localized patches[37,43]. Using selective adaptation Perizonius et al.[54] have recently shown that the spatial frequency channels of the human visual system have a local, rather than global, character.

The ability of observers to discriminate between gratings of different frequencies was first reported to behave according to a Weber law[55]. Spatial frequency discrimination thresholds are remarkably low: subjects can discriminate between suprathreshold gratings which differ only 2-5% in spatial frequency[55-59]. Discrimination is generally worse at low spatial frequencies[60-62]. However, recent results show that spatial frequency discrimination is not a smoothly monotonic function of spatial frequency[56,70,89]. Results of suprathreshold spatial frequency discrimination tasks show that gratings with periods that differ less than the distance between two foveal photoreceptors can be discriminated[63]. Therefore, spatial frequency discrimination may be regarded as a form of hyperacuity. Hirsch and Hylton[56] compared the performance of the visual system for spatial frequency and spatial separation discrimination tasks and found that the performance in both tasks was indeed similar.

The results of experiments determining spatial frequency discrimination thresholds for simple gratings[43] and for the constituent components of compound gratings[33,34,63,64] have led to the suggestion that each spatial frequency channel is "labelled" or "tagged" with the spatial frequency to which the channel is most sensitive[43,65]. However, near detection threshold, gratings of different spatial frequencies can only be perfectly discriminated when their spatial frequencies differ by 1 octave or more[43,60,64,66]. This seems to preclude the far sharper discrimination found for suprathreshold gratings. Moreover, selective adaptation experiments have shown that, although the detection threshold is most elevated at the adaptation frequency, the discrimination threshold is most elevated at a frequency some distance removed from the adaptation frequency[57].

As was first suggested by Campbell et al.[55] the gross disparity between the high contrast spatial frequency discrimination thresholds and the estimated bandwidths of the spatial frequency channels can be explained using a principle derived from Hering's theory of color vision[67,68]. In color vision it is generally assumed that wavelength discrimination in a particular part of the spectrum reflects the rate of change with wavelength of the response in three opponent color channels with overlapping spectral sensitivity profiles[69]. Similar to this view suprathreshold spatial frequency discrimination may be determined by the relative- or differential- simultaneous activities of either multiple overlapping psychophysical channels tuned to different spatial frequencies or, equivalently, size-tuned neural elements[55-59]. An opponent size-selective mechanism will discriminate best among spatial frequencies that lie in the region where its sensitivity function has the greatest slope. Its performance is limited by its noise level rather than by its spatial frequency bandwidth. This may explain the observed 2-5% precision in spatial frequency discrimination. The occurance of peaks and troughs in the spatial frequency discrimination function[56,70] may be a demonstration of the existence of a small and discrete set of size-selective mechanisms[57,71]. Shifts in perceived size have also been attributed to a shift in the relative responses of different size-tuned mechanisms[72].

The notion that spatial frequency discrimination is mediated by differential-mechanism responses has been formulated both as a line-element model[71,72] and as an opponent-size model[57-59]. The line-element model provides a reasonable fit to the data from supra- and near-threshold spatial frequency discrimination studies[71] as well as to results obtained from experiments using selective adaptation[72]. All these models used independent detectors and therefore they neglected the effect of lateral inhibition or facilitation between localized detectors[73-77] which might give corrections to the obtained results.

Aim of the experiment.

Koenderink[78,79] has recently argued how relative place tags may be assigned to a collection of nervous elements by the (physiologically imposed) constraints on the simultaneous/successive order of their total activity. In this view the relative spatial position of stimulus features is encoded in the correlation between the signal activities of the neural elements. Thus, the difference in the accuracy of performance of the visual system in resolution- and differential spatial displacement discrimination tasks may merely be a result from an increased uncertainty in the precision with which place tags can be assigned to the stimulus features when their corresponding contrast profiles overlap[13,80]. In fact, this may well explain the "crowding" effect observed for hyperacuity tasks[81-83].

Both the success of the aforementioned differential-mechanism models in describing the results of spatial frequency discrimination experiments and the results of Geisler and Davila[25] seem to confirm Koenderink's model. Therefore, it seems likely that there is no fundamental difference between the mechanisms that perform in hyperacuity and standard acuity or resolution tasks. In a recent paper Carlson and Klopfenstein[84] showed that a contrast detection model based on contiguous spatial frequency channels could readily predict many aspects of hyperacuity performance. There was no need to invoke specialized hyperacuity mechanisms that were fundamentally different from those underlying ordinary spatial acuity. As the

results of Harris[9] and Nahrstedt and Schooley[10] already indicated differential spatial displacement discrimination accuracy is only limited by the signal to noise ratio. Therefore, we assume that the same mechanisms are used to compute differential spatial position in resolution and hyperacuity tasks.

Invariant features of contrast detection and frequency discrimination tasks have resulted in models in which the retina is depicted as a self-similar detector array graded with respect to aperture size[65,85-90]. If these descriptions of the visual system have any validity it is a priori likely that the mechanisms that compute differential displacement are also scale invariant (i.e. do not depend on the level of resolution at which the stimulus features used in the differential displacement computation process are present).

We have recently shown that the differential spatial displacement discrimination thresholds for a three-blob alignment and a three-blob bisection task scale linearly with stimulus size over at least two decades[91]. We concluded that at all levels of resolution a similar mechanism is used to detect differential spatial displacement. If the same mechanisms are used to perform in the two-point discrimination task we expect from these results that the two-point discrimination thresholds will also scale linearly with stimulus size.

In order to test this assumption we designed an experiment to determine whether the mechanisms that subserve two-point discrimination are scale invariant. The stimuli we used in this experiment consisted of blobs with Gaussian spatial contrast profiles and Gaussian temporal envelopes presented at near detection threshold luminance contrast. This two-blob discrimination task is equivalent to the two-point discrimination task which is well documented in the literature[6,9,10,14,25].

METHODS.

Subjects.

Three male subjects, aged between 22 and 67, served in the experiment. Subject A.T. has corrected myopic vision and subject M.B. has corrected hypermetropic vision. Subject A.G. is emmetropic and has 20/15 Snellen acuity. Subjects A.T. and M.B. were highly practised. Subject A.G. underwent several training sessions before performing the measurements reported below.

Apparatus.

A PDP11/34 minicomputer in combination with a Gould deAnza IP8500 image array processor was used to generate, process and present the stimuli, record the responses and analyze the data.

The stimulus was displayed on a Philips LDH2123 monochrome monitor. The CRT was driven in a interlaced mode with a frame rate of 60 Hz. The display consisted of 512 × 512 pixels with the luminance value of each pixel quantized to 8 bits. A 512 × 512 correction matrix was added to the deAnza frame buffer to compensate for the inhomogeneity of the display.

Viewing conditions.

The display was placed in a dark room with non-reflecting black walls. Observers were seated with their heads supported by a chin rest, adjusted in height and position so that their dominant eye was on the line perpendicular to the center of the monitor screen. The use of a forehead rest prevented tilting of the head. Viewing was monocular with the subject's dominant eye. The unused eye was covered with an eye cap.

The angular dimensions of the blobs were varied by varying the viewing distance. Blobs with spread values below 1.5 min of arc were obtained by reducing the blob dimensions on the monitor screen. Viewing

distance varied from 12.5 cm to 16 m. Except for viewing distances of 12.5 cm and 25 cm (i.e. for blobs with spreads larger than 55 min of arc) viewing was through a 2 mm artificial pupil. This pupil diameter is known to be in the range of pupil diameters providing the greatest acuity[92,93]. At 12.5 cm and 25 cm the natural pupil was used in order to avoid vignetting effects. At these distances variations of accommodation and pupil size[92] had no influence on our results as the spread of the optical blur function of the eye[93] is more than two orders of magnitude smaller than the spread of the spatial contrast profile of the stimuli that were presented.

Stimuli.

The stimuli comprised two blobs with different spatial separations. The blobs had identical Gaussian spatial contrast profiles and were temporally modulated with a Gaussian envelope. The stimulus profile is given by

$$L(x,y,t) = L_b\ [1 + cw(x,y,t)]$$

where L_b denotes the background luminance and c is the threshold contrast value as determined for a single blob. The window function w(x,y,t) is given by

$$w(x,y,t) = (\exp[-((x-d/2)^2+y^2)/(2s_s^2)] + \exp[-((x+d/2)^2+y^2)/(2s_s^2)]\ \exp[-t^2/(2s_t^2)]$$

if the separation d between the means of the two Gaussian intensity distributions is greater than $2s_s$, and

$$w(x,y,t) = (\exp[-((x-d/2)^2+y^2)/(2s_s^2)] + \exp[-((x+d/2)^2+y^2)/(2s_s^2)])\ \exp[-t^2/(2s_t^2)]/\{2\exp[-(d/2)^2/(2s_s^2)]\}$$

if $d \leq 2s_s$. Because of this definition the stimulus profile of two blobs

with zero separation equals that of a single blob.

We adopt the term spread for the distance over which a Gaussian falls from 1 to $e^{-\frac{1}{2}}$, corresponding to the standard deviation measure as defined in statistics. (A spatial region with radius $2s_s$ and centered on (x,y) = (0,0) contains 92% of the total energy; a temporal interval of width $2s_t$ centered on t=0 contains 96% of the total stimulus energy). The window function is the product of spatial and temporal Gaussians with spreads of s_s and s_t respectively. Both the temporal and the spatial windows were truncated at plus and minus four times their spread (containing respectively 99.994% and 99.990% of the total stimulus energy). The threshold contrast c is defined as $(L-L_b)/L_b$, where L denotes the threshold luminance level.

The spread of the Gaussian time profile was 0.2 sec (therefore the stimulus was above one half of its peak value for 0.47 sec). The frame rate was 60 Hz and interlaced. Intermediate presentations lasted for 0.05 sec, corresponding to 3 frames. This was found to be short enough to present a perceptually smooth temporal contrast profile. The total duration of the stimulus presentation was eight times the spread of its Gaussian temporal contrast profile (i.e. if T is the moment at which the stimulus attained its maximum contrast and s_t represents the spread of the Gaussian temporal contrast profile, the presentation lasted from $T-4s_t$ to $T+4s_t$).

If we define the bandwidth of a Gaussian signal as the distance between the (negative and positive) frequency components for which the amplitude has dropped to one half of the value of the frequency component with maximum amplitude (zero frequency for a Gaussian signal) we find that the temporal bandwidth is given by $(2 * \ln 2)^{\frac{1}{2}}/(\pi * s_t)$. In our case the temporal frequency bandwidth is 1.87 Hz and the spatial frequency bandwidth is between 0.1 cy/deg and 13.4 cy/deg.

Because we were interested in the spatial displacement discrimination thresholds as a function of the levels of resolution (inner scale) of the stimuli we adopted a smooth (Gaussian) spatial stimulus contrast profile and a smooth (Gaussian) temporal stimulus contrast profile in combination with detection threshold luminance contrast (as determined for a single blob) in an attempt to stimulate only a small number (narrow range) of

frequency selective mechanisms.

We also used sharp edged (disc-like) circular stimuli. The results obtained with Gaussian blobs for a certain value of their spread were compared with the results obtained with discs with a radius of the same value.

The continued response of the visual system following the termination (offset) of briefly presented stimuli is known to generate so-called after-images, even at threshold luminance contrast[94,95]. This visual persistence has been shown to increase with decreasing stimulus contrast[96]. To avoid the possibility that the presence of after-images or memory effects would introduce (false) cues in the differential spatial discrimination task, the stimulus pattern as a whole appeared at random on one of 9 different positions, symmetrical with regard to the centre of the screen (0, ±1/16, ±2/16, ±3/16, ±4/16 times the size of the spread of the Gaussian blob profile), both in the horizontal and vertical directions. If the stimulus pattern would appear in the same position in each trial, comparison (using either the presence of after-images or memory effects) of successive impressions of the stimulus extent would have introduced an unwanted cue for the discrimination judgement.

The stimulus was superposed on a 100 cd/m^2 (300 Td for the 2 mm pupil) luminance background level. The luminance level of the background was chosen such as to operate in the photopic domain.

Procedure.

After adaptation of the subject to the background luminance level the contrast detection threshold for a single Gaussian blob was determined by means of a staircase method. Threshold was defined as the stimulus contrast level at which 80% of the presentations was detected. Thresholds were determined at the start of each session and in between separate runs. Pilot experiments showed that the contrast detection threshold of the overall stimulus pattern was independent of the separation of the two blobs. The two-blob discrimination tasks were performed at the threshold luminance contrast level.

For the two-blob acuity tasks no use was made of a fixation mark. The continuous presence of a fixation mark on the centre of the monitor screen would probaly have changed the detection thresholds for the blobs. A discontinuously present fixation mark (e.g. a light spot, turned on in the intervals between two consecutive stimulus presentations and interrupted on presentation of the stimuli) could activate transient mechanisms which might in turn interfere with the low-frequency selective mechanisms under study. Therefore the subjects were instructed to fixate on the centre of the monitor screen.

For the two-blob discrimination task we made use of a two-alternative forced choice method. Each trial consisted of two consecutive presentation intervals. In the first experiment one interval contained a single blob, the other one two blobs with a spatial separation d. The order of presentation of the single- and the double-blob configurations was random. The double-blob configuration was randomly oriented along the vertical or along the horizontal. At the onset of the first presentation of each trial a warning tone was presented once. The onset of the second interval of a trial was announced by the occurence of two consecutive warning tones. After completion of a trial (consisting of two consecutive stimulus presentations) the subject had to indicate (forced choice) whether the double blob had been presented in the first or in the second trial interval. Immediately after the subject had responded to a trial a new presentation was started. The separation d between the two blobs was varied during a run. By withholding his answer for a while the subject was able to take a short rest. In case no decision could be made because one or more blobs were not detected (and in that case only) the subject could skip his obligation to answer and go on to the next presentation. In this case the missed presentation would be randomly incorporated into the sequence of remaining trials. This situation occurred in about 20% of the presentations.

As noted before, when the distance between two blobs increases not only the separation between the two peaks in the resulting light distribution (assuming they are resolved) changes but the absolute luminance of the trough between the peaks and the contrast ratio between the peaks and the trough vary also. We are interested in discrimination

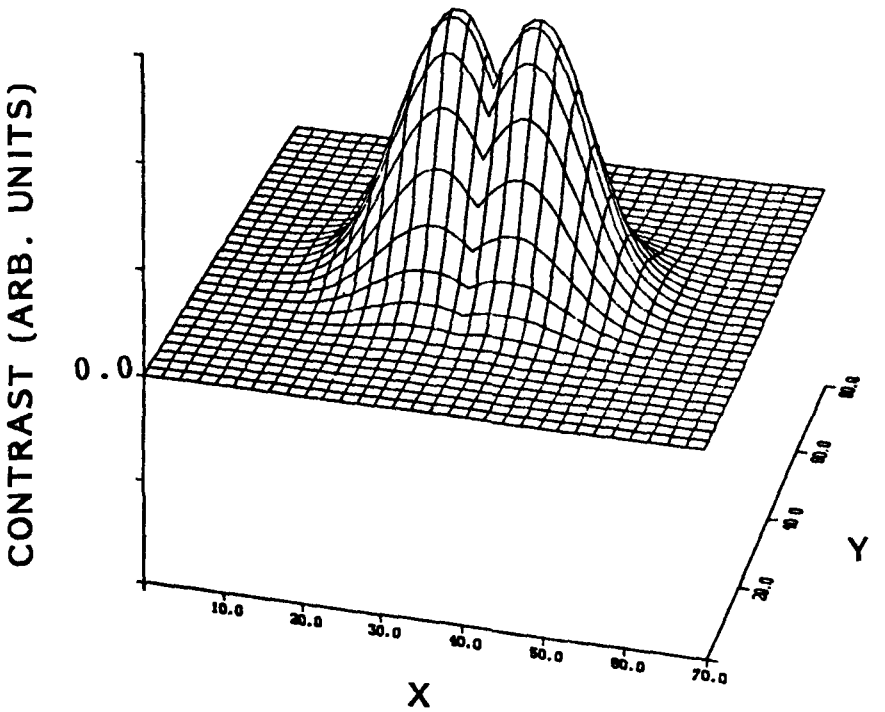

Figure 1. The resulting spatial contrast profile obtained by taking the local maximum of the spatially overlapping contrast profiles of two Gaussian blobs with equal spreads.

judgements that are only based on the relative stimulus extent. We did not want our subjects to compare the extremal contrast values between two consecutive stimulus presentations. Therefore, the stimulus was scaled so that the spatial luminance contrast of the peak(s) in the stimulus profile was independent of the separation of the two blobs. This result could also have been obtained by taking the local maximum value of both blob contrast profiles at each position. However, as shown in Fig. 1, this would have resulted in a sharp dip in the final luminance profile. Such a sharp dip is clearly visible, probably due to the activation of edge detectors (Kulikowsky and King-Smith[73], 1973), and therefore provides an unwanted cue for the discrimination task under study.

Fig. 2a shows the stimulus contrast profile for values of the inter-blob separation d ranging from 0 (top) to 3 (bottom) times the spread s_s of the Gaussian blob. Notice that $d=2s_s$ corresponds to the Sparrow resolution limit. As can be inferred from the Schwartz inequality, it seems a priori reasonable to assume that the weighting function of the detector most actively responding to a given stimulus must match the stimulus contrast profile. We assumed a DOG-like spatial weighting function for the receptive fields. This weighting function was obtained by taking the Laplacian of a two dimensional Gaussian. The DOG-like weighting function thus obtained has the advantage that it can be characterized by only one parameter, namely the spread of the underlying Gaussian. Moreover, it has a zero spatial integral. We computed the response of layers of (continuously distributed) receptive fields of the same spread to the presence of a Gaussian blob and as a function of the spread of the receptive fields. We found that the response is maximal for a layer with receptive fields that have a spread equal to $(N/(N-1))^{\frac{1}{2}}$ times the spread of the Gaussian spatial intensity distribution if N is the power that is used in the spatial probability summation. In our simulation study we took the squared mean of the response of all receptive fields within a layer. Therefore we have N=2. As a result the spread of the receptive fields within the layer most actively responding to the presence of a Gaussian blob equals $2^{\frac{1}{2}}$ times the spread of the spatial contrast profile of the Gaussian blob. Fig. 2b shows the corresponding stimulus profiles from Fig. 2a after convolution with the forementioned DOG-like receptive field

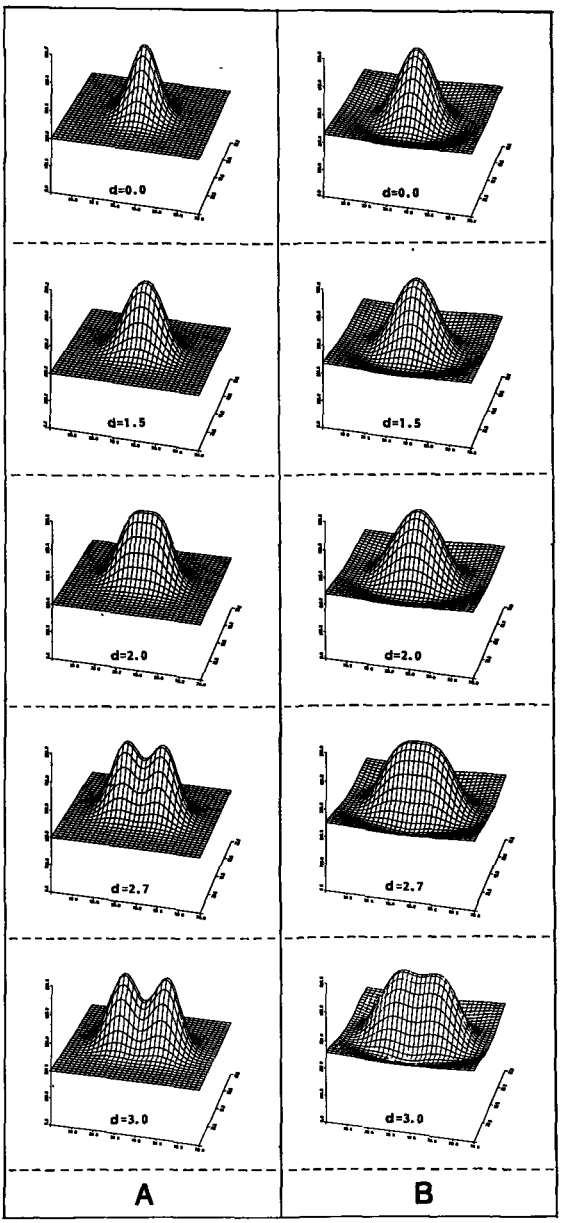

Figure 2. The spatial stimulus contrast profile as used in the two-blob separation discrimination experiments. Fig. 2a shows the spatial stimulus contrast profile for values of the blob separation parameter d ranging from 0 (top) to 3 (bottom). Fig. 2b shows the corresponding stimulus profiles from Fig. 2a after convolution with the DOG-like weighting function of the most actively responding fields.

weighting functions with a spread of $2^{\frac{1}{2}}$ times the spread of the Gaussian blobs. We assumed that the spread of the most actively responding receptive fields is independent of the separation of the two blobs. This is a good approximation as our numerical model studies showed that the spread of the receptive fields in a layer responding most actively to the simultaneous presence of two blobs never (i.e. for no value of their spatial separation d) differed more than 7% of the spread of the receptive fields in the layer responding most actively to the presence of a single blob. From Fig. 2b we see that after convolution with the receptive field weighting function of the most actively responding receptive fields the Sparrow resolution limit is reached when the inter-blob separation d is approximately $2.7s_g$.

In the abovementioned experimental procedure the flux in both trial intervals is not the same. As we wanted to rule out the possibility that subjects used flux differences to perform in the discrimination task[97] we divised a second experiment, similar to the first one, in which each trial interval presents the same amount of flux. In this experiment both trial intervals contain two blobs separated by the same distance d. However, in one interval the separation is along the vertical and in the other along the horizontal. The order of presentation of the vertical and horizontal stimulus configurations in a trial is chosen at random. In this second experiment the subject has to indicate which interval contained the blobs that were separated along the vertical.

In both experiments adaptive Probit estimation[98] was used to measure the differential spatial displacement discrimination thresholds. APE is a modified method of constant stimuli. It allows bias-free threshold determination with high precision for a relatively small number of trials. Threshold is defined as the standard deviation of the cumulative normal psychometric function (corresponding to half the difference between the 17% and 83% points) and was estimated by Probit analysis[99]. Each individual estimate is the standard deviation of the response error distribution from a run of 80 trials preceded by 20 practice trials. Thresholds quoted are the r.m.s. of at least 3 individual estimates. Standard errors for this procedure are typically of the order of 10% of the standard deviation.

The order in which the thresholds were determined was not systematic.

RESULTS.

Contrast detection thresholds were measured at the start of each run. We found that the detection thresholds remained constant during the sessions and were reproduced in separate sessions. As we already noticed in previous experiments[91] the contrast detection thresholds of the Gaussian blobs are nearly independent of their angular dimensions. Fig. 3 shows the contrast detection thresholds of the Gaussian blobs for three subjects. Subject MB had difficulties with detecting blobs larger than approximately 30 min of arc.

As a comparison two subjects (AT and MB) also measured the contrast detection thresholds for sharp edged circular discs with a radius value equal to the spread of the Gaussian blobs. The discs were modulated with the same temporal envelope as the one used for the Gaussian blobs. In Fig. 3 the contrast detection thresholds obtained for discs of a certain radius are compared with the contrast detection thresholds of blobs with a spread of the same value. This comparison is of course rather arbitrary as one cannot be sure what fraction of the spatial contrast profile of the Gaussian blobs actually contributes to their detection. Therefore, there is no simple equivalence relation between the spread of the Gaussian blobs and the radius of the circular discs. Our results show that the contrast detection thresholds for discs with radii larger than approximately 1.5 min of arc (i) are lower than the (nearly constant) contrast detection thresholds of the Gaussian blobs and (ii) decrease with increasing angular dimensions of the discs.

The differential spatial displacement discrimination thresholds for the two-blob task as a function of the angular dimensions of the blobs are shown in Fig. 4. The thresholds were defined as those displacements which resulted in a rate of 83% correct discrimination judgements. The stimuli were temporally modulated with a Gaussian envelope with a spread of 0.2 sec. They were scaled by varying the viewing distance. Therefore, the ratio between the total extent of the background (outer scale) and the

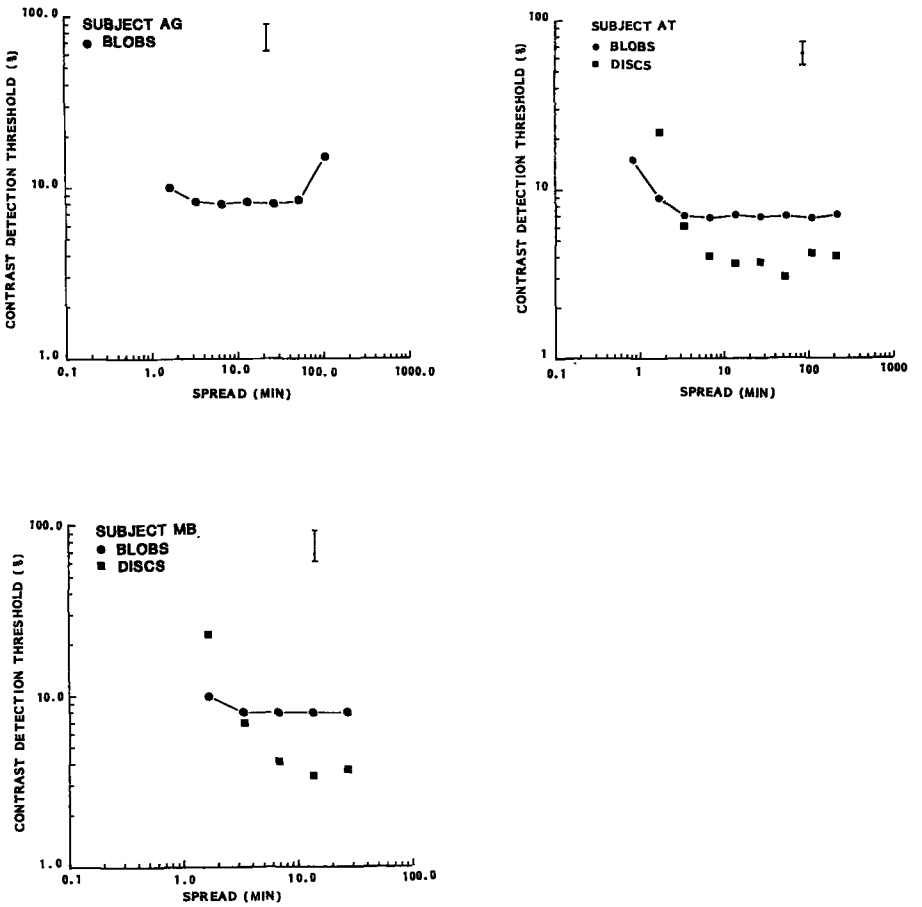

Figure 3. Contrast detection thresholds for Gaussian blobs and (sharp-edged) circular discs as a function of their spatial scale parameters (respectively spread and radius). All stimuli were temporally modulated with a Gaussian envelope with a spread of 0.2 sec. The error bar represents two standard errors.

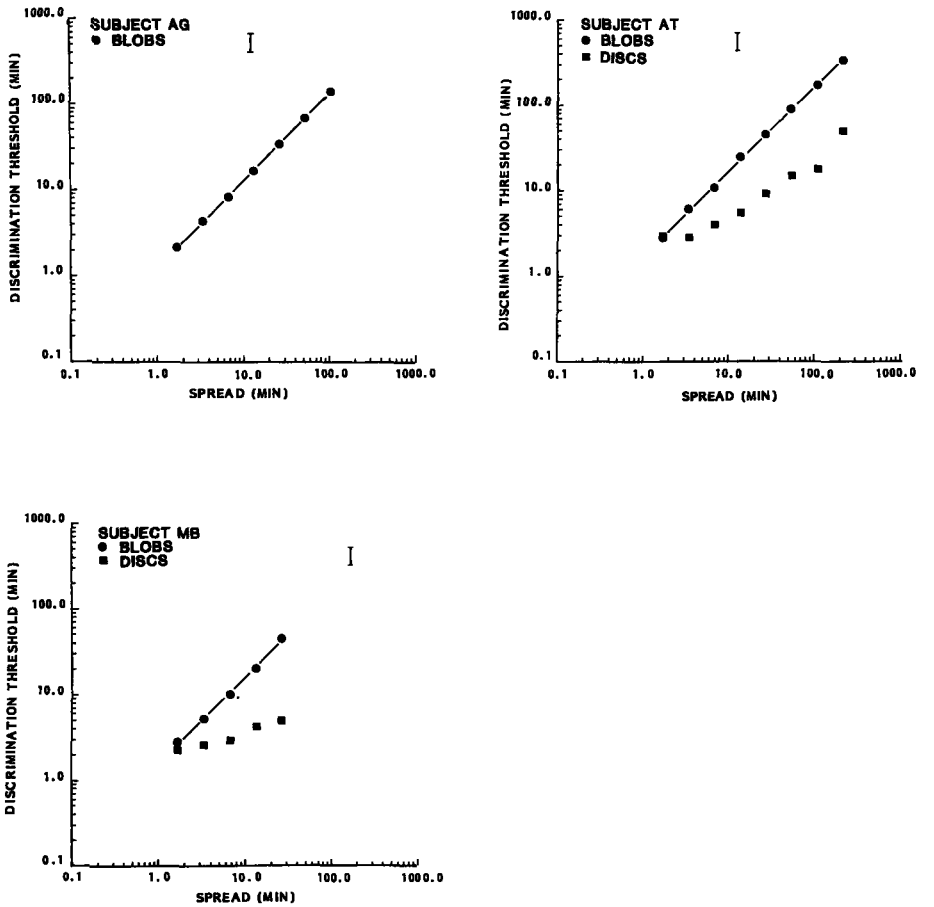

Figure 4. Separation discrimination thresholds for Gaussian blobs (all subjects) and circular discs (subjects AT and MB) as a function of the stimulus scale represented by the spread of the Gaussian blobs (respectively the radius of the circular discs). All stimuli were temporally modulated with a Gaussian envelope with a spread of 0.2 sec. The solid line indicates the result from a least square fit of an exponential curve to the data points. The error bar represents two standard errors.

spread of the Gaussian blobs (inner scale) was kept constant; i.e. at all viewing distances the stimuli were geometrically similar. We found no differences between the results obtained from the experiments in which the flux in both trial intervals differed and the results from the experiments in which the flux in both trial intervals was equal. We computed a least-square fit of an exponential curve to our data points (represented by the solid lines in Fig. 4). Only data points for spreads larger than 1.5 min of arc were used in the calculation of the regression lines. The least-square curves thus obtained closely fit the data points. The correlation coefficients (r^2) range in value between 0.99 and 1.00. The powers obtained for the exponential curves range between 0.98 and 1.01. We may therefore conclude that the differential spatial displacement discrimination thresholds for the two-blob task are a constant fraction of the angular dimensions of the blobs, at least for blobs with spreads larger than approximately 1.5 min of arc.

The differential spatial displacement discrimination thresholds we measured were all smaller than 1.7 times the spread of the Gaussian blobs s_g (The actual value of the proportionality constant for subjects AG, AT and MB was respectively 1.4 ± 0.1, 1.5 ± 0.2 and 1.7 ± 0.2). Therefore, the thresholds were always below the Sparrow resolution limit of $2s_g$ and far below the Sparrow resolution limit which is valid after the convolution of the stimulus profiles with the weighting function of the most actively responding receptive fields and which is approximately $2.7s_g$.

For two subjects (AT and MB) we measured the differential spatial displacement discrimination thresholds for sharp edged circular discs. In Fig. 4 the results of these measurements are shown as a function of the angular dimension of the radius of the discs. If the differential spatial displacement discrimination thresholds for discs of a certain radius are compared with the thresholds obtained for Gaussian blobs with a spread of the same value we see that, for radius values larger than approximately 1.5 min of arc, the thresholds for discs are lower than for blobs. For increasing radius width of the discs the discrepancy between the relative displacement acuity thresholds for discs and for blobs increases.

DISCUSSION.

The constancy of the measured contrast detection threshold values for the Gaussian blobs as a function of their angular dimensions is in agreement with the results of Arend[100-101] who found that low frequency selective spatial channels are equal in sensitivity when the temporal changes of retinal illuminance are equal. This result seems to indicate that we have succeeded in stimulating only a small range of low spatial frequency selective mechanisms.

For stationary stimuli the rate of local temporal illuminance change on the retina, dL/dt, is the product of the rate of movement of the stimulus pattern with respect to the retina, ds/dt, and the spatial rate of change of illuminance at that locus in the retinal image, dL/ds. At high spatial frequencies even the limited eye movements of fixation will produce rapid temporal changes which will lower the detection threshold. This may explain the difference found between the detection thresholds for sharp and blurred stimuli on prolonged presentations[102] and the equality of those thresholds for short presentation durations[103].

Also in our case small involuntary eye movements may explain the difference found between the detection thresholds of the Gaussian blobs and the discs as a function of their angular dimensions. Due to the presence of the sharp edges of the spatial contrast profile of the discs small involuntary eye movements may activate high spatial frequency sensitive mechanisms. For increasing angular dimensions of the discs the number of activated high frequency mechanisms will increase. For increasing angular dimensions of the Gaussian blobs the activation of high spatial frequency selective mechanisms due to small involuntary eye movements will decrease because of the decreasing spatial rate of change of the spatial contrast profile of the stimulus. Moreover, Keesey[104] has demonstrated that visual acuity is neither enhanced nor impaired by the involuntary eye movements that are present during the inspection of a test object. Therefore, we assume that we may safely ignore the influence of small involuntary eye movements on the results of our two-blob acuity measurements.

The results show that the differential spatial displacement discrimination thresholds for the two-blob task scale linearly with stimulus size over a range of at least two decades. For a certain value of the spreads of the Gaussian blobs the differential spatial displacement discrimination threshold is always below the Sparrow resolution limit.

Due to the fact that the relative localization experiment was performed at threshold luminance contrast (contrast level at which 80% of the presentations is seen) in a small fraction of the presentations no answer could be obtained. The uncertainty in the spatial position in which the stimulus pattern as a whole appeared probably caused an additional increase of the number of trials in which a stimulus presentation was missed[105,106]. If only one presentation in a trial is missed it may occur that the presentation in which the stimulus is detected contains two blobs which are clearly separated. In this case a subject can still reach a decision. We actually noted that even small separations sufficed to obtain a correct discrimination in this case. This is in agreement with the results of Westheimer[107] who noted that subjects were able to develop an accurate internal standard against which the instantaneous impression could be judged.

We found no differences between results obtained from experiments in which the flux in the first and second trial interval differed and the results from those experiments in which the flux in both trial intervals was the same. Therefore, we conclude that subjects could perform in the two-blob discrimination task without the help of information obtained from the detection of flux differences between two consecutive stimulus presentations. This result is in agreement with that of Westheimer[107] who found that the differential width discrimination thresholds for a bright bar were about the same in equal-flux and in equal-luminance situations.

We will now discuss what strategy the visual system might use to perform differential spatial displacement discrimination judgements. Hering[27] postulated the theory of mean local sign. According to this theory the visual system can perform relative localization tasks with an accuracy of a fraction of a retinal receptor diameter by taking the mean of the place tags of a collection of retinal photoreceptors. The increase in differential displacement discrimination thresholds found for two- and

three-dot tasks with increasing interdot seperation[108] indicates that the visual system is unable to access and compare the absolute retinal position of activated retinal receptors. Koenderink[78,79] has recently argued how relative place tags may be assigned to a collection of nervous elements by the (physiologically imposed) constraints on the simultaneous/successive order of their total activity. In this view the relative spatial position of stimulus features is encoded in the distribution of the simultaneous activities of the neural elements. Thus, the difference in the accuracy of performance of the visual system in so-called resolution- and differential spatial displacement discrimination tasks may merely result from a decreased precision with which place tags can be assigned to the stimulus features when their corresponding contrast profiles overlap (i.e. when they are not clearly resolved[13,80]). In fact, this may well explain the "crowding" effect observed for hyperacuity tasks[81-83].

Both the success of differential-mechanism models in describing the results of spatial frequency discrimination- and selective adaptation-experiments[57-59,71,72] and the results of Geisler and Davila[25] seem to confirm Koenderink's model. Therefore, as Carlson and Klopfenstein[84] already noted, it seems likely that there is no fundamental difference between the mechanisms that perform in hyperacuity- and standard acuity- or resolution-tasks. Therefore, we assume that the same mechanisms are used to compute differential spatial position in resolution- and hyperacuity tasks.

We have argued before[91] that it is likely that our stimuli will only stimulate a small range of spatial frequency selective mechanisms (only receptive fields with spatial dimensions of the order of those of the retinal projection of the Gaussian blobs will contribute significantly to their detection) when the Gaussian blobs are at their respective detection threshold luminance contrast level. Assuming that we have indeed succeeded in stimulating only a small number of receptive fields within a narrow range of receptive field widths and noting from our results that the differential spatial displacement discrimination thresholds scale linearly with blobsize we may conclude that these thresholds scale linearly with the level of resolution at which the stimulus features are present. If the

visual system would use different strategies to encode relative location at different levels of resolution one would expect to find indications for regions of transition between the ranges in resolution space in which the different mechanisms are active. However, our data, as well as those of Hirsch and Hylton[56,89], provide no indication for the existence of different mechanisms to encode relative position. Therefore, it seems that the visual system assigns relative location tags to receptive fields on all levels of resolution. These can then in turn be used to compute the differential spatial displacement of stimulus features at a certain level of resolution to an accuracy which is a constant multiple of the prevailing receptive field width at that level of resolution. As argued before, these place tags may be encoded in the constraints imposed on the simultaneous activity in the ganglion cell network[78,79].

We conclude that the human visual system seems to use one strategy to detect differential spatial displacement, whether the components of a stimulus pattern can be resolved or not, and independent of the level of resolution at which these stimulus features are present. The accuracy that can be obtained for differential spatial displacement discrimination tasks is directly determined by the accuracy with which stimulus components can be discriminated as spatially resolved, individual features.

Acknowledgements - We thank Prof.Dr. M.A. Bouman and Ad de Goffau for acting as patient observers. The help of our software engineers Mike van Eekhout and Henk Simons was invaluable. We are indebted to Dr. B. Nienhuis, Herman Snippe and Piet Bijl for their valuable suggestions and contributions. We thank Dr. R.J. Watt and Dr. A.P. Andrews for kindly providing us with a listing of their APE program. This work was supported by the Dutch Foundation for the Advancement of Pure Research (ZWO).

REFERENCES.

1. Rayleigh, Lord J.W.S. Collected papers. Vol. 3, p.84. Cambridge Univ. Press. Cambridge, England (1902).
2. Barakat, R Application of apodization to increase two-point resolution by the Sparrow criterion. I. Coherent illumination. J. Opt. Soc. Am. 52, 276-283 (1962).
3. Born, M. and Wolf, E. Principles of optics. 3rd ed., p.524. Pergamon Press Inc., New York (1965).
4. Sparrow, G. On spectroscopic resolving power. Astrophys. J. 44, 76-86 (1916).
5. Ramsay, B.P., Cleveland, E.L. and Koppius, O.T. Criteria and the intensity-epoch slope. J. Opt. Soc. Am. 31, 26-33 (1941).
6. Grimes, D. Nyyssonen and Thompson, B.J. Two-point resolution with partially coherent light. J. Opt. Soc. Am. 57, 1330-1334 (1967).
7. Thompson, B.J. Image formation with partially coherent light. In: Progress in Optics, Vol. VII, pp. 171-230. Ed. Wolf, E. North-Holland Publ. Comp., Amsterdam, London (1969).
8. Toraldo di Francia, G. Resolving power and information. J. Opt. Soc. Am. 45, 497-501, (1955).
9. Harris, J.L. Resolving power and decision theory. J. Opt. Soc. Am. 54, 606-611 (1964).
10. Nahrstedt, D.A. and Schooley, L. Alternative approach in decision theory as applied to the resolution of two point images. J. Opt. Soc. Am. 69, 910-912 (1979).
11. Aulhorn, E. and Harms, H. Visual perimetry. In: Handbook of sensory physiology VII/4, 102-145. Springer Verlag, New York (1972).
12. Westheimer, G. Visual acuity and spatial modulation thresholds. In: Handbook of sensory physiology VII/4, 170-187. Springer Verlag, New York (1972).
13. Westheimer, G. The spatial sense of the eye. Invest. Opthalmol. Vis. Sci. 893-912 (1979).
14. Helmholtz, H. von. Handbuch der physiologischen Optik. Translation by Southall, J.P.C., Vol. I. Dover Publications Inc., New York (1962).

15. Walls, G.K. Factors in human visual resolution. J. Opt. Soc. Am. 33, 487-505 (1943).
16. Ogle, K.N. On the resolving power of the human eye. J. Opt. Soc. Am. 41, 517-520 (1951).
17. Westheimer, G. Modulation thresholds for sinusoidal light distribution on the retina. J. Physiol. 152, 67-74 (1960).
18. Volkmann, A.W. Physiologische Untersuchingen im Gebiete der Optik. Breitkopf & Hartel, Leipzig (1863).
19. Wülfing, E.A. Über den kleinsten Gesichtswinkel. Z. Biol. 29, 199-202 (1892).
20. Westheimer, G. and McKee, S.P. Spatial configurations for visual hyperacuity. Vision Res. 17, 941-947 (1977).
21. Westheimer, G. Diffraction theory and visual hyperacuity. Am. J. of Optometry and Physiological Optics 53, 362-364 (1975).
22. Westheimer G. and McKee, S.P. Visual acuity in the presence of retinal image motion. J. Opt. Soc. Am. 65, 847-850 (1975).
23. Westheimer, G. and McKee, S.P. Integration regions for visual hyperacuity. Vision Res. 17, 89-93 (1977).
24. Klein, S.A. and Levi, D.M. Hyperacuity thresholds of 1 sec: theoretical predictions and empirical validation. J. Opt. Soc. Am. A2, 1170-1190 (1985).
25. Geisler, W.S. and Davila, K.D. Ideal discrimination in spatial vision: two-point stimuli. J. Opt. Soc. Am. A2, 1483-1497 (1985).
26. Geisler, W.S. Physical limits of acuity and hyperacuity. J. Opt. Soc. Am. A1, 775-782 (1984).
27. Hering, E. Über die Grenzen der Sehschärfe. Ber.Math.-phys. Cl. d. Königl. Sächs-Gesell. Wiss. Leipzig. Naturwiss. Teil 16-24 (1899).
28. Tonner, F. Die Messung der Empfindungsfläche und Sehschärfe unter variabelen Bedingungen im gleichen Versuch. Pflügers Archiv 247, 149-159 (1943).
29. Tonner, F. Die Grösse der Empfindungsfläche eines Lichtpunktes und der Zapfenraster. Pflügers Archiv 247, 168-182 (1943).
30. Tonner, F. Die Sehschärfe. Pflügers Archiv 247, 183-193 (1943).
31. Campbell, F.W. and Robson, J. Application of Fourier analysis to the visibility of gratings. J. Physiol. 197, 551-566 (1968).

32.Blakemore, C. and Campbell, F.W. On the existence of neurons in the human vision system selectively sensible to the orientation and size of retinal images. J. Physiol. 203, 237-260 (1969).

33. Graham, N. and Nachmias, J. Detection of grating patterns containing two spatial frequencies: a comparison of single- channel and multiple- channel models. Vision Res. 11, 251-259 (1971).

34. Sachs, M.B., Nachmias, J. and Robson, J.G. Spatial frequency channels in human vision. J. Opt. Soc. Am. 61, 1176-1186 (1971).

35. Campbell, F.W., Cooper, G.F. and Enroth-Cugell, C. The spatial selectivity of the visual cells of the cat. J. Physiol. 203, 223-235 (1969).

36. Shapley, R. and Lennie, P. Spatial frequency analysis in the visual system. Ann. Rev. Neurosci. 8, 547-583 (1985).

37. Graham, N., Robson, J.G. and Nachmias, J. Grating summation in fovea and periphery. Vision Res. 18, 815-825 (1978).

38. Quick, R.F., Mullins, W.W. and Reichert, T.A. Spatial summation effects in two-component grating thresholds. J. Opt. Soc. Am. 68, 116-121 (1978).

39. Legge, G.E. Space domain properties of a spatial frequency channel in human vision. Vision Res. 18, 959-969 (1978).

40. Wilson, H.R. and Bergen, J.R. A four mechanism model for threshold spatial vision. Vision Res. 19, 19-32. (1979)

41. Robson, J.G. and Graham, N. Probability summation and regional variation in contrast sensitivity across the visual field. Vision Res. 21, 409-418 (1981).

42. Bergen, J.R., Wilson, H.R. and Cowan, J.D. Further evidence for four mechanisms mediating vision at threshold: sensitivity to complex gratings and aperiodic stimuli. J. Opt. Soc. Am. 69, 1580-1587 (1979).

43. Watson, A.B. and Robson, J.G. Discrimination at threshold: labelled detectors in human vision. Vision Res. 21, 1115-1122 (1981).

44. Watson, A.B. Summation of grating patches indicates many types of detector at one retinal location. Vision Res. 22, 17-25 (1982).

45. Stromeyer, C.F. and Klein, S. Evidence against narrowband spatial frequency channels in human vision: the detectability of frequency

modulated gratings. Vision Res. 15, 899-910 (1975).

46. Graham, N. and Rogowitz, B. Spatial pooling properties deduced from the detectability of FM and quasi-AM gratings: a reanalysis. Vision Res. 16, 1012-1026 (1976).

47. Graham, N. Visual detection of aperiodic spatial stimuli by probability summation among narrow band channels. Vision Res. 17, 637-652 (1977).

48. Pantle, A. and Sekuler, R. Size detecting mechanisms in human vision. Science 162, 1146-1148 (1968).

49. Thomas, J.P. and Kerr, L.G. Evidence of role of size- tuned mechanisms in increment threshold task. Vision Res. 11, 647-655 (1971).

50. Nakayama, K. and Roberts, D.J. Line-length detectors in the human visual system: evidence from selective adaptation. Vision Res. 12, 1709-1713 (1972).

51. Bagrash, F.M. Size-selective adaptation: psychophysical evidence for size-tuning and the effects of stimulus contour and adapting flux. Vision Res. 13, 575-598 (1973).

52. Thomas, J.P. and Shimamura, K.K. Perception of size at the detection threshold: its accuracy and possible mechanisms. Vision Res. 14, 535-543 (1974).

53. Bagrash, F.M., Thomas, J.P. and Shimamura,K.K. Size-tuned mechanisms: correlation of data on detection and apparant size. Vision Res. 14, 937-942 (1974).

54. Perizonius, E., Schill, W., Geiger, H. and Roehler, R. Evidence of the local character of spatial frequency channels in the human visual system. Vision Res. 25, 1233-1240 (1985).

55. Campbell, F.W., Nachmias, J. and Jukes, J. Spatial-frequency discrimination in human vision. J. Opt. Soc. Am. 60, 555-559 (1970).

56. Hirsch, J. and Hylton, R. Limits of spatial-frequency discrimination as evidence of neural interpolation. J. Opt. Soc. Am. 72, 1367-1374 (1982).

57. Regan, D. and Beverly, K.I. Spatial-frequency discrimination and detection comparison of postadaptation thresholds. J. Opt. Soc. Am. 73, 1684-1690 (1983).

58. Burbeck, C.A. and Regan, D. Independence of orientation and size in spatial discrimination. J. Opt. Soc. Am. 73, 1691-1694 (1983).

59. Regan, D. Masking of spatial-frequency discrimination. J. Opt. Soc. Am. A2, 1153-1159 (1985).

60. Furchner, C.S., Thomas, J.P. and Campbell, F.W. Detection and discrimination of simple and complex patterns at low spatial frequencies. Vision Res. 17, 827-836 (1977).

61. Green, M., Corwin, T. and Schor, C. Spatiotemporal variation in the square/sine ratio: evidence of independent channels at low spatial frequencies. Vision Res. 21, 423-425 (1981).

62. Stromeyer, C.F., Klein, S., Dawson, B.M. and Spillman, L. Low-spatial frequency channels in human vision: adaptation and masking. Vision Res. 22, 225-233 (1982).

63. Jamar, J.H.T., Campagne, J.C. and Koenderink, J.J. Detectability of amplitude modulation and frequency modulation of suprathreshold sine-wave gratings. Vision Res. 22, 407-416 (1982).

64. Nachmias, J. and Weber, A. Discrimination of simple and complex gratings. Vision Res. 15, 217-223 (1975).

65. Hirsch, I., Hylting, R. and Graham, N. Simultaneous recognition of low spatial-frequency components. Vision Res. 22, 365-375 (1982).

66. Woodward, M. Ettinger, E.R. and Yager, D. The spatial frequency discrimination function at low contrasts. Spatial Vis. 1, 13-17 (1985).

67. Hering, E. Über individuelle Verschiedenheiten des Farbensinnes. Lotos, Prague (1885).

68. Hering, E. Outlines of a theory of the light sense. Translated by Hurvich, L.M. and Jameson, D., Harvard, Cambridge, Mass. (1964).

69. Marriott, F.H.C. Nervous transmission of colour information. In: The Eye. 2nd ed., vol. 2A. Ed.: Davson, H., Academic Press, New York (1976).

70. Richter, E.S. and Yager, D. Spatial-frequency difference thresholds for central and peripheral viewing. J. Opt. Soc. Am. A1, 1136-1139 (1984).

71. Wilson, H.R. and Gelb, D.J. Modified line-element theory for spatial-frequency and width discrimination. J. Opt. Soc. Am. A1, 124-131

(1984).

72. Wilson, H.R. and Regan, D. Spatial-frequency adaptation and grating discrimination: predictions of a line-element model. J. Opt. Soc. Am. A1, 1091-1096 (1984).

73. Kulikowsky, J.J. and King-Smith, P.E. Spatial arrangement of line, edge and grating detectors revealed by subthreshold summation. Vision Res. 13, 1455-1478 (1973).

74. King-Smith, P.E. and Kulikowsky, J.J. Lateral interaction in the detection of composite spatial patterns. J. Physiol. 234, 5-6 (1973).

75. King-Smith, P.E. and Kulikowsky, J.J. The detection of gratings by independent activation of line detectors. J. Physiol. 247, 237-271 (1975).

76. Rentschler, I. and Hilz, R. Evidence for discrimination in line detection. Vision Res. 16, 1299-1302 (1976).

77. Wilson, H.R., Phillips, G., Rentschler, I. and Hilz, R. Spatial probability summation and disinhibition in psychophysically measured line-spread functions. Vision Res. 19, 593-598.

78. Koenderink, J.J. Simultaneous order in nervous nets from a functional standpoint. Biol. Cybern. 50, 35-41 (1984).

79. Koenderink, J.J. The concept of local sign. In: Limits in Perception. Eds. Doorn, J. van, Grind, W.A. van de and Koenderink, J.J. VNU Science Press, Utrecht, 495-547 (1984).

80. Westheimer, G. Diffraction theory and visual hyperacuity. Am. J. of Optometry and Physiological Optics 53, 362-364 (1976).

81. Westheimer, G. and Hauske, G. Temporal and spatial interference with Vernier acuity. Vision Res. 15, 1137-1141 (1975).

82. Westheimer, G., Shimamura, K. and McKee, S.P. Interference with line-orientation sensitivity. J. Opt. Soc. Am. 66, 332-338 (1976).

83. Levi, D.M., Klein, S.A. and Aitsebaomo, A.P. Vernier acuity, crowding and cortical magnification. Vision Res. 25, 963-977 (1985).

84. Carslon, C.R. and Klopfenstein, R.W. Spatial-frequency model for hyperacuity. J. Opt. Soc. Am. A2, 1747-1751 (1985).

85. Koenderink, J.J. Current models of contrast processing. In: Spatial Contrast, Report of a workshop held in Amsterdam, 1976. Spekreijse,

H. and Tweel, L.H. van der, eds. Amsterdam-Oxford-New York: North Holland (1977).

86. Koenderink, J.J. and Doorn, A.J. van. Visual detection of spatial contrast; influence of location in the visual field, target extent and illuminance level. Biol. Cybern. 30, 157-167 (1978).

87. Koenderink, J.J. and Doorn, A.J. van. Invariant features of contrast detection: an explanation in terms of self-similar detector arrays. J. Opt. Soc. Am. 72, 83-87 (1982).

88. Hartmann, G. Recursive features of circular receptive fields. Biol. Cybern. 43, 199-208 (1982).

89. Hirsch, J. and Hylton, R. Spatial-frequency discrimination at low frequencies: evidence for position quantization by receptive fields. J. Opt. Soc. Am. A2, 128-135 (1985).

90. Burton, G.J., Haig, N.D. and Moorhead, I.R. A self-similar stack model for human and machine vision. Biol. Cybern. 53, 397-403 (1986).

91. Toet, A., Eekhout, M.P. van, Simons, H.L.J.J. and Koenderink J.J. Scale invariant features of differential spatial displacement discrimination. Vision Res. (in press).

92. Leibowitz, H. The effect of pupil size on visual acuity for photometrically equated test fields at various levels of illuminance. J. Opt. Soc. Am. 42, 416-422 (1952).

93. Campbell, F.W. and Gubisch, R.W. Optical quality of the human eye. J. Physiol. 186, 558-578 (1966).

94. Bowen, R.W., Pola J. and Matin, L. Visual persistence: effects of flash luminance, duration and energy. Vision Res. 14, 295-303 (1974).

95. Bowling, A. and Lovegrove, W. The effect of stimulus duration on the persistence of gratings. Percept. & Psychophys. 27, 574-578 (1980).

96. Bowling, A., Lovegrove, W. and Mapperson, B. The effect of spatial frequency and contrast on visual persistence. Perception 8, 529-539 (1979).

97. Enroth-Cugell, C. and Shapley, R.M. Flux, not retinal illumination, is what cat retinal ganglion cells really care about. J. Physiol. 233, 311-326 (1973).

98. Watt, R.J. and Andrews. APE: Adaptive probit estimation of psychometric function. Curr. Psychol. Rev. 1, 205-214 (1981).
99. Finney, D.J. Probit Analysis, 3rd edn. Cambridge Univ. Press (1971).
100. Arend, L.E. Temporal determinants of the form of the spatial contrast threshold MTF. Vision Res. 16, 1035-1042 (1976a).
101. Arend, L.E. Response of the human eye to spatially sinusoidal gratings at various exposure durations. Vision Res. 16, 1311-1315 (1976b)
102. Shapley, R. Gaussian bars and rectangular bars: the influence of width and gradient on visibility. Vision Res. 1457-1462 (1974).
103. Hood, D.C. The effects of edge sharpness and exposure duration on detection threshold. Vision Res. 13, 759-766 (1973).
104. Keesey, U.T. Effects of involuntary eye movements in visual acuity. J. Opt. Soc. Am. 50, 769-774 (1960).
105. Cohn, T.E. and Lasley, D.J. Detectability of a luminance increment: effect of spatial uncertainty. J. Opt. Soc. Am. 64, 1715-1719 (1974).
106. Cohn, T.E. and Wardlaw, J.C. Effect of large spatial uncertainty on foveal increment detectability. J. Opt. Soc. Am. A2, 820-825 (1985).
107. Westheimer, G. Spatial configurations for visual hyperacuity. Vision Res. 17, 941-947 (1977).
108. Beck, J. and Halloran, T. Effects of spatial separation and retinal eccentricity on two-dot Vernier acuity. Vision Res. 25, 1105-1111 (1985).
109. DeValois, R.L., Albrecht, D.G. and Thorell, L.G. Spatial frequency selectivity of cells in macaque visual cortex. Vision Res. 22, 545-559 (1982).
110. Yager, D., Kramer, P., Shaw, M. and Graham, N. Detection and identification of spatial frequency: models and data. Vision Res. 24, 1021-1035 (1984).

CHAPTER II.4.

Differential spatial displacement discrimination with interfering stimuli.

ABSTRACT.

Similar to the three-dot alignment hyperacuity task, differential spatial displacement discrimination thresholds were determined for a configuration of three blobs with Gaussian spatial contrast profiles at threshold luminance contrast. Thresholds that were determined in the presence of interfering stimuli were identical to thresholds that were determined without interfering stimuli. The thresholds scale linearly with the stimulus size over at least two decades. We conclude that (i) the mechanisms that compute differential spatial displacement for the three-blob alignment task are not disturbed by the presence of interfering stimuli, even when these enter the region over which the computations are performed and (ii) at all levels of resolution similar mechanisms are used to compute differential spatial displacement.

INTRODUCTION.

The human visual system is extremely sensitive to changes in the relative position of features in the visual field (Volkmann, 1863; Wülfing, 1892; Westheimer and McKee, 1977b). However, the apparent position of a certain feature may change due to the introduction of additional features nearby Köhler and Wallach, 1944; Fendick, 1983; Badcock and Westheimer, 1985). Therefore, it seems that the visual system computes relative place tags for some kind of centroids in the retinal luminance distribution (Watt and Morgan, 1983; Watt et al., 1983; Gendick, 1984; Badcock and Westheimer, 1985). The spatial regions within which these computations are performed are restricted (Westheimer and McKee, 1977a). It has been shown that the introduction of additional features in such a processing region has a detrimental effect on letter acuity (e.g.

Flom et al., 1963a,b; Bouman, 1970; Jacobs, 1979), on stereopsis (Butler and Westheimer, 1978) and on differential spatial displacement discrimination accuracy (Westheimer and Hauske, 1975; Westheimer et al., 1976; Andriessen and Bouman, 1976; Breitmeyer, 1978; Watt et al., 1983; Essock et al., 1983; Levi et al., 1985; Williams and Essock, 1986). There are indications that the spatial extent of the processing modules mediating differential spatial displacement discrimination is proportional to the discrimination threshold, both in foveal-, peripheral- and amblyopic- vision (Levi and Klein, 1985; Levi et al., 1985). Experiments using dichoptically presented stimuli have shown that these processing regions probably reflect central (cortical) neural interactions (Flom et al., 1963a; Westheimer and Hauske, 1975; Westheimer et al., 1976), rather than retinal ones. Moreover, an electrophysiological analogue to spatial interference has been determined with cortical potentials (Steinman et al., 1984, 1985).

As first noted by Fendick (1984) it is important not to confound the notions of "acuity" and "accuracy" for differential spatial displacement discrimination in the presence of interfering stimuli. Interfering stimuli may change the apparent position of the features constituting the target stimulus. The degree of change in apparent position of a feature will depend on the distance of that feature from the interfering stimulus. When the features in a target stimulus have different distances to the interfering feature (e.g. a Vernier stimulus with flanking bars parallel to the stimulus) the induced changes in their apparent positions will also be different. For instance, in case of an alignment task this effect will introduce a zero offset; i.e. a subject will judge the stimulus features to be in perfect alignment when there is in fact an actual (non-zero) spatial displacement. However, the acuity with which spatial variations about this apparent (subjective) zero-offset situation can be discriminated may be unimpaired (Fendick, 1984). In this case the "accuracy" for alignment is degraded but the "acuity" for noting differential spatial displacements remains unhampered after the introduction of interfering stimuli. Thus, any measure based on a single point on the psychometric curve will confound the effects of a shift in the mean apparent position of the target stimulus and a change in the

differential spatial displacement discrimination threshold.

Badcock and Westheimer (1985a,b) performed Vernier acuity and jump detection experiments with perturbing flanking lines and determined both the mean and the width of the corresponding psychometric curves. They found that the presence of the interfering flanks had no significant influence on the differential spatial displacement discrimination thresholds. However, the mean value was changed in each condition; i.e. the presence of a flank caused a change in the apparent position of the targets. By studying the influence of flanking lines on the apparent position of the target they determined the structure of the localization contribution function. These results are in agreement with those of Morgan and Ward (1985) who found that small spatial intervals could be discriminated from a standard with a high degree of accuracy, even in the presence of flanking bars that were given a randomly perturbed postion. Therefore, it seems that the presence of interfering stimuli has no detrimental effect on differential spatial displacement discrimination accuracy, as long as they can be clearly resolved from the target stimuli.

In a previous experiment (Toet et al., 1987) we determined differential spatial displacement discrimination thresholds for a configuration of three blobs with Gaussian spatial contrast profiles at threshold luminance contrast. The blobs were arranged one above the other at equal spatial intervals. Thresholds were determined for spatial displacements of the middle blob both orthogonal to and along the axis joining the centers of the outer two blobs. Thresholds for both tasks were obtained as a function of the resolution or "inner scale" and the total extent or "outer scale" of the stimulus pattern. It was found that, for both tasks, the thresholds increased linearly with increasing inner scale of the stimulus pattern for a constant ratio of the outer- and inner-scale parameters. At all levels of resolution there appeared to be two outer scale regimes in which different strategies are used to compute differential spatial displacements. Independent of the level of resolution (inner scale parameter of the stimulus configuration) transition between those regions occurs when the outer scale parameter is a constant multiple (approximately 25) of the inner scale parameter. It was argued that the different processing regimes might reflect the existence of spatial

regions or processing modules (extending up to 25 times the inner scale parameter) in which differential spatial displacement computations are performed directly. Differential spatial displacement computations performed on stimuli extending over more than 25 times their inner scale parameter (i.e. over more than the spatial extent of a single processing module) probably involve an intermediary stage of comparison of the activity of adjoining regions (i.e. indirect computation modes). Similar conclusions were reached by other researchers (e.g. Westheimer, 1981; Gelb and Wilson, 1983; Levi and Klein, 1985; Levi et al., 1985).

We designed an experiment to test whether it is possible to manifest the existence of the forementioned hypothetical processing modules by means of a differential spatial displacement discrimination task in combination with interfering stimuli. If it is in principle possible to perturb a differential spatial discrimination task it seems likely that interfering stimuli presented within the processing module that is performing in a spatial displacement discrimination task may have a detrimental effect on the discrimination accuracy, whereas interfering stimuli present in different processing regions will interfere less (or not at all) with the discrimination process. With regard to our previous results (Toet et al., 1987) and assuming that differential spatial displacement discrimination can indeed be perturbed by interfering stimuli we expect that the degree of perturbance will be maximal within a region extending over approximately 25 times the inner scale parameter of the target stimulus and centered on this stimulus. The relative spatial localization task we devised is equivalent to the three-dot alignment hyperacuity task which is well documented in the literature (Ludvigh, 1953; Ludvigh and McKinnon, 1967; Andrews et al., 1973; Andrews and Miller, 1978; Beck and Schwartz, 1979; Watt, 1984).

METHODS.

Subjects.

Three male subjects, aged between 22 and 30, served in the experiment. Subject A.T. has corrected myopic vision. The other subjects are all emmetropic and have 20/15 Snellen acuity. All subjects are highly practised.

Apparatus.

A PDP 11/34 minicomputer in combination with a Gould deAnza IP8500 image array processor was used to generate, process and present the stimuli, record the responses and analyze the data.

The stimulus was displayed on a Philips LDH2123 monochrome monitor. The CRT was driven in an interlaced mode with a framerate of 60 Hz. The display consisted of 512 × 512 pixels with the luminance value of each pixel quantized to 8 bits. A 512 × 512 correction matrix was added to the deAnza frame buffer to compensate for the inhomogeneity of the display.

Viewing conditions.

The display was placed in a dark room with nonreflecting black walls. Observers were seated with their heads supported by a chin rest adjusted in height and position so that their dominant eye was on the line perpendicular to the centre of the monitor screen. The use of a forehead rest prevented tilting of the head. Viewing was monocular with the subject's dominant eye. The unused eye was covered with an eye cap. Viewing distance varied from 10 cm to 10 m. Except for viewing distances below 1 m viewing was through a 2 mm artificial pupil. Below 1 m the natural pupil was used in order to avoid vignetting effects. At these distances variations of accommodation had no influence on our results as the spread of the optical blur function of the eye is more than two orders of magnitude smaller than the spread of the spatial contrast profile of the stimuli that were presented.

Stimuli.

The target stimuli used in this experiment comprised three blobs arranged one above the other at equal spatial intervals. The blobs had identical Gaussian spatial contrast profiles and were modulated with a Gaussian temporal envelope. Their luminance distribution is given by

$$L(x,y,t) = L_b\ [1 + cw(x,y,t)]$$

where L_b denotes the background luminance and c is the threshold contrast value as determined for a single blob. The window function w(x,y,t) is given by

$$w(x,y,t) = \exp[-(x^2+y^2)/(2s_s^2)-t^2/(2s_t^2)]$$

We adopt the term spread for the distance over which a Gaussian falls from 1 to $e^{-\frac{1}{2}}$, corresponding to the standard deviation measure as defined in statistics. (A spatial region with radius $2s_s$ and centered on (x,y)=(0,0) contains 92% of the total energy; a temporal interval of width $2s_t$ centered on t=0 contains 96% of the total stimulus energy). The window function is the product of spatial- and temporal- profiles with spreads of s_s and s_t respectively. Both the temporal and the spatial windows were truncated at plus and minus four times their spread (containing respectively 99.994% and 99.990% of the total energy in a blob). The threshold contrast c is defined as $(L-L_b)/L_b$, where L denotes the threshold luminance level.

The spread of the Gaussian temporal envelope was 0.2 sec (therefore the stimulus was above one half of its peak value for 0.47 sec). The frame rate was 60 Hz and interlaced. Intermediate presentations lasted for 0.05 sec., corresponding to 3 frames. This was found to be short enough to present a perceptually smooth temporal contrast profile. The total duration of the stimulus presentation was eight times the spread of its Gaussian temporal contrast profile (i.e. if T is the moment at which the stimulus attained its maximum contrast and s_t represents the spread of the Gaussian tempral contrast profile, the presentation lasted from $T-4s_t$ to

$T+4s_t$).

If we define the bandwidth of a Gaussian signal as the distance between the (negative and positive) frequency components for which the amplitude has dropped to one half of the value of the frequency component with maximum amplitude (zero frequency for a Gaussian signal), we find that the temporal bandwidth is given by $(2*\ln 2)^{\frac{1}{2}}/(\pi*s_t)$. In our case the temporal frequency bandwidth is 1.87 Hz and the spatial frequency bandwidth is between 0.1 cy/deg and 53.6 cy/deg.

The distance between the centres of the outer two blobs of the target stimulus was 20 times their spread. The middle blob appeared on the line through the middle of and orthoaxial to the line segment joining the centres of the outer two blobs.

The interfering stimuli were either Gaussian blobs identical to the blobs constituting the target stimulus or sharp edged circular discs with a radius value equal to the spread of the Gaussian blobs. The entire stimulus pattern was modulated with the same Gaussian temporal envelope.

Fig. 1 represents the spatial stimulus configurations that were used in the experiment. The three filled dots represent the target stimulus. The two outer blobs of the target configuration were aligned along the vertical (v). The middle blob appeared somewhere on the horizontal (h) with a small offset from the vertical (v). The two open dots represent the interfering stimuli. These were either two Gaussian blobs, identical to those constituting the target configuration, or two sharp edged circular discs with radii equal to the spreads of the Gaussian blobs in the target stimulus. The dashed lines (v' and h') represent an orthoaxial system with an origin that coincides with the center of the target system and that has been rotated with respect to the coordinate system of the target stimulus (v and h). The two interfering stimuli appeared each on a different axis of this rotated orthoaxial system, randomly on the positive or negative side of those axes, and at a prescribed distance (R) from the centre of the target configuration. Therefore, their positions were on a circle which was centered on the the middle of the target configuration (or, equivalently, on the centre of both coordinate systems). At the start of a run both the radius value of this circle (R) and the angle over which the primed system had to be rotated (θ) were prescribed. They both remained

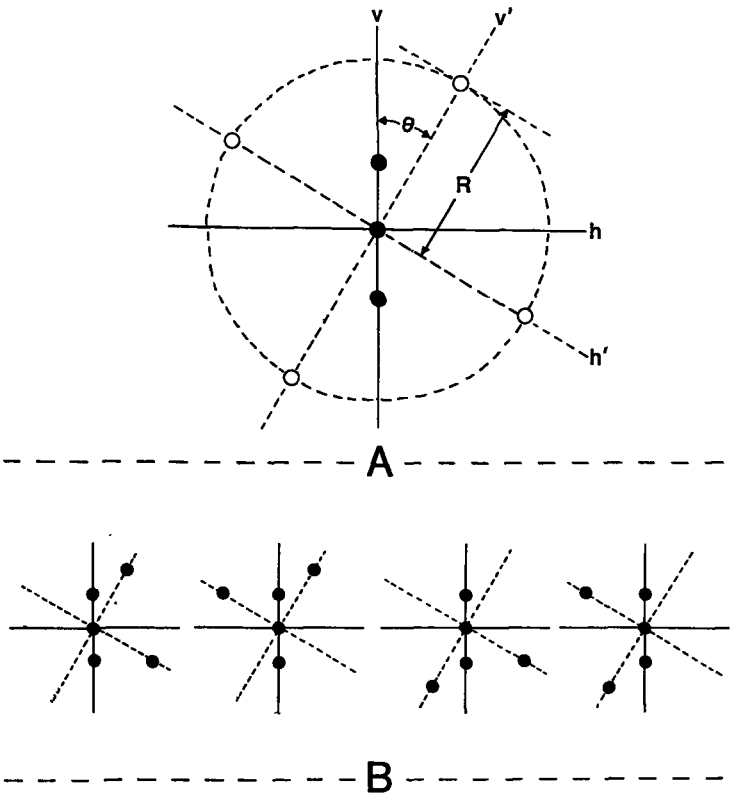

Figure 1. Symbolic representation of all different spatial stimulus configurations that were used in the experiment. **A.** The three filled dots represent the three-blob alignment target stimulus. The open dots represent the possible positions of the interfering stimuli (two of which, on different axes, are actually simultaneously realized on each stimulus presentation). **B.** All stimulus configurations that were actually realized in the experiment.

constant during a complete run.

We chose for ± 30° as the angle of rotation of the primed system. Interfering blobs flanking the outer two blobs of the target configuration (on the vertical v) would provide an additional alignment cue. In a previous paper (Toet et al., 1987) we determined the three-blob alignment discrimination thresholds as a function of the separation of the outer two blobs. We found that the thresholds remained constant for separations up to 25 times the spread of the Gaussian blobs. For larger separations the thresholds showed a Weber behaviour as a function of the separation of the outer blobs. In this experiment we wanted to investigate the influence of interfering stimuli on the three-blob alignment discrimination thresholds in both regions (i.e. the constant threshold region and the Weber region). Therefore, we could not use interfering blobs flanking the outer two blobs of the target configuration. For large separations of the interfering stimuli such a configuration would yield results that confound the output of the two regions. For a rotation angle of the primed system of 0° the interfering blobs would appear on both axes of the target coordinate system. The blob that appears on the horizontal (h) will then provide a distance cue (discrimination of separation between the middle blob of the target configuration and the horizontal interfering blob) and the blob appearing on the vertical (v) will provide an additional alignment cue. A rotation angle of ±45° results in a configuration of interfering blobs that will either provide an additional alignment cue or a bisection cue (depending on which of the four possible interfering stimulus configurations is actually realized). Therefore, we chose for an absolute value of the rotation angle of 30° as this seems to result in a spatial arrangement of the interfering stimuli that provides no obvious cues that might be helpful in performing the three-blob alignment discrimination task.

Because we are interested in the differential spatial displacement discrimination thresholds as a function of the level of resolution (inner scale) of the stimuli, we adopted a smooth (Gaussian) spatial stimulus contrast profile and a smooth (Gaussian) temporal stimulus contrast profile, in combination with detection threshold luminance contrast (as foveally determined for a single blob) in an attempt to stimulate only a

small number (narrow range) of frequency selective mechanisms. An extensive motivation for the exact choice of the stimulus profiles was given in a previous paper (Toet et al., 1987).

The continued response of the visual system following the termination (offset) of briefly presented stimuli is known to generate so-called afterimages, even at threshold luminance contrast (Bowen et al., 1974; Bowling et al., 1980). This visual persistence has been shown to increase with decreasing stimulus contrast (Bowling et al., 1979). To avoid the possibility that the presence of afterimages or memory effects would introduce (false) cues in the differential spatial displacement discrimination task the stimulus pattern as a whole (i.e. the entire combination of target- and interfering- stimuli) appeared at random on one of 9 different positions, symmetrical with regard to the centre of the screen (0, ±3/16, ±6/16, ±9/16, ±12/16 times the size of the spread of the blob profile), both in the horizontal and vertical directions. If the stimulus pattern had appeared in the same position in each trial comparison (using either the presence of afterimages or memory effects) of successive displacements of the middle blob relative to the axis through the outer two would have introduced a (false) cue for the localization judgement.

The stimuli were superposed on a 100 cd/m^2 (300 Td for the 2 mm pupil) luminance background level. The luminance level of the background was chosen such as to operate in the photopic domain.

Procedure.

After adaptation of the subject to the background luminance level the contrast detection threshold for a single Gaussian blob was determined by means of a staircase method. Threshold was defined as the contrast level for which 80% of the stimulus presentations are detected. Thresholds were determined at the start of each session and between separate runs. The differential spatial displacement discrimination tasks were performed at detection threshold luminance contrast as (foveally) determined for a single blob.

For all three-blob alignment acuity tasks no use was made of a fixation mark because it would have presented a cue for the task to be performed. Therefore, the subjects were instructed to fixate on the centre of the monitor screen.

At the onset of each stimulus presentation a buzzer signal sounded. After completion of the presentation the subject had to choose (forced choice) between a left or right displacement of the middle blob relative to the axis defined by the outer two blobs. Immediately after the subject had responded to a trial a new presentation was started. By withholding his answer for a while the subject was able to take a short rest. If one or more of the target blobs were not detected (and in that case only) the subject could skip his obligation to answer and go on to the next presentation. In this case the missed presentation was randomly incorporated into the sequence of remaining trials. This situation occurred in about half of the number of presentations.

Adaptive probit estimation (APE: see Watt and Andrews, 1981) was used to determine the differential spatial displacement discrimination thresholds. APE is a modified method of constant stimuli. It allows bias-free threshold determination with high precision for a relatively small number of trials. Threshold is defined as the standard deviation of the cumulative normal psychometric function (corresponding to half the difference between the 17% and 83% points) and was estimated by Probit analysis (Finney, 1971). Each individual estimate is the standard deviation of the response error distribution from a run of 80 trials preceded by 20 practice trials. Thresholds quoted are the r.m.s. of at least 3 individual estimates. Standard errors for this procedure are typically of the order of 10% of the standard deviation.

The order in which the thresholds were determined was not systematic.

RESULTS AND DISCUSSION.

The differential spatial displacement discrimination thresholds determined both with and without interfering stimuli are shown in Fig. 2 as a function of the inner scale parameter (spread) of the stimulus

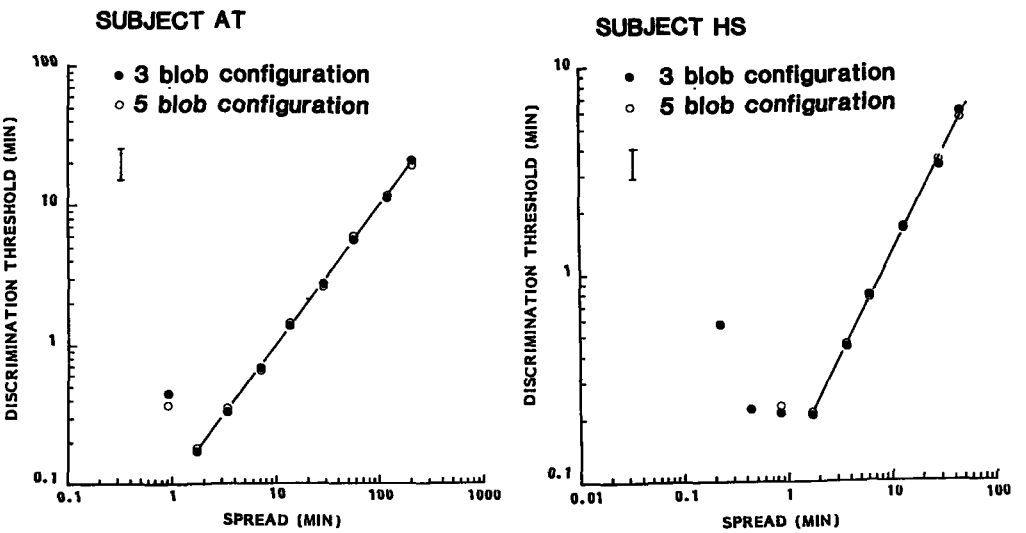

Figure 2. Differential spatial displacement discrimination thresholds for the three-blob alignment task as a function of the stimulus scale represented by the spread of the Gaussian blobs. The filled dots represent the results from experiments without interfering stimuli. For blobspreads smaller than 2 min of arc the open dots represent the mean of thresholds determined with interfering stimuli at R=12, 16, 20, 24, 28 and 32 times the corresponding blobspread. For blobspreads larger than 2 min of arc the open dots represent the mean of thresholds determined with interfering stimuli at R=8, 12, 16, 20, 24, 28 and 32 times the corresponding blobspread. All stimuli were temporally modulated with a Gaussian envelope with a spread of 0.2 sec. The solid line indicates the result from a least square fit of an exponential curve to the data points. The error bar represents two standard errors for thresholds determined without interfering stimuli and four standard errors for thresholds determined with interfering stimuli.

pattern. We found that the presence of interfering stimuli had no noticeable influence on the discrimination threshold values. Except for blobspreads smaller than 2 min of arc, the data in Fig. 2 that represent the discrimination thrèsholds in conditions with interfering stimuli were obtained by taking the mean value of thresholds determined for respectively R=8, 12, 16, 20, 24, 28 and 32 times the corresponding inner scale parameter. When the inner scale parameter (i.e. the angular dimensions of the spread of the blobs) became smaller than approximately 1.5 min of arc the presence of interfering stimuli within a radius of 10 times the inner scale parameter severly impaired the three-dot alignment task. Although all stimuli remained resolved for these values of the spatial parameters the task became hard to perform because of the confusing nature of the stimulus pattern as a whole. Subjects reported that for these parameter values it was no longer obvious which blobs constituted the target stimulus and which blobs merely represented the interfering stimuli. The data in Fig. 2 that represent the differential spatial displacement discrimination thresholds in conditions with interfering stimuli and for blobspreads smaller than 2 min of arc were obtained by taking the mean value of thresholds determined for respectively R=12, 16, 20, 24, 28 and 32 times the corresponding inner scale parameter (thus omitting the condition in which R=8 times the inner scale parameter). For spreads smaller than 1 min of arc thresholds rise, probably due to the fact that subjects can no longer resolve the stimulus pattern.

Experiments using selective adaptation to spatial frequency gratings have demonstrated that thresholds for spatial frequency discrimination are most elevated at a frequency some distance removed from the adaptation frequency (Regan and Beverly, 1983). We repeated the determination of the three-blob alignment discrimination thresholds in the presence of sharp edged circular discs as interfering stimuli. These interfering stimuli introduce a large range of spatial frequency components which might interfere with the mechanisms mediating the differential spatial displacement discrimination task studied. The radius value of the discs was always equal to the value of the spread of the Gaussian blobs that constitute the target stimulus. Moreover, we adopted a contrast value of

30% for the discs which was far above their contrast detection threshold (which depended on their angular dimensions and was never more than 7%). Still, we found that the presence of these interfering stimuli had no noticeable influence on the three-blob alignment discrimination thresholds when they were located at more than 8 times the inner scale parameter from the centre of the target stimulus.

In a previous experiment (Toet et al., 1987) we found that there are two outer scale regimes at all levels of resolution in which different strategies are used to compute differential spatial displacements. Independent of the level of resolution (inner scale parameter of the stimulus configuration) transition between those regions occurs when the outer scale parameter is a constant multiple (approximately 25) of the inner scale parameter. It was argued that the different processing regimes might reflect the existence of spatial regions or processing modules (extending up to 25 times the inner scale parameter) in which differential spatial displacement computations are performed directly. We designed the present experiment to test whether it is possible to manifest the existence of these hypothetical processing modules by means of a differential spatial displacement discrimination task in combination with interfering stimuli. However, as we found that the presence of interfering stimuli had no influence on the performance in the three-blob alignment task we cannot draw any further conclusions about the possible existence of processing modules mediating differential spatial displacement discrimination.

The drawn lines in Fig. 2 represent the result of a least-square fit of exponential curves to our data points. Only data points for spreads larger than 1.5 min of arc were used in the calculation of the regression lines. The least-square curves thus obtained closely fit the data points. The correlation coefficients (r^2) range in value from 0.99 to 1.00. The powers obtained for the exponential curves range between 0.98 and 1.00. Thus, the differential spatial displacement discrimination thresholds for the three-blob alignment task are a constant fraction of the stimulus size over a range of at least two decades. In a previous paper (Toet et al., 1987) we interpreted these results as evidence for the fact that the human visual system uses a single strategy to compute differential spatial

displacements at all levels of resolution.

Our results are in agreement with those of other researchers who found that differential spatial displacement discrimination accuracy was not degraded by the presence of interfering stimuli (Badcock and Westheimer, 1985a,b; Fendick, 1984; Morgan and Ward, 1985). We conclude that the mechanisms that compute differential spatial displacements in case of the three-blob alignment task are not disturbed by the presence of interfering stimuli even when these enter the region over which the computations are performed and independent of the level of resolution on which the features of the interfering stimuli are represented.

Acknowledgements - We thank Henk Simons and Mike van Eekhout for providing us with the necessary software. We are indebted to Dr. R.J. Watt and Dr. P.A. Andrews for sending us their APE software. This work was supported by the Dutch Foundation for the Advancement of Pure Research.

REFERENCES.

Andrews D.P., Butcher A.K. and Buckley B.R. (1973) Acuities for spatial arrangement in line figures: human and ideal observers compared. Vision Res. 13, 599-620.

Andrews D.P. and Miller D.T. (1978) Acuity for spatial separation as a function of stimulus size. Vision Res. 18, 615-619.

Andriessen J.J. and Bouman H. (1979) Eccentric vision: adverse interaction between line segments. Vision Res. 16, 71-78.

Badcock D.R. and Westheimer G. (1985a) Spatial location and hyperacuity: centre/surround localization contribution function has two substrates. Vision Res. 25, 1259-1267.

Badcock D.R. and Westheimer G. (1985b) Spatial location and hyperacuity: flank position within the centre and surround zones. Spatial Vision 1, 3-11.

Beck J. and Schwartz T. (1979) Vernier acuity with dot test objects. Vision Res. 19, 313-319.

Bouman H. (1970) Interaction effects in parafoveal letter recognition. Nature 226, 177-178.

Bowen R.W., Pola J. and Matin L. (1974) Visual persistence: effects of flash luminance, duration and energy. Vision Res. 14, 295-303.

Bowling A., Lovegrove W. and Mapperson B. (1979) The effect of spatial frequency and contrast on visual persistence. Perception 8, 529-539.

Bowling A. and Lovegrove W. (1980) The effect of stimulus duration on the persistence of gratings. Percept. & Psychophys. 27, 574-578.

Breitmeyer B.G. (1978) Disinhibition in metacontrast masking of Vernier acuity targets: sustained channels inhibit transient channels. Vision Res. 18, 1401-1405.

Butler T. and Westheimer G. (1978) Interference with stereoscopic acuity: spatial, temporal and disparity tuning. Vision Res. 18, 1387-1392.

Essock E.A., Williams R.A. and Enoch, J.M. (1983) Areas of spatial interactions about a hyperacuity target. Invest. Ophthal. Vis. Sci. suppl. 23, p. 92.

Fendick M.G. (1983) Parameters of the retinal light distribution of a bright line which correspond to its attributed spatial location. Invest. Ophthal. Vis. Sci. suppl. 23, p. 92 (A).

Fendick M.G. (1984) Dissociation of Vernier "acuity" and Vernier "accuracy". Invest. Ophthal. Vis. Sci. suppl. 25, p. 144 (A).

Finney D.J. (1971) Probit analysis, 3rd edn. Cambridge Univ. Press.

Flom M.C., Heath G.G. and Takahashi E. (1963a) Contour interaction and visual resolution: Contralateral effects. Science 142, 979-980.

Flom M.G., Weymouth F.W. and Kahnemann D. (1963b) Visual resolution and contour interaction. J. Opt. Soc. Am. 53, 1026-1032.

Foley J.M. (1976) Successive stereo and Vernier position discrimination as a function of dark interval duration. Vision Res. 16, 1269-1273.

Gelb D.J. and Wilson H.R. (1983) Shifts in perceived size as a function of contrast and temporal modulation. Vision Res. 23, 71-82.

Hess R.F. and Jacobs R.J. (1979) A preliminary report of acuity and contour interactions across the amblyope's visual field. Vision Res. 19, 1403-1408.

Jacobs R.J. (1979) Visual resolution and contour interaction in the fovea and periphery. Vision Res. 19, 1187-1195.

Klein S.A. and Levi D.M. (1985) Hyperacuity thresholds of 1 sec: theoretical predictions and empirical validation. J. Opt. Soc. Am. A2, 1170-1190.

Köhler W. and Wallach H. (1944) Figural after-effects: an investigation of visual processes. Proc. Am. Phil. Soc. 88, 269-357.

Levi D.M. and Klein S.A. (1983) Spatial localization in normal and amblyopic vision. Vision Res. 23, 1005-1017.

Levi D.M. and Klein S.A. (1985) Vernier acuity and amblyopia. Vision Res. 25, 979-991.

Levi D.M., Klein S.A. and Aitsebaomo A.P. (1985) Vernier acuity, crowding and cortical magnification. Vision Res. 25, 963-977.

Ludvigh E. (1953) Direction sense of the eye. Am. J. Ophthal. 36, 139-142.

Ludvigh E. and McKinnon P. (1967) The effect of orientation on the three dot alignment test. Am. J. Ophthal. 64, 261-265.

Morgan M.J. and Ward R.M. (1985) Spatial and spatial-frequency primitives in spatial-interval discrimination. J. Opt. Soc. Am. A2, 1205-1210.

Regan D. and Beverly K.I. (1983) Spatial-frequency discrimination and detection comparison of postadaptation thresholds. J. Opt. Soc. Am. 73, 1684-1690.

Steinman S.B., Levi D.M., Manny R.E. and Klein S.A. (1984) Spatial interference with cortical potentials evoked by Vernier offsets. Invest. Ophthal. Vis. Sci. suppl. 25, p. 144 (A).

Steinman S.B., Levi D.M., Klein S.A. and Manny R.E. (1985) Selectivity of the evoked potential for Vernier offset. Vision Res. 25, 951-961.

Toet, A., Eekhout M.P., Simons H.L.J.J. and Koenderink J.J. (in press) Scale invariant features of differential spatial displacement discrimination. Vision Res.

Volkmann A.W. (1863) Physiologische Untersuchungen im Gebiete der Optik. Breitkopf & Hartel, Leipzig.

Watt R.J. (1984) Towards a general theory of the visual acuities for shape and spatial arrangement. Vision Res. 24, 1377-1386.

Watt R.J. and Andrews D.P. (1981) APE: Adaptive probit estimation of psychometric function. Curr. Psychol.Rev. 1, 205-214.

Watt R.J. and Morgan M.J. (1983) Mechanisms responsible for the assesment of visual location: theory and evidence. Vision Res. 23, 97-109.

Watt R.J., Morgan M.J. and Ward R.M. (1983) Stimulus features that determine the visual location of a bright bar. Invest. Opthal. Vis. Sci. 24, 66-71.

Westheimer G. (1981) Visual hyperacuity. In: Progress in sensory physiology I: 1-30. Eds. Autrum, H., Ottoson, D., Perl, E.R. and Schmidt, R.F. Springer Verlag, New York.

Westheimer G. and Hauske G. (1975) Temporal and spatial interference with Vernier acuity. Vision Res. 15, 1137-1141.

Westheimer G. and McKee S.P. (1977a) Integration regions for visual hyperacuity. Vision Res. 17, 89-93.

Westheimer G. and McKee S.P. (1977b) Spatial configurations for visual hyperacuity. Vision Res. 17, 941-947.

Westheimer G., Shimamura K. and McKee S.P. (1976) Interference with line-orientation sensitivity. J. Opt. Soc. Am. 66, 332-338.

Williams R.A., and Essock E.A. (1986) Areas of spatial interaction for a hyperacuity stimulus. Vision Res. 26, 349-360.

Wülfing E.A. (1892) Über den kleinsten Gesichtswinkel. Z. Biol. 29, 199-202.

CHAPTER II.5.

Differential spatial displacement discrimination thresholds for stimuli with mixed increment/decrement features.

ABSTRACT.

Similar to the three-dot alignment hyperacuity task, differential spatial displacement discrimination thresholds were determined for a configuration of three blobs at threshold luminance contrast. The blobs had either Gaussian- or DOG-like spatial contrast profiles and were modulated with a Gaussian temporal envelope. The differential spatial displacement discrimination thresholds determined for homogeneous configurations of either incremental or decremental blobs were identical to the thresholds determined for different heterogeneous configurations of mixed incremental/decremental blobs. The thresholds are a constant fraction of the stimulus size over a range of almost two decades. We conclude that (i) the mechanisms that compute differential spatial displacement show no increment/decrement dichotomy and (ii) at all levels of resolution similar mechanisms are used to compute differential spatial displacement.

INTRODUCTION.

In 1874 Hering[1] (Chap. 2) postulated separate mechanisms for the sensations of "brightness" and "darkness". Helmholtz[2] (Section 19) argued that the visual sensations of white and black (or light and dark) were qualitatively distinct.

At the retinal level bipolar and ganglion cells posses circularly symmetric receptive fields as do the cells of the lateral geniculate bodies[3-5]. The so-called on-centre cells respond when a spot lighter than the background covers the circular receptive field centre, but this response is suppressed when the surrounding annular area of the receptive

field is stimulated with an incremental stimulus. The off-centre cells respond with an excitatory response when their surround area is stimulated with an incremental stimulus, or, equivalently, when a spot darker than the background is projected onto their centre. Jung[6-8] has proposed the existence of two visual systems: a B-system which responds to luminance increments and signals "brighter", and a D-channel which is sensitive to luminance decrements and signals "darker". The B-system is thought to reflect the activity of on-center off-surround receptive fields and the D-system the activity of off-center on-surround receptive fields.

Neurophysiological research has demonstrated the existence of a differential stratification of the on- and off-centre cells, both for brisk transient Y-cells[9] and for brisk sustained X-cells[10]. This strengthens the argument that the corresponding detector units form two spatially independent channels. The separation into a brightness (on) and darkness (off) system is preserved through the lateral geniculate nucleus[11] and maintained as two separate channels on into the visual cortex[12]. Their exact cortical termination is unknown. The duality of the channels can still be recognized in the simple cells of lamina IV of the visual cortex because such cells have corresponding discharge centres.

The nature of the visual mechanisms that signal the sign of a luminance change is still not very clear. Psychophysics has dealt mostly with incremental stimuli. Less work has been done on the response of the visual system to decremental stimuli. The experiments that have been performed to test the increment-decrement dichotomy yield evidence that is hardly conclusive and mostly even of conflicting nature.

(1) There is evidence that luminance decrements are slightly more detectable than luminance increments[13-19]. Blackwell[20] found a difference only for large stimuli and low adaptation brightnesses: in this case the thresholds for decremental stimuli were lower than those for incremental stimuli. Other authors[21-25] report that they found no significant differences between decremental and incremental detection thresholds[23]

(2) Novak[26] determined increment and decrement contrast detection thresholds near a light-dark boundary. For one subject there was no difference in the thresholds whereas the other subject showed different thresholds. However, Remole[27] demonstrated consistent asymmetries in the

brightness versus darkness enhancement at contrast borders.

(3) Grating detection threshold elevation due to adaptation to high contrast gratings has been shown to be selective for the widths of the light bars but not for the widths of the dark bars[28]. However, Georgeson and Reddin[29] found separate but equally strong selectivity for light- and dark-bar widths in a similar experiment.

(4) The results from experiments studying the influence of selective adaptation on perceived spatial frequency[30-32] and the effect of adaptation to white or black bars on the perceived widths of white and black test bars[32] seemed to confirm the assumption that black and white grating components are processed independently. However, using combined adaptation to rectangular wave gratings of a certain frequency alternating with sine wave gratings of twice this frequency, Cavanagh et al.[33] demonstrated that black and white grating components are not processed independently. They propose mechanisms that are sensitive to the relative phase relations among the spatial frequency components of the input.

(5) Walraven[34] studied the perceived colour contrast as a function of increment and decrement stimulus contrast. His results suggested that chromatic colour vision is subserved only by incremental discontinuities in the intensity profile of the light stimulus; decremental input seems to feed only into the achromatic system, generating a "blackness" signal.

(6) Studies comparing the influence of flash duration[35] and flicker rate[36-38] on the apparent stimulus contrast have demonstrated an asymmetry in the processing of incremental and decremental stimuli. However, Glad and Magnussen[39] found that brightness and darkness enhancement during intermittent stimulation were symmetrical. Cohn and Lasley[40] showed that the discrimination of pulsed increments from decrements improves relative to the frequency of their detection when the adaptation level is decreased or the stimulus duration is increased. This result suggests the existence of two independent channels operating at low adaptation levels and long stimulus durations and preserving the sign of the stimulus contrast, versus a mechanism operating at high adaptation levels and short stimulus durations that obscures the sign of the stimulus contrast.

(7) Vicars and Lit[41] found that reaction times for suprathreshold flashes of small target spots were independent of stimulus contrast for

dark spots but depended on stimulus contrast for light spots.

(8) Krauskopf[16] showed that adaptation to a temporal luminance sawtooth differentially elevated thresholds for luminance increments and decrements.

The accuracy with which the human visual system can determine changes in the relative spatial position of features in the visual field is extremely high[42-44]. This precision, coined "hyperacuity" by Westheimer[45], is possible for a variety of spatial localization tasks[44] and remains unaffected by movement of the stimuli across the retina over several min of arc[46,47]. Thresholds for the accuracy obtained in these tasks are typically a few sec of arc, which is an order of magnitude below the size of the foveal photoreceptors.

The results of spatial frequency discrimination experiments have led to the view that spatial frequency discrimination may be determined by the relative- or differential-simultaneous activities of either multiple overlapping psychophysical channels tuned to different spatial frequencies or, equivalently, size-tuned neural elements[48-52]. Koenderink[53,54] has recently argued how relative place tags may be assigned to a collection of nervous elements by the (physiologically imposed) constraints on the simultaneous/successive order of their total signal activity. In these views the relative spatial position of stimulus features is encoded in the correlation between the signal activities of the neural elements. If the mechanisms that signal increment/decrement luminance changes really form two separate systems one would expect the differential spatial position discrimination accuracy to be higher for tasks that require comparison of the relative spatial position of stimulus features that are represented within the same system than for tasks that involve the comparison of the spatial position of features represented in different systems.

Some researchers have investigated the influence of wavelength of illumination[55-59] or contrast reversal[60,61] on differential spatial displacement discrimination thresholds. However, as far as we know no previous experiments have been performed to test differential spatial displacement discrimination with stimuli that have features that are simultaneously represented in different psychophysical channels.

We designed an experiment to test whether it is possible to manifest an increment/decrement dichotomy by means of a differential spatial displacement discrimination task. The stimuli we used in this experiment consisted of three blobs with either Gaussian or DOG-like spatial contrast profiles and a Gaussian temporal envelope. Because they are bandlimited in the frequency domain these stimuli are likely to activate only a small range of spatial frequency selective mechanisms (i.e. only receptive fields with spatial dimensions of the order of those of the retinal projection of the blobs will make a significant contribution to their detection) thereby providing us with a precise control over the resolution of the stimuli. We determined differential spatial displacement discrimination thresholds for different configurations of incremental and decremental blobs as a function of the resolution parameter of the blobs. The relative localization task we used is equivalent to the three-dot alignment hyperacuity task which is well documented in the literature[62-67].

METHODS.

Subjects.

Four male subjects, aged between 22 and 30, served in the experiment. Subject A.T. has corrected myopic vision. The other subjects are all emmetropic and have 20/15 Snellen acuity. Subjects A.T., M.E., and H.S. were highly practised. Subject H.W. underwent several training sessions before performing the measurements reported below.

Apparatus.

A PDP 11/34 minicomputer in combination with a Gould deAnza IP8500 image array processor was used to generate, process and present the stimuli, record the responses and analyze the data.

The stimulus was displayed on a Philips LDH2123 monochrome monitor. The CRT was driven in an interlaced mode with a frame rate of 60 Hz. The

display consisted of 512 × 512 pixels with the luminance value of each pixel quantized to 8 bits. A 512 × 512 correction matrix was added to the deAnza frame buffer to compensate for the inhomogeneity of the display.

Viewing conditions.

The display was placed in a dark room with nonreflecting black walls. Observers were seated with their heads supported by a chin rest, adjusted in height and position so that their dominant eye was on the line perpendicular to the center of the monitor screen. The use of a forehead rest prevented tilting of the head. Viewing was monocular with the subject's dominant eye. The unused eye was covered with an eye cap. Viewing distance varied from 10 cm to 10 m. Except for viewing distances below 1 m viewing was through a 2 mm artificial pupil. Below 1 m the natural pupil was used in order to avoid vignetting effects. At these distances variations of accommodation had no influence on our results as the spread of the optical blur function of the eye is more than two orders of magnitude smaller than the spread of the spatial contrast profile of the stimuli that were presented.

The stimuli were superposed on a 100 cd/m^2 (300 Td for the 2 mm pupil) luminance background level. The luminance level of the background was chosen such as to operate in the photopic domain.

Stimuli.

The stimuli comprised different spatial arrangements of three blobs. The spatial contrast profiles of the blobs was given by either a Gaussian function or by the second derivative (Laplacian) of a Gaussian function. In the sequel we will refer to these profiles as respectively G- and G"-blobs. All blobs were temporally modulated with the same Gaussian envelope. The luminance distribution for the G-blobs is given by

$$L(x,y,t) = L_b[1+cw(x,y,t)]$$

where L_b denotes the background luminance and c is the threshold contrast value as determined for a single blob. The window function w(x,y,t) is

given by

$$w(x,y,t) = \pm\exp[-(x^2+y^2)/(2s_s^2)-(t^2/2s_t^2)]$$

A positive sign of the window function corresponds to an incremental blob; a negative sign to a decremental blob. The luminance distribution for the G"-blobs is given by

$$L(x,y,t) = L_b[1+cw"(x,y,t)]$$

where L_b and c represent the same parameters as above. The window function w"(x,y,t) is given by

$$w"(x,y,t) = \pm\{1-(x^2+y^2)/(2s_s{}^2)\}*\exp[-(x^2+y^2)/(2s_s^2)-(t^2/2s_t^2)]$$

A positive sign corresponds with a G"-blob with an increment-centre, a negative sign implies a decrement-centre.

We adopt the term spread for the distance over which a Gaussian falls from 1 to $e^{-\frac{1}{2}}$, corresponding to the standard deviation measure as defined in statistics. The spatial profiles of both G- and G"-blobs are completely characterized by their spreads. (For G-blobs a spatial region with radius $2s_s$ and centered on (x,y) = (0,0) contains 92% of the total energy; a temporal interval of width $2s_t$ centered on t = 0 contains 96% of the total stimulus energy. G"-blobs have a zero-valued spatial, and therefore temporal, integral). The window function is the product of spatial- and temporal-profiles with spreads of s_s and s_t respectively. Both the temporal and the spatial windows were truncated at plus and minus four times their spread (containing respectively 99.994% and 99.990% of the total stimulus energy in a G-blob). The threshold contrast c is defined as $(L-L_b)/L_b$, where L denotes the threshold luminance level.

The spread of the Gaussian temporal envelope was 0.2 sec (therefore the stimulus was above one half of its peak value for 0.47 sec). The frame rate was 60 Hz and interlaced. Intermediate presentations lasted for 0.05 sec, corresponding to 3 frames. This was found short enough to present a perceptually smooth temporal contrast profile. The total duration of the

stimulus presentation was eight times the spread of its Gaussian temporal contrast profile (i.e. if T is the moment at which the stimulus attained its maximum contrast and s_t represents the spread of the Gaussian temporal contrast profile, the presentation lasted from $T-4s_t$ to $T+4s_t$).

If we define the bandwidth of a Gaussian signal as the distance between the (negative and positive) frequency components for which the amplitude has dropped to one half of the value of the frequency component with maximum amplitude (zero frequency for a Gaussian signal), we find that the temporal bandwidth is given by $(2*\ln 2)^{\frac{1}{2}}/(\pi*s_t)$. In our case the temporal frequency bandwidth is 1.87 Hz. For G-blobs the spatial frequency bandwidth is between 0.10 cy/deg and 8.37 cy/deg. For G"-blobs the position of the centre-frequencies range between 0.22 and 22.34 cy/deg and their bandwidths (defined as the distance between the power-spectrum components at half-height) are approximately 1.75 octaves.

Because we were interested in the differential spatial displacement discrimination thresholds as a function of the level of resolution (inner scale) of the stimuli we adopted a smooth (Gaussian and Laplacian of Gaussian) spatial stimulus contrast profile and a smooth (Gaussian) temporal stimulus contrast profile in combination with detection threshold luminance contrast (as foveally determined for a single blob) in an attempt to stimulate only a small number (narrow range) of frequency selective mechanisms.

The continued response of the visual system following the termination (offset) of briefly presented stimuli is known to generate so-called after-images, even at threshold luminance contrast[68,69]. This visual persistence has been shown to increase with decreasing stimulus contrast[70]. To avoid the possibility that the presence of after-images or memory effects would introduce (false) cues in the differential spatial displacement discrimination task the stimulus pattern as a whole appeared at random on one of 9 different positions, symmetrical with regard to the centre of the screen (0, ±3/16, ±6/16, ±9/16, ±12/16 times the size of the spread of the blob profile) both in the horizontal and vertical directions. If the stimulus pattern had appeared in the same position in each trial comparison (using either the presence of after-images or memory effects) of successive displacements of the middle blob relative to the

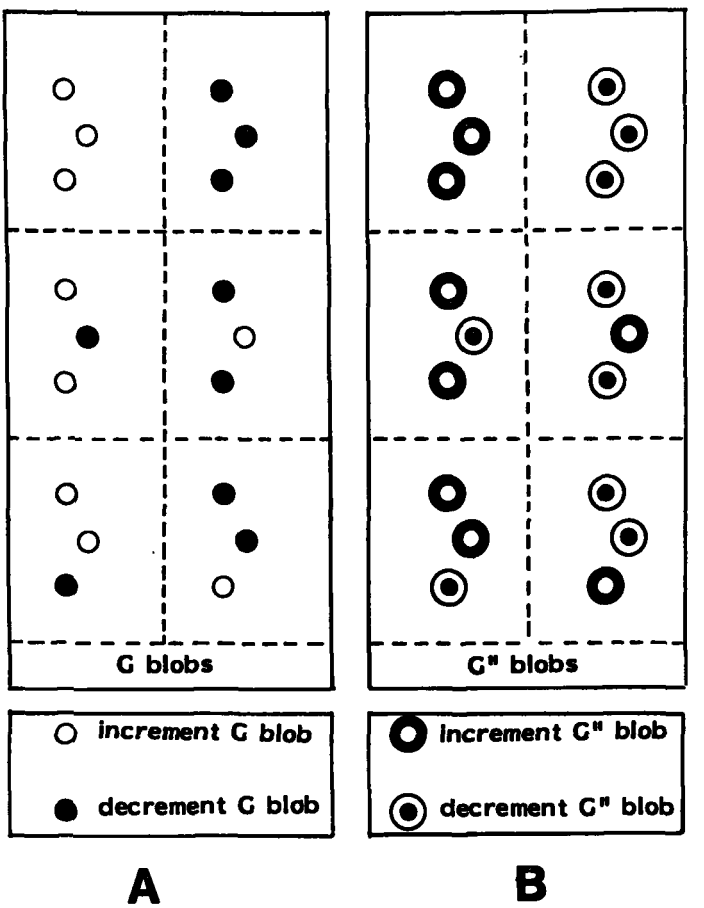

Figure 1. Symbolic representation of all spatial configurations of G- (Fig. 1a) and G"- (Fig. 1b) blobs that were used in the differential spatial displacement discrimination experiments. A spot with a light centre represents an incremental blob; a spot with a dark centre implies a decremental blob.

axis through the outer two would have introduced a (false) cue for the localization judgement.

Fig. 1 represents all spatial configurations of incremental and decremental G- (Fig.1a) and G"- (Fig. 1b) blobs that were used in the experiment. The distance between the centres of the outer two blobs was 14 times the spread of their spatial contrast profile. At this separation the blobs appeared clearly resolved. The middle blob appeared on the line through the middle of and orthoaxial to the line segment joining the centres of the outer two blobs. In the sequel we will refer to stimulus configurations containing only identical blobs as **homogeneous stimuli.** Stimulus configurations containing blobs of opposite contrast polarity will be called **heterogeneous stimuli.**

The angular dimensions of the blobs were varied by varying the viewing distance. Therefore, the ratio between the total extent of the background and the spread of the blobs was kept constant; i.e. at all viewing distances the stimuli were geometrically similar. For blobs with a spread smaller than 27 min of arc viewing was through a 2 mm artificial pupil. For blobs with a spread larger than 27 min of arc the natural pupil was used in order to avoid vignetting effects.

Procedure.

After adaptation of the subject to the background luminance level the contrast detection threshold for a single G- or G"-blob was foveally determined by means of a staircase method. Threshold was defined as the contrast level for which 80% of the stimulus presentations are detected. Thresholds were determined at the start of each session and between separate runs. The differential spatial displacement discrimination tasks were performed at detection threshold luminance contrast as (foveally) determined for a single blob.

For all three-blob alignment acuity tasks no use was made of a fixation mark because it would have presented a cue for the task to be performed. Therefore, the subjects were instructed to fixate on the centre of the monitor screen.

At the onset of each stimulus presentation a buzzer signal sounded.

After completion of the presentation the subject had to choose (forced choice) between a left or right displacement of the middle blob relative to the axis defined by the outer two blobs. Immediately after the subject responded to a trial a new presentation was started. By withholding his answer for a while the subject was able to take a short rest. In case no decision could be made because one or more blobs were not detected (and in that case only) the subject could skip his obligation to answer and go on to the next presentation. In this case the missed presentation was randomly incorporated into the sequence of remaining trials. This situation occurred in about 80% of the presentations.

Adaptive probit estimation (APE[71]) was used to determine the differential spatial displacement discrimination thresholds. APE is a modified method of constant stimuli. It allows bias-free threshold determination with high precision for a relatively small number of trials. Threshold is defined as the standard deviation of the cumulative normal psychometric function (corresponding to half the difference between the 17% and 83% points) and was estimated by Probit analysis[72]. Each individual estimate is the standard deviation of the response error distribution from a run of 80 trials preceded by 20 practice trials. Thresholds quoted are the r.m.s. of at least 3 individual estimates. Standard errors for this procedure are typically of the order of 10% of the standard deviation.

The order in which the thresholds were determined was not systematic.

RESULTS.

Contrast detection thresholds were determined at the start of each run of the alignment task. We found that the detection thresholds remained constant during the sessions and were reproduced in separate sessions. Thresholds for blobs with decremental centres were systematically slightly lower than thresholds for blobs with incremental centers. The detection thresholds were approximately 8%; the difference between the thresholds for incremental and decremental blobs was approximately 1% (the standard errors being typically less than 0.1%).

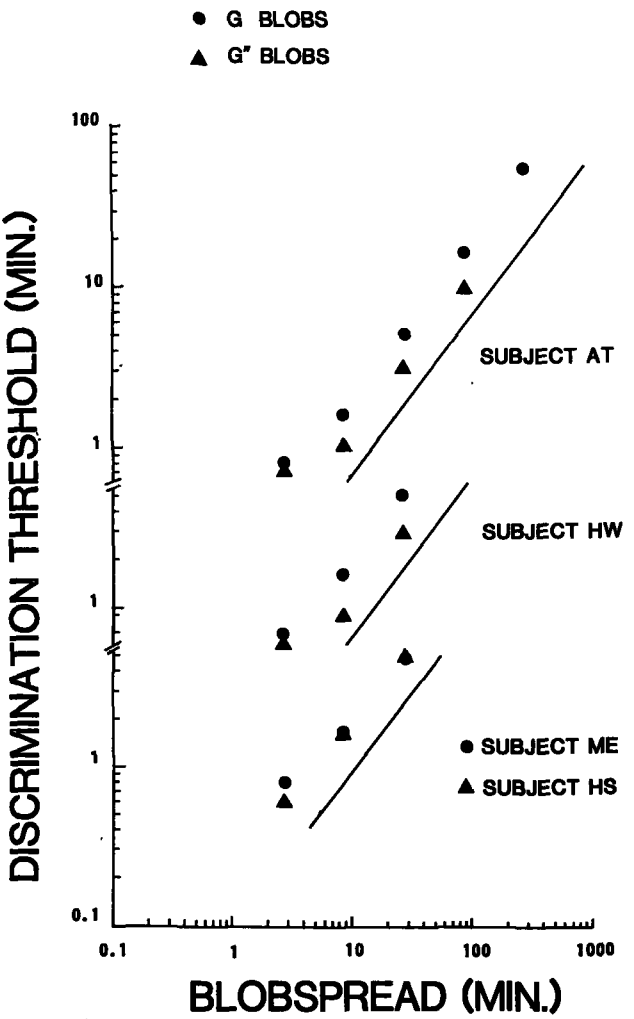

Figure 2. The mean values of the differential spatial displacement discrimination thresholds determined for all different (homogeneous and heterogeneous) stimulus configurations of Fig. 1 as a function of the angular dimensions of the blobs. The solid line represents the Weber fraction. The standard error is less than symbol height.

Table I shows the results of the performance of four subjects in the three-blob differential spatial displacement discrimination task for different configurations of incremental and decremental (G- and G"-) blobs and as a function of the angular dimensions of the blobs. Two subjects (AT and HW) performed all tests with both G- and G"-blobs. The other two subjects (ME and HS) were tested with different configurations of either G- (ME) or G"- (HS) blobs. The standard errors in the quoted threshold values are typically less than 10%. For a constant value of the spread of either G- or G"-blobs we found no significant systematical difference between the differential spatial displacement discrimination thresholds determined for homogeneous and heterogeneous configurations. Even the standard errors within the individual estimates were of the same magnitude in both cases. As the results of subjects AT and HW show, the differential spatial displacement discrimination thresholds for a configuration of G"-blobs of a certain spread are always lower than those of a similar configuration of G-blobs of the same spread and determined for one and the same subject.

The mean values of the differential spatial displacement discrimination thresholds determined for all different (homogeneous and heterogeneous) stimulus configurations are shown in Fig.2 as a function of the angular dimensions of the blobs. For blobspreads larger than 3 min of arc the differential spatial displacement discrimination thresholds are a fixed fraction of the spread of the blobs (akin to Weber's law). For blobspreads smaller than 3 min of arc the thresholds are larger than this fraction. This is probably a result of the fact that the width of the pointspread function of the eye is no longer negligible compared to these values of the spread of the blob-profiles. In this case the just noticeable differential spatial displacement is limited by the (optical and neural) blur function of the eye.

Table I. DIFFERENTIAL SPATIAL DISPLACEMENT DISCRIMINATION THRESHOLDS FOR DIFFERENT CONFIGURATIONS OF INCREMENTAL AND DECREMENTAL G- AND G"- BLOBS. The different stimulus configurations are symbolically denoted by plus (+) and minus (-) signs. The plus sign stands for an incremental (G- or G"-) blob, and the minus sign for a decremental (G- or G"-) blob. The left most sign corresponds to the other blob, and the rightmost sign to the lower blob in the actual stimulus configuration. Standard errors are typically less than 10% of the quoted threshold values.

BLOB SPREAD (min of arc)	CONFIGU-RATIONS	DISCRIMINATION THRESHOLDS (MIN OF ARC)					
		SUBJECT AT		SUBJECT HW		SUBJECT ME	SUBJECT HS
		G-blobs	G"-blobs	G-blobs	G"-blobs	G-blobs	G"-blobs
2.69	+ + +	0,8	0,7	0,7	0,5	0,8	0,6
	- - -	0,8	0,7	0,7	0,7	0,8	0,7
	+ - +	0,9	0,8	0,7	0,6	0,8	0,6
	- + -	0,8	0,8	0,7	0,6	0,8	0,7
	+ + -	0,8	0,7	0,7	0,6	0,8	0,6
	- - +	0,8	0,7	0,7	0,7	0,8	0,6
8,50	+ + +	1,6	1,0	1,6	0,9	1,5	1,6
	- - -	1,6	0,9	1,5	0,9	1,6	1,5
	+ - +	1,6	1,0	1,6	1,0	1,6	1,6
	- + -	1,7	1,0	1,6	0,9	1,5	1,5
	+ + -	1,6	0,9	1,6	0,9	1,5	1,5
	- - +	1,6	1,0	1,6	1,1	1,7	1,6
26,86	+ + +	5,0	3,0	5,0	2,7	4,8	4,6
	- - -	5,0	2,9	4,7	2,7	4,4	4,9
	+ - +	4,8	3,0	5,0	2,9	4,7	4,5
	- + -	5,2	3,0	5,0	2,9	5,0	4,3
	+ + -	5,1	2,8	5,0	2,9	5,0	4,9
	- - +	4,9	3,0	5,0	3,2	5,4	5,1
84,97	+ + +	15,9	9,3				
	- - -	17,5	8,9				
	+ - +	14,9	10,1				
	- + -	16,4	10,4				
	+ + -	16,1	9,7				
	- - +	17,0	8,6				

DISCUSSION.

The slightly lower contrast detection thresholds for the decrement blobs relative to the thresholds for the increment blobs is in agreement with observations of other researchers[13-19].

Due to the fact that relative localization experiment was performed at threshold luminance contrast (contrast level at which 80% of the presentations is seen) in about 60% of the presentations no answer could be obtained. The uncertainty in the spatial position in which the stimulus pattern as a whole appeared probably caused an additional increase of the number of trials in which a part of the stimulus configuration was not detected[74,75].

We found that differential spatial displacement discrimination thresholds obtained with homogeneous stimuli were equal to those obtained with heterogeneous stimuli. As argued before, if separate systems are signalling increment/decrement luminance changes one would expect higher differential spatial displacement discrimination thresholds for tasks involving heterogeneous stimuli than for tasks involving homogeneous stimuli. The absence of a bright/dark dichotomy may be due to the high background luminance used in these experiments[40].

In an earlier paper[73] we demonstrated that the differential spatial displacement discrimination thresholds for the three-blob alignment task are a constant fraction of the stimulus size. Our present results show that this scaling is also found for stimuli with mixed increment/decrement features. We have argued before[73] that this implies that the visual system uses the same strategy to encode relative spatial position, independent of the level of resolution at which the stimulus features are represented. If the visual system uses different strategies to encode relative location at different levels of resolution one would expect to find indications for regions of transition between the ranges in resolution space in which the different mechanisms are active. However, our data[73], as well as those of Hirsch and Hylton[49,76], provide no indication for the existence of different mechanisms to encode relative position. Therefore, it seems that the visual system assigns relative location tags to receptive fields on all levels of resolution. These can then in turn be used to compute the

differential spatial displacement of stimulus features at a certain level of resolution to an accuracy which is a constant fraction of the prevailing receptive field width at that level of resolution. These place tags may be encoded in the constraints imposed on the simultaneous activity in the ganglion cell networks[53,54].

We conclude that the human visual system seems to use one strategy to detect differential spatial displacement independent of the contrast polarity of the stimulus features and independent of the level of resolution at which these stimulus features are present.

Acknowledgements - The help of our software engineers and observers Mike van Eekhout and Henk Simons was invaluable. We thank Huub van de Wouden for acting as a patient observer. We are indebted to Dr. R.J. Watt and Dr. A.P. Andrews for kindly providing us with a listing of their APE program. The work was supported by the Dutch Foundation for the Advancement of Pure Research (Z.W.O.).

REFERENCES.

1. Hering, E. (1874). Zur Lehre vom Lichtsinne. IV. Über die sogenannte Intensität der Lichtempfindung und über die Empfindung des Schwarzen. Sber. Akad. Wiss. Wien, Abt. III, 69, 85-104.
2. Helmholtz, H.L.F. von (1962). Physiological optics. (Edited by Southall, J.P.C. Translated from the 3rd German edn. Dover Publications Inc., New York, 1962).
3. Kaneko, A. (1970) Physiological and morphological identification of horizontal, bipolar and amacrine cells in goldfish retina. J. Physiol. 207, 623-633.
4. Kuffler, S.W. (1953). Discharge patterns and functional organization of mammalian retina. J. Neurophysiol. 16, 37-68.
5. Hubel, D.H. and Wiesel, T.N. (1961). Integrative action in the cat's lateral geniculate body. J. Physiol. 155, 385-398.

6. Jung, R. (1961). Korrelationen von Neuronentätigkeit und Sehen. In: Neurophysiologie und Psychophysik des visuellen Systems. Ed. by R. Jung and H. Kornhuber, 410-435. Berlin-Göttingen, Heidelberg. Springer Verlag.
7. Jung, R. (1972). Neurophysiological and psychophysical correlates in vision research. In: Brain and Human Behaviour. Ed. by Karczmar, A.G. and Eccles, J.C., 209-258. Berlin-Heidelberg-New York. Springer Verlag.
8. Jung, R. (1973). Visual perception and neurophysiology. In: Handbook of sensory physiology, Vol. VII/3A. Ed. by Jung, R., 1-152. Berlin-Heidelberg-New York. Springer Verlag.
9. Peichl, L. and Wässle, H. (1981). Morphological identification of on- and off-centre brisk transient (Y) cells in the cat retina. Proc. R. Soc. Lond. B 212, 139-156.
10. Wässle, H. Boycott, B.B. and Illing, R.B. (1981). Morphology and mosaic of on- and off-beta cells in the cat retina and some functional considerations. Proc. R. Soc. Lond. B 212, 177-195.
11. Cleland, B.G., Dubin, M.W. and Levick, W.R. (1971). Sustained and transient neurones in the cat's retina and lateral geniculate nucleus. J. Physiol. 217, 473-496.
12. Hubel, D.H. and Wiesel, T.N. (1968). Receptive fields and functional architecture of monkey striate cortex. J. Physiol. 195, 215-243.
13. Boynton, R.M., Ikeda, M. and Stiles, W. (1964). Interactions among chromatic mechanisms as inferred from positive and negative increment thresholds. Vision Res. 4, 87-117.
14. Cohn, T.E. and Lasley, D.J. (1975). Spatial summation of foveal increments and decrements. Vision Res. 15, 389-399.
15. Kelly, D.H. and Savoie, R.E. (1978). Theory of flicker and transient responses. III. An essential nonlinearity. J. Opt. Soc. Am. 68, 1481-1490.
16. Krauskopf, J. (1980). Discrimination and detection of changes in luminance. Vision Res. 20, 671-677.
17. Legge, G.E. and Kersten, D. (1983). Light and dark bars; contrast discrimination. Vision Res. 23, 473-483.

18. Patel, A.S. and Jones, R.W. (1968). Increment and decrement visual thresholds. J. Opt. Soc. Am. 58, 696-699.
19. Short, A.D. (1966). Decremental and incremental visual thresholds. J. Physiol. 185, 646-654.
20. Blackwell, H.R. (1946). Contrast thresholds of the human eye. J. Opt. Soc. Am. 36, 624-643.
21. Vos, J.J., Lazet, A. and Bouman, M.A. (1956). Visual contrast thresholds in practical problems. J. Opt. Soc. Am. 46, 1065-1068.
22. Bouman, M.A. and Blokhuis, E.W.M. (1952). The visibility of black objects against an illuminated background. J. Opt. Soc. Am. 42, 525-528.
23. Herrick, R.M. (1956). Foveal luminance discrimination as a function of the duration of the decrement or increment in luminance. J. Comp. Physiol. Psychol. 49, 437-443.
24. Rashbass, C. (1970). The visibility of transient changes of luminance. J. Physiol. 210, 165-186.
25. Roufs, J.A.J. (1974). Dynamic properties of vision. IV. Thresholds of decremental flashes, incremental flashes and doublets in relation to flicker fusion. Vision Res. 14, 831-852.
26. Novak, S. (1969). Comparison of increment and decrement thresholds near a light-dark boundary. J. Opt. Soc. Am. 59, 1383-1384.
27. Remole, A. (1977). Brightness enhancement versus darkness enhancement at a border. Vision Res. 17, 1095-1100.
28. Nagshineh, S. and Ruddock, K.H. (1978). Properties of length selective adaptation mechanisms in human vision. Biol. Cybern. 31, 37-47.
29. Georgeson, M.A. and Reddin, S.K. (1981). Adaptation to gratings: Equal spatial selectivity for light and dark bar width variation. Vision Res. 21, 419-421.
30. Blakemore, C. and Sutton, P. (1969). Size adaptation: A new aftereffect. Science 166, 245-247.
31. Burton, G.J., Nagshineh, S. and Ruddock, K.H. (1977). Processing by the human visual system of the light and dark contrast components of the retinal image. Biol. Cybern. 27, 189-197.
32. DeValois, K.K. (1977). Independence of black and white: Phase-specific adaptation. Vision Res. 17, 209-215.

33. Cavanagh, P. (1981). Evidence against independent processing of black and white pattern features. Perception and Psychophysics 29, 423-428.
34. Walraven, P.L. (1977). Color signals from incremental and decremental light stimuli. Vision Res. 17, 71-76.
35. White, T.W., Irvin, G.E. and Williams, M.C. (1980). Asymmetry in the brightness and darkness Broca-Sulzer effect. Vision Res. 20, 723-726.
36. Magnussen, S. and Glad, A. (1975a). Brightness enhancement during flicker: perceptual correlates of neuronal B- and D-systems in human retina. Expl. Brain Res. 22, 399-413.
37. Magnussen, S. and Glad, A. (1975b). Temporal frequency characteristics of spatial interaction in human vision. Expl. Brain Res. 23, 519-528.
38. Magnussen, S. and Glad, A. (1975c). Effects of steady surround illumination on the brightness and darkness enhancement of flickering lights. Vision Res. 15, 1413-1416.
39. Glad, A. and Magnussen, S. (1972). Darkness enhancement in intermittent light: an experimental demonstration. Vision Res. 12, 111-115.
40. Cohn, T.E. and Lasley, D.J. (1985). Discrimination of luminance increments and decrements. J. Opt. Soc. Am. A2, 404-407.
41. Vicars, W. and Lit, A. (1975). Reaction time to incremental and decremental target changes at various photopic background levels. Vision Res. 15, 261-265.
42. Volkmann, A.W. (1863) Physiologische Untersuchungen im Gebiete der Optik. Breitkopf & Hartel, Leipzig.
43. Wülfing, E.A. (1892). Über den kleinsten Gesichtswinkel. Z. Biol. 29, 199-202.
44. Westheimer, G. and McKee, S.P. (1977b). Spatial configurations for visual hyperacuity. Vision Res. 17, 941-947.
45. Westheimer, G. (1975). Visual acuity and hyperacuity. Invest. Ophthal. Visual Sci. 14, 570-572.
46. Westheimer, G. and McKee, S.P. (1975). Visual acuity in the presence of retinal image motion. J. Opt. Soc. Am. 65, 847-850.
47. Westheimer, G. and McKee, S.P. (1977a). Integration regions for visual hyperacuity. Vision Res. 17, 89-93.

48. Campbell, F.W., Nachmias, J. and Jukes, J. (1970). Spatial frequency discrimination in human vision. J. Opt. Soc. Am. 60, 555-559.

49. Hirsch, J. and Hylton, R. (1982). Limits of spatial-frequency discrimination as evidence of neural interpolation. J. Opt. Soc. Am. 72, 1367-1374.

50. Regan, D. and Beverly, K.I. (1983). Spatial-frequency discrimination and detection comparison of postadaptation thresholds. J. Opt. Soc. Am. 73, 1684-1690.

51. Burbeck, C.A. and Regan, D. (1983). Independence of orientation and size in spatial discrimination. J. Opt. Soc. Am. 73, 1691-1694.

52. Regan, D. (1985). Masking of spatial-frequency discrimination. J. Opt. Soc. Am. A2, 1153-1159.

53. Koenderink, J.J. (1984a). Simultaneous order in nervous nets from a functional standpoint. Biol. Cybern. 50, 35-41.

54. Koenderink, J.J. (1984b). The concept of local sign. In: Limits in Perception. Eds. Doorn, A.J. van, Grind W.A. van de and Koenderink, J.J. VNU Science Press, Utrecht, 495-547.

55. Baker, K.E. (1949). Some variables influencing Vernier acuity. J. Opt. Soc. Am. 39, 567-576.

56. Foley-Fisher, J.A. (1968). Measurements of Vernier acuity in white and coloured light. Vision Res. 8, 1055-1065.

57. Foley-Fisher, J.A. (1973). The effect of target line length on Vernier acuity in white and blue light. Vision Res. 13, 1447-1454.

58. Morgan, M.J. and Aiba, T.S. (1985). Positional acuity with chromatic stimuli. Vision Res. 25, 689-695.

59. Mulligan, J.B. and Krauskopf, J. (1983). Vernier acuity for chromatic stimuli. Invest. Ophthal. Vis. Sci. suppl. 24, 276.

60. Leibowitz, H. (1955). Some factors influencing the variability of Vernier adjustments. Am. J. Psychol. 68, 266-273.

61. Watt, R.J. and Morgan M.J. (1983). The recognition and representation of edge blur: evidence for spatial primitives in human vision. Vision Res. 23, 1465-1477.

62. Andrews, D.P., Butcher, A.K. and Buckley, B.R. (1973). Acuities for spatial arrangement in line figures: human and ideal observers compared. Vision Res. 13, 599-620.

63. Andrews, D.P. and Miller, D.T. (1978). Acuity for spatial separation as a function of stimulus size. Vision Res. 18, 615-619.

64. Beck, J. and Schwartz, T. (1979). Vernier acuity with dot test objects. Vision Res. 19, 313-319.

65. Ludvigh, E. (1953). Direction sense of the eye. Am. J. Ophth. 36, 139-142

66. Ludvigh E., McKinnon, P. (1967). The effect of orientation on the three dot alignment test. Am. J. Opth. 64, 621-265.

67. Watt, R.J. (1984). Towards a general theory of the visual acuities for shape and spatial arrangement. Vision Res. 24, 1377-1386.

68. Bowen, R.W., Pola, J. and Matin, L. (1974). Visual persistence: effects of flash luminance, duration and energy. Vision Res. 14, 295-303.

69. Bowling, A. and Lovegrove, W. (1980). The effect of stimulus duration on the persistence of gratings. Percept. & Psychophys. 27, 574-578.

70. Bowling, A., Lovegrove, W. and Mapperson, B. (1979). The effect of spatial frequency and contrast on visual persistence. Perception 8, 529-539.

71. Watt, R.J. and Andrews, D.P. (1981). APE: Adaptive probit estimation of psychometric function. Curr. Psychol. Rev. 1, 205-214.

72. Finney, D.J. (1971). Probit analysis, 3rd edn. Cambridge Univ. Press.

72. Toet, A., Eekhout, M.P. van, Simons, H.L.J.J. and Koenderink, J.J. (in press). Scale invariant features of differential spatial displacement discrimination. Vision Res.

73. Cohn, T.E. and Lasley, D.J. (1974). Detectability of a luminance increment: effect of spatial uncertainty. J. Opt. Soc. Am. 64, 1715-1719.

74. Cohn, T.E. and Wardlaw, J.C. (1985). Effect of large spatial uncertainty on foveal luminance increment detectability. J. Opt. Soc. Am. A2, 820-825.

75. Hirsch, J. and Hylton, R. (1985). Spatial-frequency discrimination at low frequencies: evidence for position quantization by receptive fields. J. Opt. Soc. Am. A2, 128-135.

76. Westheimer, G. (1977). Spatial configurations for visual hyperacuity. Vision Res. 17, 941-947.

77. Westheimer, G. (1979). The spatial sense of the eye. Invest. Ophthalmol. Vis. Sci. 18, 893-912.

78. Westheimer, G. and Hauske, G. (1975). Temporal and spatial interference with Vernier acuity. Vision Res. 15, 1137-1141.

79. Westheimer, G., Shimamura, K. and McKee, S.P. (1976). Interference with line-orientation sensitivity. J. Opt. Soc. Am. 66, 332-338.

80. Yager, D., Kramer, P., Shaw, M. and Graham, N. (1984). Detection and identification of spatial frequency: models and data. Vision Res. 24, 1021-1035.

CHAPTER II.6.

Differential spatial displacement discrimination thresholds for Gabor patches.

ABSTRACT.

Differential spatial displacement discrimination thresholds were determined for a configuration of three identical Gaussian modulated patches of sinusoidal grating presented with equal orientation and at threshold luminance contrast. The patches were arranged one above the other at equal spatial intervals. The orientation of the bars of the sinusoidal grid constituting the patches was orthogonal to the axis joining the centres of the outer two patches. Thresholds were determined for displacements of the middle patch both orthogonal to and along the axis joining the outer two patches. Thresholds for both tasks were obtained as a function of both the spatial frequency of the sinusoidal grating and the spatial scale parameter of the Gaussian envelope of the patches.

We found that the differential spatial displacement discrimination thresholds for both tasks are a constant fraction of the spatial scale parameter of the Gaussian envelope of the sinusoidal grating patches and are independent of the spatial frequency of the modulated grating. We conclude that the human visual system is capable of assigning a single location tag to an entire Gaussian modulated patch of sinusoidal grating. The accuracy with which the relative position of such a Gabor patch can be determined is a constant fraction of its spatial extent (spread of the Gaussian spatial envelope).

key-words: hyperacuity, 3-dot alignment task, 3-dot bisection task, resolution, threshold contrast, Gabor stimuli.

INTRODUCTION.

Campbell and Robson (1968) suggested a multiple-channel model for pattern vision. In this model a spatial intensity distribution is processed in parallel by many separate channels, each selectively sensitive to a narrow range of spatial frequencies or bar widths of sinusoidal gratings. Nowadays there is abundant psychophysical (e.g. Blakemore and Campbell, 1969; Graham and Nachmias, 1971; Sachs et al., 1971) and neurophysiological (e.g. Campbell et al., 1969; Movshon et al., 1978; DeValois et al., 1982) evidence consistent with this hypothesis.

The spatial frequency description of the psychophysical channels is equivalent to a description in terms of collections of spatially overlapping detectors with different spatial weighting functions (e.g. Shapley and Lennie, 1985). Thus, a channel can be thought of as an array of detectors, each subserving a different part of the visual field but responding to the same range of bar widths or spatial frequencies.

Recent theories generally suppose that a pattern is detected whenever the integrated product of the retinal intensity distribution caused by the presence of a stimulus pattern and the weighting function of a detector, plus noise, exceeds the threshold value for at least one detector (e.g. Graham et al., 1978; Legge, 1978; Wilson and Bergen, 1979; Robson and Graham, 1981). There is still disagreement on the number of detectors with different weighting functions subserving the same retinal area. However, recent evidence suggests that their number may be quite small (Graham et al., 1978; Bergen et al., 1979; Wilson and Bergen, 1979; Watson and Robson, 1981; Watson, 1982). It has been suggested that the apparent sharp tuning of the spatial frequency channels may be due to the effects of spatial probability summation of the response of localized detector units at different spatial positions (Stromeyer and Klein, 1975; Graham and Rogowitz, 1976; Graham, 1977; Bergen et al., 1979; Wilson and Bergen, 1979).

Psychophysical evidence for the existence of size selective mechanisms, i.e. detectors maximally sensitive to visual targets with sizes in a particular range and existing at a single location was first reported by Pantle and Sekuler (1968). Their results were later confirmed

by experiments using selective adaptation (Thomas and Kerr, 1971; Nakayama and Roberts, 1972; Bagrash, 1973), size discrimination tasks at detection threshold (Thomas and Shimamura, 1974; Bagrash et al., 1974) and by discrimination experiments with spatially localized patches (Graham et al., 1978; Watson and Robson, 1981). Using selective adaptation, Perizonius et al. (1985) have recently shown that the spatial frequency channels of the human visual system have a local rather than global character.

The effect of presenting a stimulus with a narrow bandlimited spatial frequency characteristic is to elicit mainly the properties of mechanisms with a comparable spatial frequency characteristic. Because the receptive fields in the visual system overlap and interact, the overall response to a stimulus pattern near detection threshold depends upon the total activity in a relatively large class of subunits and is subject to some form of spatial probability summation. For different stimuli with the same spatial extent and presented at contrast detection threshold the number of detectors involved in the their detection will depend on their spatial frequency content. According to Hering's (1899) "mean local sign" theory the visual system can perform relative spatial localization tasks with an extremely high accuracy by taking the mean of the place tags assigned to a collection of individual detector units. Evidence for this theory has been presented by Westheimer (1977), who showed that stimuli which are by themselves subthreshold, devoid of contours or even of contrary information content can be pooled and used for a differential spatial discrimination judgement precise to a few seconds of arc in the human fovea. Thus, it is in principle possible that the accuracy with which the spatial position of a stimulus can be determined is some function of its spatial frequency content. For instance, the spatial position of the centroid of a large number of detectors with narrow spatial weighting functions (small uncertainty in spatial position) can (theoretically) be determined with a higher accuracy than the spatial position of the centroid of a small number of detectors with broad spatial weighting functions (large uncertainty in spatial positon).

It is known that differential spatial displacement discrimination thresholds depend on the prevailing spatial frequency of the stimulus

rest prevented tilting of the head. Viewing was monocular with the subject's dominant eye. The unused eye was covered with an eye cap. In experiments 1 and 2 the viewing distances were respectively 50 cm and 1 m. In both experiments the natural pupil was used in order to avoid vignetting effects.

Stimuli.

The target stimuli used in this experiment comprised three grating patches arranged one above the other at equal spatial intervals. The blobs had identical spatial contrast profiles and were modulated with a Gaussian temporal envelope. Their luminance distribution at a point (x,y) at time t is specified by

$$L(x,y,t) = L_b[1 + cw(x,y,t)*\sin(2\pi fy)]$$

where x and y are respectively along the horizontal and the vertical, L_b denotes the background luminance, f denotes the spatial frequency of the sinusoidal grating and c is the threshold contrast value as determined for a single patch. The window function w(x,y,t) is given by

$$w(x,y,t) = \exp[-(x^2+y^2)/(2s_s^2) - (t^2/2s_t^2)]$$

Such a sinusoidal patch looks like a fuzzy-edged circle containing alternating dark and light fuzzy-edged stripes (see Fig.1). This kind of stimulus is sometimes called a Gabor patch. As a comparison to the results obtained with Gabor patches of different spatial frequencies we performed some measurements with plain Gaussian modulated incremental blobs. These are obtained by replacing the sine term in the formula of the Gabor blobs by a constant of value 1.

Note that the sinusoidal component was always presented in the sine phase relative to the center of the Gaussian envelope. As a result, the mean overall stimulus luminance was equal to that of the background. The Gaussian window served to confine the stimuli in space time as well as in

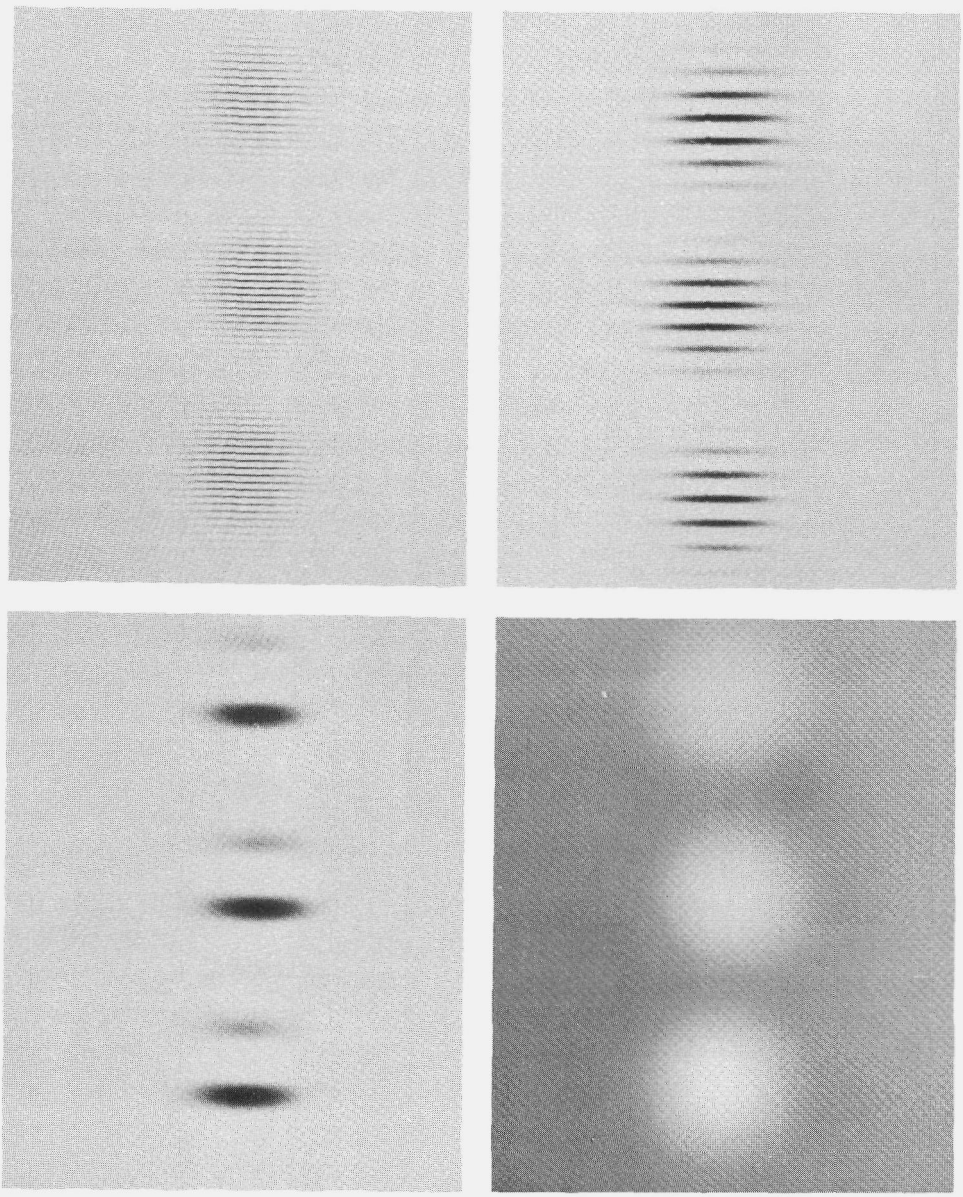

Figure 1. a-d: Photographs of the alignment stimuli for respectively Gabor patches with a spatial frequency of their grating component of 6.0, 1.9 and 0.6 cy/deg (a-c) and for three plain Gaussian modulated incremental blobs (d). Note in each case the small displacement of the middle patch relative to the axis joining the centres of the outer two patches.

spatial- and temporal- frequency. This was done in an attempt to stimulate only a small number (narrow range) of frequency selective mechanisms. If we define the bandwidth of a Gaussian signal as the distance between the (negative and positive) frequency components for which the amplitude has dropped to one half of the value of the frequency component with maximum amplitude, we find that the temporal bandwidth is given by $(2*\ln 2)^{\frac{1}{2}}/(\pi*s_t)$. In our case, the temporal frequency bandwidth is 1.87 Hz, and the spatial frequency bandwidth is between 0.21 cy/deg and 2.1 cy/deg. The spatial frequency of the sinusoidal grating varied between 0.6 cy/deg and 6.0 cy/deg.

We adopt the term spread for the distance over which a Gaussian falls from 1 to $e^{-\frac{1}{2}}$, corresponding to the standard deviation measure as defined in statistics. The window function is the product of spatial- and temporal-profiles with spreads of s_s and s_t respectively. Both the temporal and the spatial windows were truncated at plus and minus four times their spread. The threshold contrast c is defined as $(L-L_b)/L_b$, where L denotes the threshold luminance level.

The spread of the Gaussian temporal envelope was 0.2 sec (therefore the stimulus was above one half of its peak value for 0.47 sec). The frame rate was 60 Hz and interlaced. Intermediate presentations lasted for 0.05 sec, corresponding to 3 frames. This was found to be short enough to present a perceptually smooth temporal contrast profile. The total duration of the stimulus presentation was eight times the spread of its Gaussian temporal profile (i.e. if T is the moment at which the stimulus attained its maximum contrast and s_t represents the spread of the Gaussian temporal contrast profile, the presentation lasted from $T-4s_t$ to $T+4s_t$).

The distance between the centres of the outer two blobs of the target stimulus was 10 times their spread. The middle patch appeared either along the horizontal (alignment task) or along the vertical (bisection task) through the midpoint of the line segment joining the centres of the outer two patches and with a small displacement relative to this point. The orientation of the bars of the sinusoidal grid (along the x-direction) constituting the patches was also orthogonal to the axis joining the outer two patches (along the y-direction). If the orientation of the bars had been along the axis joining the outer two patches (along the x-direction),

subjects could perform in the alignment task by aligning the large scale patches using only one or more of their constituting small scale bars (subunits) as a position cue, e.g. by aligning the center (most visible) period of the grating patches. Because we were interested in the discrimination accuracy of subjects for differential spatial displacements of a Gabor patch as a whole we took care to exclude this possibility.

The continued response of the visual system following the termination (offset) of briefly presented stimuli is known to generate so-called after-images, even at threshold luminance contrast (Bowen et al., 1974; Bowling and Lovegrove, 1980). This visual persistence has been shown to increase with decreasing stimulus contrast (Bowling et al., 1979). To avoid the possibility that the presence of after-images or memory effects would introduce (false) cues in the differential spatial displacement discrimination task, the stimulus pattern as a whole appeared at random on one of 9 different positions, symmetrical with regard to the centre of the screen (0, ±3/16, ±6/16, ±9/16, ±12/16 times the size of the spread of the blob profile), both in the horizontal (x) and vertical (y) directions. If the stimulus pattern had appeared in the same position in each trial, comparison (using either the presence of after-images or memory effects) of successive displacements of the middle blob relative to the midpoint of the axis through the outer two would have introduced a (false) cue for the localization judgement.

The stimuli were superposed on a 100 cd/m^2 (300 Td for the 2 mm pupil) luminance background level. The luminance level of the background was chosen such as to operate in the photopic domain.

Experimental procedures.

After adaptation of the subject to the background luminance level the contrast detection threshold for a single (Gaussian or Gabor) blob was determined by means of a staircase method. Threshold was defined as the contrast level for which 80% of the stimulus presentations are detected. Thresholds were determined at the start of each session and between separate runs. The differential spatial displacement discrimination tasks were performed at detection threshold luminance contrast as (foveally)

determined for a single blob.

For all three-patch displacement discrimination tasks no use was made of a fixation mark because it would have presented a cue for the task to be performed. Therefore the subjects were instructed to fixate on the centre of the monitor screen.

At the onset of each stimulus presentation a buzzer signal sounded. After completion of the presentation the subject had to choose (forced choice) between a left or right displacement of the middle blob relative to the line segment defined by the outer two blobs in case of the alignment task and between a displacement up- or downwards relative to the midpoint of this line segment in case of the bisection task. Immediately after the subject had responded to a trial a new presentation was started. By withholding his answer for a while the subject was able to take a short rest. In case no decision could be made because one or more blobs were not detected (and in that case only) the subject could skip his obligation to answer and go on to the next presentation. In this case the missed presentation was randomly incorporated into the sequence of remaining trials. This situation occurred in about half of the number of presentations.

Adaptive probit estimation (APE; see Watt and Andrews, 1981) was used to determine the differential spatial displacement discrimination thresholds. APE is a modified method of constant stimuli. It allows bias-free threshold determination with high precision for a relatively small number of trials. Threshold is defined as the standard deviation of the cumulative normal psychometric function (corresponding to half the difference between the 17% and 83% points) and was estimated by Probit analysis (Finney, 1971). Each individual estimate is the standard deviation of the response error distribution from a run of 80 trials preceded by 20 practice trials. Thresholds quoted are the r.m.s. of at least 3 individual estimates. Standard errors for this procedure are typically of the order of 10% of the standard deviation.

The order in which the thresholds were determined was not systematic.

RESULTS.

Contrast detection thresholds were determined at the start of each run of the three-patch displacement discrimination tasks. We found that the contrast detection thresholds remained constant during the sessions and were reproduced in separate sessions.

The differential spatial displacement discrimination thresholds were defined as those spatial displacements which resulted in a rate of 83% correct localization judgements. All stimuli were temporally modulated with a Gaussian envelope with a spread of 0.2 sec. The ratio of the separation of the outer two blobs and the spread of the Gaussian spatial envelope of the blobs (i.e. the overall spatial extent of the patches) was kept constant. We chose for a ratio of 10. This resulted in a stimulus pattern in which the blobs appeared clearly resolved.

Due to the fact that the differential spatial localization experiments were performed at threshold luminance contrast (contrast level at which 80% of the presentations is seen) in about half of the presentations no answer could be obtained. An additional number of stimulus presentations is probably missed due to the uncertainty in the spatial position in which the pattern as a whole appeared (Cohn and Lasley, 1974; Cohn and Wardlaw, 1985).

Experiment 1.

In experiment 1 we determined the differential spatial displacement discrimination thresholds for the three-patch alignment and bisection tasks as a function of the spatial frequency of the sinusoidal grating component of the blobs. The spatial frequency of this grating component varied between 0.6 c/deg and 6.0 c/deg. All blobs used in this experiment had a Gaussian spatial envelope with a spread of 53.7 min of arc. The results are shown in Figure 2. As a comparison we measured for both tasks the differential spatial displacement discrimination thresholds for plain Gaussian modulated incremental blobs. (The value of this threshold is represented by the level of the dashed lines in Fig. 2.)

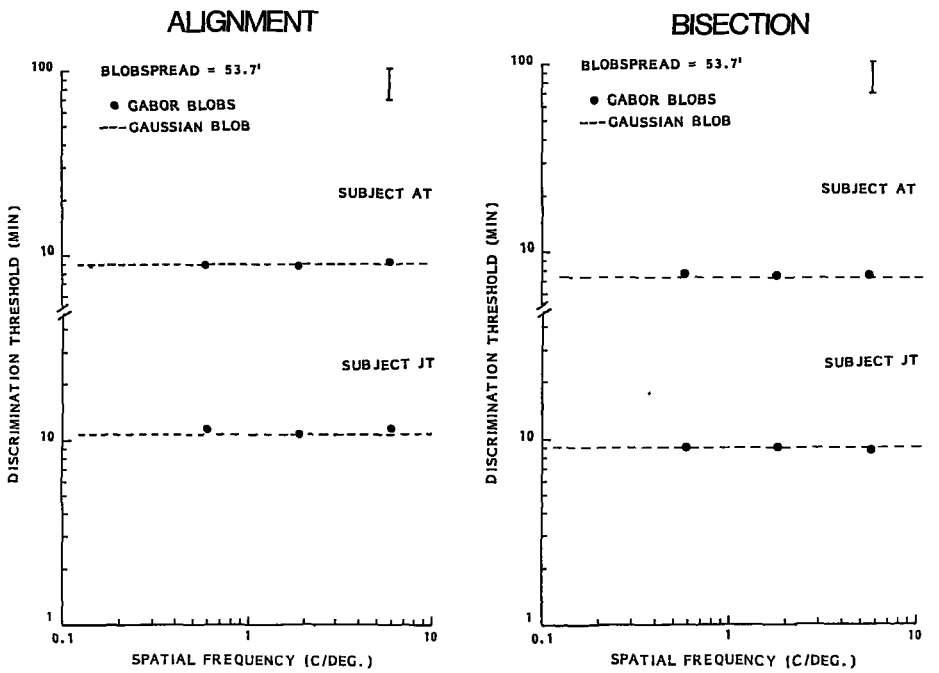

Figure 2. Differential spatial displacement discrimination thresholds for Gaussian modulated patches of sinusoidal grating (Gabor blobs) as a function of the spatial frequency of the sinusoidal grating component of the blobs. The dashed lines indicate the threshold level for Gaussian modulated incremental blobs. All stimuli were temporally modulated with a Gaussian envelope with a spread of 0.2 sec. The spatial spread of all blobs was 53.7 min of arc. The error bar represents two standard errors.

As shown in Fig. 2, we found no variation of the differential spatial displacement discrimination thresholds of the Gabor patches with variation of the spatial frequency of their sinusoidal grating component. Moreover, the differential spatial displacement discrimination thresholds determined for the Gabor blobs were not systematically different from those determined for Gaussian modulated incremental blobs.

Experiment 2.

The results from Experiment 1 indicate that the accuracy with which the overall position of a grating patch can be determined is independent of the spatial frequency of its sinusoidal component (at least over the range of spatial frequencies used in this study). As a further check on this result we performed Experiment 2 in which we determined the differential spatial displacement discrimination thresholds for both three-patch displacement discrimination tasks as a function of the spread of the Gaussian spatial envelope of the sinusoidal grating patches. The value of this spread varied between 10.7' and 107.4'. All Gabor patches used in this experiment had a sinusoidal grating component with a spatial frequency of 2.23 c/deg. As a comparison, we measured the differential spatial displacement discrimination thresholds for Gaussian modulated incremental blobs as a function of the spread of their Gaussian spatial envelopes (which is in fact a replication of an earlier experiment: see Toet et al., 1987).

The results of Experiment 2 (depicted in Figs. 3 and 4) show that the differential spatial displacement discrimination thresholds for the Gabor blobs scale with the spread of their Gaussian spatial envelopes (for a constant spatial frequency of their sinusoidal grating component). Again, the differential spatial displacement discrimination thresholds determined for grating patches with a certain spread of their Gaussian spatial envelope were not systematically different from those determined for Gaussian modulated incremental blobs of the same spread.

We computed a least-square fit of an exponential curve to the data points of Figs. 3 and 4. For the Gabor blob results (of subjects AT and JT

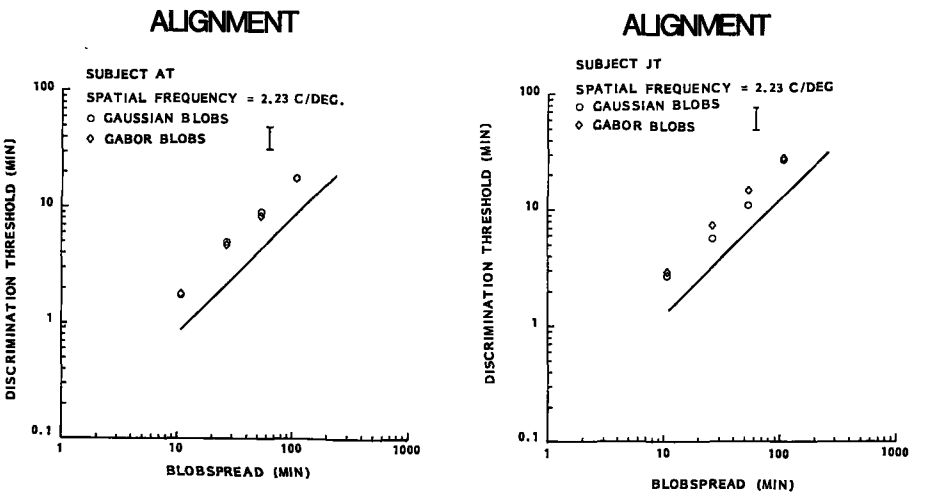

Figure 3. Three-patch alignment discrimination thresholds for both Gaussian modulated patches of sinusoidal grating (Gabor blobs) and Gaussian modulated incremental blobs as a function of the spread of the Gaussian spatial envelopes of the blobs. The spatial frequency of the Gabor blobs was 2.23 c/deg. The solid line represents the Weber fraction. All stimuli were temporally modulated with a Gaussian envelope with a spread of 0.2 sec. The error bar represents two standard errors.

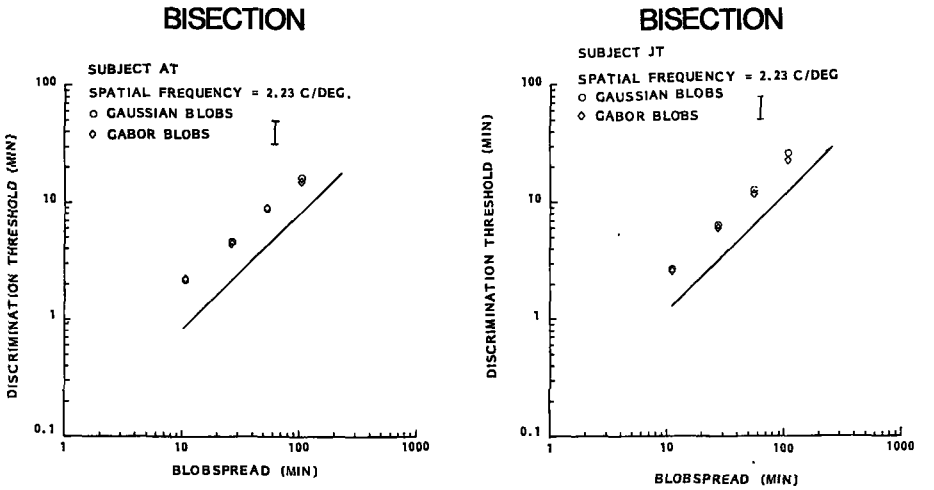

Figure 4. As Figure 3 for the three-patch bisection task.

respectively) the correlation coefficients (r^2) were all 1.00 and the powers obtained for the exponential curves ranged between 0.98 and 0.99. A similar fit to the data for the Gaussian incremental blob results yielded values ranging from 0.99 to 1.00 for the correlation coefficients and from 0.99 to 1.00 for the powers of the exponential curves. We may therefore conclude that the differential spatial displacement discrimination thresholds for the Gabor blobs are a constant fraction of the spread of their Gaussian envelopes.

DISCUSSION.

There is nowadays abundant evidence that the human visual system analyses a retinal light distribution with a range of linear spatial frequency- or size-selective elements that transduce the spatial information of the retinal image in an independent fashion (Campbell and Robson, 1968; Wilson and Bergen, 1979; for a review see Braddick et al., 1978). In a later stage this spatially extended information is combined to allow inferences about the spatial structure of the image.

The experiments described in this paper were performed to test the influence of the spatial frequency content of a stimulus on the accuracy with which subjects can determine relatively small changes in its spatial position. In view of the aforementioned facts and the considerations already mentioned in the introduction we were confident to find some manifestation of this influence. However, we found that the differential spatial displacement discrimination thresholds for Gaussian modulated patches of sinusoidal grating were a constant fraction of the spread of their Gaussian spatial envelope and were independent of the spatial frequency of their sinusoidal grating component.

Other researchers have shown that location is assigned to some widespread property (e.g. centroid or first moment) of a retinal light distribution, rather than to a local feature thereof (Watt et al., 1983; Westheimer and McKee, 1977). It is generally assumed that the visual system performs some kind of interpolation on the representation of the sampled stimulus intensity distribution after convolution with the optical

blur function of the visual system (Barlow, 1979). Morgan and Watt (1982, 1984) have shown that Vernier acuity for the position of a cosine luminance modulation is unaffected when the modulation is represented by discrete spatial samples at intervals up to 2-3 min of arc (i.e. if the sampling rate is more than 20 c/deg). Thus, the profile represented by the samples could be discerned with undiminished spatial accuracy even when the samples themselves were visually resolved. Their results can be explained with a simple difference of Gaussians (DOG) model of receptive field organization (see Wilson and Bergen, 1979) providing a long-range interpolation (neural blurring) beyond the spacing of the retinal mosaic. Our results indicate that the visual system assigns location to the grating patches using their entire spatial intensity distribution. In our experiments interpolation after merely blurring the stimuli (i.e. after a convolution with a receptive field weighting function of some kind) is clearly of no avail to determine the spatial position of the grating patches because this would only affect the global modulation depth but not the spatial structure of our stimulus pattern. Our results suggest that the visual system assigns a location tag to some kind of centroid of the spatial features of the grating patches. For instance, if the visual system processes the bars of opposite contrast polarity of the grating patches in independent channels (as suggested by Burton et al., 1977) it might compute a centroid for the bright and dark bars separately and assign position to a weighted mean of these outcomes regarding this as the final position of the entire stimulus distribution. In the same way position could be assigned to the centroids of peaks (Hirsch and Hylton, 1982) or edges (Marr and Hildreth, 1980) present in the retinal luminance distribution.

We conclude that the human visual system is capable to assign a single location tag to a Gaussian modulated patch of sinusoidal grating. The accuracy with which the position of such a Gabor patch can be determined is a constant fraction of its spatial extent (i.e. the spread of its Gaussian spatial envelope).

Acknowledgements - We thank Ad de Goffau for producing the necessary software and Jan Toet for acting as a patient observer. We are indebted to Dr. R.J. Watt and Dr. D.P. Andrews for kindly providing us with a listing of their APE program. This work was supported by the Dutch Foundation for the Advancement of Pure Research (ZWO).

REFERENCES.

Andrews D.P., Butcher A.K. and Buckley B.R. (1973) Acuities for spatial arrangement in line figures: human and ideal observers compared. Vision Res. 13, 599-620.

Andrews D.P. and Miller D.T. (1978) Acuity for spatial separation as a function of stimulus size. Vision Res. 18, 615-619.

Bagrash F.M. (1973) Size-selective adaptation: psychophysical evidence for size-tuning and the effects of stimulus contour and adapting flux. Vision Res. 13, 575-598.

Bagrash F.M., Thomas J.P. and Shimamura K.K. (1974) Size-tuned mechanisms: correlation of data on detection and apparent size. Vision Res. 14, 937-942.

Barlow H.B. (1979) Reconstructing the visual image in space and time. Nature 279, 189-190.

Beck J. and Schwartz T. (1979) Vernier acuity with dot test objects. Vision Res. 19, 313-319.

Bergen J.R., Wilson H.R. and Cowan J.D. (1979) Further evidence for four mechanisms mediating vision at threshold: sensitivity to complex gratings and aperiodic stimuli. J. Opt. Soc. Am. 69, 1580-1587.

Blakemore C. and Campbell F.W. (1969) On the existence of neurons in the human vision system selectively sensible to the orientation and size of retinal images. J. Physiol. 203, 237-260.

Bowen R.W., Pola J. and Matin L. (1974) Visual persistence: effects of flash luminance, duration and energy. Vision Res. 14, 295-303.

Bowling A. and Lovegrove W. (1980) The effect of stimulus duration on the persistence of gratings. Percept. & Psychophys. 27, 574-578.

Bowling A., Lovegrove W. and Mapperson B. (1979) The effect of spatial frequency and contrast on visual persistence. Perception 8, 529-539.

Braddick O., Campbell F.W. and Atkinson J. (1978) Channels in vision: basic aspects. In: Handbook of Sensory Physiology (Eds. Held R., Leibowitz H.W. and Teuber H.L.), Vol. 8, Springer, Berlin.

Burton G.J., Nagshineh S. and Ruddock K.H. (1977) Processing by the human visual system of the light and dark contrast components of the retinal image. Biol. Cybern. 27, 189-197.

Campbell F.W., Cooper G.F. and Enroth-Cugell C. (1969) The spatial selectivity of the visual cells of the cat. J. Physiol. 203, 223-235.

Campbell F.W. and Robson J. (1968) Application of Fourier analysis to the visibility of gratings. J. Physiol. 197, 551-566.

Cohn T.E. and Lasley D.J. (1974) Detectability of a luminance increment: effect of spatial uncertainty. J. Opt. Soc. Am. 64, 1715-1719.

Cohn T.E. and Wardlaw J.C. (1985) Effect of large spatial uncertainty on foveal luminance increment detectability. J. Opt. Soc. Am. A2, 820-825.

Daugman J.G. (1980) Two-dimensional spectral analysis of cortical receptive field profiles. Vision Res. 20, 847-856.

Daugman J.G. (1985a) Representational issues and local filter models of two-dimensional spatial visual encoding. In : Models of the Visual Cortex, 96-107. Eds. Rose, D. and Dobson V.G. John Wiley, New York, London.

Daugman J.G. (1985b) Uncertainty relation for resolution in space, spatial frequency and orientation optimized by two-dimensional visual cortical filters. J. Opt. Soc. Am. A2, 1160-1169.

DeValois R.L., Albrecht D.G. and Thorell L.G. (1982) Spatial frequency selectivity of cells in macaque visual cortex. Vision Res. 22, 545-559.

Finney D.J. (1971) Probit Analysis, 3rd edn. Cambridge Univ. Press.

Gabor D.(1946) Theory of communication. J. Inst. Electr. Eng. 93, 429-457.

Graham N. (1977) Visual detection of aperiodic spatial stimuli by probability summation among narrowband channels. Vision Res. 17, 637-652.

Graham N. and Nachmias J. (1971) Detection of grating patterns containing two spatial frequencies: a comparison of single-channel and multiple-channel models. Vision Res. 11, 251-259.

Graham N., Robson J.G. and Nachmias J. (1978). Grating summation in fovea and periphery. Vision Res. 18, 815-825.

Graham N. and Rogowitz B. (1976) Spatial pooling properties deduced from the detectability of FM and quasi-AM gratings: a reanalysis. Vision Res. 16, 1021-1026.

Hirsch J. and Hylton R. (1982) Limits of spatial-frequency discrimination as evidence of neural interpolation. J. Opt. Soc. Am. 72, 1367-1374.

Hirsch J. and Hylton R. (1985) Spatial-frequency discrimination at low frequencies: evidence for position quantization by receptive fields. J. Opt. Soc. Am. A2, 128-135.

Legge G.E. (1978) Space domain properties of a spatial frequency channel in human vision. Vision Res. 18, 959-969.

Levi D.M. and Klein S.A. (1983) Spatial localization in normal and amblyopic vision. Vision Res. 23, 1005-1017.

Levi D.M., Klein S.A. and Aitsebaomo A.P. (1985) Vernier acuity, crowding and cortical magnification. Vision Res. 25, 963-977.

Ludvigh E. (1953) Direction sense of the eye. Am. J. Ophth. 36, 139-142.

Ludvigh E. and McKinnon P. (1967) The effect of orientation on the three dot alignment test. Am. J. Ophth. 64, 261-265.

Marr D. and Hildreth E. (1980) Theory of edge detection. Proc. R. Soc. Lond. B 207, 187-217.

Morgan M.J. and Watt R.J. (1982) Mechanisms of interpolation in human spatial vision. Nature 299, 553-555.

Morgan M.J. and Watt R.J. (1984) Spatial frequency interference effects and interpolation in Vernier acuity. Vision Res. 24, 1911-1919.

Movshon J.A., Thompson I.D. and Tolhurst D.J. (1978) Spatial summation in the receptive fields of the simple cells in the cat's striate cortex. J. Physiol. 283, 53-77.

Nakayama K. and Roberts D.J. (1972) Line length detectors in the human visual system: evidence from selective adaptation. Vision Res. 12, 1709-1713.

Pantle A. and Sekuler R. (1968) Size detecting mechanisms in human vision. Science 162, 1146-1148.

Perizonius E., Schill W., Geiger H. and Roehler R. (1985) Evidence on the local character of spatial frequency channels in the human visual system. Vision Res. 25, 1233-1240.

Quick R.F., Mullins W.W. and Reichert T.A. (1978) Spatial summation

effects in two-component grating thresholds. J. Opt. Soc. Am. 68, 116-121.

Robson J.G. and Graham N. (1981) Probability summation and regional variation in contrast sensitivity across the visual field. Vision Res. 21, 409-418.

Sachs M.B., Nachmias J. and Robson J.G. (1971) Spatial-frequency channels in human vision. J. Opt. Soc. Am. 61, 1176-1186.

Shapley R. and Lennie P. (1985) Spatial frequency analysis in the visual system. Ann. Rev. Neurosci. 8, 547-583.

Stromeyer C.F., Klein S. (1975) Evidence against narrow-band spatial frequency channels in human vision: the detectability of frequency modulated gratings. Vision Res. 15, 899-910.

Thomas J.P. and Kerr L.G. (1971) Evidence of role of size-tuned mechanisms in increment threshold task. Vision Res. 11, 647-655.

Thomas J.P. and Shimamura K.K. (1974) Perception of size at the detection threshold: its accuracy and possible mechanisms. Vision Res. 14, 535-543.

Toet A., Eekhout M.P. van, Simons H.L.J.J. and Koenderink J.J. (1987) Scale invariant features of differential spatial displacement discrimination. Vision Res. In press.

Watson A.B. (1982) Summation of grating patches indicates many types of detector at one retinal location. Vision Res. 22, 17-25.

Watson A.B. and Robson J.G. (1981) Discrimination at threshold: labelled detectors in human vision. Vision Res. 21, 1115-1122.

Watt R.J. (1984) Towards a general theory of the visual acuities for shape and spatial arrangement. Vision Res. 24, 1377-1386.

Watt R.J. and Andrews D.P. (1981) APE: Adaptive probit estimation of psychometric function. Curr. Psychol. Rev. 1, 205-214.

Watt R.J., Morgan M.J. and Ward R.M. (1983) Stimulus features that determine the visual location of a bright bar. Invest. Ophthal. Vis. Sci. 24, 66-71.

Westheimer G. and McKee S.P. (1977) Integration regions for visual hyperacuity. Vision Res. 17, 89-93.

Wilson H.R. and Bergen J.R. (1979) A four mechanism model for threshold spatial vision. Vision Res. 19, 19-32.

CHAPTER II.7.

Effects of blur and eccentricity on differential spatial displacement discrimination thresholds.

ABSTRACT.

Similar to the two-point discrimination acuity task and the three-dot alignment hyperacuity task, differential spatial displacement discrimination thresholds were determined for stimuli consisting of blobs with Gaussian spatial and temporal envelopes presented at detection threshold luminance contrast. Thresholds were determined as a function of eccentricity along the horizontal meridian of the visual field (from 45° nasal to 65° temporal) with the spatial spread or blur parameter of the blobs as a scale parameter.

The results show that the performance of the visual system in differential spatial displacement discrimination tasks becomes progressively more homogeneous for a progressive increase in the blur parameter of the stimuli. Scaling (i) the three-blob alignment results with estimates of the cortical magnification factor and (ii) the two-blob separation discrimination results with their corresponding neural blur parameter shows an impressive isotropy and blur scale-invariance for the mechanisms mediating differential spatial displacement discrimination across the visual field. These results are interpreted in terms of a scaled sampling lattice model of the visual system in combination with an automatic scale-selection mechanism.

key-words: hyperacuity, 3-dot alignment task, 2-point discrimination, stimulus blur, resolution, threshold contrast, periphery, cortical magnification

INTRODUCTION.

Most mechanisms mediating visual detection and discrimination of spatial patterns are spatially inhomogeneous. This is probably the result of inhomogeneities in the composition of the retina and the distribution of functional connections between the retinal output and the cortical input. Several attempts were made to relate the decline in visual performance with eccentricity to changes in the anatomy and physiology of the visual system (Weymouth, 1958; Cowey and Rolls, 1974; Rovamo et al., 1978; Koenderink et al., 1978; Drasdo, 1977; Virsu and Rovamo, 1979; Schwartz, 1980, 1983). For a large number of discrimination tasks it was found that visual performance is essentially independent of eccentricity if the stimulus size is scaled such that the number of stimulated ganglion cells or the stimulated cortical area are almost the same at any eccentricity.

It has been shown that thresholds for differential spatial displacement discrimination (or so-called hyperacuity) tasks rise faster with eccentricity than visual resolution thresholds (Bourdon, 1902; Westheimer, 1982). Recently, Livingstone and Hubel (1985) have suggested that this might reflect the difference in the rates of increase with eccentricity between the mean receptive field sizes of simple cells mediating acuity and of complex cells which reside at a higher stage in the visual pathways and are assumed to be involved in the assesment of spatial localization. Levi et al. (1985) have shown that the fall-off in Vernier acuity (i.e. hyperacuity) is compatible with recent estimates of cortical magnification (Dow et al., 1981; Tootell et al., 1982; Van Essen et al., 1984) while the decline in grating acuity is consistent with retinal factors. This seems to indicate that resolution is limited by retinal processes while differential spatial displacement discrimination is limited by cortical processes.

Discrimination thresholds based on the relative spatial location of stimulus features are known to be less affected by optical blur than discrimination thresholds based on the spatial resolution of stimulus features (Hartridge, 1923; Stigmar, 1971; Foley-Fisher, 1977; Westheimer, 1979; Enoch and Williams, 1983; Watt et al., 1983; Watt and Morgan, 1984;

Williams et al., 1984). Hering (1899) postulated the theory of mean local sign. According to this theory the visual system can perform differential spatial displacement discrimination tasks with an accuracy of a fraction of a foveal photoreceptor diameter by taking the mean of the place tags of a collection of retinal receptors. There are indications that the visual system actually performs a computational process of this kind (Levi and Klein, 1986; Westheimer and McKee, 1977). In this view the accuracy with which the visual system can assign place tags to the mean or centroid of each feature in a retinal intensity distribution will depend on the resolution of the stimulus features. Blurring two features which are clearly resolved does not necessarily have to deteriorate this accuracy. Moreover, it is even thought to be essential in attaining optimal accuracy in some hyperacuity tasks (Fahle and Poggio, 1981, 1984; Hirsch and Hylton, 1985; Morgan and Watt, 1982, 1983; Snyder, 1982; Williams et al., 1984). The precision with which two stimulus features can be resolved is limited by the precision with which the flux density in the image plane can be determined (Harris, 1964; Westheimer, 1976). Blurring two barely resolved stimulus features will cause a further decrease of this precision. As a result, the spatial separation discrimination thresholds will increase. Therefore, blur may have an asymmetrical effect on acuity- (resolution or spatial separation discrimination) and hyperacuity- (differential spatial displacement discrimination) tasks. Thus, there is no apparent need to invoke separate mechanisms mediating these different tasks.

Invariant features of contrast detection and spatial frequency discrimination tasks have resulted in models in which the retina is depicted as a self-similar detector array graded with respect to aperture size (Koenderink, 1977; Koenderink and van Doorn, 1978, 1982; Hartmann, 1982; Hirsch and Hylton, 1982, 1985; Burton et al., 1986). If these descriptions of the visual system have any validity it is a priori likely that the mechanisms that compute differential spatial displacements are also scale invariant (i.e. do not depend on the spatial scale- or blur-parameter of the stimulus features). Therefore, it seems possible that the notions of acuity and hyperacuity can be generalized to low resolution tasks in which differential spatial displacement is computed from the

output of detectors with large aperture sizes (large receptive field sizes).

In previous experiments we determined discrimination thresholds for (i) three-blob alignment- and bisection- (hyperacuity) tasks (Toet et al., 1987) and (ii) for a two-blob discrimination (acuity) task (Toet and Koenderink, 1987) as a function of the blur parameters of the stimuli. The stimuli were oriented along the vertical or horizontal meridian. For both tasks we found that the discrimination thresholds were a constant fraction of the blur parameters of the stimuli. From these results we concluded that at all levels of resolution a similar mechanism is used to detect differential spatial displacements. Moreover, we suggested that there is no fundamental difference between the mechanisms that perform in hyperacuity- and in acuity- or resolution- tasks. The difference in the accuracy of performance of the visual system in resolution- and differential spatial displacement discrimination- tasks may merely result from a decreased accuracy with which the position of the stimulus features can be determined when their corresponding contrast profiles overlap (Westheimer, 1976, 1979).

In the literature there are only a few studies investigating the effects of retinal eccentricity and stimulus blur on spatial resolution and differential spatial displacement discrimination thresholds (Enoch et al., 1984; Levy-Schoen, 1977). However, the blur parameter of the stimuli was neither well-defined nor systematically varied in any of these experiments. We devised experiments in which the blur parameter of the stimuli is well-defined and easy to vary. The stimuli we use consisted of blobs with Gaussian spatial profiles and Gaussian temporal envelopes presented at detection threshold luminance contrast. Because they are roughly bandlimited in the frequency domain these stimuli are likely to activate only a small range of spatial frequency selective mechanisms, thereby providing us with a measure for the blur parameter of the blobs (namely the spread of their Gaussian spatial contrast profiles). We use these stimuli to determine spatial resolution- and differential spatial displacement discrimination- thresholds, both as a function of the blur parameter of the stimuli and as a function of retinal eccentricity.

In this paper we will determine differential spatial displacement discrimination thresholds for a configuration of three blobs arranged one above the other at equal spatial intervals. Thresholds will be determined for displacements of the middle blob orthogonal to the axis joining the outer two blobs. For a configuration of two blobs with overlapping (Gaussian) spatial contrast profiles we will determine spatial resolution- or separation-discrimination thresholds. For both tasks thresholds will be determined as a function of the eccentricity in the visual field of the midpoint of the stimulus pattern (which is located somewhere along the horizontal meridian) with the spread of the blobs as a (blur-) scale parameter. The three-blob alignment task is equivalent to the three-dot alignment hyperacuity task which is well documented in the literature (Andrews et al., 1973; Andrews and Miller, 1978; Beck and Schwartz, 1979; Ludvigh, 1953; Ludvigh and McKinnon, 1967; Watt, 1984). The two-blob separation discrimination task also has its two-dot resolution equivalent in the literature (Helmholtz, 1909; Harris, 1964; Nyyssonen-Grimes and Thompson, 1967; Nahrstedt and Schooley, 1979; Geisler and Davila, 1985).

GENERAL METHODS.

Subjects.

Two male subjects, aged 27 and 30, served in the experiments. Both subjects have corrected myopic vision. Subject A.T. is highly practised. Subject H.S. underwent several training sessions before performing the measurements reported below.

Apparatus.

A PDP11/34 minicomputer in combination with a Gould deAnza IP8500 image array processor was used to generate, process and present the stimuli, record the responses and analyze the data.

The stimulus was displayed on a Philips LDH2123 monochrome monitor.

The CRT display was equipped with white D phosphor. The CRT was driven in an interlaced mode with a frame rate of 60 HZ. The display consisted of 512 × 512 pixels with the luminance value of each pixel quantized to 8 bits. A 512 × 512 correction matrix was added to the deAnza frame buffer to compensate for the inhomogeneity of the display.

Viewing conditions.

The display was placed in a dark room with nonreflecting black walls. Observers were seated with their heads supported by a chin rest, adjusted in height and position so that their dominant eye was on the line perpendicular to the center of the monitor screen. The use of a forehead rest prevented tilting of the head. For both subjects testing was monocular with the non-dominant eye patched via a black occluder. In Experiment 1 a 2 mm artificial pupil was used. In Experiment 2 viewing was with the natural pupils. For measurements in the far periphery (eccentricities larger than 25°) no optical correction was applied to correct for the refractive errors of the observers. As errors in refraction do not seem to influence peripheral visual acuity (Millidot et al., 1975) we assume that the absence of such a correction does not have a detrimental effect on our results. For tasks performed in the near periphery we applied the foveally determined optical correction.

The stimulus was superposed on a 100 cd/m^2 (300 Td for the 2 mm pupil) luminance background level. The luminance level of the background was chosen such as to operate in the photopic domain.

Stimuli.

The stimuli comprised a number of blobs with identical Gaussian spatial contrast profiles and Gaussian temporal envelopes. Their luminance is given by

$$L(x,y,t) = L_b[1+cw(x,y,t)]$$

where L_b denotes the background luminance and c is the threshold contrast value as determined for a single blob. The window function w(x,y,t) is given by

$$w(x,y,t) = \exp[-(x^2+y^2)/(2s_s^2)-(t^2/(2s_t^2))]$$

We adopt the term spread for the distance over which a Gaussian falls from 1 to $e^{-1/2}$, corresponding to the standard deviation measure as defined in statistics. (A spatial region with radius $2s_s$ and centered on (x,y)=(0,0) contains 92% of the total energy; a temporal interval of width $2s_t$ centered on t=0 contains 96% of the total stimulus energy). The window function is the product of spatial and temporal Gaussians with spreads of s_s and s_t respectively. Both the temporal and the spatial windows were truncated at plus and minus four times their spread (containing respectively 99.994% and 99.990% of the total stimulus energy). The threshold contrast c is defined as $(L-L_b)/L_b$, where L denotes the threshold luminance level.

The spread of the Gaussian temporal envelope was 0.2 sec (therefore the stimulus was above one half of its peak value for 0.47 sec). The frame rate was 60 Hz and interlaced. Intermediate presentations lasted for 0.05 sec, corresponding to 3 frames. This was found to be short enough to present a perceptually smooth temporal contrast profile. The total duration of the stimulus presentation was eight times the spread of its Gaussian temporal envelope (i.e. if T is the moment at which the stimulus attained its maximum contrast and s_t represents the spread of the Gaussian temporal contrast profile, the presentation lasted from $T-4s_t$ to $T+4s_t$). This stimulus presentation duration comfortably exceeds the critical duration of both fovea and periphery.

If we define the bandwidth of a Gaussian signal as the distance between the (negative and positive) frequency components for which the amplitude has dropped to one half of the value of the frequency component with maximum amplitude (zero frequency for a Gaussian signal) then we find that the temporal bandwidth is given by $(2*\ln 2)^{\frac{1}{2}}/(\pi*s_t)$. In our case the temporal frequency bandwidth is 1.87 Hz and the spatial frequency

bandwidth is between 0.21 cy/deg and 20.09 cy/deg.

Because we are interested in the differential spatial displacement discrimination thresholds as a function of the resolution of the stimuli we adopted a smooth (Gaussian) spatial stimulus contrast profile and a smooth (Gaussian) temporal stimulus contrast profile in combination with detection threshold luminance contrast (as determined for a single blob) in an attempt to stimulate only a small number (narrow range) of frequency selective mechanisms. We adopt the spread of the spatial contrast profiles of the Gaussian blobs as their resolution- or blur-parameter.

Experimental procedures.

After adaptation of the subject to the background luminance level the contrast detection threshold for a single blob was determined by means of a staircase method. Threshold was defined as the contrast level for which 80% of the stimulus presentations are detected. Thresholds were determined at the start of each session and in between separate runs. The differential spatial displacement discrimination tasks were performed at detection threshold luminance contrast as determined for a single blob.

For all differential spatial displacement discrimination tasks that involved stimulus presentations along the vertical meridian no use was made of a fixation mark because it would have presented a cue for the task to be performed and it would have interfered with the detection of the stimuli. In this case the subjects were instructed to fixate on the centre of the monitor screen. For peripherally performed measurements a small black dot, situated on the horizontal through the centre of the monitor screen, was used as a fixation mark.

At the onset of each stimulus presentation a buzzer signal sounded. After completion of the presentation the subject had to report (forced choice) his decision for the task in hand. Immediately after the subject had responded to a trial a new presentation was started. By withholding his answer for a while the subject was able to take a short rest. In case no decision could be made because one or more blobs were not detected (and in that case only) the subject could skip his obligation to answer and go

on to the next presentation. In this case the missed presentation was randomly incorporated into the sequence of remaining trials. This situation occurred in about half of the number of presentations.

Adaptive probit estimation (APE; see Watt and Andrews, 1981) was used to determine the differential spatial displacement discrimination thresholds. APE is a modified method of constant stimuli. It allows bias-free threshold determination with high precision for a relatively small number of trials. Threshold is defined as the standard deviation of the cumulative normal psychometric function (corresponding to half the difference between the 17% and 83% points) and was estimated by Probit analysis (Finney, 1971). Each individual estimate is the standard deviation of the response error distribution from a run of 80 trials preceded by 20 practice trials. Thresholds quoted are the r.m.s. of at least 3 individual estimates. Standard errors for this procedure are typically of the order of 10% of the standard deviation.

The data were gathered over a period of two weeks in irregular order.

The three-blob alignment task.

The stimuli comprised three blobs arranged one above the other at equal spatial intervals. The blobs had identical (Gaussian) spatial and temporal envelopes. The spread of the temporal envelopes was 0.2 sec. The distance between the centres of the outer two blobs of the target stimulus was 24 times their spread. Therefore, all stimuli were geometrically similar, independent of the value of their resolution parameter. We adopted the spatial spread (or the blur parameter) of the blobs as the spatial scale parameter of the stimulus pattern. The middle blob appeared on the line through the middle of and orthoaxial to the line segment joining the centres of the outer two blobs. On each stimulus presentation the displacement of the middle blob was selected randomly from a number of preset magnitudes using APE. After completion of a stimulus presentation the subject had to choose between a left or right displacement of the middle blob relative to the axis defined by the outer two blobs.

The two-blob discrimination task.

The stimuli comprised two blobs with different spatial separations. The stimulus profile is given by

$$L(x,y,t)=L_b[1+cw(x,y,t)]$$

where L_b denotes the background luminance and c is the threshold contrast value as determined for a single blob. The window function w(x,y,t) is given by

$$w(x,y,t)=(\exp[-((x-d/2)^2+y^2)/(2s_s^2)]+\exp[-((x+d/2)^2+y^2)/(2s_s^2)])\times \exp[-t^2/(2s_t^2)]$$

if the separation d between the means of the two Gaussian intensity distributions is greater than $2s_s$ and

$$w(x,y,t)=(\exp[-((x-d/2)^2+y^2)/(2s_s^2)]+\exp[-((x+d/2)^2/(2s_s^2)])\times \exp[-t^2/(2s_t^2)]/(2\exp[-(d/2)^2/(2s_s^2)])$$

if $d<2s_s$. Because of this definition the stimulus profile of two blobs with zero separation equals that of a single blob. The spread of the temporal envelope (s_s) was 0.2 sec. We adopted the spatial spread (or the blur parameter) of the blobs as the spatial scale parameter of the entire stimulus pattern.

For the two-blob separation discrimination task we made use of a two-alternative forced choice method. Each trial consisted of two consecutive presentation intervals. Both trial intervals contain two blobs separated by the same distance d. However, in one interval the separation is along the vertical and in the other along the horizontal. At the onset of the first presentation interval of each trial a warning tone is presented once. The onset of the second presentation interval of a trial is announced by the occurence of two consecutive warning tones. After completion of a trial (consisting of two consecutive stimulus

presentations) the subject has to indicate (forced choice) which interval contained the blobs that were separated along the vertical. The order of presentation of the vertical and horizontal stimulus configurations in a trial is chosen at random. APE is used to select on each presentation the spatial separation of the two blobs randomly from a number of preset magnitudes.

Another way to make up the two-blob discrimination experiment would have been to present a single blob in one presentation interval and two blobs with a spatial separation d in the other interval. In this case the order of the presentation of the single- and double-blob configurations would have to be random. The two-blob configuration could then be randomly oriented either along the vertical or along the horizontal. However, this form of the experiment would leave the possibility that subjects perform in the spatial separation discrimination task by using either flux differences (in case of equal contrast values of the different stimulus configurations) or contrast differences (in case of the different stimulus configurations presenting equal flux) between the two intervals of a single trial. In the procedure used in this paper only the orientation of the stimulus varies between the consecutive trial intervals, thereby keeping the flux and luminance contrast levels constant. Thus, the only discrimination cue available to the subjects is the orientation of the stimulus pattern.

Because the total stimulus extent (i.e. the spatial separation of the blobs) is varied through a run, the total flux presented by the stimulus will also be different in each trial. In a previous study (Toet and Koenderink, 1987) we performed numerical calculations with a model representing a continuous distribution of layers of sampling units with different aperture sizes. The results from these calculations indicated that, if this model is realistic, the detection thresholds for two-blob stimuli should not vary more than 10% with the separation of the two blobs. Psychophysical experiments we performed in the same study validated this prediction. Moreover, as flux differences present no information about the orientation of the stimulus pattern, we assume that flux differences throughout a run are not available as a cue for the subjects to perform in the spatial separation discrimination task.

When the distance between two blobs increases not only the separation between the two peaks in the resulting light distribution (assuming they are resolved) changes, but the absolute luminance of the trough between the peaks and the contrast ratio between the peaks and the trough vary also. We do not want the contrast of the stimuli to vary with their relative spatial extent, as this would result in contrast values being either above or below the detection threshold value (which is nearly independent of the spatial extent of the stimuli). Therefore, the stimulus is scaled so that the spatial luminance contrast of the peak(s) in the stimulus profile is independent of the spatial separation of the two blobs. This result can also be obtained by taking the local maximum value of both blob contrast profiles at each position. However, this would result in a sharp dip in the final luminance profile. Such a sharp dip is clearly visible (Kulikowksy and King-Smith, 1973) and therefore provides an unwanted clue for the discrimination task under study.

EXPERIMENT I: Determination of three-blob alignment acuity and two-blob separation discrimination at 0° eccentricity.

Foveal contrast detection thresholds were determined at the start of each run of the three-blob alignment and the two-blob separation discrimination tasks. We found that the contrast detection thresholds remained constant during the sessions and were reproduced in separate sessions.

Due to the fact that the differential spatial localization experiments were performed at threshold luminance contrast (contrast level at which 80% of the presentations is seen) in about 60% of the presentations no answer could be obtained.

The differential spatial displacement discrimination thresholds for the three-blob alignment and the two-blob separation discrimination tasks determined for a range of eccentricities along the horizontal meridian and with the angular dimensions of the blobs as a blur parameter are shown in respectively Figs. 1 and 2. The thresholds were defined as those spatial displacements which resulted in a rate of 83% correct localization

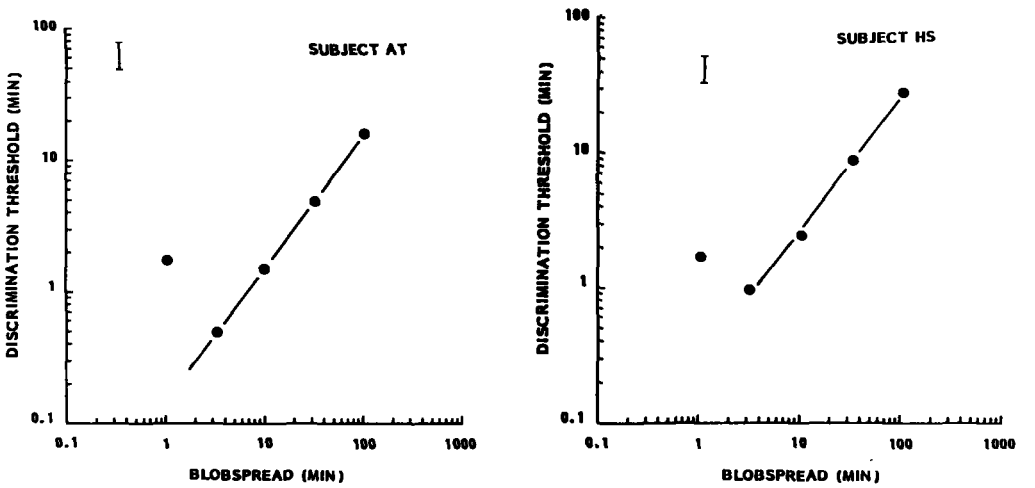

Figure 1. Differential spatial displacement discrimination thresholds for the three-blob alignment task as a function of the blur parameter of the blobs and for geometrically similar stimuli presented along the vertical meridian.

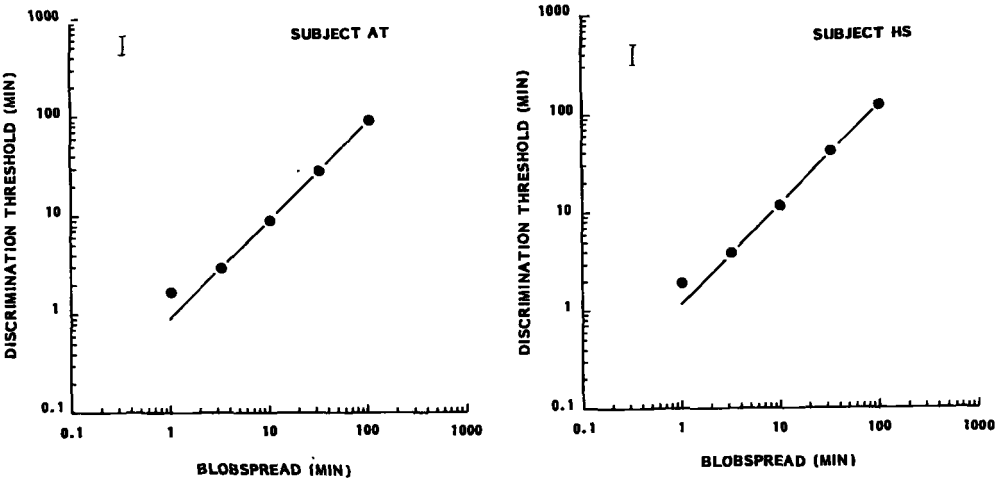

Figure 2. Spatial separation discrimination thresholds for the two-blob discrimination task as a function of the blur parameter of the blobs and for foveal fixation.

judgements. We computed a least-square fit of an exponential curve to our data points. Only data points for spreads larger than 2 min of arc were used in the calculation of the regression lines. The least-square curves thus obtained closely fit the data points. The correlation coefficients (r^2) range in value between 0.99 and 1.00. The powers obtained for the exponential curves range between 0.98 and 1.01. We may therefore conclude that the differential spatial displacement discrimination thresholds for the three-blob alignment and the two-blob separation discrimination tasks are a constant fraction of their spatial scale parameters, at least for blobs with spreads larger than approximately 2 min of arc (and, in case of the three-blob alignment task, for a separation between the outer two blobs of 24 times the blob spread or resolution parameter).

For blobs with spreads smaller than 2 min of arc the differential spatial displacement acuity thresholds rise. This is probably a result of the fact that the resolution parameter of the blobs (their spatial spread) is no longer large compared to the blur function of the eye. In this case, the just noticable differential spatial displacement will be limited by the (optical and neural) pointspread function of the eye rather than by the resolution parameter of the blobs.

EXPERIMENT II: Determination of three-blob alignment acuity and two-blob separation discrimination as a function of eccentricity in the visual field.

At each eccentricity contrast detection thresholds were determined (by means of a staircase method) for blobs centered on the horizontal meridian. This was done at the start of each run of the three-blob alignment and the two-blob separation discrimination task. We found that the contrast detection thresholds remained constant during the sessions and were reproduced in separate sessions.

The differential spatial localization experiments were performed at threshold luminance contrast (contrast level at which 80% of the presentations is seen). As a result, in about 60% of the presentations no answer could be obtained, probably because one more blobs were

subthreshold.

It is well-known that the periphery is strongly susceptible to the effects of practice (Fendick and Westheimer, 1983; Frisen and Glansholm, 1975; McKee and Westheimer, 1978; Johnson and Leibowitz, 1974; Saugstad and Lie; 1964; Westheimer, 1982). However, we found no appreciable change in performance after approximately 300 presentations for each stimulus condition. Therefore, we assume that learning effects play no significant role in our experiments.

The differential spatial displacement discrimination thresholds for the three-blob alignment and the two-blob separation discrimination tasks as a function of eccentricity in the visual field and with the spread of the blobs as a scale parameter are shown in respectively Figs. 3 and 4. The three-blob alignment stimuli were oriented along the vertical (i.e. orthogonal to the horizontal meridian). This was done to assure that they were everywhere tangent to the isopters (i.e. along the direction in which the variation in spatial visual acuity is supposed to be minimal). The two-blob separation discrimination stimuli were oriented either parallel to the vertical or along the horizontal. All stimuli were centered on the horizontal meridian. We adopted the eccentricity of the midpoint of a stimulus configuration as the "effective eccentricity" of the entire stimulus configuration.

The results, depicted in Figs. 3 and 4, show that the variation of three-blob alignment accuracy with the effective eccentricity in the visual field is generally larger than the variation of two-blob discrimination accuracy. For both discrimination tasks the 128' condition has generally the largest threshold values (with the exception of the results of the three-blob task in the nasal field of subject A.T.) while the variation of the thresholds across the visual field is minimal for this condition. Thus, for large values of the blur parameter the visual system is nearly homogeneous for both spatial discrimination tasks.

At 0° eccentricity the thresholds for both spatial discrimination tasks strictly increase with an increasing blur parameter of the stimulus pattern. Generally, this is also the case for thresholds determined at larger eccentricities, although in some cases the reversed condition was found (e.g. the 8.06' condition for both subjects in the three-blob

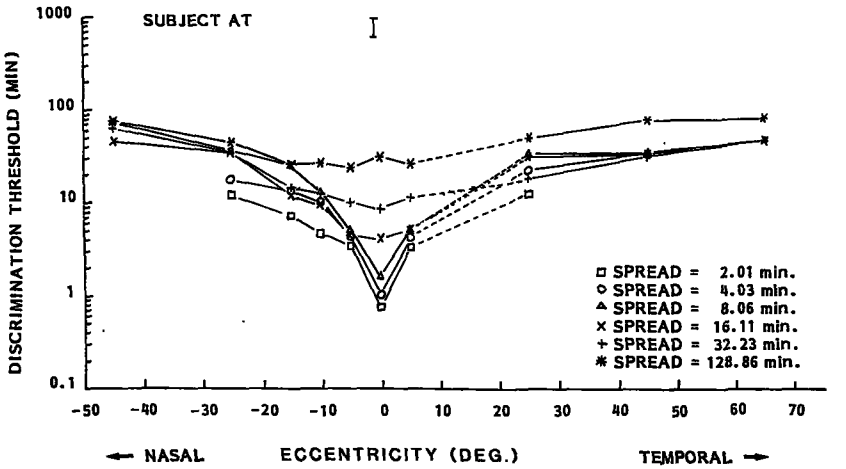

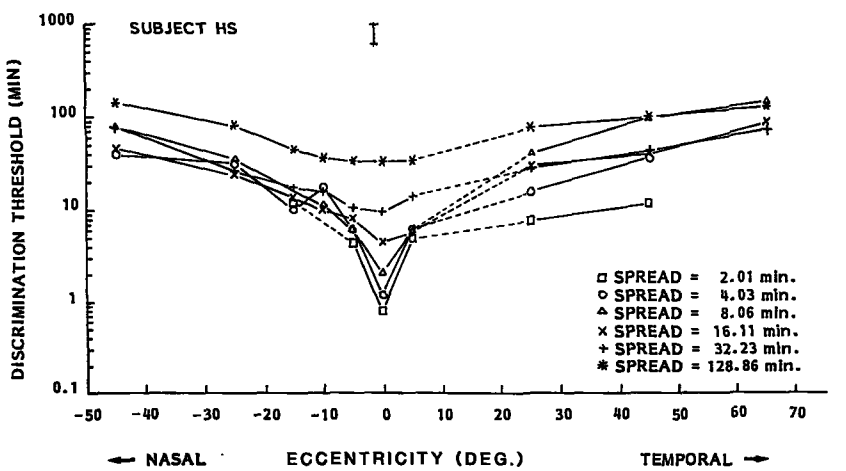

Figure 3. Differential spatial displacement discrimination thresholds for the three-blob alignment task as a function of eccentricity in the visual field and for different values of the blur parameter of the blobs.

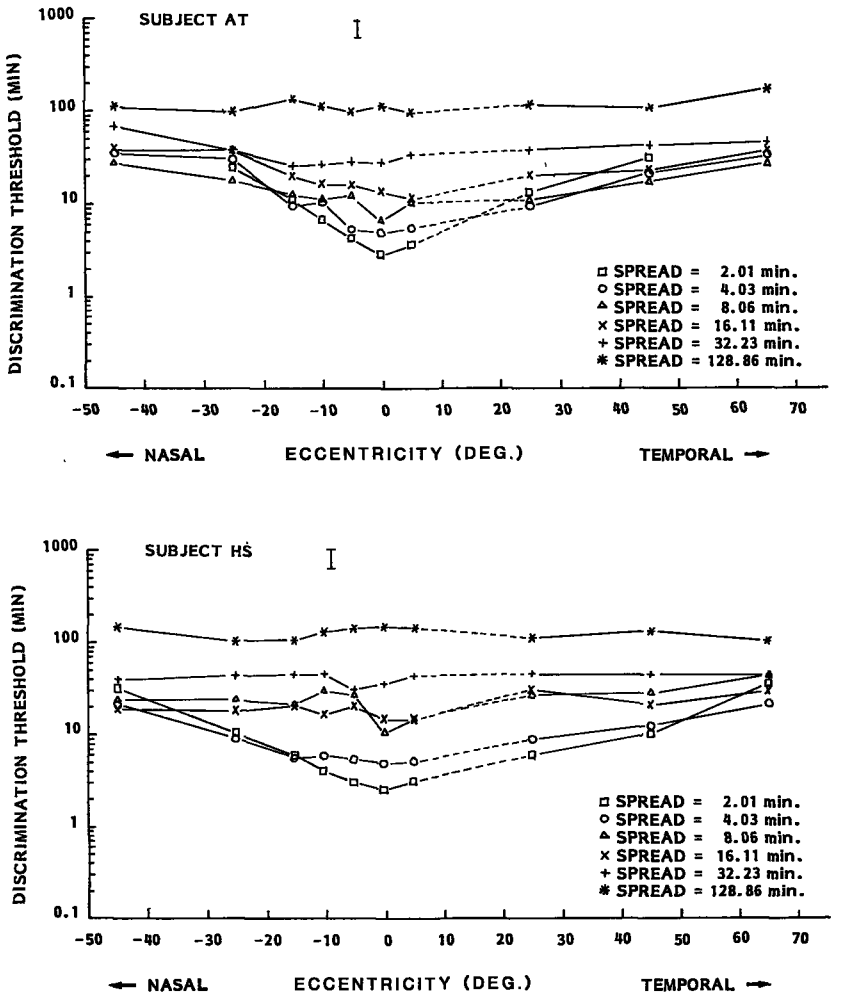

Figure 4. Spatial separation discrimination thresholds for the two-blob discrimination task as a function of eccentricity in the visual field and for different values of the blur parameter of the blobs.

alignment task and the 2.01' condition for both subjects in the two-blob discrimination task). The relative foveal decrease in discrimination accuracy (i.e. the increase in the thresholds) with an increasing blur parameter is of the same order of magnitude for both tasks. Figure 3 shows that the thresholds for the three-blob task tend to near a common upper limit in the far periphery. Convergence to a common upper limit is slower for the two-blob discrimination thresholds.

Subject H.S. had great difficulties performing the three-blob alignment task at 10° in the nasal visual field. This is reflected in the lack of data and the hump around -10° for some curves in Fig. 3. This subject reported that he had no difficulties in distinguishing three clearly resolved blobs, but he was unable to comment on their spatial order. At this eccentricity he had no problems in performing the two-blob acuity measurements (Fig. 4). This loss of ability to determine the spatial order of the blobs in the three-blob alignment task was also found in the far periphery of both subjects. This is the cause of the lack of the data on the 2.01' and 4.03' conditions in the far periphery. For these conditions the subjects were not only unable to determine the spatial order of the blobs but they noticed more blobs than the number that was actually presented (often as many as 7 or 8 blobs were seen on the presentation of a three-blob alignment stimulus).

SCALING THE RESULTS.

MB-scaling.

In order to be able to compare the performance of the visual system across eccentricities and stimulus blur parameters we applied a scaling to the differential spatial displacement discrimination thresholds of both tasks. The results of Experiment I indicate that the foveally determined differential spatial displacement discrimination thresholds for geometrically similar stimuli are independent of the absolute extent of these stimuli when scaled with their corresponding blur parameters. We will now investigate whether this scale invariance is valid at all

eccentricities in the visual field.

Several studies (Cowey and Rolls, 1974; Danile and Whitteridge, 1961; Drasdo, 1977; Rolls and Cowey, 1970; Whitteridge and Daniel, 1961) have shown that the increase of the minimal angle of resolution with retinal eccentricity follows the reciprocal of the cortical magnification factor M. This factor M was defined as the linear extent of primary (striate) visual cortex to which 1 deg of visual angle projects. In this section we will adopt the eccentricity of the location of the midpoint of a stimulus pattern as the eccentricity that characterizes the location of the entire stimulus pattern. We will refer to this eccentricity as the "effective eccentricity". Suppose that differential spatial displacement discrimination thresholds and "standard acuity" (or resolution) thresholds scale in a similar way with retinal eccentricity. Then we expect that the thresholds for the two-blob separation discrimination and the three-blob alignment acuity tasks will be nearly independent of the effective eccentricity of the stimuli when they are multiplied with the corresponding estimates of M.

Figs. 5 and 6 represent the thresholds as depicted in Figs. 3 and 4 after scaling with the blur parameter of the stimulus pattern and with Drasdo's prediction of the cortical magnification factor (based on his estimates of the ganglion cell receptive field density; see: Drasdo, 1977, formula (1)). In the sequel we will refer to this type of scaling as "MB-scaling" (cortical magnification factor and blur parameter scaling).

As was expected from the results of Experiment 1, the thresholds for both tasks coincide at 0° after scaling. However, this scale invariance is lost immediately outside the vertical meridian. Except for stimuli with blur parameters larger than approximately 8 min of arc and presented in the near periphery the performance of the visual system in the three-blob discrimination task is nearly independent of eccentricity after scaling. The scaled thresholds generally decrease (i.e. the relative spatial displacement discrimination accuracy increases) with increasing blur parameters of the stimuli. For stimuli with blur parameters larger than approximately 8 min of arc scaled thresholds increase with decreasing eccentricity in the near periphery. This decrease in relative accuracy is greatest for the stimuli with the largest blur parameters. In case of the

MB SCALING

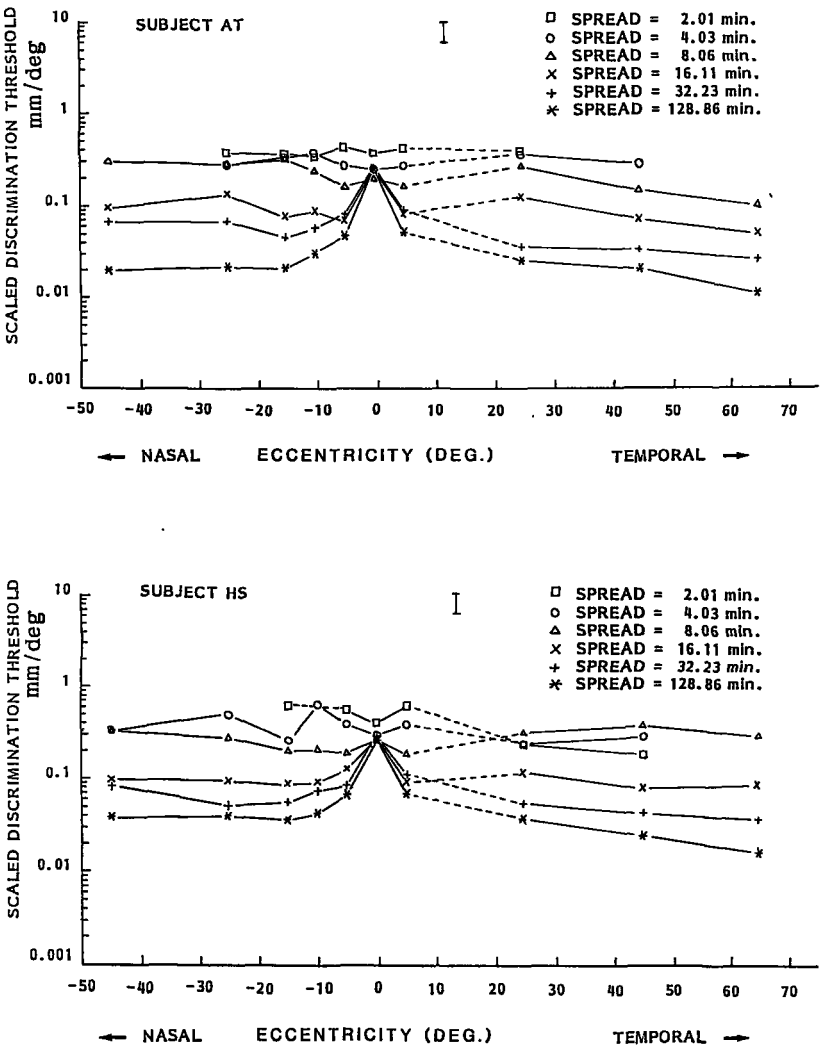

Figure 5. The three-blob alignment discrimination thresholds from Figure 3 after the application of the MB-scaling procedure and expressed in mm extent on the visual cortex per degree of the visual field.

MB SCALING

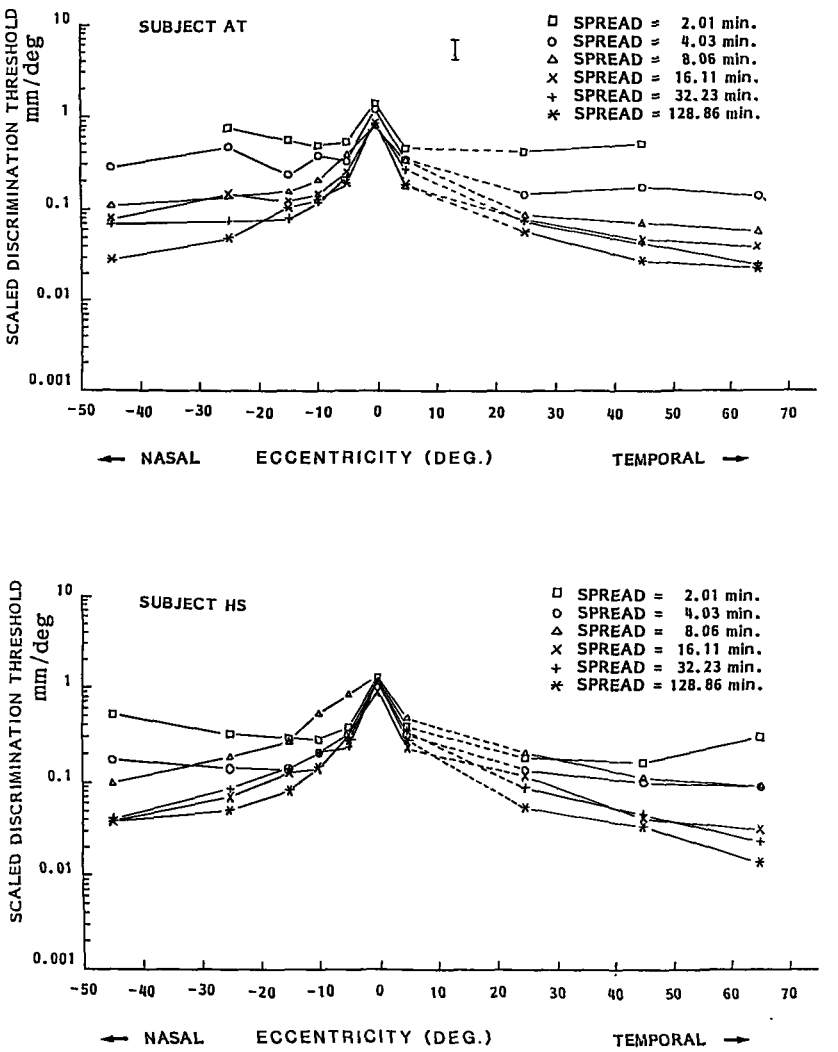

Figure 6. The two-blob separation discrimination thresholds from Fig. 4 after the application of the MB-scaling procedure and expressed in mm extent on the visual cortex per degree of the visual field.

two-blob discrimination task (Fig. 6) we notice a larger variation of the scaled discrimination thresholds with eccentricity in the near periphery. For this task all scaled thresholds increase with decreasing eccentricity in the near periphery. The slow decrease of the scaled threshold values for the two-blob task with increasing eccentricity in the far periphery is probably due to an overestimation of the cortical magnification factor M. Drasdo's scaling formula is only valid over a limited range of eccentricities while we applied it across the entire visual field. Therefore, this is probably merely a manifestation of the non-isotropy of the cortical magnification factor.

Levi et al. (1985) propagated the use of different scaling formulae for tasks that are assumed to involve either cortical or retinal processing. Our results do not change significantly when we rescale our data with their formulae. We merely notice a somewhat less pronounced decrease in accuracy for the near peripheral results of the two-blob discrimination task when their retinal scaling formula was applied.

C-scaling.

As noted before, after the application of MB-scaling the three-blob alignment acuity thresholds for stimuli with blur parameters larger than approximately 8 min of arc and presented in the near periphery show relatively large variations with eccentricity whereas the thresholds for this task and for the other conditions are nearly independent of eccentricity. This fact and the sudden loss of blur-scale invariance outside the vertical meridian both seem to indicate that our choice of the scaling parameters may be inappropriate. Therefore, we will scale the results of Figs. 3 and 4 anew, this time adopting a new definition for the effective eccentricity of a stimulus pattern. For the two-blob separation discrimination stimuli we will use the sum of the eccentricity of the midpoint of the stimulus configuration and the angular value of the spread of the blobs as the effective eccentricity that characterizes the performance of the visual system. For a three-blob alignment stimulus we will adopt the absolute eccentricity of the two most remote blobs (i.e.

the blobs with the largest eccentricity) as the (effective) eccentricity characterizing the location of the entire stimulus pattern. The difference of the value of the cortical magnification factor M resulting from the present definition of the effective eccentricity and the one resulting from the definition used in the previous section will be relatively small for stimuli with small blur parameters or stimuli that are located in the far periphery. However, for stimuli with large blur parameters and stimuli located in the near periphery this difference will be relatively large. Note that the separate effects of total stimulus extent and eccentricity in the visual field are both taken into account by our present choice of the effective eccentricity of the stimulus pattern.

We adopt the following approximate relation between the "cortical magnification factor" M and the effective eccentricity E of the stimulus pattern:

$$M(E) = M_0/(1.0 + 3.0*E^2/E_{\frac{1}{2}}^2)^{\frac{1}{2}}$$

where M_0 is the value of M at the foveal projection in mm/deg, E is the effective eccentricity expressed in degrees and $E_{\frac{1}{2}}$ is the eccentricity in degrees at which M equals half of the value at the fovea. The rationale for the adoption of a second order scaling relation is that it has a continuous first derivative at the fovea whereas a first order approximation (like the one used by Levi et al., 1985) has a foveal discontinuity in its first derivative. The requirement of a continuous first derivative seems reasonable when we relate the scaling relation to its probable neuroanatomical equivalent: the ganglion cell density function. Similar to the increase of the minimal angle of resolution with retinal eccentricity we will assume that the differential spatial displacement discrimination thresholds are proportional to the reciprocal of the cortical magnification factor M. We can obtain two individual estimates for $E_{\frac{1}{2}}$ from the results of the 2.01', 4.03' and 8.06' conditions for stimuli with their midpoint at 0° (i.e. oriented along the vertical meridian). By taking the mean of these two estimates we find that $E_{\frac{1}{2}}$ equals 0.8±0.2 deg for subject HS and 1.4±0.3 deg for subject AT. An estimate for M_0 can be obtained by calculating the area of a part of the striate cortex, using our estimate of the magnification factor M and equating this result with corresponding estimates that can be made from

the results of other researchers. This is done as follows. A good approximation of the data of Cowey and Rolls (1974) is given by

$$M(E) = M_0/(1.0 + E/E_{\frac{1}{2}})$$

where all parameters have the same meaning as in the formula described above; M_0 = 15.1 mm/deg and $E_{\frac{1}{2}}$ = 1.22 deg. Integrating both estimates of M from 0° to 60° eccentricity and equating the results we find that M_0 equals 19±4 mm/deg for subject AT and 31±6 mm/deg for subject HS. The choice of the upper integration limit (60°) is of course rather arbitrary. However, we found that the results obtained by varying the upper boundary between 20° and 180° were within the error range of our estimates. Thus, we feel that our present results may provide a useful approximation for M_0.

The estimated value of $E_{\frac{1}{2}}$ for subject HS (0.8±0.2 deg) is consistent with other recent estimates of this parameter for cortical magnification and for a variety of hyperacuity tasks (see Levi et al., 1985). The value of $E_{\frac{1}{2}}$ for subject AT is large compared to these recent estimates (although it is within the error range of some of the estimates mentioned in Table 1 of Levi et al., 1985).

Using a value of 0.8 for $E_{\frac{1}{2}}$ Levi et al. (1985) showed that Vernier acuity is as good in the periphery as it is centrally when scaled with the cortical magnification factor. Our present estimates of $E_{\frac{1}{2}}$ and M_0 are of course not very accurate. However, the values of M computed with the estimates of these parameters for both of our subjects differ typically less than 10%. We will scale our results with the estimate for M derived from the results of subject HS as his value of $E_{\frac{1}{2}}$ corresponds best to the value that was adopted by Levi et al. (1985) and that resulted in a scaling which closely fitted their results. Note that the specific value chosen for M_0 is not critical as we are only interested in the relative change of M with eccentricity. Thus, we get the following expression for M(E):

$$M(E) = 31.0/(1.0 + E^2/0.22)^{\frac{1}{2}}.$$

In the sequel we will refer to this type of scaling as "C-scaling" (as this scaling is thought to be induced by the effects of cortical processing).

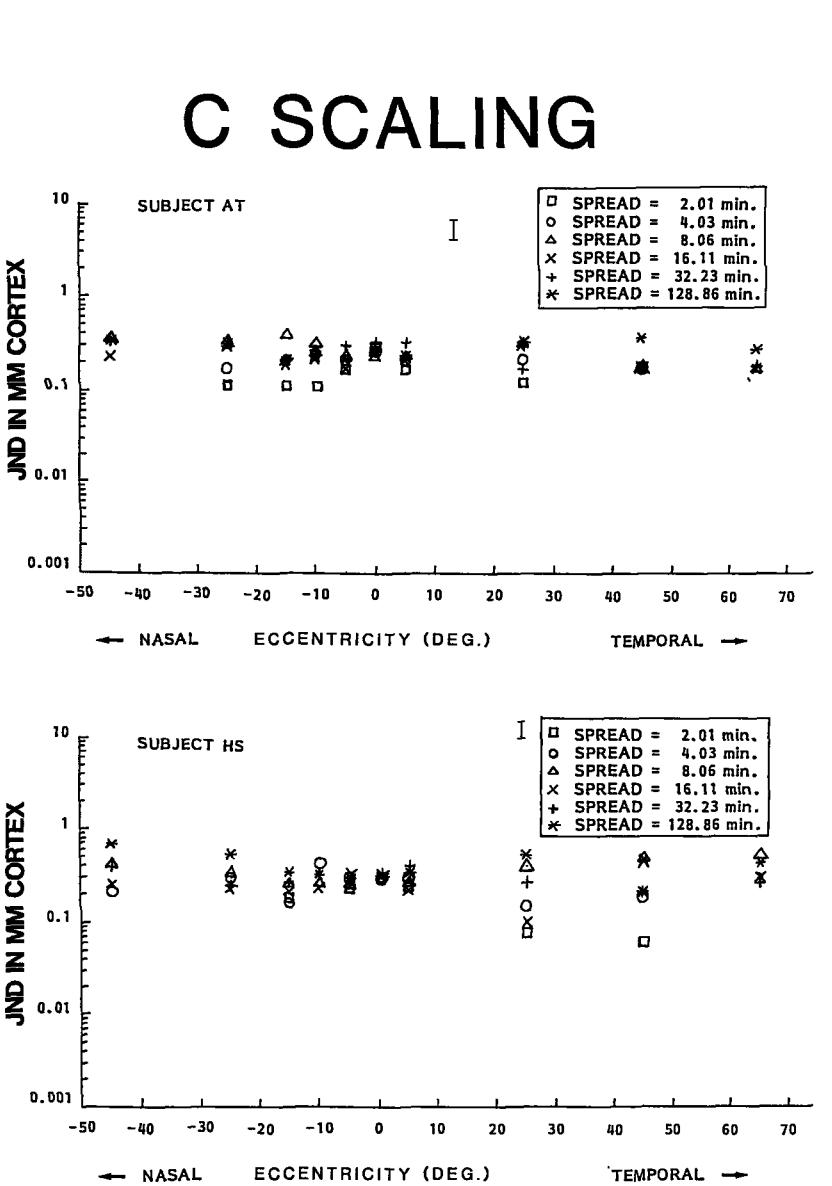

Figure 7. The three-blob alignment discrimination thresholds from Fig. 3 after the application of the C-scaling procedure and expressed in mm extent on the visual cortex.

C SCALING

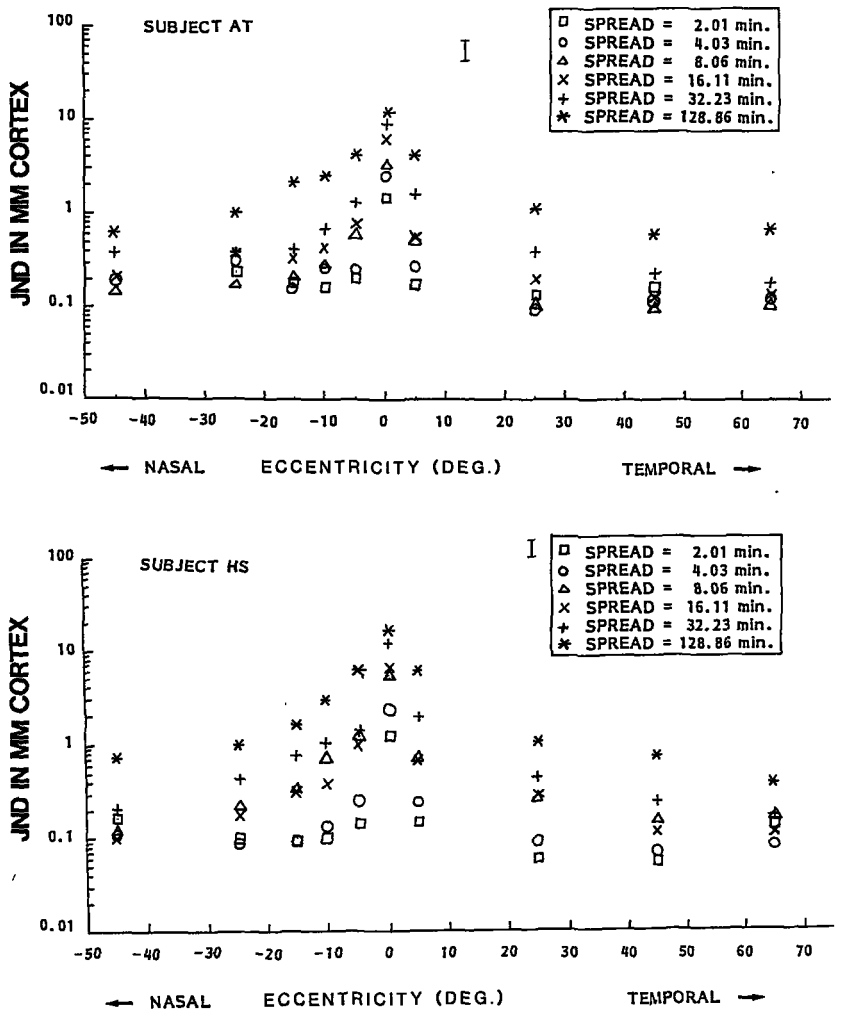

Figure 8. The two-blob separation discrimination thresholds from Fig. 4 after the application of the C-scaling procedure and expressed in mm extent on the visual cortex.

We replotted the data of Figures 3 and 4 in terms of cortical distances. The results are shown in Figures 7 and 8 respectively. All thresholds are expressed in mm extent on the primary visual cortex. The thresholds are depicted as a function of the eccentricity (in the visual field) of the midpoint of the stimulus pattern. These data were obtained by calculating for each stimulus configuration the appropriate effective eccentricity and multiplying the corresponding discrimination thresholds by the estimate of M derived from the abovementioned C-scaling formula.

Figure 7 shows that the functions from Figure 3 that describe the alignment discrimination thresholds for different values of the blur parameter of the stimuli and that are widely disparate in the near periphery collapse to a more or less unitary function after C-scaling (i.e. at each eccentricity the C-scaled alignment discrimination thresholds vary over less than one decade when the blur parameter of the stimulus configuration varies over almost two decades). This function appears to be approximately constant across the visual field. These results show that C-scaled three-blob alignment discrimination for geometrically similar stimuli is (i) independent of the blur parameter of the stimuli and (ii) as good in the periphery as it is foveally.

Figure 8 shows that C-scaling is of no avail to reduce the disparity in the functions from Figure 4 (i.e. the results of the two-blob discrimination task). At each eccentricity in the visual field the scaled thresholds generally increase with an increase in the value of the blur parameter. For a constant value of the blur parameter we notice a sharp increase in the thresholds in the near periphery. The C-scaled two-blob separation discrimination thresholds vary over more than a decade, both across the visual field and across the range of applied blur parameters (the maximum variation in the entire data set of each subject extends over more than two decades). Thus, these results suggest that C-scaling may not be appropriate for the two-blob separation discrimination task.

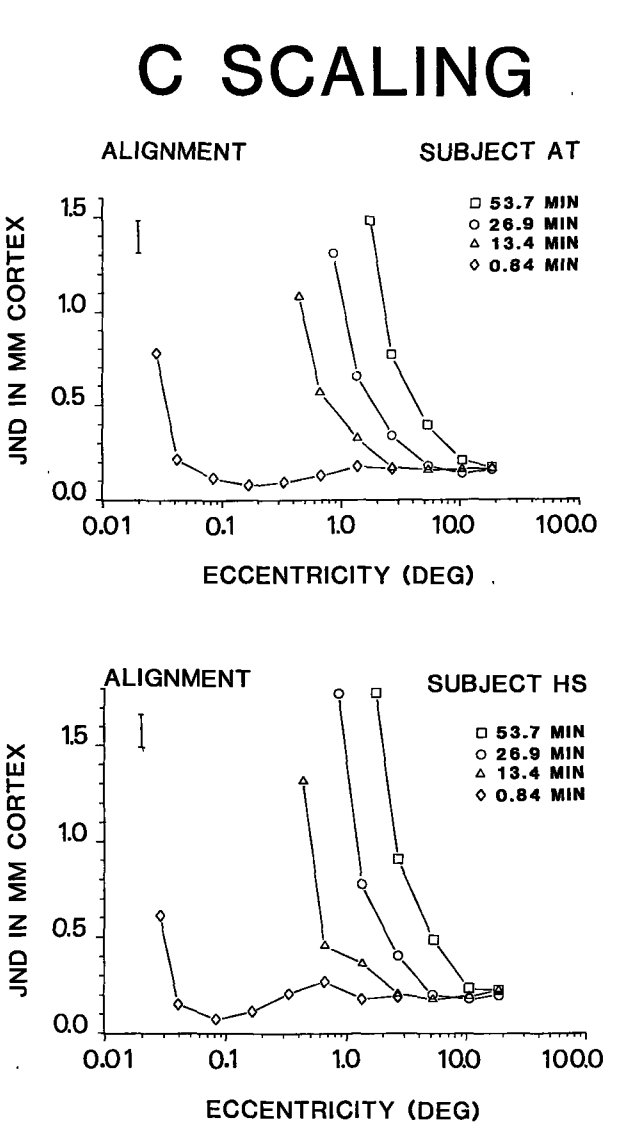

Figure 9. The C-scaled three-blob alignment discrimination thresholds for stimulus presentations along the vertical meridian as a function of the eccentricity of the outer two blobs and for four different values of the blur parameter (results from Toet et al., 1987).

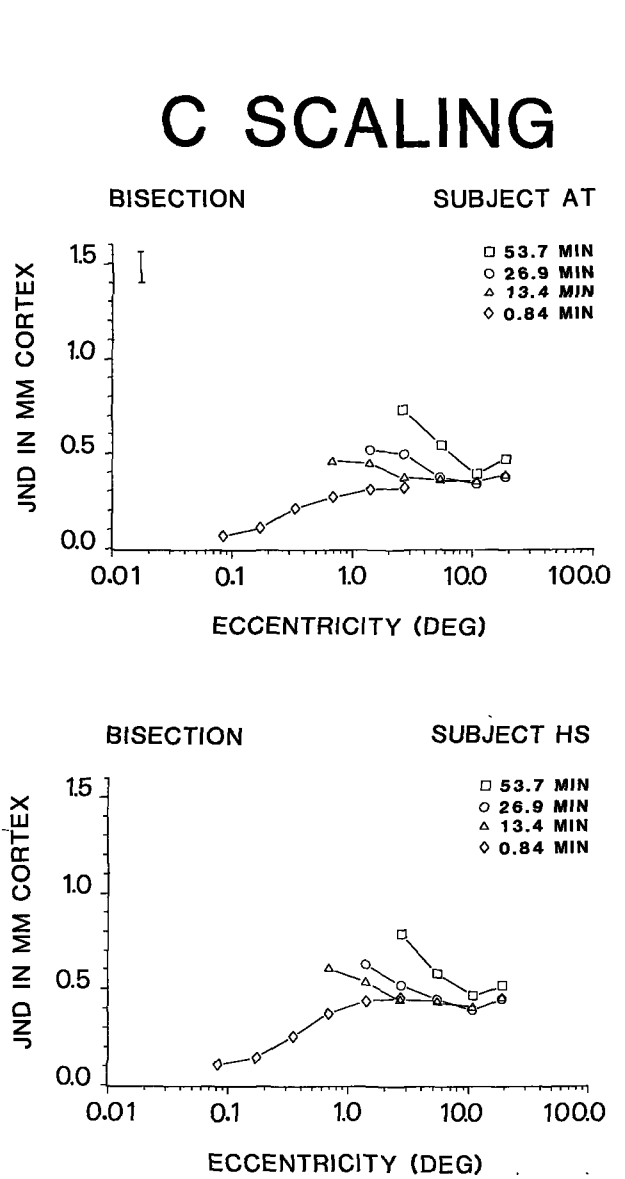

Figure 10. The C-scaled three-blob bisection discrimination thresholds for stimulus presentations along the vertical meridian as a function of the eccentricity of the outer two blobs and for four different values of the blur parameter (results from Toet et al., 1987).

C-scaling applied to earlier results.

The stimuli we used in our present three-blob alignment discrimination experiments were all geometrically similar (i.e. the ratio of the distance between the outer two blobs and their blur parameter was equal for all stimuli). In a previous paper we determined differential spatial displacement discrimination thresholds for the three-blob alignment task and a three-blob bisection task as a function of the separation of the outer two blobs with the blob spread as a spatial (blur) scale parameter (see Figures 3 and 4 from Toet et al., 1987). All stimuli were oriented along the vertical meridian. As in Experiment I, we found that the alignment discrimination thresholds are a constant fraction of the blur parameter of the stimulus pattern for a constant ratio of this parameter and the separation of the outer two blobs (i.e. for geometrically similar stimuli at decreasing levels of resolution). Moreover, we showed that this fraction depends only on the ratio of the separation of the outer two blobs and the blur parameter. However, the results of the C-scaling procedure seem to indicate that the accuracy of differential spatial displacement discrimination is completely determined by the eccentricity of the most remote blobs. In this case our previous findings may reflect a mere side effect of the geometrical scaling procedure that was applied to these stimuli. That this is not the case can be seen from Figures 9 and 10. These Figures show the data from Toet et al. (1987) expressed in mm on the primary visual cortex (produced by C-scaling) and plotted as a function of the effective eccentricity of the stimulus pattern. If the discrimination thresholds only depend on the effective eccentricity the data points for stimuli with the same effective eccentricity should coincide, independent of the value of the blur parameter. Figures 9 and 10 show that this is not the case. The curves describing the thresholds for stimuli with the same value of their blur parameter only tend to near a common limit for stimulus extents that are large relative to this parameter.

In the sequel we will refer to the ratio of the distance between the outer two blobs of a three-blob (alignment- or bisection-) stimulus and its blur parameter as the "relative extent" of the stimulus. Figures 11

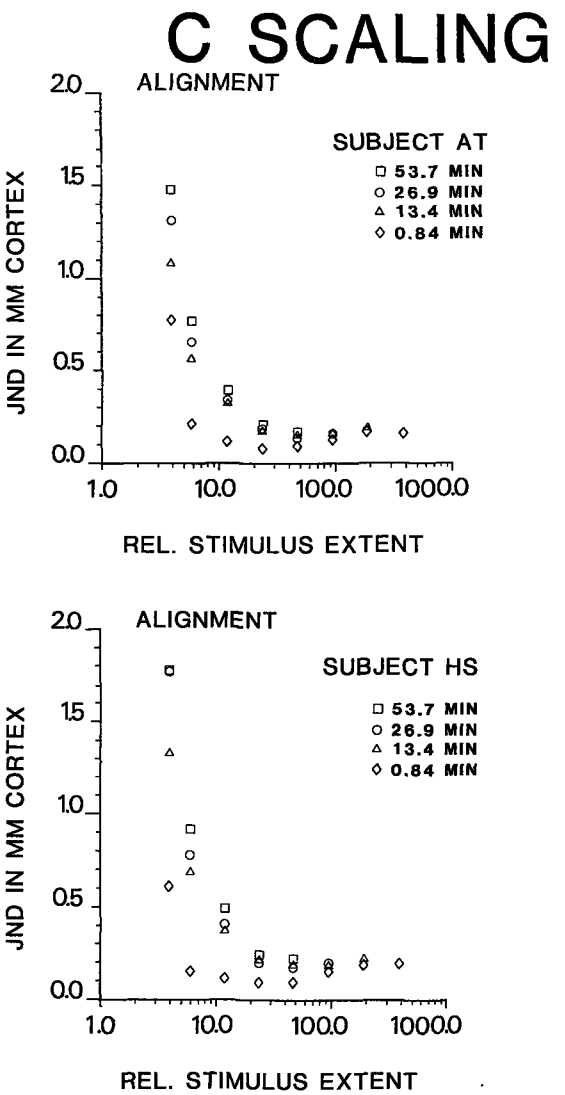

Figure 11. The C-scaled three-blob alignment discrimination thresholds from Fig. 9 as a function of the relative stimulus extent (i.e. the stimulus extent divided by the blur parameter of the blobs).

C SCALING

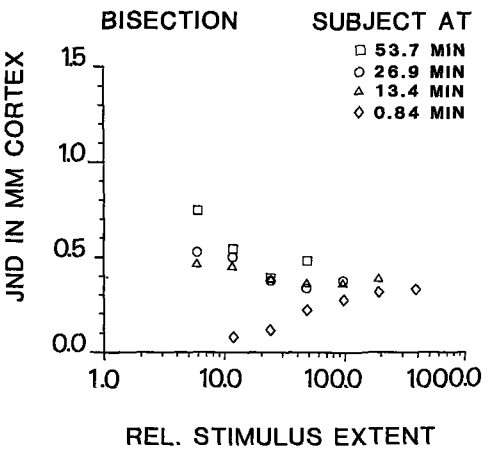

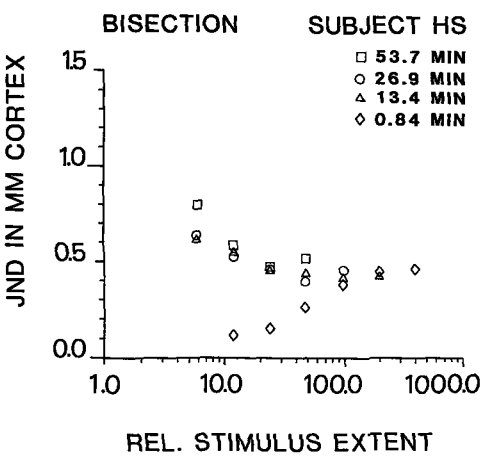

Figure 12. The C-scaled three-blob bisection discrimination thresholds from Fig. 10 as a function of the relative stimulus extent (i.e. the stimulus extent divided by the blur parameter of the blobs).

and 12 show the data from Figures 9 and 10 as a function of the relative stimulus extent. From these Figures we see that stimuli with the same relative extent and a blur parameter larger than 0.84' produce identical discrimination thresholds independent of the value of the blur parameter when their relative extent is larger than approximately 10. Moreover, these Figures show that the thresholds near a common and approximately constant (in case of the alignment task about 0.15 mm for our choice of M_0 = 31 mm/deg and about 0.07 mm for M_0 = 15 mm/deg ; see Cowey and Rolls, 1974) limit for increasing values of the relative stimulus extent. For values of the relative stimulus extent larger than approximately 20 the ratio of the total extent of the stimulus and its corresponding differential spatial displacement discrimination threshold is approximately constant. We find a ratio of appproximately 1/70 for the alignment task and about 1/30 for the bisection task. These ratios are the same as those determined by Levi et al. (1985) for similar tasks. They are also comparable to the ratio 1/40 found by Hirsch and Hylton (1982, 1985) for a spatial-frequency discrimination task. For relative stimulus extents smaller than approximately 20 the thresholds are no longer a constant fraction of the total stimulus extent.

From the foregoing we conclude that the three-blob displacement discrimination acuity is a function of both (i) the effective eccentricity and (ii) the relative extent of the stimulus pattern.

R-scaling.

The results of the previous section indicate that C-scaling may not be appropriate in case of the two-blob separation discrimination task. As Levi et al. (1985) suggested, retinal and cortical processes may impose different limits on psychophysical performance. Thus, while some (e.g. standard acuity- or resolution-) tasks may be limited primarily by optical (e.g. the blur function of the eye) or retinal (e.g. cone density) factors, other tasks may be primarily limited by cortical processing (Westheimer, 1982; Barlow, 1979, 1981). As we already noted in the Introduction, it seems likely that the limits set by retinal factors will

have a more pronounced effect on the results of the two-blob task than on those of the three-blob task. The former is limited by the accuracy with which two different flux estimates originating from neighbouring points of the retina can be discriminated, whereas the latter is limited by the precision with which the relative position of different features in the visual field can be determined.

In this section we will investigate the influence of retinal limitations on the performance of subjects in the differential spatial displacement discrimination tasks presented in this paper. We expect that the two-blob separation discrimination thresholds will scale with the extent of the receptive fields that respond most actively to their presentation. As we remarked before, the nature of our stimuli is such that we expect that only receptive fields with spatial dimensions of the order of those of the retinal projections of the blobs will make a significant contribution to their detection when they are presented at detection threshold luminance contrast (this is intuitively clear from the consideration of the Schwarz-inequality and the convolution product of the spatial contrast profile of a blob and the receptive field weighting function for a range of values of the spatial scale parameter of this function). Thus, we may adopt the spread of a blob as a measure for the extent of the retinal processing units involved in its detection.

Merely scaling the results of Figure 4 with the blur parameter of the stimuli is clearly of no avail to reduce the disparity between the different curves. Only the data points for the stimuli that have a midpoint located at 0° will coincide after this scaling has been applied. If we interpret the results of Figure 4 in terms of retinal factors we can regard this disparity as a result of the inhomogeneous structure of the visual field. We will therefore scale the results of the two-blob separation discrimination and the three-blob alignment acuity tasks as follows. Thresholds determined for stimuli with an effective eccentricity at which the smallest receptive fields have an angular diameter that is smaller than the angular size of the blur parameter will be scaled with the blur parameter of the stimulus itself. The thresholds for all other stimuli will be scaled with the diameter of the smallest receptive fields present at the effective eccentricity of those stimuli. In the sequel we

will refer to the thus defined scale parameter as the "effective blur parameter". The rationale of this choice is our assumption that the two-blob separation discrimination accuracy will scale with the spatial extent of the receptive fields that respond most actively to their presentation. As argued before, the angular dimensions of these receptive fields will be comparable to the blur parameter. When all receptive fields present at a certain eccentricity have a diameter larger than the blur parameter of the stimulus the most actively responding ones will be those with the smallest diameter. Thus, the blur parameter of the stimulus pattern is only valid as a scale parameter when detector units with a size that is comparable to this blur parameter are (abundantly) present over the entire area of the stimulus pattern. Otherwise the spatial discrimination accuracy will be limited by the smallest detector units that are distributed over the entire stimulus area. In the sequel we will refer to this scaling procedure as "R-scaling" (as this scaling is thought to reflect the effects of retinal limitations). We assume that the diameter of the smallest receptive fields that are present at a certain eccentricity E is E/100 (from the value of acuity, e.g. Koenderink et al., 1978c). Note that we rather arbitrarily compare the diameter of the receptive fields with the blur parameter of the blobs in our definition of the effective blur parameter. However, as both (a) the fraction of the spatial contrast profile of the blobs that is used in the detection process and (b) the proportionality constant in the relation between the eccentricity and the diameter of the smallest receptive fields are only known within an order of magnitude we feel that this is no serious restriction to our argument.

Figure 13 shows the results of the application of R-scaling to the two-blob separation discrimination thresholds from Figure 4. At each eccentricity the R-scaled separation discrimination thresholds vary over less than one decade when the blur parameter of the blobs varies over almost two decades. The variation in the thresholds across the visual field is also over less than a decade. The largest variation is found for the 8' condition near 10° nasal for subject HS. As we noticed before, this subject has some pecularities in his functioning at that particular eccentricity. Thus, it appears that the curves from Figure 4 that describe the two-blob separation discrimination thresholds for different values of

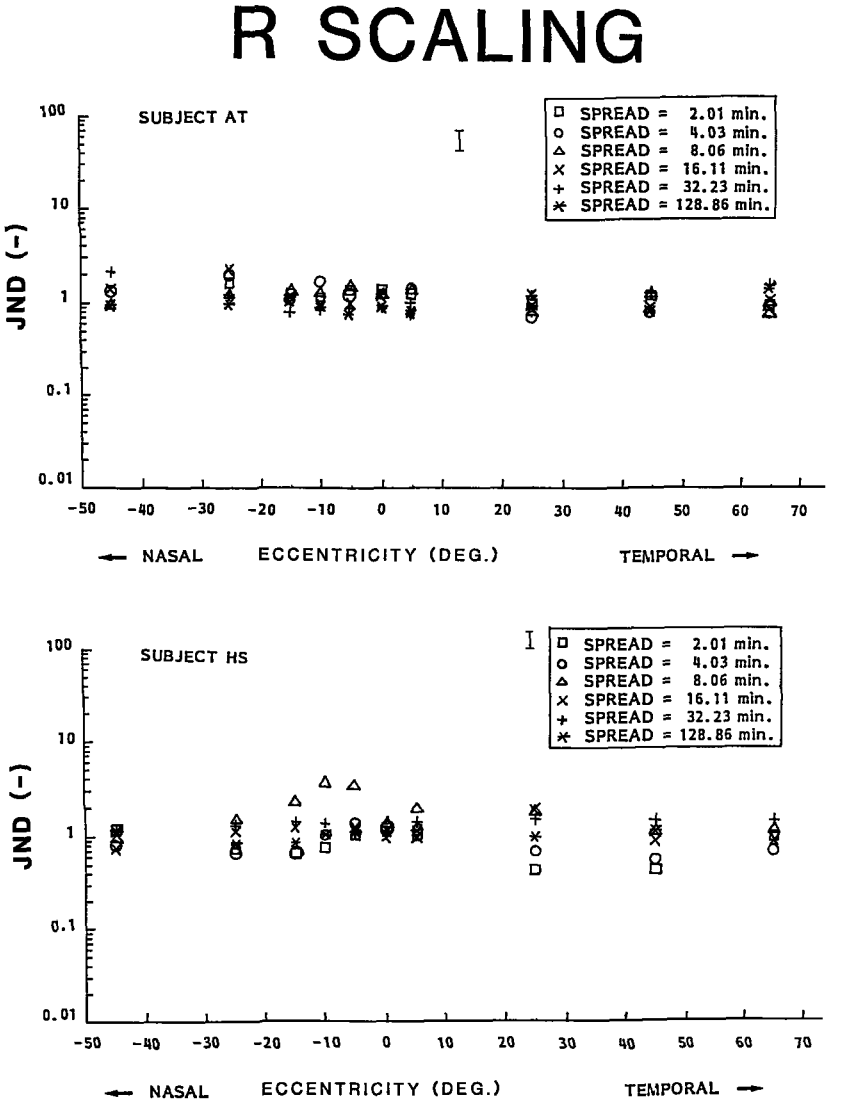

Figure 13. The two-blob separation discrimination thresholds from Fig. 4 after the application of the R-scaling procedure.

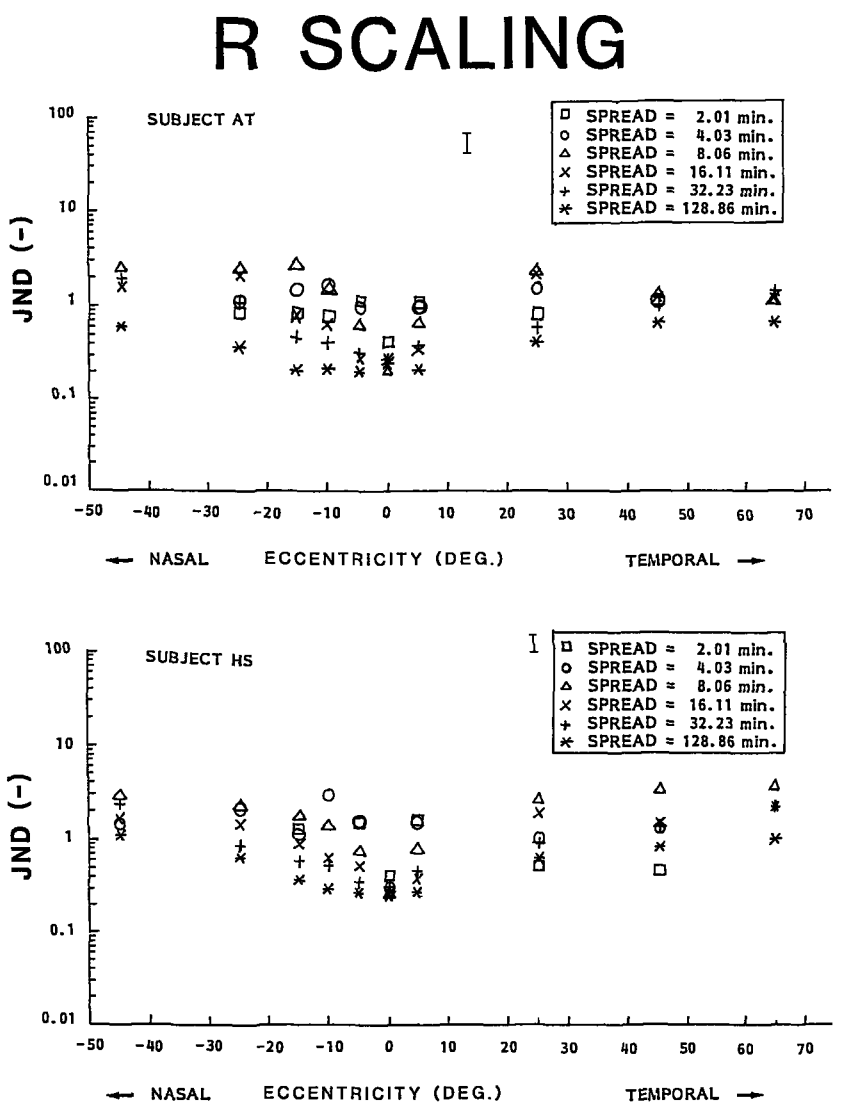

Figure 14. The three-blob alignment discrimination thresholds from Fig. 3 after the application of the R-scaling procedure.

the blur parameter of the stimuli and that are widely disparate in the near periphery collapse to a more or less unitary function after R-scaling. This function appears to be approximately constant across the visual field. These results show that R-scaled two-blob separation discrimination is (i) independent of the blur parameter of the blobs and (ii) as good in the periphery as it is foveally.

Figure 14 shows that R-scaling only partly reduces the disparity in the functions from Figure 3 (i.e. the results of the three-blob alignment discrimination task). As expected from the results of Figure 2 (Experiment I) the discrimination thresholds at 0° coincide after R-scaling. At all other eccentricities in the visual field and for values of the blur parameter larger than approximately 8 min of arc the scaled thresholds generally decrease with an increase in the value of the blur parameter. Although the sharp foveal dip in the curves from Figure 3 and for blur parameters smaller than approximately 10 min of arc is considerably reduced we still notice a decrease in the R-scaled thresholds in the near periphery. The R-scaled three-blob alignment discrimination thresholds vary over more than a decade, both across the visual field and across the range of applied blur parameters. Thus, these results suggest that R-scaling may not be appropriate for the three-blob alignment discrimination task.

DISCUSSION.

Frisen and Glansholm (1975) stressed the need to include an optical blur factor whenever results from studies on peripheral vision, using external target stimuli, are to be analyzed in terms of retinal architecture. Lack of exact knowledge of this factor hinders a meaningful analysis of this kind. This is clearly demonstrated by the results of Enoch et al. (1984), who determined two-dot orientation acuity as a function of retinal eccentricity for different degrees of stimulus blur. Their results are remarkably similar to our three-blob alignment discrimination results. However, their method of blurring the stimuli (with the use of ground glass plates) provides no exact blur parameters.

Moreover, they used high-contrast targets. Therefore, they had to restrict their conclusion to the statement that blur generally raises the spatial discrimination thresholds while the overall shape of the curves describing the spatial discrimination thresholds as a function of eccentricity remains similar. The same comments apply to the study of Levy-Schoen (1977). The results of her spatial discrimination experiments, as a function of eccentricity and stimulus size, show an increased homogeneity of the visual system for larger stimulus sizes. The same effect is demonstrated by our results. However, because Levy-Schoen's stimuli consisted of high-contrast line figures she had no control over the range of stimulated size-selective mechanisms. Therefore, it is not possible on the basis of her results to draw any further conclusions about the mechanisms that are used in the assessment of relative location.

In the experiments reported in this paper we used blobs with Gaussian spatial contrast profiles and Gaussian temporal envelopes presented at detection threshold luminance contrast. Because they are roughly bandlimited in the spatial frequency domain these stimuli are likely to activate only a small range of spatial frequency selective mechanisms. Thus, the spatial spread or blur parameter of the blobs provides us with a precise measure for the resolution of the stimuli. In case of foveal fixation we have shown that the differential spatial displacement discrimination thresholds for (i) the two-blob separation discrimination task and (ii) the three-blob alignment task and for stimuli that are geometrically similar are a constant fraction of the blur parameter. Immediately outside the fovea this scaling breaks down.

In the two-blob discrimination experiment the separation of the two blobs was at random oriented along the horizontal meridian or orthogonal to it. Therefore, our results probably confound to some extent differences in accuracy in either direction. However, the visual field is probably nowhere isotropic over the range of stimulus extents used in our experiments. Therefore, we do not believe that our results would change significantly if the separation of the two blobs had only been along the vertical (or, alternatively, if we had chosen a paradigm that allowed separate processing of the results from both stimulus-orientations).

Scaling our results with estimates of the cortical magnification factor (Drasdo, 1977; Levi et al., 1985) and the blur parameter of the stimuli (the MB-scaling procedure) revealed that the performance of the visual system is homogeneous for the three-blob task when the blur parameter of the stimuli is less than approximately 8 min of arc. After MB-scaling a decreased relative accuracy of spatial discrimination performance was found in the near periphery in case of (i) the three-blob task for stimuli with scale parameters larger than approximately 8 min of arc and for (ii) the two-blob task in general. The apparent superiority of the fovea over the periphery of the visual field, as far as spatial displacement discrimination is concerned (Westheimer, 1982), is no longer found after MB-scaling. Except for the three-blob task and blur parameters smaller than 8 min of arc it is even transformed into a relative inferiority for both spatial displacement discrimination tasks.

Because MB-scaling of our results shows (i) a decreased homogeneity of the performance of the visual system in the two- and three-blob tasks for an increasing value of the blur parameter and (ii) a sudden loss of blur-scale invariance outside the vertical meridian we felt that this type of scaling was inappropriate for these tasks. We therefore introduced the C-scaling procedure. We adopted a second order eccentricity-dependent size-scaling relation with only one free parameter ($E_{\frac{1}{2}}$). We furthermore assumed that the accuracy of the performance of the visual system is determined by the eccentricity of the most remote blobs of the stimulus configuration or the so-called effective eccentricity of a stimulus. The results obtained by applying the C-scaling procedure to the discrimination thresholds for geometrically similar stimuli in the three-blob alignment task suggest that the differential spatial displacement discrimination accuracy of the visual system is nearly independent of (i) the blur parameter and (ii) the effective eccentricity of the stimuli when the discrimination thresholds are expressed in terms of extent on the primary visual cortex. By C-scaling the results from an earlier experiment (Toet et al., 1987) we showed that the three-blob alignment discrimination accuracy depends mainly on the relative stimulus extent when expressed in terms of cortical distances[x)]

Our results show that C-scaling does not reduce the disparity in the two-blob results. Because it seems likely that these discrimination thresholds are primarily limited by retinal factors we introduced the R-scaling procedure which accounts for the effects of retinal inhomogeneity. The results obtained from the R-scaling routine indicate that the two-blob separation discrimination thresholds are a constant fraction of the spatial (blur) scale parameter of the detector units that are thought to respond most actively to their presentation or the so-called effective blur parameter. The results show that R-scaling does not completely reduce the disparity in the three-blob alignment discrimination thresholds (as determined for the different conditions).

Invariant features of contrast detection and spatial frequency discrimination tasks have resulted in models in which the retina is depicted as a self-similar detector array graded with respect to aperture size (Koenderink, 1977; Koenderink and van Doorn, 1978, 1982; Hartmann, 1982; Hirsch and Hylton, 1982, 1985; Burton et al., 1986). There is both psychophysical (Koenderink et al., 1978a-c) and electrophysiological (DeValois et al., 1982) evidence for a progressive loss of high- spatial frequency- (or, equivalently, small size-) selective mechanisms with increasing retinal eccentricity. Moreover, it has been demonstrated that the lower boundary of the spatial extent of the processing units present at a certain retinal location is proportional to the retinal eccentricity of that spot (Koenderink, 1978a-c). Thus, in terms of a scaled lattice model of spatial vision, progressive finer detector arrays are restricted to progressive smaller eccentricities. Therefore, it seems likely that spatial localization thresholds will only scale with the blur parameter of the stimuli for tasks that involve the localization of stimulus features within a retinal area in which the entire range of size-selective processing units is (abundantly) present. Thus, a stimulus with small-

x) It would be interesting to see whether the disparity in our present results can be further reduced by scaling the stimuli such that their cortical extent is a constant multiple of the spread of the smallest psychophysical hypercolumns thought to reside at the effective eccentricity of the stimulus. In this way one could try to produce stimuli that have images at the cortical lattice that are approximately geometrically similar.

sized features may extend over areas where there are no, or not enough, mechanisms that are optimally tuned to its detection. In this case the processing mechanisms will have to switch to the output of an array of detectors of larger aperture size (i.e. to the layer of detectors with the smallest aperture size that still covers the entire area over which the stimulus extends and still responds appreciably to the presence of the stimulus). This is the rationale for our adoption of the effective eccentricity as a scale parameter for the results of the three-blob task. Moreover, all stimuli with features smaller than the limit set by the aperture size of the finest detector array present at some eccentricity will be processed by the same detector array (which is in fact too coarse for optimal processing). Spatial localization thresholds can therefore no longer be expected to scale with the blur parameter of the stimuli. Therefore we introduced the effective blur parameter as a scale parameter for the results of our two-blob experiments. In this view, the increased homogeneity of the visual system for localization tasks involving stimuli with large scale parameters, as found in our experiments, is presumably due to the fact that the coarser sampling units extend to larger eccentricities (with the implicit assumption that the visual spatial localization function is uniform across the visual field). Plateaus of constant acuity as a function of retinal eccentricity and centred on the fovea have indeed been found for photopic resolution (Lie, 1980) and form identification (Levy- Schoen, 1977) tasks. However, there is no strict reason to expect isosensitivity plateaus in curves describing spatial discrimination thresholds as a function of eccentricity because the loss of small-sized feature detectors towards the periphery is gradual and because the visual system may also be functionally non-uniform across the visual field (Orban, 1985).

As already suggested by Hirsch and Hylton (1985) the visual system may use a single strategy to encode positional information independent of the level of resolution of the stimulus features. It merely has to adapt the size of its yardstick to the resolution or total extent of the stimulus pattern by means of an automatic scale-selection mechanism. Suppose that the scale-selecting mechanism chooses the sampling lattice such that the effective lattice spacing is roughly proportional to the

spatial scale of the measurement that has to be performed. Moreover, we will assume that the visual system determines relative distances by counting lattice points. In this case the absolute differential spatial displacement discrimination accuracy will be dominated by the effective spacing of the applied neural grid. However, the relative accuracy will remain constant. This may explain our results that (i) the three-blob alignment discrimination thresholds for geometrically similar stimuli presented along the vertical meridian and (ii) the two-blob separation discrimination thresholds are a constant fraction of the effective blur parameter (which is for the first kind of stimuli always equal to the actual blur parameter or the spread of the blobs). The Weber-law behaviour shown by our results for the alignment- and the bisection- discrimination thresholds as a function of the stimulus extent and for relative stimulus extents larger than approximately 20 is an indication for the fact that the effective resolution of the visual system scales with the stimulus extent over this range. In this view an equal amount of cortical area may be allocated for processing geometrically similar stimuli at different levels of resolution. This may explain our result that the three-blob alignment discrimination thresholds, expressed in mm extent on the primary visual cortex, are identical for geometrically similar stimuli with the same relative extent.

Our alignment discrimination results are in agreement with the results of Levi et al. (1985) who showed that Vernier acuity is as good in the periphery as it is centrally when scaled with recent estimates of the cortical magnification factor. The difference between the fall-off in relative localization acuity and the decline of standard acuity with eccentricity can be explained by the abovementioned scaled lattice model of spatial vision and is probably a result from the fact that resolution is primarily limited by retinal structure while position acuity is mainly limited by cortical processes.

In summary, our results show that the performance of the visual system in differential spatial displacement discrimination tasks becomes progressively more homogeneous for a progressive increase in the blur parameter of the stimuli. Scaling (i) our three-blob alignment results with the effective eccentricity and (ii) our two-blob separation

discrimination results with the effective blur parameter shows an impressive isotropy and blur scale invariance for the mechanisms mediating differential spatial displacement discrimination across the visual field. These results are all in favour of a scaled sampling lattice model of the visual system in combination with an automatic scale-selection mechanism (as proposed by Koenderink, 1978 and Hirsch and Hylton, 1985). The scale-selection mechanism is supposed to choose a lattice of sampling units with a quantization spacing (sampling unit aperture size) that is proportional to the resolution or the total extent of the stimulus.

Acknowledgements - The help of Mike van Eekhout, Henk Simons and Ad de Goffau, with the production of the necessary software, is greatly appreciated. We thank Dr. R.J. Watt and Dr. D.P. Andrews for kindly sending us a listing of their APE program. This work was supported by the Dutch Foundation for the Advancement of Pure Research (ZWO).

REFERENCES.

Andrews, D.P., Butcher, A.K. and Buckley, B.R. (1973) Acuities for spatial arrangement in line figures: human and ideal observers compared. Vision Res. 13, 599-620.

Andrews, D.P. and Miller, D.T. (1978) Acuity for spatial separation as a function of stimulus size. Vision Res. 18, 615-619.

Barlow, H.B. (1979) Reconstructing the visual image in space and time. Nature 279, 189-190.

Barlow, H.B. (1981) Critical limiting factors in the design of the eye and visual cortex. Proc. R. Soc. Lond. B212, 1-34.

Beck, J. and Schwartz, T. (1979) Vernier acuity with dot test objects. Vision Res. 19, 313-319.

Bourdon, B. (1902) La Perception Visuelle de l'Espace. Scheicher, Paris.

Burton, G.J., Haig, N.D. and Moorhead, I.R. (1986) A self-similar stack model for human and machine vision. Biol. Cybern. 53, 397-403.

Cowey, A. and Rolls, E.T. (1974) Human cortical magnification factor and its relation to visual acuity. Expl. Brain Res. 21, 447-454.

Daniel, P.M. and Whitteridge, D. The representation of the visual field on the cerebral cortex in monkeys. J. Physiol. Lond. 159, 203-221.

DeValois, R.L., Albrecht, D.G. and Thorell, L.G. (1982) Spatial frequency selectivity of cells in macaque visual cortex. Vision Res. 22, 545-559.

Dow, B.M., Snyder, R.G., Vautin, R.G. and Bauer, R. (1981) Magnification factor and receptive field size in foveal striate cortex of the monkey. Expl. Brain Res. 44, 213-228.

Drasdo, N. (1977) The neural representation of visual space. Nature 266, 554-556.

Enoch, J.M. and Williams, R.A. (1983) Development of clinical tests of vision: initial data on two hyperacuity paradigms. Percept. & Psychophys. 33, 314-322.

Enoch, J.M., Williams, R.A., Essock, E.A. and Barricks, M. (1984) Hyperacuity perimetry: Assessment of macular function through ocular opacities. Arch. Ophthal. 102, 1164-1168.

Fahle, M. and Poggio, T. (1984) Visual hyperacuity: spatiotemporal interpolation in human vision. Proc. R. Soc. Lond. B 213, 451-477.

Fahle, M. and Poggio, T. (1984) Visual hyperacuity: spatiotemporal interpolation in human vision. In: Image Understanding 1984, 49-77. Ullman, S. and Richards, W. eds. Ablex Publ. Corp., Norwood, New Jersey.

Fendick, M. and Westheimer, G. (1983) Effects of practice and the separation of test targets on foveal and peripheral stereoacuity. Vision Res. 23, 145-150.

Finney, D.J. (1971) Probit analysis, 3rd edn. Cambridge Univ. Press.

Foley-Fisher, J.A. (1977) Contrast, edge-gradient, and target line width as a factor in Vernier discrimination. Optica Acta 24, 179-186.

Frisen, L. and Glansholm, A. (1975) Optical and neural resolution in peripheral vision. Invest. Ophthal. Vis. Sci. 14, 528-536.

Geisler, W.S. and Davila, K.D. (1985) Ideal discrimination in spatial vision: two-point stimuli. J. Opt. Soc. Am. A2, 1483-1497.

Hartridge, H. (1923) Visual discrimination and the resolving power of the eye. J. Physiol. 57, 52-67.

Harris, J.L. (1964) Resolving power and decision theory. J. Opt. Soc. Am. 54, 606-611.

Helmholtz, H. von (1909) Handbuch der Physiologischen Optik. Translation by Southall, J.P.C., Vol. I. Dover Publications Inc., New York, 1962.

Hering, E. (1899) Über die Grenzen der Sehschärfe. Ber. Math.-phys. Cl.d. Königl. Sächs. Gesell. Wiss. Leipzig Naturwiss. Teil 16-24.

Hartmann, G. (1982) Recursive features of circular receptive fields. Biol. Cybern. 43, 199-208.

Hirsch, J. and Hylton, R. (1982) Limits of spatial-frequency discrimination as evidence of neural interpolation. J. Opt. Soc. Am. 72, 1367-1374.

Hirsch, J. and Hylton, R. (1985) Spatial-frequency discrimination at low frequencies: evidence for position quantization by receptive fields. J. Opt. Soc. Am. A2, 128-135.

Hubel, D.H. and Wiesel, T.N. (1974) Uniformity of monkey striate cortex: a parallel relationship between field size, scatter and magnification factor. J. Comp. Neurol. 158, 295-305.

Johnson, C.A. and Leibowitz, H.W. (1974) Practice, refractive error and feedback as factors influencing peripheral motion thresholds. Percept. Psychophys. 15, 276-280.

Koenderink, J.J. (1977) Current models of contrast processing. In: Spatial Contrast, Report of a workshop held in Amsterdam, 1976; Spekreijse, H. and Tweel, L.H. van der, eds., Amsterdam-Oxford-New York: North Holland.

Koenderink, J.J. and Doorn, A.J. van (1978) Visual detection of spatial contrast; influence of location in the visual field, target extent and illuminance level. Biol. Cybern. 30, 157-167.

Koenderink, J.J. and Doorn, A.J. van (1982) Invariant features of contrast detection: an explanation in terms of self-similar detector arrays. J. Opt. Soc. Am. 72, 83-87.

Koenderink, J.J., Bouman, M.A., Bueno de Mesquita, A.E., Slappendel, S. (1978a) Perimetry of contrast detection thresholds of moving spatial sine wave patterns. I. The near peripheral visual field (eccentricity 0-8°. J. Opt. Soc. Am. 68, 845-849.

Koenderink, J.J., Bouman, M.A., Bueno de Mesquita, A.E., Slappendel, S. (1978b) Perimetry of contrast detection thresholds of moving spatial sine wave patterns. II. The far peripheral visual field (eccentricity 0-

50°. J. Opt. Soc. Am. 68, 850-854.

Koenderink, J.J., Bouman, M.A., Bueno de Mesquita, A.E., Slappendel, S. (1978c) Perimetry of contrast detection thresholds of moving spatial sine wave patterns. III. The target extent as sensitivity controlling parameter. J. Opt. Soc. Am. 68, 854-860.

Koenderink, J.J., Bouman, M.A., Bueno de Mesquita, A.E., Slappendel, S. (1978d) Perimetry of contrast detection thresholds of moving spatial sine wave patterns. IV. The influence of mean retinal illuminance. J. Opt. Soc. Am. 68, 860-865.

Kulikowski, J.J. and King-Smith, P.E. (1973) Spatial arrangement of line, edge and grating detectors revealed by subthreshold summation. Vision Res. 13, 1455-1478.

Levi, D.M. and Klein, S.A. (1986) Sampling in spatial vision. Nature 320, 360-362.

Levi, D.M., Klein, S.A. and Aitsebaomo, A.P. (1985) Vernier acuity, crowding and cortical magnification. Vision Res. 25, 963-977.

Levy-Schoen, A. (1977) Form identification in peripheral vision. Optica Acta 24, 139-145.

Lie, I. (1980) Visual detection and resolution as a function of retinal locus. Vision Res. 20, 967-974.

Livingstone, M.S. and Hubel, D.H. (1985) Spatial relationship and extrafoveal vision. Nature 315, p.285.

Low, F.N. (1951) Peripheral visual acuity. Am. Med. Ass. Archiv. Ophthal. 45, 80-99.

Ludvigh, E. (1953) Direction sense of the eye. Am. J. Ophthal. 36, 139-142.

Ludvigh, E. and McKinnon, P. (1967) The effect of orientation on the three dot alignment test. Am. J. Ophth. 64, 261-265.

McKee, S.P. and Westheimer, G. (1978) Improvement in Vernier acuity with practice. Perception and Psychophys. 24, 258-262.

Millidot, M. Johnson, C.A., Lamont, A. and Leibowitz, H.W. (1975) Effect of dioptrics on peripheral visual acuity. Vision Res. 15, 1357-1362.

Morgan, M.J. and Watt, R.J. (1982) Mechanisms of interpolation in human spatial vision. Nature 299, 553-555.

Morgan, M.J. and Watt, R.J. (1983) On the failure of spatiotemporal

interpolation: a filtering model. Vision Res. 23, 997-1004.

Nahrstedt, D.A. and Schooley, L. (1979) Alternative approach in decision theory as applied to the resolution of two point images. J. Opt. Soc. Am. 69, 910-912.

Nyyssonen-Grimes, D. and Thompson, B.J. (1967) Two-point resolution with partially coherent light. J. Opt. Soc. Am. 57, 1330-1334.

Orban, G.A. (1985) Visual cortex and retinal eccentricity: uniformity or non-uniformity? In: Models of the Visual Cortex. Rose, D. and Dobson, V.G. eds. John Wiley & Sons Ltd, New York.

Rovamo, J., Virsu, V. and Nasanen, R. (1978) Cortical magnification factor predicts the photopic contrast sensitivity of peripheral vision. Nature 271, 54-56.

Saugstad, P. and Lie, I. (1980) Training of peripheral visual acuity. Scand. J. Psychol. 5, 218-224.

Schwartz, E.L. (1980) A quantative model of the functional architecture of human striate cortex with application to visual illusion and cortical texture analysis. Biol. Cybern. 37, 63-76.

Schwartz, E.L. (1980) Cortical mapping and perceptual invariance. A reply to Cavanagh. Vision Res. 23, 831-835.

Snyder, A.W. (1982) Hyperacuity and interpolation by the visual pathways. Vision Res. 22, 1219-1220.

Stigmar, G. (1971) Blurred visual stimuli. II: The effect of blurred visual stimuli on Vernier and stereo acuity. Acta Ophthal. 49, 364-379.

Toet, A., Eekhout, M.P. van, Simons, H.L.J.J. and Koenderink, J.J. (1987) Scale invariant features of differential spatial displacement discrimination. Vision Res. In press.

Toet, A. and Koenderink, J.J. (1987) Two-point discrimination at low resolution. Submitted to J. Opt. Soc. Am. A

Tootell, R.B., Silverman, M.S., Switkes, E. and DeValois, R.L. (1982) Deoxyglucose analysis of retinotopic organization in primate striate cortex. Science 218, 902-904.

Van Essen, D.C., Newsome, W.T. and Maunsell, J.H.R. (1984) The visual field representation in striate cortex of the macaque monkey: Asymmetries, anisotropies, and individual variability. Vision Res. 24, 429-448.

Virsu, V. and Rovamo, J. (1979) Visual resolution, contrast sensitivity, and the cortical magnification factor. Expl. Brain Res. 37, 475-494.

Watt, R.J. (1984) Towards a general theory of the visual acuities for shape and spatial arrangement. Vision Res. 24, 1377-1386.

Watt, R.J. and Andrews, D.P. (1981) APE: Adaptive probit estimation of psychometric function. Curr. Psychol. Rev. 1, 205-214.

Watt, R.J. and Morgan, M.J. (1984) Spatial filters and the localization of luminance changes in human vision. Vision Res. 24, 1387-1397.

Watt, R.J., Morgan, M.J. and Ward, R.M. (1983) The use of different cues in Vernier acuity. Vision Res. 23, 991-995.

Westheimer, G. (1976) Diffraction theory and visual hyperacuity. Am. J. Optom. & Physiol. Optics 53, 362-364.

Westheimer, G. (1979) The spatial sense of the eye. Invest. Ophthal. Vis. Sci. 18, 893-912.

Westheimer, G. (1982) The spatial grain of the perifoveal visual field. Vision Res. 22, 157-162.

Westheimer, G. and McKee, S.P. (1977) Integration regions for visual hyperacuity. Vision Res. 17, 89-93.

Weymouth, F.W. (1958) Visual sensory units and the minimal angle of resolution. Am. J. Opthal. 46, 102-113.

Whitteridge, D. and Daniel, P.M. (1961) The representation of the visual field on the calcarine cortex. In: The visual system: neurophysiology and psychophysics. Eds. Jung, R. and Kornhuber, H. Springer Verlag. Berlin.

Williams, R.A., Enoch, J.M. and Essock, E.A. (1984) The resistence of selected hyperacuity configurations to retinal image degradation. Invest. Ophthal. Vis. Sci. 25, 389-399.

CHAPTER II.8.

The visual assessment of the spatial location of a bright bar.

ABSTRACT.

Vernier acuity, three-line interval bisection and line-width discrimination experiments were performed for a target bar stimulus with an asymmetrical orthoaxial contrast profile. This was done in an attempt to identify the nature of the spatial primitives that are involved in the visual coding of spatial location. We conclude that both the zero-crossings and the centroid or extremum of the zero-bounded region of the neural activity distribution that is elicited by the presentation of the target bar are in principle available to perception. It probably depends on the spatial characteristics of the applied stimulus pattern and the adopted strategy which features are actually used in different localization tasks.

key-words: Vernier acuity bisection linewidth discrimination centroids zero-crossings

INTRODUCTION.

Spatial vision requires the analysis of the spatial relations of features in the perceived intensity distribution. In order to perform this analysis a visual system has to build an internal representation of the spatial structure of its visual environment using the signals transmitted by its individual photoreceptors. Ideal photoreceptors transform the spatial distribution of an environmental intensity pattern into a set of flux measurements. Lotze (1884) suggested that the signal activity of the optic nerve fibers encode labels or "local-signs" stating from which part of the sensorium the signals originate. These place-tags may be encoded in

the simultaneous excitatory activity pattern in the central nervous system that is elicited by the stimulus presentation (Koenderink, 1984a,b). In this view, the lower limit of accuracy for the determination of retinal local signs is obviously set by the diameter of the retinal photoreceptors.

Differential spatial displacement discrimination (or hyperacuity-) thresholds of less than 5 sec of arc indicate that the visual system can determine changes in the relative spatial position of features in the visual field that are an order of magnitude smaller than the diameter of the foveal photoreceptors (Volkmann, 1863; Wülfing, 1892; Westheimer and McKee, 1977b; Klein and Levi, 1985). To explain this high degree of accuracy it has been suggested that the visual system computes place tags for a collection of simultaneously activated retinal photoreceptors (Hering, 1899). These place tags may in principle be computed with an accuracy that exceeds the spatial dimensions of the photoreceptors themselves.

It is still largely unknown which features of a spatial intensity distribution are used in the visual assessment of its spatial structure. In other words, we do not know (i) in what way the constitution of a collection of retinal receptors to which a local sign is attached depends on the distribution of their signal activities and (ii) how the signals of the individuals are weighted in the process of computing a mean local sign. This immediately raises the question whether the location attributed to a stimulus is a function of its entire (global) retinal light distribution or of one or more of its local features. For instance, the position of a bright bar may be characterized by local features such as its edges or by features that are determined by the entire light distribution such as its center or mean.

Several experiments have been performed to investigate the representation of the spatial structure of an intensity distribution by the human visual system. The results of some of these experiments suggest that the visual system utilizes the luminance distribution within a restricted region of about 2'-3' of arc, and assigns the location of a stimulus to that of the centroid (first moment) of its corresponding weighted retinal intensity distribution (Westheimer and McKee, 1977a; Badcock and

Westheimer, 1985a,b). Watt et al. (1983) and Watt and Morgan (1983a) found that the perceived position of an asymmetrical retinal luminance profile consisting of a pair of unresolved lines was determined by their relative luminances. They investigated which features of the retinal light distribution, or its neurally filtered derivative, account best for their psychophysical data. They were able to show convincingly that the position of a peak or threshold edges (defined as the first value in the light distribution that exceeds some threshold set by the intensity of the background light and the intrinsic noise level) in the retinal intensity distribution are not available to perception. They were not able to distinguish between the use of zero-crossings in the second derivative of the retinal intensity distribution (i.e. the inflexion points of this distribution) or its arithmetic mean as features to which location may be assigned. Moreover, they found that subjects could not discern the direction of the luminance asymmetry of a bar pair unless the two bars were theoretically resolved (i.e. when there existed a minimum between two maxima in the joint light distribution of the bar pair). However, they provided no reference stimulus for this task. Thus, they determined detection thresholds for contrast differences within the stimulus profile and not spatial separation discrimination thresholds. The detection of contrast differences may also play a role in their width discrimination and Vernier acuity experiments. They concluded that the processes of extracting a mean or zero-crossings in the second derivative (processes which rely on an accurate recording of luminance asymmetries) obliterate any small scale asymmetry; i.e. the luminance asymmetries are used in the assessment of location but have no individual representation in the visual system.

It has been shown that the results of a large number of experiments investigating the representation of the spatial structure of an intensity distribution by the human visual system can be explained by assuming that the primitives in this representation correspond to local features of the second derivative of the retinal luminance profile (e.g. regions of inactivity or zero-crossings and extrema or central moments of zero-bounded regions in the simultaneous excitatory activity pattern in the central nervous system: Watt and Morgan, 1983a,b, 1984, 1985; Watt, 1984;

Mather and Morgan, 1986).

The number of zero-crossings in the second derivative of the retinal image of two parallel bars depends on their spatial separation in the visual field (varying from two when they are close together to four when they are clearly separated). Thus, Watt and Morgan's (1983a) and Badcock and Westheimer's (1985a,b) stimuli confound asymmetry or centroid detection and the discrimination of the number or the pronouncedness of inflexion points in the retinal image. Therefore, these experiments provide no conclusive evidence that the visual system integrates a retinal intensity distribution to determine an interpolated value for a local sign. It may still be the case that the location of a stimulus is represented by a weighted mean of some of its more or less pronounced features.

This paper seeks to identify the nature of the spatial primitives that are involved in the visual coding of spatial location. We devised some experiments to test if the visually perceived position of a bright bar is completely determined by the position of the inflexion points in the resulting retinal intensity distribution, independent of the spatial characteristics of the distribution between the inflexion points. The spatial extent of a bright bar is defined as the area where its contrast profile differs from zero. The extent of the bar stimuli that were used in the experiments reported in this paper is finite in all directions. In the sequel we will call the direction of the largest extent of a bar its axial direction. The direction orthogonal to the axial direction will be called the orthoaxial direction. A line in the axial direction and through the midpoint of the orthoaxial extent of a bar will be called its axis. The target stimuli we used consisted of bars that have an orthoaxial spatial contrast profile with a high degree of asymmetry and no inflexion points. Inflexion points in the resulting retinal images of these stimuli arise on the edges of the bar profiles due to convolution with the optical pointspread function of the eye. Because the target stimuli have only a limited width (defined as their total orthoaxial extent) and no inflexion points there will only be two inflexion points in the orthoaxial direction of their retinal projection. The spatial separation of these two inflexion points is determined by the width of the input bars. Two bars that are

mirror symmetrical with respect to a line parallel to their axis produce retinal images which have inflexion points with the same spacing (i.e. that have identical contour width). If the visual system uses only the zero-crossings in the second derivative of the retinal projection of a bar to determine its spatial location, there should be no difference in the perceived spatial location of the bar when it is substituted for its mirror image such that the inflexion points coincide in both cases. We used our asymmetrical bar stimuli for the assessment of Vernier-, bisection- and line-width discrimination acuity.

GENERAL METHODS.

Subjects.

Two male subjects AG and CS, aged respectively 25 and 27, and one female subject EO, aged 25, served in the experiments reported below. Subjects CS and EO both have corrected myopic vision. Subject CS is highly practised. The subjects AG and EO both underwent several training sessions before performing the measurements reported below.

Apparatus.

A PDP11/34 minicomputer in combination with a Gould deAnza IP8500 image array processor was used to generate, process and present the stimuli, record the responses and analyze the data.

The stimuli were displayed on a Tektronix 634 monochrome monitor. The CRT was driven in an interlaced mode with a frame rate of 60 Hz. The display was equipped with P45 phosphor and had a resolution of 512 × 512 pixels in a screen area of 87.8 × 87.8 mm. The luminance value of each pixel was quantized to 8 bits. A 512 × 512 correction matrix was added to the deAnza frame buffer to compensate for the inhomogeneity of the display. A lookup table was used to correct for non-linearities in the variation of the luminance of the display with the applied gray level signal.

Stimuli.

The experiments we describe in this paper were performed to find out whether the visually perceived position of a bright bar is completely determined by the location of the inflexion points in the resulting retinal intensity distribution, independent of the spatial characteristics of the intensity distribution between these points. Our stimuli consist of bright bars. The spatial contrast profiles of these bars is such that the retinal images of these stimuli, resulting after convolution with the optical pointspread function of the eye, have only two inflexion points in their orthoaxial direction. If inflexion points are available to perception their relative distances may provide a cue to discriminate a bar profile from its mirror image (the term "mirror image" will be used to denote the image of a bar stimulus that is obtained when it is mirrored with respect to its axis). Bar stimuli which have no inflexion points in their orthoaxial contrast profile will not provide this cue.

The orthoaxial contrast profile we adopted for our target stimulus is given by

$$L_t(x,y) = L_b[1+cw_t'(x)]$$

where L_b denotes the background luminance. The parameter c will be referred to as contrast. The window function $w_t'(x)$ is given by

$$w_t'(x) = w_t(x) \; / \; w_{tmax}$$

were $w_t(x)$ is in turn given by

$$w_t(x) = (a-x) * \ln(1+b*x) \; ; \; 0 \leq x \leq a.$$
$$w_t(x) = 0 \; ; \; x < 0 \text{ or } x > a.$$

The parameters a and b determine respectively the width (total orthoaxial extent) and the asymmetry of the orthoaxial spatial contrast profile of the bar. w_{tmax} denotes the maximum value of $w_t(x)$ over the range $0 \leq x \leq a$.

The results of Westheimer and McKee (1977a) and Badcock and Westheimer (1985a,b) suggest that the visual system uses the luminance distribution within a region extending up to 2'-3' in the assessment of the spatial location of a stimulus. Together with the results from so-called "crowding" experiments this has been interpreted as an indication for the existence of individual differential spatial displacement processing units (Levi et al., 1985). We chose a=175 arcsec. This results in a target stimulus with an orthoaxial spatial contrast profile that has an extent that is comparable to the extent of the abovementioned hypothetical processing units. By restricting the orthoaxial spatial extent of our stimuli within the influence sphere of a single processing unit we hope to minimize the interfering influence of large scale (global) localization processes that probably involve an intermediary stage of comparison of the activity of units in adjoining regions. Only by bypassing these indirect computation modes we have a chance to reveal the way in which the elementary units that contribute to the visual assessment of spatial location actually function.

Discrimination between the detection of inflexion points and other spatial characteristics of the retinal intensity distribution is theoretically only possible when the relative spatial variation between these features exceeds the known limits of the differential spatial displacement discrimination capability of the visual system. Our choice of b=5/9 results in a target stimulus with an asymmetry of its orthoaxial spatial contrast profile that is large enough to induce relative spatial separations between the different features in its retinal projection and that of its mirror image that exceed the thresholds for differential spatial displacement discrimination. Thus if one or (a combination of) more of these features are available to perception this should become apparent from our results. (In the sequel we will present exact figures for the width of the spatial intervals separating the different stimulus features. Moreover, we will indicate how their possible use by the visual system in the assessment of the spatial location of the target stimulus may be reflected in the results from our experiments.)

The orthoaxial contrast profile we adopted for our reference bar stimuli is given by

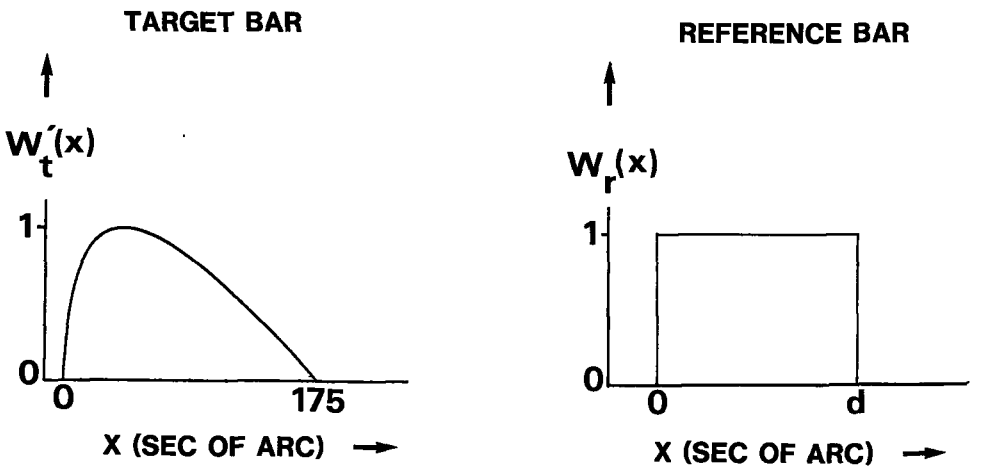

Figure 1. Schematical representation of the orthoaxial spatial contrast profiles of the target bar (a) and the reference bar (b).

$$L_r(x,y) = L_b[1+cw_r(x)]$$

where L_b again denotes the background luminance and c is the contrast value of the reference bar. The window function $w_r(x)$ is given by

$$w_r(x) = 1 \; ; \; 0 \leq x \leq d.$$
$$w_r(x) = 0 \; ; \; x < 0 \text{ or } x > d.$$

Thus, the parameter d determines the width of the orthoaxial spatial contrast profile of the equiluminant reference bar. The orthoaxial spatial contrast profiles of both our target- and reference-stimuli are represented in Figure 1.

Viewing conditions.

The display was placed in a dark room with non-reflecting black walls. Observers were seated with their heads supported by a chin rest, adjusted in height and position so that their dominant eye was on the line perpendicular to the center of the monitor screen. The use of a forehead rest prevented tilting of the head. Viewing was monocular with the subject's dominant eye. The unused eye was covered with an eye cap. The viewing distance was 7.30 m. At this distance, one pixel subtended 4.84 arc sec and the entire screen 0.69 degree.

The stimulus was superposed on a 170 cd/m^2 (540 Td for the 2 mm pupil; 1450 Td for the 3.3 mm pupil) luminance background level. The luminance level of the background was chosen such as to operate in the photopic domain.

The precision with which the relative location of a bright bar can be perceived will depend on its contrast. Therefore we performed all our experiments for three different contrast values. The contrast values we used were respectively 19%, 41% and 79%. These values were chosen such that the edges of the stimuli were clearly visible for the highest contrast value (79%), whereas the stimulus was only dimly visible (i.e.

the subjects had the impression that they could not discern its edges) for the lowest contrast value that was used (19%).

The spacing and pronouncedness of the inflexion points in the resulting retinal image of the stimuli will also depend on the actual form and size of the optical pointspread function. The point- or line-spread function of the eye is largely determined by its pupil size. In our experiments we used two different artificial pupils with a diameter of respectively 2 mm and 3.3 mm. The 2 mm pupil is in the range of pupil diameters that provide the narrowest line spread profiles (and therefore an optimum resolution; see: Campbell and Gubisch, 1966; Gubisch, 1967; Fry, 1970). For this aperture size the linespread function consists roughly of a Gaussian core and an exponential "skirt". The approximately Gaussian core is the ideal (diffraction limited) line image; the skirt represents stray light coming from scatter and defects of focus. For the 3.3 mm pupil the core width decreases and the skirt of the linespread function becomes more dominant.

The four different conditions used in all experiments are summarized in Table I.

Table I. The different conditions used in the experiments.

CONDITION NR.	PUPIL SIZE (mm)	CONTRAST (%)
I	2.0	79
II	2.0	41
III	2.0	19
IV	3.3	41

The order in which the spatial localization experiments were performed for all different conditions was not systematic.

Experimental procedures.

A run was started when the subject had adapted to the background luminance level. At the onset of each stimulus presentation a buzzer signal sounded. After completion of the presentation the subject had to report (forced choice) his decision for the task in hand by pressing the appropiate one of two digital switches. Immediately after the subject had responded to a trial a new presentation was started. By withholding his answer for a while the subject was able to take a short rest. In case of a missed presentation (and in that case only) the subject could skip the obligation to answer by pressing a third knob. In this case the missed presentation was randomly incorporated into the sequence of remaining trials and a new presentation was started.

Adaptive probit estimation (APE; see Watt and Andrews,1981 for details) was used to determine the subject's error response distribution in the different forced choice tasks. APE is a modified method of constant stimuli. It allows a bias-free determination of a psychometric function with high precision for a relatively small number of trials. Probit analysis (Finney, 1971) was used to determine the mean of the cumulative normal psychometric function (corresponding to the point of subjective equality or PSE). Each individual estimate is the mean of the response error distribution from a run of 70 trials preceded by 14 practice trials. Probit analysis also estimates the standard error of this statistic. At least 10 replications were performed for each stimulus condition. The data points quoted are the r.m.s. of these individual estimates with the standard deviation of their dispersion serving as a second measure of the standard error. These two measures are always close and relatively small (typically less than 7% of the standard deviation).

In some of our experiments we determined the perceived position of a target stimulus relative to a (simultaneously present) reference stimulus. Since the perceived location of the reference stimulus is unknown the experiments need to be devised such that this reference location does not enter our results (thereby resulting in an unknown offset error). Therefore we measured the perceived location of a target stimulus as well as that of its mirror image (both positions taken relative to the

reference location). The difference of these two positions is independent of the perceived reference location and represents the perceived location of the target stimulus relative to some physical feature of its spatial contrast profile.

We chose for a procedure that integrated two localization experiments in a single run: one for a target stimulus and a second one for its mirror image. The procedure was as follows. In a single run of the experiment the two target stimuli were presented an equal number of times. On each trial the program made a random choice between the presentation of the target stimulus or its mirror image. For both targets the same fixed repertoire of test locations was available. APE was used to select the test locations at which the stimuli were actually presented. The subject's judgements for both targets were processed separately. Thus, a single run resulted in two psychometric functions. Probit analysis produced the mean of the underlying error response distributions for each of these two functions. The location at which the target stimulus was actually perceived is given by the mean of these two PSE's. The data we present are the weighted mean of (typically more than 10) of these location estimates. As mentioned before, each individual PSE is the mean of the response error distribution from a number of 70 trials preceded by 14 practice trials. Thus, a single target location estimate is the result of a run consisting of 140 trials preceded by 28 practice trials.

EXPERIMENTS.

We computed numerical predictions for the perceived locations of several stimulus features to compare with the results of our subjects in the psychophysical experiments. Although the exact mechanism subserving hyperacuity is unknown it is sometimes attributed to some kind of neural interpolation process (Barlow, 1979; Morgan and Watt, 1982). Mathematically, interpolation can be carried out by convolving the sampled function with an appropriate frequency-limited function. Physically, such a function is provided by the combination of the optical and neural linespread functions. For the spatial linespread function we adopted the

Laplacian of a one-dimensional normalized Gaussian. This function closely resembles the well known DOG-profile which has been successfully used to fit line-spread function data (e.g. King-Smith and Kulikowsky, 1975; Hines, 1976; Wilson, 1978). We will adopt the term spread for the distance over which a Gaussian falls from 1 to $e^{-\frac{1}{2}}$, corresponding to the standard deviation measure as defined in statistics. Our particular choice of the linespread function is completely characterized by the spread of the underlying Gaussian.

For different values of the spatial scale parameter of the linespread function we computed an approximation of the continuous one-dimensional convolution product of this function and the asymmetrical orthoaxial spatial contrast profile of our target bar stimulus. In case of a discrete convolution product (representing a discretely spaced collection of receptive fields) the outcome depends on the actual position of the stimulus relative to the sampling lattice. In the visual system the effects of small involuntary eye movements serve to reduce the effect of this positional preference. To simulate this effect we computed an approximation of the continuous convolution product.

Figure 2 shows all different features that were extracted from the resulting simulated activity distribution. First there are the local features such as

(i) the zero-crossings in the orthoaxial direction of the activity distribution. These correspond to the inflexion points in the retinal illuminance distribution.

(ii) the extrema (peaks and troughs). These features were first suggested by Frisby and Mayhew (1980) and more recently by Watt and Morgan (1983b).

Then there are the global features that are determined by an entire part of the activity distribution, such as

(iii) the midpoint of the zero-crossings.

(iv) the centroid or first moment of a zero- bounded region of activity.

Mechanisms that assign location to a bar using one or (a combination of) more of these features may either be unitary, in that there is only one locus of position for a narrow bright bar, or compound, when an individual position is attributed to two or more different features of the stimulus. The fundamental difference between these two types of models is that for

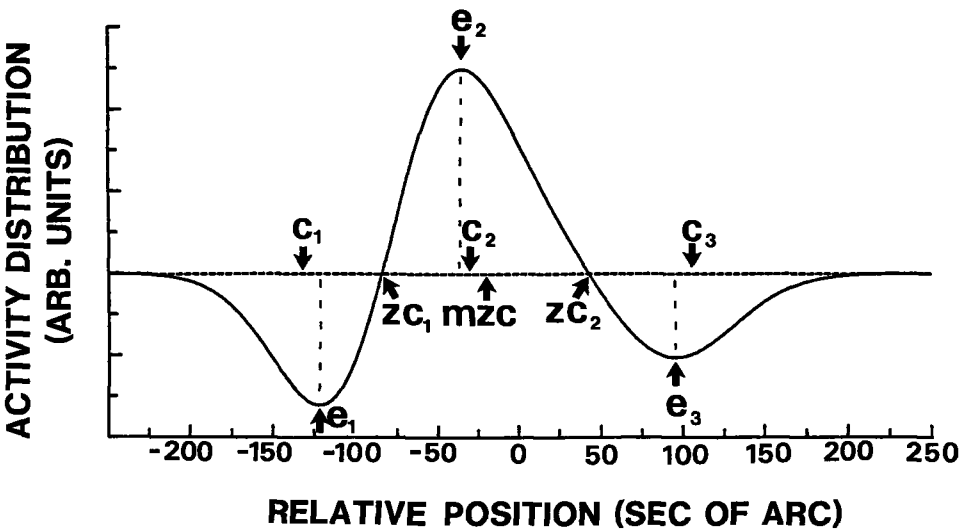

Figure 2. Schematical representation of the orthoaxial profile of the simulated neural response distribution corresponding to the target stimulus. The zero-crossings of this distribution are indicated by ZC_1 and ZC_2. MZC indicates the midpoint of ZC_1 and ZC_2. E_1, E_3 and E_2 indicate the extrema of respectively the (two) outer and the (single) inner zero-bounded regions of activity. The centroids of these regions are respectively indicated by C_1, C_3 and C_2.

instance the edges are represented independently in the compound models, whereas the unitary mechanisms produce a single representation for the entire stimulus. It may be the case that different mechanisms are used to perform different spatial localization tasks.

We computed the position of several different features of the asymmetrical orthoaxial target bar profile after convolution with the linespread function and relative to the midpoint of the input profile. The relative positions thus obtained will be compared with the results of the psychophysical experiments that yield the perceived location of the target bar stimulus relative to its axis. The relative positions of all features were determined for a range of values of the spatial scale parameter of the linespread function. Thus, the outcome from this simulation study provides us with baseline conditions against which we can gauge the performance of the subjects in our psychophysical experiments.

There exists both psychophysical and physiological evidence that the response of the early stages of the visual pathway increases with intensity according to a nonlinear saturation function of the kind

$$R_i = i * R_{max}/(i+H)$$

where R_i denotes the response amplitude to a light of intensity i, R_{max} is the maximum response amplitude and H is a constant determining the degree of nonlinearity. H represents the intensity level at which half the maximum response is elicited. Small values of H result in a strong nonlinearity, while the transform becomes approximately linear for very large values of H. The transform has been successfully fitted to retinal responses (e.g. Naka and Rushton, 1966; Norman and Werblin, 1974; Valeton and van Norren, 1984) and to psychophysical data (e.g. Hood et al., 1979; Maudarbocus and Ruddock, 1973; Legge and Kersten, 1983). Models for edge localization incorporating this transform have been shown to be capable of producing accurate predictions for the relative perceived position of differently blurred edges (Morgan et al., 1984; Mather and Morgan, 1986).

The actual value of H depends on the state of retinal light adaptation. Mather and Morgan (1986) determined a value for H that was 200% of the maximum display luminance or 3.16 log td (for a 2 mm artificial pupil). This result is comparable with psychophysical estimates derived from flash detection thresholds (2.0-4.3 log td in Hood et al.,

1979, Fig. 2) and with data from extracellular recordings in monkey retina (3.5-6.3 log td in Valeton and van Norren, 1983, Table I). In our experiments the background luminance was 2.73 log td and the maximum stimulus luminance was 2.98 log td (both data for the 2.0 mm artificial pupil). As these values are comparable to the one used by Mather and Morgan we adopted their ratio of 200%, resulting in a value of 3.3 log td for H. (Actually, their background luminance was an order of magnitude lower than ours. However, they presented a stimulus of 417 td at the location of the target stimulus in between trials. Therefore, we feel that we may compare their situation with the one described in this paper.)

Figure 3 illustrates the influence of the actual value of H on the results of some of our numerical predictions. This figure represents the position of the positive zero-bounded centroid and the position of the middle of the interval defined by the two zero-crossings in the simulated resulting activity distribution as a function of H. All positions are taken relative to the axis of the target bar. The spatial scale parameter of the linespread function was (arbitrarily) taken as 60". H is varied from 10 td to 10^5 td. For H=10^5 td the positive centroid is located at a distance of 22.71" from the middle of the bar profile and the middle of the zero-crossings is at 20.68" from this middle. These values are nearly equal to those that are obtained without compression (respectively 22.73" and 20.71"). Figure 3 allows us to estimate the errors in the calculated position of the different stimulus features that are made due to an incorrect choice of the value of H. This figure shows that relatively large variations in H result in variations in the calculated (relative) positions that are small relative to the separation of the different stimulus features. Thus, we feel confident that our choice of H will give a good indication of the effects of a possible compressive nonlinear transform on the luminance profiles.

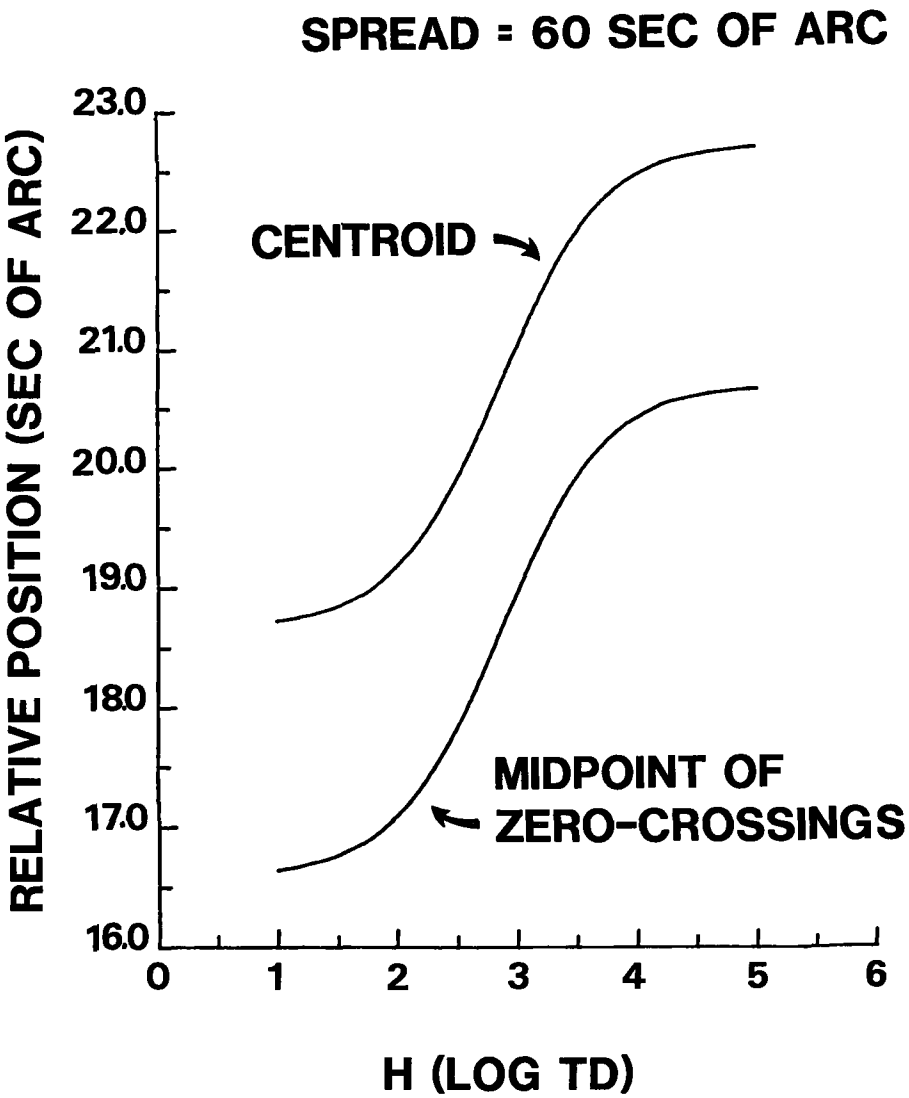

Figure 3. The dependency of the relative positions of (i) the middle zero-bounded centroid and (ii) the midpoint of the interval defined by the two zero-crossings from Figure 2 on the degree of nonlinearity of the neural response saturation function. All positions are taken relative to the axis of the target bar.

EXPERIMENT I: Bar width discrimination.

On each trial of this experiment an equiluminant reference bar and the previously described asymmetrical target bar were presented simultaneously in a Vernier configuration. This particular configuration was chosen to prevent the introduction of temporal cues. These may for instance result from horizontal sequential scanning eye movements when the two bars are presented next to each other (and with the same orientation). To avoid Vernier type of positional (e.g. boundary misalignment) cues, the axis of the lower bar appeared at random on one of 7 different positions, centered in the orthoaxial direction with respect to the middle of the upper bar (the actual displacements being spectively 0", ±4.84", ±9.68", ±14.52"). The orientation of both bars was parallel to the vertical. The axis of the upper bar coincided with the vertical through the centre of the CRT display. The width of the reference bar was randomly selected from a number of preset magnitudes using APE. The asymmetrical bar had a width of 175". To reduce the pronouncedness of luminance cues the luminance of the reference bar was set to 80% of the maximal luminance of the target bar. Both bars had a length of 18' and their vertical separation (when their main axes were aligned) was 5'. The subject's task was to report whether the width of the lower bar was larger or smaller than that of the upper bar. The maximum stimulus presentation duration was 5 sec. Immediately after a subject had indicated his decision by pressing one of the response buttons a new presentation was started.

To eliminate offset errors that may arise due to a difference between the perceived and the veridical orientation of the stimulus pattern (in case the subject uses an orientation cue; see Sullivan et al., 1972), the program randomly placed the target stimulus either below or on top of the reference stimulus. The subject's responses for these two conditions were processed separately. The final equivalent width estimate equals the mean of the PSE's of both error response distributions. Each datum point represents the r.m.s. of at least ten of these estimates with the standard deviation of their distribution serving as a measure of dispersion, defined as the standard error.

We will now assume that the visual system assigns a location to individual features of the activity distribution that is elicited by the presentation of the stimulus pattern. In this case both the centroid and the extremum of the middle zero-bounded region in the orthoaxial activity profile provide no cue for the width discrimination task. The visual system can only perform this task by comparing the distance between two related features in the orthoaxial profile of the neural activity distribution. Therefore, we restricted our simulation experiments to the extraction of the relative spatial separation of pairs of related features.

This particular experiment serves two purposes. Firstly it provides us with information about the features that may be utilized by subjects in performing the width discrimination task. Secondly it yields the width of the reference bar for which it has the same perceived total orthoaxial extent as the target bar (and which will be used in the following experiments).

Results and discussion.

Figure 4 represents the individual data for two observers and the results of some numerical predictions. The drawn curves in this figure were obtained by computing the distances between respectively (i) the outer centroids, (ii) the two zero-crossings and (iii) the outer two extrema (troughs) of the orthoaxial profile of the simulated neural activity distribution. This distribution was obtained by convolving the contrast profile of the target bar stimulus with the previously described linespread function. We calculated the spatial separation of the aforementioned entities (i.e. the distance between the related features in the simulated activity distribution) for a range of values of the spatial scale parameter of the linespread function. The value of this parameter is varied between 20" and 300". For each point on the curves that were thus obtained we thereafter computed the width of a reference bar that would elicit an activity distribution (after convolution with a linespread function with the same value for its spatial scale parameter as that used

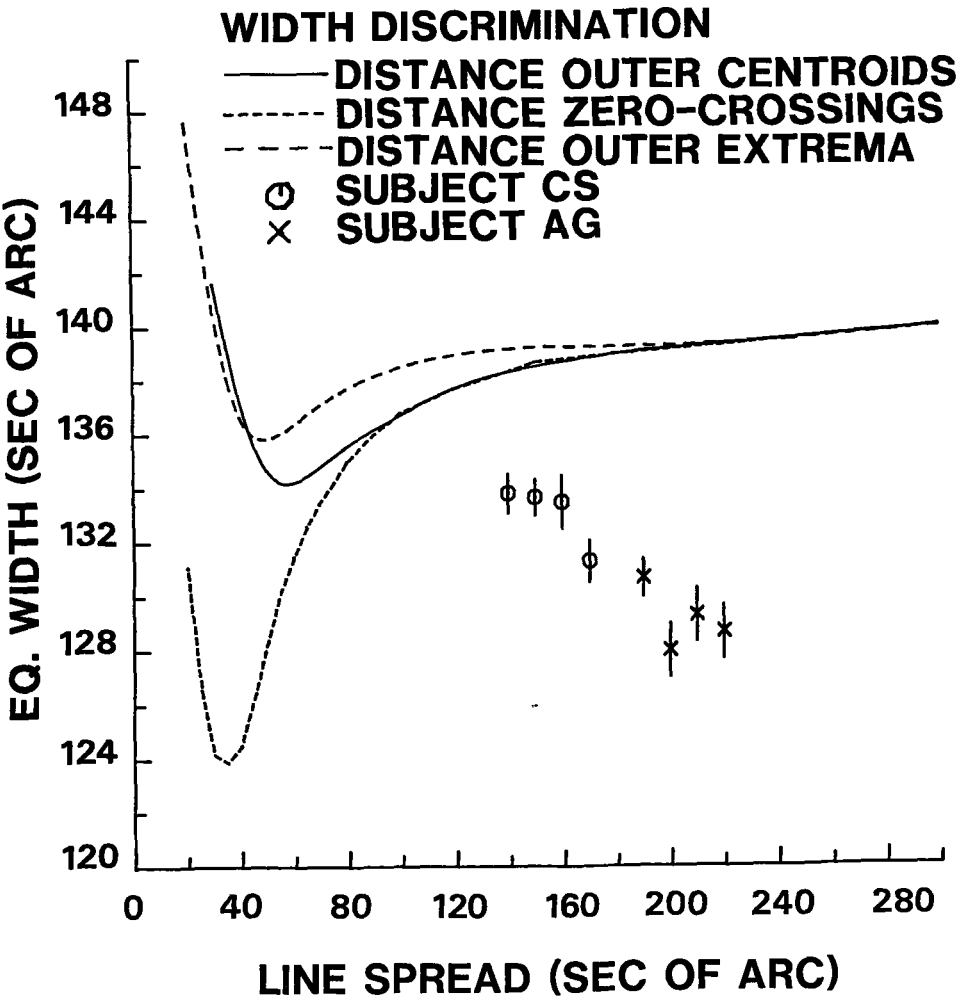

Figure 4. The results of the width discrimination experiment for subjects CS and AG. This Figure also shows the computed distances between respectively (i) the outer two centroids (solid line), (ii) the two zero-crossings (dotted line) and (iii) the outer two extrema (dashed line) of the orthoaxial profile of the simulated neural activity distribution. All positions are taken relative to the axis of the target bar.

to obtain the data point under consideration) with the same spacing of its corresponding features. In the sequel we will call the value thus obtained the "equivalent width" of the target bar stimulus. (Note that the equivalent width is defined with respect to the particular features under consideration) The smallest value of the spatial scale parameter we used (20") yields a linespread function that is comparable with the smallest linespread function that has been determined for the human visual system and with incoherent light (and which is well approximated by a Gaussian with a spread of 24": see Campbell and Gubisch, 1966). For values of the spatial scale parameter larger than 300" the locations of the different features are nearly independent of the actual value of this parameter. These simulation results provide a baseline against which we can gauge the performance of our subjects; i.e. we can check whether one or more of the abovementioned features of the neural activity distribution may have been utilized by the subjects.

The data points indicating the results of our width discrimination experiments represent the width of the reference bar for which its orthoaxial extent was perceived to be equal to that of the target bar. In Figure 4 these points are arbitrarily positioned somewhere along the horizontal axis. This was done because the actual value of the spatial scale parameter of the (combination of the optical and neural) linespread function of the subjects is unknown. However, the order of the data points from left to right corresponds with the conditions I to IV as described in the previous section.

If the horizontal line through a data point intersects with one of the theoretical curves then it is in principle possible that the features that were used in the computation of the equivalent width of this intersection point were also used by the subjects to perform in the width discrimination task. By determining the intersection points corresponding to the individual psychophysical data points and by taking into account their standard errors we obtain a range of values for the spatial scale parameter of the linespread function. This range corresponds to a collection of linespread functions that result in a simulated activity distribution for the asymmetrical bar stimulus with a computed equivalent width that is within the error range of the perceived equivalent width of

the equiluminous bar. Thus, we may obtain an impression of the spatial scale of the visual mechanisms that are involved in the process of width discrimination.

Contrary to our expectations the results of Figure 4 show no clear dependency of the perceived equivalent widths on the value of the stimulus contrast and the diameter of the artificial pupil. The results of subject CS are nearly independent of the stimulus contrast (conditions I to III) whereas those of subject AG vary heavily. An increase of the pupil diameter (condition IV) causes a decrease in the perceived equivalent width for subject CS, whereas the result of subject AG is not significantly different from his results in the conditions II and III.

Figure 4 shows that the results of the width discrimination experiment can in principle be explained by the assumption that the zero-crossings in the orthoaxial activity distribution are used in the visual assessment of the width of the bars. The lower part of the curve describing the equivalent width of the interval determined by the centroids of the outer two zero-bounded regions of activity is only just within the error range of the results of subject CS for the conditions I to III.

TABLE II. Results of the width discrimination experiment.

subject	condition nr.	perceived width (sec of arc)	spread (sec of arc)	error range spread (± 1 SE) (sec of arc)
CS	I	133.8 ± 0.7	73	68 - 77
	II	133.7 ± 0.7	72	67 - 76
	III	133.5 ± 1.0	70	64 - 77
	IV	131.3 ± 0.8	59	57 - 63
AG	I	130.7 ± 0.7	57	55 - 60
	II	128.0 ± 1.0	49	47 - 52
	III	129.3 ± 1.0	53	50 - 56
	IV	128.7 ± 1.0	51	48 - 54

The perceived equivalent widths in all different conditions are presented in Table II. Table II also presents the estimated extent of the hypothetical processing units that are involved in the width discrimination process, under the assumption that the visual system discriminates the extent of the interval delineated by the zero-crossings in the orthoaxial profile of the neural response distribution.

In our simulation experiments we also applied the previously described nonlinear response saturation transform to the stimulus luminance profile. As a result all curves in Figure 4 were shifted upwards over a distance corresponding to approximately 2". In this case the results of the width discrimination experiment can only be explained by the assumption that the visual system determines the equivalent width of the interval determined by the zero-crossings in the orthoaxial profile of the neural response distribution elicited by the stimulus pattern.

In summary, the results from this experiment seem to rule out the possibility that the visual system detects the distance between either the

extrema or the centroids of the outer two zero-bounded regions of activity in the neural response distribution. However, it seems possible that the zero-crossings in the neural activity distribution are extracted.

EXPERIMENT II: Vernier acuity.

The stimulus we used in this experiment consisted of one target bar with an asymmetrical orthoaxial contrast profile and one reference bar with a constant valued contrast profile. Except for its centroid, the latter bar provides only edge cues. As in a conventional Vernier experiment, the bars were placed one above the other (and oriented along the vertical). The asymmetrical bar had a width (i.e. an entire orthoaxial extent) of 175". The luminance of the bar with the constant valued contrast profile was 80% of the maximal luminance of the asymmetrical bar. It was given a width for which it had the same perceived orthoaxial extent as the asymmetrical bar (as determined for each subject in the previous experiment). The length of both bars was 18' and their vertical separation (when their edges were aligned) was 5'. The orthoaxial separation between the axes of both bars was always centered on the vertical through the middle of the CRT display. The subject's task is to report, by pressing the appropriate one of two digital switches, whether the top line was shifted to the right or left of the lower line. The offset in position was varied randomly from side to side and selected from a number of preset magnitudes, using APE.

It has been argued that orientation cues may be available for performing Vernier acuity tasks (Sullivan et al., 1972). To eliminate offset errors that may arise due to a difference between the perceived orientation and the veridical orientation of the stimulus pattern, we randomly placed the target stimulus either below or on top of the reference stimulus. The subject's responses for these two conditions were processed separately. The final location estimate equals the mean of the PSE's of both error response distributions. Each datum point represents the r.m.s. of at least ten of these estimates with the standard deviation of their distribution serving as a measure of dispersion, defined as the standard error.

ARTIST'S IMPRESSION OF
THE VERNIER STIMULUS

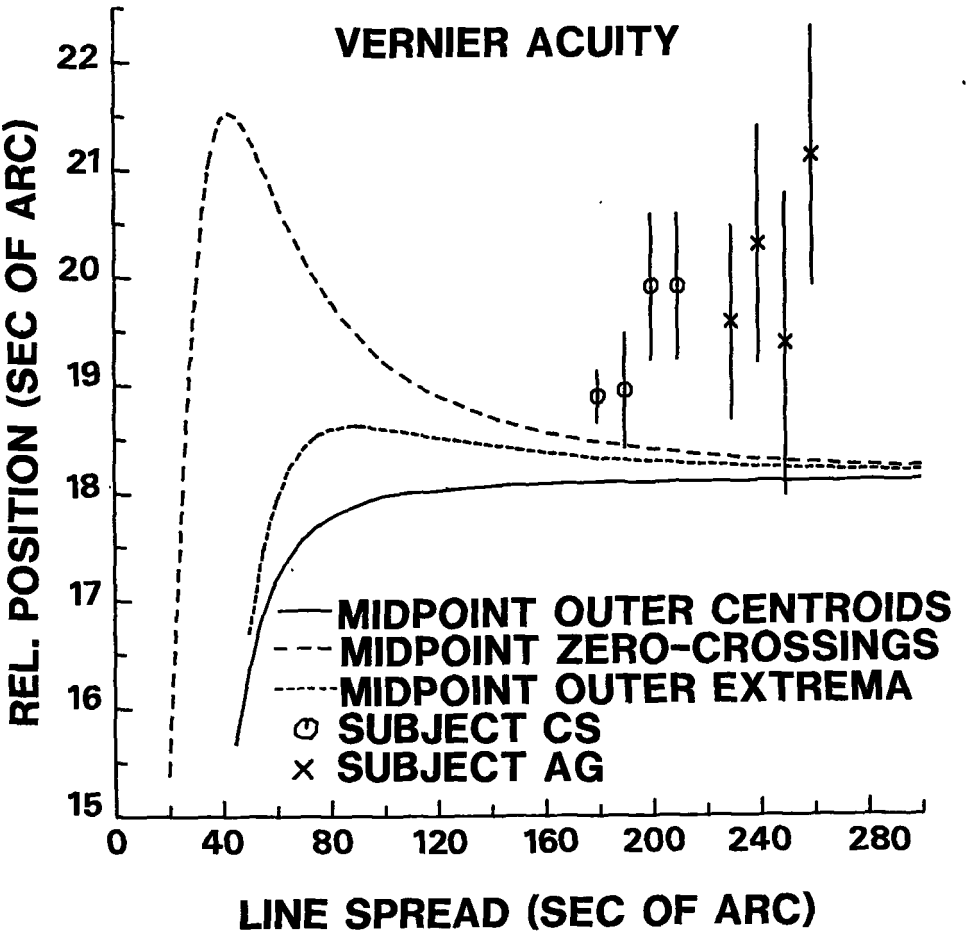

Figure 5. The results of the Vernier acuity experiment for subjects CS and AG. This Figure also shows the relative location of the centra of the spatial intervals delineated by respectively (i) the outer two centroids (solid line), (ii) the two zero-crossings (dashed line) and (iii) the outer two extrema (dotted line) of the orthoaxial profile of the simulated neural activity distribution. All positions are taken relative to the axis of the target bar.

Results and discussion.

Figure 5 represents the individual data for two observers and the results of some numerical simulations of the Vernier acuity experiment. The drawn curves in this figure were obtained by computing the distances between the centre of the asymmetrical orthoaxial contrast profile of the input test stimulus and the centra of the spatial intervals delineated by respectively (i) the outer centroids, (ii) the two zero-crossings and (iii) the outer two extrema (troughs) of the orthoaxial profile of the simulated neural response distribution that is thought to be elicited by the presence of this test stimulus.

The data points indicating the results of our subjects in the Vernier acuity experiments represent the distance between the axis of the target bar and the perceived middle of the equiluminous reference bar when both are perceived to be in alignment, or, equivalently, the distance between the axis of the target bar and the position at which it is perceived to be located. These data points are again arbitrarily positioned somewhere along the horizontal axis of Figure 5. Their order from left to right corresponds with the conditions I to IV as described in the previous section.

The results of Figure 5 show no consistent dependency of the perceived relative locations of the target stimulus on the value of the stimulus contrast. An increase of the pupil diameter (condition IV) seems to cause an increase in the separation between the middle of the target bar and its perceived location, although this effect is too small to be significant. The results of subject CS for conditions III and IV are even identical.

Figure 5 shows that the results of the Vernier acuity experiment can in principle be explained by the assumption that the visual system assigns the location of the bar to the middle of the zero-crossings in the orthoaxial neural response distribution. Only two of the data points (the results of condition II for subject CS and condition III of subject AG) can possibly be explained by one of the other abovementioned mechanisms.

TABLE III. Results of the Vernier experiment.

subject	condition nr.	relative perceived position of bar (sec of arc)	spread (sec of arc)	error range spread (±1 SE) (sec of arc)
CS	I	18.89 ± 0.24	120	100 - 140
	II	18.94 ± 0.53	115	90 - 200
	III	19.91 ± 0.68	75	60 - 100
	IV	19.91 ± 0.68	75	60 - 100
AG	I	19.6 ± 0.9	85	65 - 140
	II	20.3 ± 1.1	67	47 - 100
	III	19.4 ± 1.4	90	59 - ∞
	IV	21.1 ± 1.2	53	30 - 76

The distance between the axis of the target bar and the position at which it is perceived to be located are presented in Table III for all different conditions. Table III also presents the estimated extent of the hypothetical processing units that are involved in the localization process, under the assumption that the visual system assigns the location of the bar to the middle of the interval delineated by the zero-crossings in the orthoaxial neural response distribution.

In the present simulation experiments we again applied the previously described nonlinear response saturation transform to the asymmetrical luminance profile of the test stimulus. As a result all curves in Figure 5 were shifted downwards over a distance corresponding to approximately 1". In this case the results of the Vernier acuity experiment can only be explained by the assumption that the visual system determines the middle of the interval defined by the zero-crossings in the orthoaxial profile of

the neural response distribution elicited by the presentation of the stimulus pattern.

The results from this experiment are in agreement with those of the width-discrimination experiment. Both experiments seem to rule out the possibility that the visual system assigns a location to a combination of either the extrema or the centroids of the outer two zero-bounded regions of activity in the neural response distribution. The results of both experiments can in principle be explained by a mechanism that assigns the location of a bar to the zero-crossings in its corresponding neural response distribution.

EXPERIMENT III: Bisection discrimination.

The stimulus we used for the bisection experiment consisted of three vertically oriented bars placed next to each other. The length of the bars was 26'.The middle (target) bar had an asymmetrical orthoaxial contrast profile with a total orthoaxial extent of 175". The outer two (reference) bars had a constant valued contrast profile. Thus, for each of these reference bars the position of their mean or centroid and the position of the middle of the interval delineated by their edges coincided. This has the advantage that the perceived position of the target bar, relative to the two reference bars, was only determined by the characteristics of its orthoaxial contrast profile (i.e. the perceived location of each of the reference bars was assumed to be uniquely determined and to be at the middle of their contrast profile). The luminance of both reference bars was 80% of the maximal luminance of the asymmetrical bar. Their total orthoaxial extent (width) was 2 min of arc.

A number of discrete positions were available for testing. These were equally spaced and centered around the location of the physical mean of the reference interval. On each trial the target stimulus was positioned randomly on one of these locations using APE. The subject's (forced choice) task was to report whether the target stimulus appeared to the left or to the right of the midpoint of the reference interval. In the previous section we have described how the offset errors were eliminated in this case.

In a three line interval bisection experiment there are different strategies a subject may use to perform the task. One strategy is to determine the (subjective) middle of the interval constituted by the outer two reference bars. Thereafter, the position of the target bar may be judged relative to that of this subjective middle. This procedure would involve the comparison of the mean local sign of the reference bars (or, equivalently, of the interval between the two reference bars) with the location attributed to the target bar. Note that both local signs may be computed in parallel. Therefore, this strategy requires no scanning eye movements. Another strategy would be to compare the width of the two spatial intervals constituted by the three bars. Comparison of the mean local signs of the two spatial intervals is clearly of no avail to obtain a bisection judgement. This procedure seems to require the explicit comparison of the differences of the local signs of the two reference bars and that of the target bar. Therefore, we suspect that this strategy may depend on scanning eye movements, or, equivalently, the use of temporal cues.

In this paper we tried to establish the features of the spatial contrast profile of a stimulus that are used in the visual assessment of its spatial location. We didn't want to confuse the issue by using tasks that depend on the ability to perform geometrical calculations or scanning eye movements (and which may involve global or temporal processing strategies). Therefore, we tried to stimulate the use of the first strategy (i.e. comparison of the mean local signs of the two reference bars and that of the target bar). This was done as follows:

- The outer two reference bars were continuously present. The subjects were instructed to fixate on the middle of the interval delineated by these bars.
- If the distance between the two reference bars was too large the subjects tended to use scanning eye movements to determine the middle of the interval these bars constitute. We found 10' a convenient separation for which the subjects had no difficulties maintaining a steady fixation (i.e. for which they had an instantaneous impression of the location of the middle of the interval).
- The presentation of the target bar lasted for only 0.5 sec.

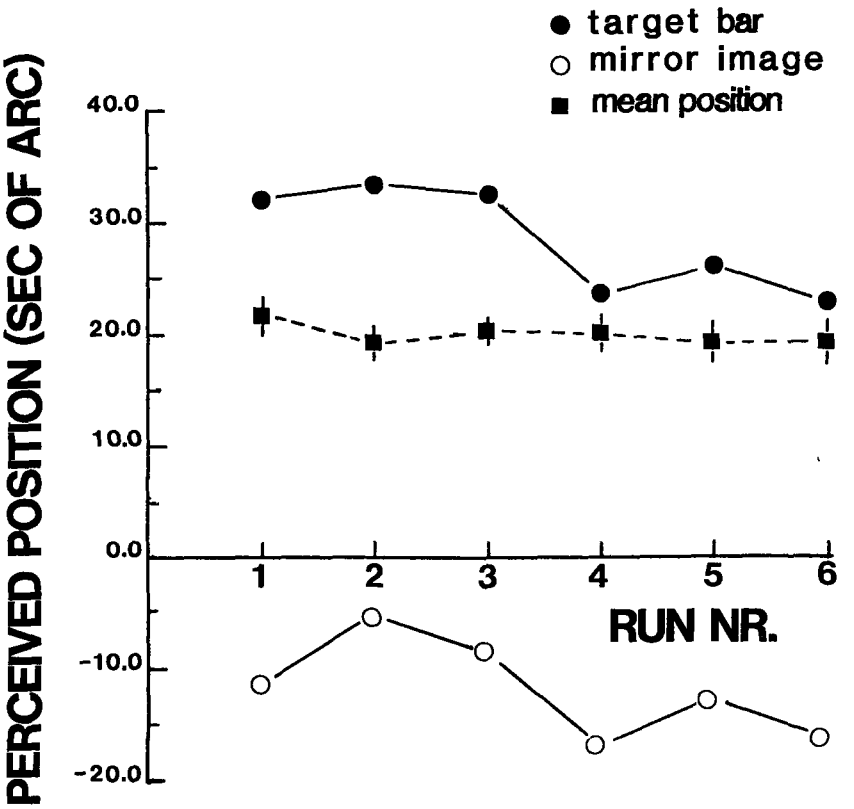

Figure 6. Example of the variation of respectively the perceived location P_1 of a target bar (upper drawn line) and the perceived position P_2 of its mirror image (lower drawn line), both taken relative to the physical middle of the reference interval, over a number of runs of the bisection discrimination experiment. The dashed line indicates the perceived location P of the target bar relative to its axis. P was obtained by taking half the difference of P_1 and P_2 (i.e. $P=\frac{1}{2}(P_1-P_2)$). Note that the variation in P is smaller than the individual variations in respectively P_1 and P_2.

Results and discussion.

As we have mentioned before, we obtained a single localization estimate from two simultaneously performed interwoven runs for a target stimulus and its mirror (left-right reversed) image. A single localization estimate can of course also be obtained from two consecutive runs. However, in this case a shift in the subject's criterium for response (corresponding for instance to a shift in the perceived location of the middle of the reference interval) will cause an offset error in the final estimate of the perceived target position. This offset error will be eliminated when the above described interwoven procedure is applied. This effect is clearly illustrated by Figure 6. This figure shows that the variations in the perceived locations of the target stimulus and its mirror image relative to the physical middle of the reference interval and obtained by the above described interwoven measuring procedure are (i) larger than the standard error in the individual values and (ii) highly correlated. However, the variations in half the difference of both distances (corresponding to the perceived location of the target bar relative to its axis) are within the (relatively small) standard error. When the perceived position of the target stimulus and its mirror (left-right reversed) image, relative to the physical middle of the reference interval, are computed separately by taking the mean of their respective location estimates derived from a number of (typically 10) interwoven runs before taking half the difference of the perceived positions of both stimuli then the external error is considerably larger than the internal one (chisquare = 4 ... 10). However, when half the difference of the perceived location of the target stimulus and its mirror image is computed for each individual pair of estimates (that results from a single interwoven run) before computing the mean of these values then both errors are comparable (chisquare = 0.8 ... 1.0). The same effects were noted in the previous two experiments.

Figure 7 represents the individual data for two observers and the results of some numerical simulations of the bisection discrimination experiment. The drawn curves in this figure were obtained by computing the distances between the centre of the asymmetrical orthoaxial contrast

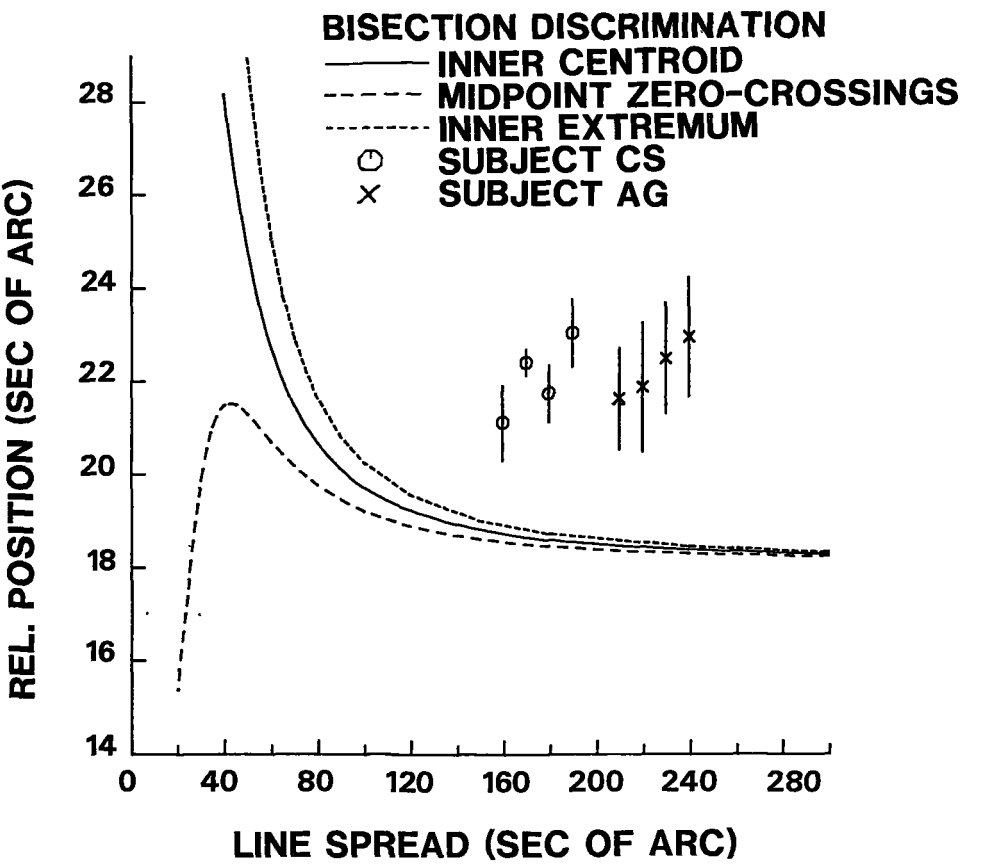

Figure 7. The results of the bisection discrimination experiment for subjects CS and AG. This Figure also shows the relative location of respectively (i) the centroid (solid line), (ii) the midpoint of the two zero-crossings (dashed line) and (iii) the extremum of the inner zero-bounded region (dotted line) of the orthoaxial profile of the simulated neural activity distribution. All positions are taken relative to the axis of the target bar.

profile of the input test stimulus and respectively (i) the centroid or (ii) the extremum (peak) of the zero-bounded region of activity and (iii) the middle of the two zero-crossings of the orthoaxial profile of the simulated neural response distribution that is thought to be elicited by the presence of this test stimulus.

The data points indicating the results of our subjects in the bisection discrimination experiments represent the distance between the axis of the target stimulus and the perceived middle of the interval delineated by the two equiluminous reference bars when both are perceived to be at the same location, or, equivalently, the distance between the axis of the target bar and the position at which it is perceived to be located. Again the data points are arbitrarily positioned somewhere along the horizontal axis of Figure 7. Their order from left to right corresponds with the conditions I to IV as described in the previous section.

The results of Figure 7 show no consistent or significant dependency of the perceived location of the target bar on the value of its contrast. As was found in the previous experiment, an increase of the pupil diameter (condition IV) seems to cause an increase in the separation between the axis of the target bar and its perceived location, although this effect is again too small to be significant.

Figure 7 shows that all results of the bisection discrimination experiment can in principle be explained by the assumption that the visual system assigns the location of the target bar to either the extremum or the centroid of the zero-bounded region of activity in the orthoaxial neural response distribution. Five of the data points (the results of the conditions I and III for subject CS and the conditions I to III of subject AG) can possibly be explained by a mechanism that attributes the location of the bar to the middle of the interval delineated by the zero-crossings.

TABLE IV. Results of the bisection experiment.

subject	condition nr.	relative perceived position of bar (sec of arc)	spread (sec of arc)	error range of spread (±1 SE) (sec of arc)
CS	I	21.12 ± 0.82	74	66 - 87
	II	22.43 ± 0.29	62	60 - 64
	III	21.75 ± 0.63	67	62 - 74
	IV	23.06 ± 0.73	57	54 - 63
AG	I	21.7 ± 1.1	68	60 - 82
	II	21.9 ± 1.4	66	57 - 83
	III	22.5 ± 1.2	62	55 - 72
	IV	23.0 ± 1.3	58	52 - 69

The distance between the axis of the target bar and the position at which it is perceived to be located are presented in Table IV for all different conditions. Table IV also presents the estimated extent of the hypothetical processing units that are involved in the localization process, under the assumption that the visual system assigns the location of the bar to the centroid of the zero-bounded region of activity in the orthoaxial neural response distribution.

In the present simulation experiments we again applied the previously described nonlinear response saturation transform to the asymmetrical luminance profile of the target stimulus. As a result all curves in Figure 7 were shifted downwards over a distance corresponding to approximately 1". In this case none of the results of the bisection experiment can any longer be explained by the assumption that the visual system determines the middle of the interval defined by the zero-crossings in the orthoaxial profile of the neural response distribution elicited by the presentation of the stimulus pattern.

The results from this experiment are clearly not in agreement with those of the Vernier- and the width-discrimination experiments. As we noted before, the results of the latter two experiments seem to rule out the possibility that the visual system assigns a location to a combination of either the extrema or the centroids of the outer two zero-bounded regions of activity in the neural response distribution. However, they can in principle be explained by a mechanism that assigns a location tag to a combination of the zero-crossings in this distribution. The present results lead us to exactly the opposite conclusions.

This controversy may reflect the fact that different strategies are used to assess the location of the target bar in the different experiments. As we noted before, the width discrimination task is probably performed by comparing the relative separation of edge cues. The Vernier task may also be performed by aligning edge cues. However, in the bisection experiment the conditions were chosen such that they stimulated the comparison of the mean local signs of the reference interval and the target stimulus. To see whether we could consistently influence the results of the bisection experiment by promoting a different discrimination strategy and to find out whether the results thus obtained could in principle be explained by the same mechanism that was used to explain the results from the first two experiments, we repeated the bisection experiment for condition II. In this experiment the subjects were instructed to compare the width of the two intervals constituted by the three bars. They had to report whether the left interval was wider or smaller than the right interval. The results of this experiment are listed in Table V, together with the previously obtained results for the same condition (II). These results show that the separation between the location at which the target bar is perceived and its axis is consistently smaller when the subjects discriminate the relative width of the intervals between the three bars compared to the results of the experiment in which they determine the difference between the mean local sign of the reference interval and that of the target bar. Comparison of the results obtained by using the interval discrimination strategy with the simulated data, represented by the drawn curves in Figure 7, shows that these results can in principle also be explained by a mechanism that assigns a location tag

to the middle of the interval determined by the zero-crossings in the simulated neural activity distribution. Thus, we conclude that both the zero-crossings and the centroid or extremum of the zero-bounded region of the neural activity distribution that is elicited by the presentation of the target bar are in principle available to perception. It probably depends on the stimulus conditions and the adopted strategy which features are actually used in the different localization tasks.

TABLE V. Results of the bisection experiment for condition II.

subject	interval discrimination (sec of arc)	comparison of mean position (sec of arc)
CS	19.76 ± 0.58	22.43 ± 0.29
EO	18.4 ± 0.9	22.4 ± 1.1

SUMMARY AND CONCLUDING REMARKS.

The experiments reported here were designed to investigate the mechanisms underlying visual spatial localization. The target stimulus we used was a bright bar with an asymmetrical orthoaxial contrast profile. The reference stimuli consisted of one or two equiluminous bars.

First we determined the orthoaxial extent of a reference bar for which it presented a width impression that was identical to that of the target bar. Thereafter we determined the distance between the perceived position of the target bar and the location of its axis when it was judged to be in alignment with a reference bar that had a perceived width equivalent to that of the target bar (Vernier experiment). We found that the results of both of these experiments can in principle be explained by a mechanism that assigns a location tag to the centre of the interval determined by the zero-crossings in the simulated neural response

distribution that is thought to be elicited by the presentation of the stimulus pattern. It was shown that the application of a nonlinear saturation function to the stimulus luminance profile even strenghtens this conclusion.

In the bisection experiment we again determined the distance between the location of the axis of the target bar and the position at which it was perceived to be located. This was done for two different subjective decision criteria. In the first part of this experiment the subjects compared the perceived location of the target stimulus with the perceived position of the middle of the interval delineated by the two equiluminous reference bars. When this criterium is used the results of the bisection discrimination experiment can in principle be explained by the assumption that the visual system assigns the location of the target bar to either the extremum or the centroid of the zero- bounded region of activity in the simulated orthoaxial neural response distribution. The results of this experiment were not in agreement with the predictions for the results of a mechanism that extracts zero-crossings from the neural response distribution. In the second part of this experiment the subjects compared the width of the intervals determined by the three bars consituting the stimulus pattern. The results of this experiment can again be explained by a mechanism that attributes a location tag to the middle of the interval determined by the zero-crossings in the simulated neural response distribution.

We also repeated the Vernier experiment for different instructions to the observers. However, the results we obtained were very consistent and showed no significant variation (i.e. they varied only within one standard error) with the subjective strategy that was used to perform the experiment.

Thus, we conclude that both the zero-crossings and the centroid or extremum of a zero-bounded region of the neural activity distribution that is elicited by the presentation of a stimulus pattern are in principle available to perception. It probably depends on the spatial characteristics of the applied stimulus pattern and the adopted strategy which features are actually used in the different localization tasks. The use of zero-crossings seems to prevail in tasks requiring boundary

information like alignment- (Vernier acuity) or separation-tasks (the width discrimination task and the bisection task for the interval-width discrimination strategy). Tasks involving the comparison of mean local signs of stimulus features may require the use of the centroids or extrema in a neural response distribution.

Acknowledgements - We thank Dr.R.J.Watt and Dr.D.P.Andrews for kindly providing us with a listing of their APE program. We are indebted to Ad de Goffau and Ellie Oostveen who acted as patient observers. This work was supported by the Dutch Foundation for the Advancement of Pure Research (ZWO).

REFERENCES.

Badcock, D.R. and Westheimer, G. (1985a) Spatial location and hyperacuity: the centre/surround localization contribution function has two substrates. Vision Res. 23, 1259-1267.

Badcock, D.R. and Westheimer, G. (1985b) Spatial location and hyperacuity: flank position within the centre and surround zones. Spatial Vision 1, 3-11.

Barlow, H.B. (1979) Reconstructing the visual image in space and time. Nature 279, 189-190.

Campbell, F.W. and Gubisch, R.W. (1966) Optical quality of the human eye. J. Physiol. 186, 558-578.

Finney, D.J. (1971) Probit Analysis, 3rd edn. Cambridge Univ.Press.

Frisby, J.P. and Mayhew, J.E.W. (1980) Spatial frequency tuned channels: implications for structure and function from psychophysical and computational studies of stereopsis. Phil. Trans. R. Soc. Lond. B 290, 95-116.

Fry, G.A. (1970) The optical performance of the human eye. In: Progress in optics, Vol. VIII, 52-131.

Gubisch, R.W. (1967) Optical performance of the human eye. J. Opt. Soc. Am. 57, 407-415.

Hering, E. (1899) Über die Grenzen der Sehschärfe. Ber. Math.-phys. Cl. d. König. Sächs. Gesell. Wiss. Leipzig. Naturwiss. Teil 16-24.

Hines, M. (1976) Line spread function variation near the fovea. Vision Res. 16, 567-572.

Hood, D.C., Finkelstein, M.A. and Buckingham, E. (1979) Psychophysical tests of models of the response function. Vision Res. 19, 401-406.

King-Smith, P.E. and Kulikowsky, J.J. (1975) Pattern and flicker detection analysed by subthreshold summation. J. Physiol. 249, 519-548.

Klein, S.A. and Levi, D.M. (1985) Hyperacuity thresholds of 1 sec: theoretical predictions and empirical validation. J. Opt. Soc. Am. A2, 1170-1190.

Koenderink, J.J. (1984a) Simultaneous order in nervous nets from a functional standpoint. Biol. Cybern. 50, 35-41.

Koenderink, J.J. (1984b) Geometrical structures determined by the functional order in nervous nets. Biol. Cybern. 50, 43-50.

Legge, G.E. and Kersten, D. (1983) Light and dark bars: contrast discrimination. Vision Res. 23, 473-483.

Levi, D.M., Stanley, A.K. and Aitsebaomo, A.P. (1985) Vernier acuity, crowding and cortical magnification. Vision Res. 25, 963-977.

Lotze, H. (1884) Mikrokosmos. Hirzel, Leipzig.

Mather, G. and Morgan, M.J. (1986) Irradiation: implications for theories of edge localization. Vision Res. 26, 1007-1015.

Maudarbocus, A.Y. and Ruddock, K.H. (1973) Non-linearity of visual signals in relation to shape sensitive adaptation responses. Vision Res. 13, 1713-1738.

Morgan, M.J. and Watt, R.J. (1982) Mechanisms of interpolation in human spatial vision. Nature 299, 553-555.

Morgan, M.J., Mather, G., Moulden, B. and Watt, R.J. (1984) Intensity-response nonlinearities and the theory of edge localization. Vision Res. 24, 713-719.

Naka, K.I. and Rushton, W.A.H. (1966) S-potentials from luminosity units in the retina of fish (cyprinidae). J. Physiol. Lond. 185, 587-599.

Norman, F.A. and Werblin, F.S. (1974) Control of retinal sensitivity I. J. gen. Physiol. 63, 37-61.

Sullivan, G.D., Oatley, K. and Sutherland, N.S. (1972) Vernier acuity as affected by target length and separation. Percept. Psychophys. 12, 438-444.

Valeton, J.M. and van Norren, D. (1983) Light adaptation of primate cones: an analysis based on extracellular data. Vision Res. 23, 1539-1547.

Volkmann, A.W. (1863) Physiologische Untersuchungen im Gebiete der Optik. Breitkopf & Hartel, Leipzig.

Watt, R.J. (1984) Towards a general theory of the visual acuities for shape and spatial arrangement. Vision Res. 24, 1377-1386.

Watt, R.J. and Andrews, (1981) APE: adaptive probit estimation of psychometric function. Curr. Psychol. Rev. 1, 205-214.

Watt, R.J. and Morgan, M.J. (1983a) Mechanisms responsible for the assessment of visual location: theory and evidence. Vision Res. 23, 97-109.

Watt, R.J. and Morgan, M.J. (1983b) The recognition and representation of edge blur: evidence for spatial primitives in human vision. Vision Res. 23, 1465-1477.

Watt, R.J. and Morgan, M.J. (1984) Spatial filters and the localization of luminance changes in human vision. Vision Res. 24, 1387-1397.

Watt, R.J. and Morgan, M.J. (1985) A theory of the primitive spatial code in human vision. Vision Res. 25, 1661-1674.

Watt, R.J. Morgan, M.J. and Ward, R.M. (1983) Stimulus features that determine the visual location of a bright bar. Invest. Ophthalmol. Vis. Sci. 24, 66-71.

Westheimer, G. and McKee, S.P. (1977a) Integration regions for visual hyperacuity. Vision Res. 17, 89-93.

Westheimer, G. and McKee, S.P. (1977b) Spatial configurations for visual hyperacuity. Vision Res. 17, 941-947.

Wilson, H.R. (1978) Quantitative characterization of two types of line-spread function near the fovea. Vision Res. 18, 971-981.

Wülfing, E.A. (1892) Über den kleinsten Gesichtswinkel. Z. Biol. 29, 199-202.

Samenvatting.

Dit proefschrift behandelt een aantal aspekten van de verwerking van spatiële informatie door het menselijke visuele systeem. Centraal staat de vraag hoe de relatieve positie van objekten in het visuele veld wordt gekodeerd in de simultane signaalaktiviteit van de neurale elementen. Er wordt op twee manieren getracht inzicht in dit probleem te verkrijgen. Ten eerste (Deel I) wordt er met behulp van simulatiemodellen getoond hoe een neuraal systeem de inputsignalen die het ontvangt van zijn bijbehorende detektorruimte kan integreren tot een kontinu samenhangende gewaarwording. Ten tweede (Deel II) worden de resultaten vermeld van een paar experimenten die werden verricht om de grenzen van de nauwkeurigheid van dit integratieproces in het menselijke visuele systeem te bestuderen.

In Deel I worden twee modellen gepresenteerd die beschrijven hoe de hersenen een zuiver funktionele ordening kunnen aanbrengen in een kollektie neurale elementen door gedurende een zekere tijdsduur (ook wel leerfase genoemd) de signaalaktiviteit in die elementen te bestuderen. De achterliggende gedachten bij deze modellen zijn de volgende:

(i) Een neuraal netwerk (bijvoorbeeld de visuele cortex) heeft geen a priori informatie over de ruimtelijke struktuur (geometrie) van de met dat netwerk korresponderende detektorruimte.

(ii) Het kan deze informatie alleen verkrijgen door een studie te maken van al zijn aktivatietoestanden die gedurende een leerfase optreden.

(iii) Het neurale systeem representeert de zo verworven kennis over zijn eigen funktionele beperkingen in zijn verbindingsstruktuur.

Op grond van de tijdens de leerfase verworven kennis kan het systeem vervolgens zijn aktivatietoestanden of "waarnemingen" indelen in funktionele equivalentieklassen. Zo is het systeem in staat zowel de spatiële struktuur van de detektorruimte als die van de buitenwereld (zoals die wordt gerepresenteerd in de projektie van de buitenwereld op de met het neurale netwerk korresponderende detektorruimte) te karakteriseren. De mate waarin deze funktionele beschrijving van de opbouw van de detektorruimte overeenkomt met diens ruimtelijke (geometrische) samenhang

zoals die door een externe waarnemer zou worden beschreven hangt af van (i) de verbindingsstruktuur binnen het netwerk en (ii) de geometrische struktuur van de buitenwereld gedurende de leerfase. Een tekort aan verbindingen in een dergelijk netwerk maakt het voor het systeem onmogelijk in aktivatiepatronen met een gelijk aantal deelelementen (van ongeveer gelijke afmetingen) verschillende spatiële strukturen te onderscheiden. In dit geval kan het de deelelementen van een aktivatiepatroon alleen nog maar tellen en niet meer funktioneel ordenen. Het gevolg is dat het systeem aktivatiepatronen met hetzelfde aantal deelelementen maar een verschillende spatiële struktuur alle in dezelfde funktionele equivalentieklasse onderbrengt. Een teveel aan verbindingen heeft tot gevolg dat er slechts een beperkt aantal equivalentieklassen kan worden onderscheiden. Er bestaat dus voor een neuraal netwerk een optimale verbindingsstruktuur die (wanneer de buitenwereld voldoende struktuur bezit) in eerste instantie wordt bepaald door de geometrische struktuur van de bijbehorende detektorruimte.

In Hoofdstuk I.1 worden twee algorithmes gepresenteerd die beschrijven hoe een funktionele orde in een kollektie neurale elementen tot stand kan komen wanneer er alleen gebruik mag worden gemaakt van de funktionele relaties tussen die elementen. Het eerste algorithme maakt gebruik van de korrelaties in de signaalaktiviteit van verschillende neurale elementen. In het vervolg wordt dit algorithme aangeduid als het "covariantie-model". Het tweede algorithme gebruikt de aktivatie-coincidenties van de neurale elementen. Dit algorithme zal in het vervolg het "coincidentie-model" worden genoemd. Uitgaande van de voornoemde (covariantie- of coincidentie-) relaties konstrueren beide algorithmes een partiële funktionele orde in de kollektie neurale elementen. Door funktioneel equivalente neuronen te laten versmelten tot een funktionele eenheid of door neuronen te rekruteren die voorheen geen funktionele betekenis hadden kan er lokaal een roosterordening worden gekonstrueerd. In dit hoofdstuk worden de resultaten vermeld van enkele simulatieexperimenten die werden uitgevoerd om te bestuderen hoe het aantal funktioneel onderscheidbare elementen in de resulterende roosterordening afhangt van het aantal funktionele individuen in de partiële ordening.

In Hoofdstuk I.2 wordt besproken hoe de funktionele ordening in een neuraal netwerk kan worden gerelateerd aan de geometrie van de met dat netwerk korresponderende detektorruimte. Er wordt een algorithme gepresenteerd dat, uitgaande van de bovengenoemde funktionele orde, een abstrakt geometrisch komplex konstrueert. De algebraïsche struktuur van dit komplex representeert de geometrische en topologische struktuur van de detektorruimte. Verder wordt er besproken hoe aktivatiepatronen binnen dit komplex kunnen worden gerelateerd aan de stimuli die worden aangeboden aan de kollektie detektoren. De homologie van een abstrakt komplex kan door het uitvoeren van simpele kombinatorische operaties worden vastgesteld. Zodoende is het mogelijk dat zowel de geometrie van de detektorruimte als de topologische struktuur van de stimulus patronen objektief aanwezig zijn in de simultane funktionele orde in het neurale systeem.

Zoals reeds eerder werd vermeld worden er zowel door de geometrische struktuur van de detektorruimte als door de buitenwereld beperkingen opgelegd aan de signaalaktiviteit in een neuraal netwerk. De simultane funktionele orde die wordt geproduceerd door het covariantie- en het coincidentie-model kodeert deze beperkingen in de uiteindelijke funktionele struktuur van het netwerk. In de Hoofdstukkken I.3 en I.4 worden de resultaten gepresenteerd van een aantal simulatieexperimenten die werden uitgevoerd om de invloed te bestuderen van verschillende beperkingen van de geometrische struktuur van respektievelijk de detektorruimte en de buitenwereld op de uiteindelijke funktionele orde die in het neurale systeem ontstaat. De resultaten die worden vermeld in Hoofdstuk I.3 laten zien dat zowel het covariantie- als het coincidentie-model in staat zijn om een funktionele struktuur voort te brengen die een isomorphisme met een triangulatie toelaat, wanneer tenminste de onderliggende detektorruimte een voldoend ontwikkelde geometrische struktuur bezit. Uit resultaten die worden beschreven in Hoofdstuk I.4 blijkt dat de geometrische beperkingen van de buitenwereld worden vastgelegd in de funktionele struktuur van een netwerk zoals die door het coincidentie-model wordt geproduceerd. Er wordt in dit hoofdstuk ook aangetoond hoe bepaalde gewaarwordingen (aktiviteitspatronen) van het netwerk kunnen worden gerelateerd aan gebeurtenissen (stimuli) in de buitenwereld.

In Deel II wordt een studie gemaakt van het vermogen van het menselijke visuele systeem om de relatieve positie van objecten in het visuele veld te bepalen. Kennis omtrent dit vermogen kan inzicht verschaffen in het probleem dat in dit proefschrift centraal staat: namelijk hoe de perceptie van een kontinu visueel veld kan ontstaan uit een groot aantal losse inputsignalen. Ergens in het visuele systeem moet elke signaalbaan kunnen worden gerelateerd aan elke andere, omdat we in staat zijn de relatieve positie te schatten van twee objecten die gelijktijdig en op een willekeurige positie in het visuele veld aanwezig zijn. Door de grenzen van de nauwkeurigheid van het lokalisatievermogen te bestuderen kan het duidelijk worden hoe de relaties tussen de verschillende signaalbanen tot stand komen. Daarom wordt in Deel II bestudeerd hoe nauwkeurig verschillen in relatieve positie kunnen worden waargenomen. Het is namelijk bekend dat het menselijke visuele systeem verschillen in relatieve positie kan waarnemen die (uitgedrukt in ruimtehoeken) een orde van grootte kleiner zijn dan de afmetingen van de foveale photoreceptoren. Deze extreem hoge nauwkeurigheid wordt doorgaans toegeschreven aan een corticaal interpolatieproces dat een gewogen gemiddelde van een aantal losse inputsignalen zou berekenen. Door niet alleen de relatieve positie maar ook de resolutie van stimuli te variëren wordt in Deel II getracht meer kennis over de aard van het lokalisatievermogen te verkrijgen.

In Hoofdstuk II.1 wordt een psychofysisch experiment beschreven waarbij een proefpersoon gevraagd wordt een uitspraak te doen over de relatieve spatiële positie van drie identieke vage vlekjes. Alle vlekjes hebben een Gaussisch spatiëel luminantieprofiel. In de referentiepositie liggen de vlekjes onder elkaar en op een gelijke onderlinge afstand. Het totale stimuluspatroon is Gaussisch gemoduleerd in de tijd. De stimulus wordt aangeboden met een luminantiekontrast dat gelijk is aan de kontrast-detektie drempelwaarde van een enkel vlekje. De keuze van de stimuli is zodanig dat verwacht mag worden dat ze slechts een klein bereik van het scala van resolutie-afhankelijke kontrastdetektiemechanismen zullen aktiveren. Dit maakt het mogelijk de schaalgrootte van deze psychofysische grootheden te relateren aan de karakteristieke afmetingen van de vlekjes (te weten de schaalparameter van hun Gaussische spatiele luminantie-

profiel). Bij elke aanbieding van de stimulus is het middelste vlekje over een kleine afstand verschoven ten opzichte van het middelpunt van het lijnsegment dat de centra van de buitenste twee vlekjes verbindt (en dat vertikaal is georienteerd). Dit punt wordt in het vervolg het "referentiepunt" genoemd. Is deze verschuiving (die gelijk nul mag zijn) langs de horizontaal door het referentiepunt dan spreken we van de "orthoaxiale taak". Wanneer de uitwijkingen langs de vertikaal door dit punt liggen wordt gesproken over de "axiale-" of "bisectietaak". Uit de resultaten van Hoofdstuk II.1 blijkt dat voor de orthoaxiale taak en geometrisch gelijkvormige stimuli de juist waarneembare verplaatsing van het middelste vlekje een konstante fraktie is van de spatiele schaalparameter van dat vlekje. Deze relatie blijkt te gelden over een bereik van minstens twee decaden voor deze schaalparameter.

In Hoofdstuk II.2 wordt eerst vastgesteld dat de in Hoofdstuk II.1 gevonden schaalrelatie voor de orthoaxiale taak ook geldt voor de bisectie taak. Vervolgens worden voor beide taken de verplaatsingsdrempels gemeten als funktie van de afstand tussen de buitenste twee vlekjes, voor verschillende waarden van de schaalparameter van de vlekjes. Uit de resultaten blijkt dat er op alle niveaus van resolutie twee verschillende strategien worden gebruikt om relatieve plaatsbepalingen te verrichten. Omschakeling van het ene naar het andere mechanisme vindt plaats wanneer de afstand tussen de buitenste twee vlekjes ongeveer 25 keer de schaalparameter van de vlekjes bedraagt.

In Hoofdstuk II.3 wordt onderzocht hoe nauwkeurig het menselijke visuele systeem twee identieke vlekjes, met een afstand tussen hun centra die klein is ten opzichte van hun schaalparameter, kan onderscheiden van een enkele vlekje. De stimuli worden weer aangeboden met een kontrast gelijk aan de detektiedrempel waarde van een enkel vlekje. Ook bij dit experiment blijkt de juist waarneembare uitwijking van de beide vlekjes een konstante fraktie van de spatiele schaalparameter van de vlekjes te zijn. Wederom blijkt deze relatie te gelden over een bereik van minstens twee decaden voor de schaalparameter van de vlekjes.

De resultaten van Hoofdstuk II.2 laten zien dat er op elk niveau van resolutie twee gebieden zijn waarin relatieve plaatsbepaling op een andere manier geschiedt. In Hoofdstuk II.4 wordt een experiment beschreven

dat dient om te onderzoeken of deze verschillende gebieden korresponderen met psychofysische modulen die gespecialiseerd zijn in het bepalen van relatieve posities. Als dit het geval is mag worden verwacht dat de werking van dergelijke modulen wordt verstoord wanneer er in hun blikveld meer objekten aanwezig zijn dan alleen degenen waarvoor een relatieve plaatsbepaling wordt verlangd. Daarom wordt de orthoaxiale taak verricht in de aanwezigheid van twee storende vlekjes. De resultaten laten zien dat de nauwkeurigheid waarmee de taak kan worden verricht niet door de aanwezigheid van de twee extra vlekjes wordt beinvloed. Er kan dus op grond van dit experiment geen uitspraak worden gedaan over het al of niet bestaan van de bovengenoemde hypothetische psychofysische modulen.

Over het al of niet bestaan van verschillende mechanismes voor de detektie van increment- en decrementsignalen zijn de meningen in de literatuur sterk verdeeld. Als er inderdaad een increment/decrement dichotomie bestaat dan lijkt het waarschijnlijk dat de relatieve positie van objekten die door gelijksoortige mechanismes worden gedetekteerd met een grotere nauwkeurigheid kan worden bepaald dan de relatieve positie van objekten die door verschillende mechanismes worden gedetekteerd. Om aanwijzingen te vinden voor het bestaan van een eventuele increment/decrement dichotomy wordt in Hoofdstuk II.5 de orthoaxiale taak uitgevoerd voor verschillende kombinaties van increment- en decrement vlekjes. De nauwkeurigheid waarmee proefpersonen verschillen in de relatieve posities van de vlekjes kunnen waarnemen blijkt in alle gevallen gelijk te zijn. Dit experiment geeft dus geen enkele indikatie voor het bestaan van een increment/decrement dichotomie.

Uit de voorgaande experimenten bleek steeds dat de nauwkeurigheid waarmee verschillen in de relatieve positie van objekten in het visuele veld worden waargenomen schaalt met de resolutie van die objekten (d.w.z. met hun spatiele schaalparameter). Het lijkt daarom aannemelijk dat de juist waarneembare verschillen in de relatieve positie van clusters kleine objekten (bijv. grote vlekken die zijn opgebouwd uit kleine vlekjes) met een bepaalde karakteristieke globale afmeting en van grote objekten met eenzelfde karakteristieke afmeting niet overeen zullen komen. Om dit te onderzoeken worden in Hoofdstuk II.6 zowel de orthoaxiale taak als ook de axiale taak uitgevoerd met zogenaamde Gabor-vlekjes. Dit zijn vlekjes die

bestaan uit Gaussisch gemoduleerde sinusrasters. De experimenten worden gedaan voor verschillende waarden van de schaalparameters van de Gaussische omhullende van de vlekjes en voor verschillende spatiele frequenties van de sinusrasters. Het blijkt dat de nauwkeurigheid waarmee de beide taken kunnen worden verricht alleen afhangt van de schaalparameter van de Gaussische omhullende van de vlekjes en niet van de spatiele frequentie van de sinusrasters. Dit wijst erop dat het visuele systeem een relatieve positie toekent aan een vlek als geheel, onafhankelijk van de spatiele frequentieinhoud van zo'n vlek.

In hoofdstuk II.7 wordt onderzocht welke invloed de eccentriciteit van een stimulus in het visuele veld heeft op de nauwkeurigheid waarmee verschillen in relatieve positie kunnen worden gedetekteerd. Dit wordt zowel gedaan voor de orthoaxiale taak als voor de dubbele vlek discriminatietaak uit Hoofdstuk II.3. Het blijkt dat de isotropie van het visuele systeem toeneemt met afnemende resolutie van de stimuli. Wanneer de resultaten van de orthoaxiale taak met een schatting voor de corticale vergrotingsfaktor worden geschaald vertoont het visuele systeem een opmerkelijke isotropie en resolutie- of spatiele schaalinvariantie voor deze taak. Eenzelfde isotropie en schaalinvariantie worden gevonden voor de dubbele vlek discriminatie taak wanneer de resultaten hiervan worden geschaald met een "neurale resolutie" parameter. Deze resultaten worden kwalitatief verklaard met behulp van een model waarin wordt aangenomen dat het visuele systeem is opgebouwd uit een aantal lagen waarbinnen detektoren naar apertuurgrootte zijn gerangschikt en waarin een automatisch schaal-selektie mechanisme de resolutie van het bemonsterrooster aanpast aan de resolutie of de totale uitgestrektheid van de stimulus. Er wordt gekonkludeerd dat de nauwkeurigheid waarmee het visuele systeem funktioneert in de dubbele vlek discriminatie taak voornamelijk wordt beperkt door retinale faktoren, terwijl de nauwkeurigheid waarmee het de orthoaxiale taak verricht hoofdzakelijk wordt gelimiteerd door corticale faktoren.

In Hoofdstuk II.8 wordt tenslotte een poging ondernomen om de aard vast te stellen van de kleinste spatiele beeldelementen die het visuele systeem gebruikt bij het bepalen van de relatieve positie van objekten. Dit wordt gedaan met behulp van een Vernier-taak, een drie-lijn interval

bisectie taak en een breedte-discriminatie taak voor een test stimulus in de vorm van een balk met een asymmetrisch orthoaxiaal (overdwars) kontrast profiel. De nauwkeurigheid waarmee proefpersonen deze taken kunnen verrichten wordt vergeleken met de resultaten van een numeriek simulatiemodel. Dit model simuleert de neurale responsverdeling die ontstaat bij de perceptie van de stimulus. De positie van enkele kenmerkende punten in de gesimuleerde responsverdeling wordt vergeleken met de positie waarop de stimulus door de proefpersonen wordt waargenomen. Er blijkt dat in sommige taken de positie van de nuldoorgangen van de gesimuleerde responsverdeling, en in andere taken de positie van het zwaartepunt of het extremum van een aan beide zijden door nuldoorgangen begrensd gebied, goede overeenstemming vertonen met de waargenomen positie van de test stimulus. Er wordt gekonkludeerd dat al deze karakteristieke punten in principe kunnen worden gebruikt bij de bepaling van de relatieve positie van een object. Het is waarschijnlijk afhankelijk van de spatiele eigenschappen van de test stimulus en de aard van de te verrichten taak of van de strategie die de proefpersoon toepast van welke mogelijkheden het visuele systeem gebruik maakt.

Nawoord - De grote mate van vrijheid die ik van mijn promotor Prof. Dr. J.J. Koenderink heb gekregen om dit onderzoek te verrichten, en de frequente discussies met hem en Piet Lemmens, Bernard Nienhuis, Herman Snippe en Peter Zuidema zijn voor mij een permanente stimulus met een sterk leereffekt geweest. Jacques Jamar en Armand Lelkens ben ik zeer erkentelijk voor hun goede raad die zijn vruchten heeft afgeworpen. Ik ben Jacques bovendien dank verschuldigd voor zijn hulp bij het verkrijgen van enkele CRT's met white D phosphor. Dankzij de managementcursus die ik van Johan van Esch mocht ontvangen heb ik een bedrijfje, bestaande uit 17 (groot- en klein-) onderzoekers en aktief op 5 verschillende terreinen (te weten local sign, hyperacuity, hierarchische beeldsegmentatie en optic flow computation) succesvol weten te runnen. Peter Werkhoven ben ik dankbaar voor alle badminton- en tennislessen alsmede de urban survival training die ik van hem mocht ontvangen. De prettige samenwerking en het persoonlijke contact met Piet Bijl, Hans Blom, Kees de Graaf, Bart ter Haar Romeny, Leena Määttänen, Steve Pizer en Harry Stevens, en de konstante morele support van Ans Koenderink-van Doorn, hebben veel voor mij betekend. Mien van Deursen en Marijke Kolev hielden mij op de been met lekkere etentjes en werden door mij als tegenprestatie beloond met al mijn (over-) tikwerk. Verder wil ik Peter Faber, Hans Kolijn, Bert Mooi en Pieter Schiphorst hartelijk danken voor hun ondersteuning op elektronisch en technisch gebied. Ik ben mijn trouwe Beebje veel dank verschuldigd voor haar diensten op tekstverwerkingsgebied. Ik dank Hanneke van de Waal voor alle hulp en adviezen op grafisch gebied.

Piet Bijl, Hans Blom, Mike van Eekhout, Barbara van de Doef, Ad de Goffau, Rogier Noordenbos, Gerard Ranke, Henk Simons, Clarel Smit, Carl van Vreeswijk en Huub van de Wouden hebben ieder als student een bijdrage aan het in dit proefschrift beschreven onderzoek geleverd. De studenten Evert van Brummelen, Ad de Goffau, Leen Helmink, Jan van Lieshout en Peter Werkhoven hebben mij geholpen bij het uitoefenen van mijn beeldverwerkingstaak.

Verder gaat mijn dank uit naar Prof. Dr. M.A. Bouman, Ans Koenderink-van Doorn, Ellie Oostveen, Herman Snippe en mijn vader, die allen bereid waren als proefpersoon op te treden.

Last but certainly not least wil ik mijn ouders bedanken. Zonder hun hulp was ik nooit zo ver gekomen.

CURRICULUM VITAE.

De auteur van dit proefschrift werd op 12 oktober 1955 te Apeldoorn geboren. De middelbare schoolopleiding werd gevolgd aan het Gemeentelijk Gymnasium te Apeldoorn.

Na het behalen van het eindexamen Gymnasium β in 1974 werd nog in datzelfde jaar begonnen met de studie Wis- en Natuurkunde (studierichting N_3) aan de Rijksuniversiteit Utrecht. Het kandidaatsexamen werd behaald in 1977, waarna werd begonnen met de studie Geofysica, hoofdrichting fysica van de vaste aarde. In 1979 werd het accent verlegd naar de hoofdrichting Meteorologie- en Oceanografie. Het afstudeerwerk in deze richting werd verricht bij de vakgroep Natuur- en Weerkunde van de Landbouwhogeschool in Wageningen (o.l.v. Prof. Dr. Ir. L. Wartena en Dr. Ir. A.F.G. Jacobs), en betrof het ontwikkelen en testen van een infrarood absorptiehygrometer voor het meten van de waterdampflux in de atmospherische grenslaag m.b.v. de eddy-korrelatiemethode. Ondertussen werd tevens een begin gemaakt met de doktoraalstudie Experimentele Natuurkunde. Het afstudeerwerk in deze richting werd uitgevoerd bij de vakgroep Medische en Fysiologische Fysika (o.l.v. Prof. Dr. J.J. Koenderink), en betrof de ontwikkeling van algorithmen voor hierarchische beeldsegmentatie. Het doktoraaldiploma Experimentele Natuurkunde werd behaald in januari 1983.

Per 1 februari 1983 trad de auteur in dienst van de Stichting voor ZWO. In augustus van datzelfde jaar werd het doktoraaldiploma Geofysika verkregen (met het predikaat 'cum laude').

Het in dit proefschrift beschreven onderzoek werd uitgevoerd bij de vakgroep Medische en Fysiologische Fysika van de Rijksuniversiteit Utrecht, o.l.v. Prof. Dr. J.J. Koenderink. Gedurende dit onderzoek had de schrijver als neventaak een adviserende en begeleidende funktie bij de ontwikkeling, implementatie en praktijkevaluatie van beeldverwerkingsalgorithmen t.b.v. de vakgroepen Röntgendiagnostiek en Nucleaire Geneeskunde in het Academisch Ziekenhuis te Utrecht.

Na het beëindigen van zijn dienstverband bij ZWO treedt de auteur in dienst van een grote gloeilampenfabrikant in het zuiden des lands, om zich met digitale beeldverwerking te gaan bezighouden.

Da steh' ich nun, ich armer Tor,
Und bin so klug als wie zuvor!

Goethe.
Faust: Der Tragödie erster Teil.